Zeitschrift: IABSE reports = Rapports AIPC = IVBH Berichte
Band: 48 (1985)

Rubrik: Session D: Composite steel-concrete construction

SESSION D

Composite Steel-Concrete Construction

Construction mixte acier-béton

Verbundbau

Leere Seite
Blank page
Page vide

Case Study: One Tampa City Center

Etude de cas: One Tampa City Center

Fallstudie: One Tampa City Center

Daniel A. CUOCO
Vice President
Lev Zetlin Assoc., Inc.
New York, NY, USA

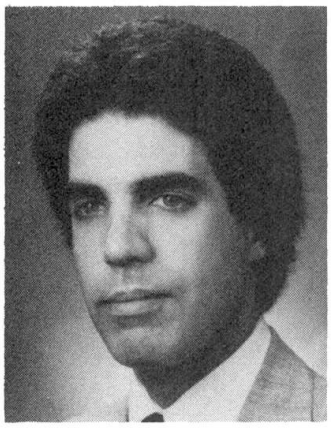

Daniel A. Cuoco is responsible for the management of major engineering and design projects at LZA, such as high-rise buildings, hotels, aerial tramways, industrial buildings, schools, airport structures, parking structures, hospitals, special structures, and investigations of structures in distress.

Charles H. THORNTON
President
Lev Zetlin Assoc., Inc.
New York, NY, USA

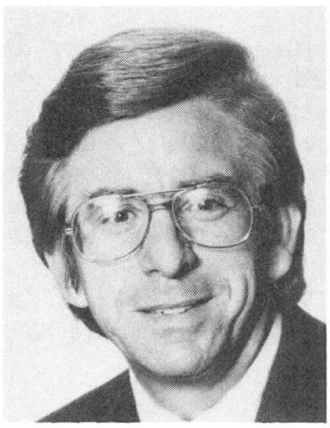

Charles H. Thornton has overall responsibility for engineering, design, research and development activities and policies at LZA. His experience includes involvement in the design and construction of projects, ranging from hospitals, arenas, industrial buildings, and high-rise buildings, to airports, transportation facilities.

SUMMARY

This paper presents a case study of One Tampa City Center, a 40-story office building located in Tampa, Florida, USA. Completed in 1982 as Florida's tallest building, the project utilizes composite steel-concrete construction for the primary structural system of the building, as well as composite subsystems and components. The composite structural system provided large clear-span areas as well as the required hurricane-wind resistance, all at minimum cost and within a tight construction schedule.

RÉSUMÉ

Cet article présente une étude de cas, le bâtiment administratif de 40 étages «One Tampa City Center», situé à Tampa. Achevé en 1982, il constitue le plus haut bâtiment de Floride. Les structures primaires et secondaires sont constituées d'éléments mixtes acier-béton. Ces structures mixtes permettent des grandes portées, assurent la résistance requise aux cyclones avec des coûts minimaux et nécessitent moins de dossiers et de plans de construction.

ZUSAMMENFASSUNG

Dieser Vortrag beinhaltet eine Fallstudie des One Tampa City Centers, eines 40stöckigen Geschäftshauses in Tampa, Florida, USA. Es wurde 1982 als Floridas höchstes Gebäude vollendet. Die primäre Tragkonstruktion sowie Tragwerksteile und Komponenten wurden in Stahl-Betonverbundbauweise ausgeführt. Mit dem Verbundtragwerk wurden grosse, frei überspannte Flächen wie auch die erforderliche Orkan-Widerstandsfähigkeit erreicht; dies alles zu minimalen Kosten und innerhalb eines gedrängten Bauprogramms.

1. GENERAL DESCRIPTION

One Tampa City Center is a 40-story office building located in Tampa, Florida, USA (Fig. 1). The building, sheathed in silver reflecting glass, has a height of 158 m and contains a gross area of 80,000 sq. m.

Completed in 1982 as Florida's tallest building, the project utilizes a composite steel-concrete structural system which consists of a slipformed concrete core in combination with structural steel framing outside the core (Fig. 2). All wind resistance is provided by the core, thus enabling the use of simple economical connections for the steel framing outside the core. The gross weight of structural steel for this project is only 39.6 kg/sq. m.

The composite structural system provides large 13.7-m clear-span areas as well as the required hurricane-wind resistance, all at minimum cost and within a tight construction schedule. Other structural systems which were evaluated during the preliminary design stage included a total structural steel frame, a post-tensioned concrete beam-and-slab system, and a prefabricated prestressed concrete joist system. It is estimated that the composite steel-concrete system resulted in overall savings to the project in excess of $1,000,000. In addition, the composite system expedited the fast-track construction schedule, allowing installation of elevators and mechanical risers in the core while the structural frame outside the core was being erected.

2. CONCRETE CORE

2.1 Design

The concrete core has a typical wall thickness of 406 mm and is stepped at the 12th and 20th Floors, corresponding to the exterior shape of the building (Fig. 3). In order to achieve the proper composite interaction of these stepped portions of the core, necessary for drift control of the building, built-up structural steel H-frames were placed in pairs within the concrete core walls at the 6th, 11th, 12th, 18th, 19th, and 20th Floors (Fig. 4).

A concrete mat having a thickness of 2.4 m forms the base of the core. Compacted soil-cement, in a unique application, transfers the mat foundation loads to limestone which lies approximately 10 m below the ground surface.

2.2 Analysis

The concrete core was analyzed utilizing a 3 dimensional finite element computer model comprised of combined membrane and beam elements. A total of 45 loading combinations were investigated, including pressure loading conditions obtained from wind tunnel testing.

Due to the fast-track nature of the project, and the lead time requirements for wind tunnel testing, the actual testing was performed subsequent to both

the structural design of the building and the awarding of a contract for the structural steel work. However, since the structural steel design was essentially unaffected by the wind loading on the building, mill ordering and fabrication of the structural steel was able to proceed unhindered. The results of the wind tunnel testing indicated significant torsional effects, which were otherwise unpredictable, and required reanalysis of the core and modification of the core wall reinforcing in several localized areas.

3. STEEL FRAMING

3.1 Beams and Girders

A typical framing plan for the upper portion of the building is shown in Fig. 5. The steel specified for the beams and girders is ASTM A572 Grade 50, F_y = 35.2 kg/sq.mm. Beams and girders utilize 19-mm-diameter x 89-mm-long shear connectors to act compositely with the floor slabs. Since the entire lateral resistance is provided by the core, beam-to-beam and beam-to-column connections are generally simple shear connections (Fig. 6).

Temporary shoring was provided for the steel beams until the concrete gained sufficient strength, in lieu of providing heavier beams to control the deflection due to the weight of wet concrete. This approach enabled the use of relatively shallow beams for large spans, e.g., a 457-mm beam for the typical 13.7-m span, which reduced the floor-to-floor dimension and the total height of the building.

3.2 Columns

The steel specified for the columns is ASTM A572 Grade 50, F_y = 35.2 kg/sq.mm. Since the columns transmit only axial forces, simple base plate and column splice details are utilized (Fig. 7).

In order to compensate for the differential shortening of the concrete core and the steel columns under dead load, column length adjustments were specified in the design and incorporated into the fabrication process.

3.3 Connection to Concrete Core

A weld-plate detail is utilized for the connection between the steel beams and the concrete core (Fig. 8). During the slipform operation, the weld-plates are set at the required locations, with the outer surface of the weld-plate set flush with the wall surface. Anchorage of the weld-plate is achieved by shear connectors which are welded to the inner surface and become embedded in the core wall. The weld-plates were oversized in order to allow for placement tolerances.

Subsequently, structural steel tees were field-welded to the weld-plates. The outstanding stem of each structural tee contained slotted holes in order to provide increased erection tolerances. The beams were connected to the tee stems using high-strength friction bolts.

In order to avoid delays to the structural steel erection due to possible out-of-tolerance field conditions of weld-plates, several types of such conditions were anticipated prior to the start of steel erection. Standardized solutions for these conditions were developed and pre-approved so that they would be readily available to be implemented whenever an out-of-tolerance condition might arise during the steel erection.

4. FLOOR CONSTRUCTION

4.1 Outside Core

The floor system outside the core area, typically spanning 2.5 m between floor beams, utilizes composite steel decking having a depth of 51 mm and a thickness of 0.91 mm. A concrete fill of 64 mm thickness is placed above the decking, and welded wire fabric is placed within the concrete fill (Fig. 9). An electrified floor system is utilized for the 3rd through 17th Floors, and a nonelectrified system is utilized for the balance of the floors.

4.2 Within Core

The typical floor construction within the core consists of cast-in-place concrete beams and slabs, with the exception of the 11th, 19th, 30th, and 37th Floors which use structural steel framing with composite steel decking and concrete fill.

Each of the steel-framed core floors was constructed as soon as the slipform reached its corresponding level. This provided stiffening for the free-standing concrete core, and also provided a protective umbrella which enabled concrete floor slabs to be placed at the floors below while the slipform operation continued. Structural steel framing was used for these protection floors in lieu of concrete in order to minimize the shutdown time of the slipform operation while these floors were being constructed.

4.3 Connection to Concrete Core

At the connection between the floor slabs (both within and outside of the core) and the core walls, intermittent keyways were provided in the core walls (Fig. 10). This enables the transmission of lateral diaphragm forces from the floor system to the core. Keyway connections were also provided at stairs and stair platforms within the core in order to maintain the structural continuity of the core at the stair shaft openings.

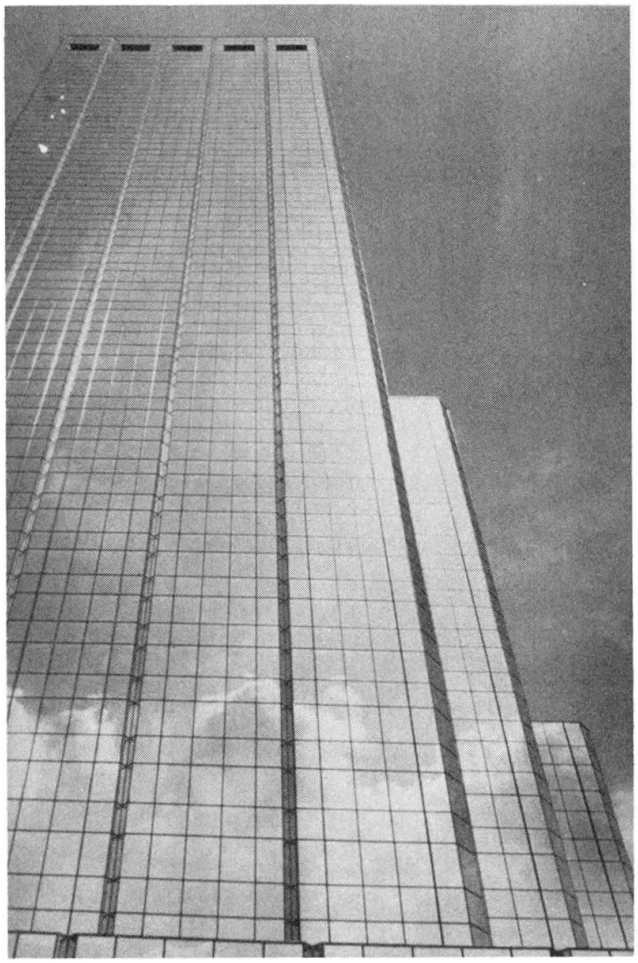

Fig.1 One Tampa City Center, Tampa, Florida, USA

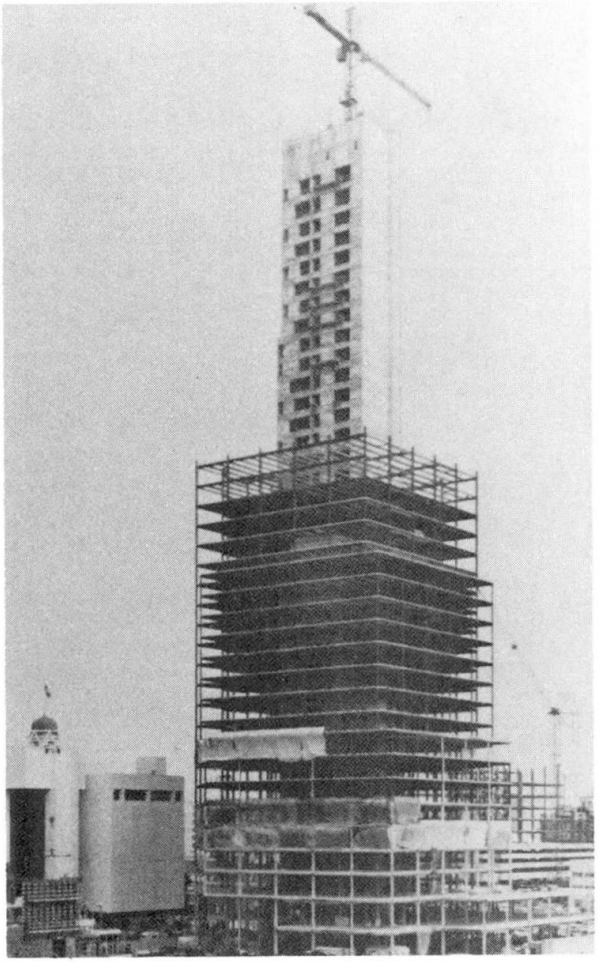

Fig.2 Composite Steel-Concrete Structural System

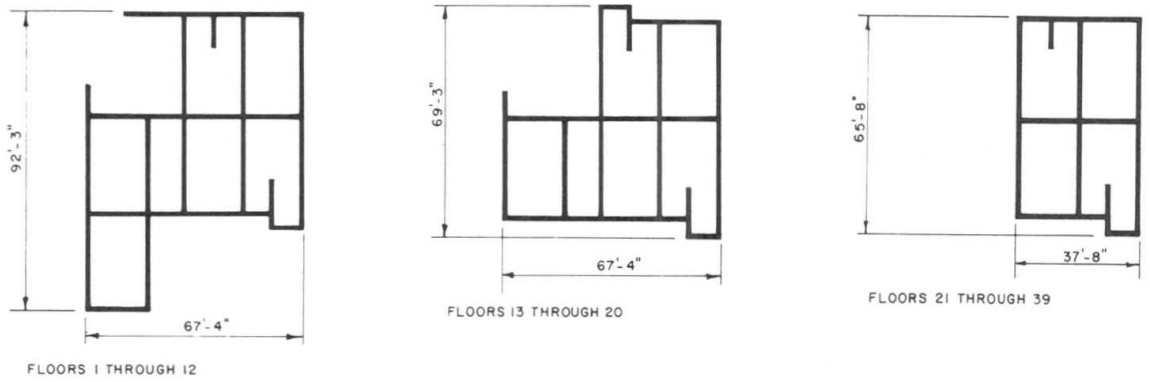

Fig.3 Concrete Core Configurations

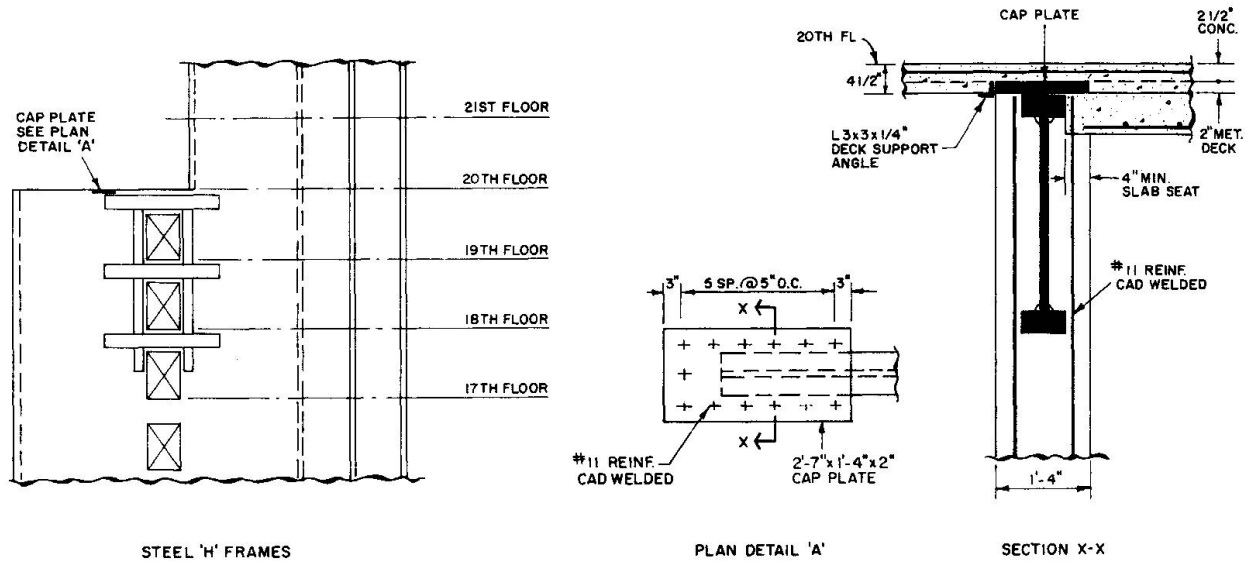

Fig.4 Structural Steel H-Frames Placed in Concrete Core

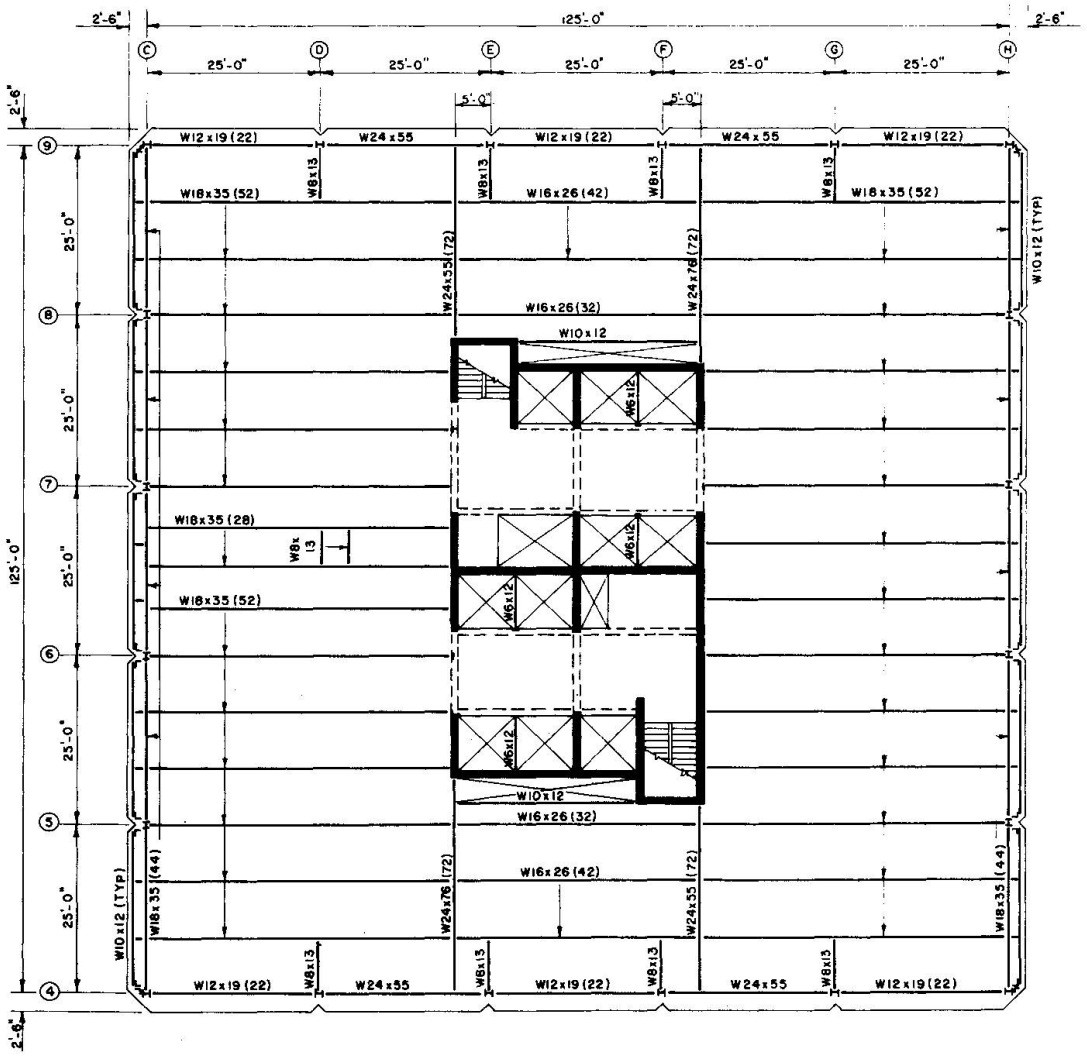

Fig.5 Typical Framing Plan

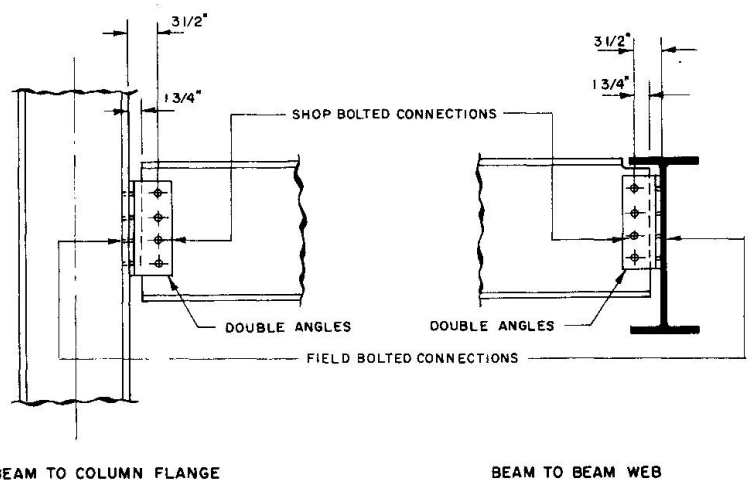

Fig.6 Typical Steel Framing Connections

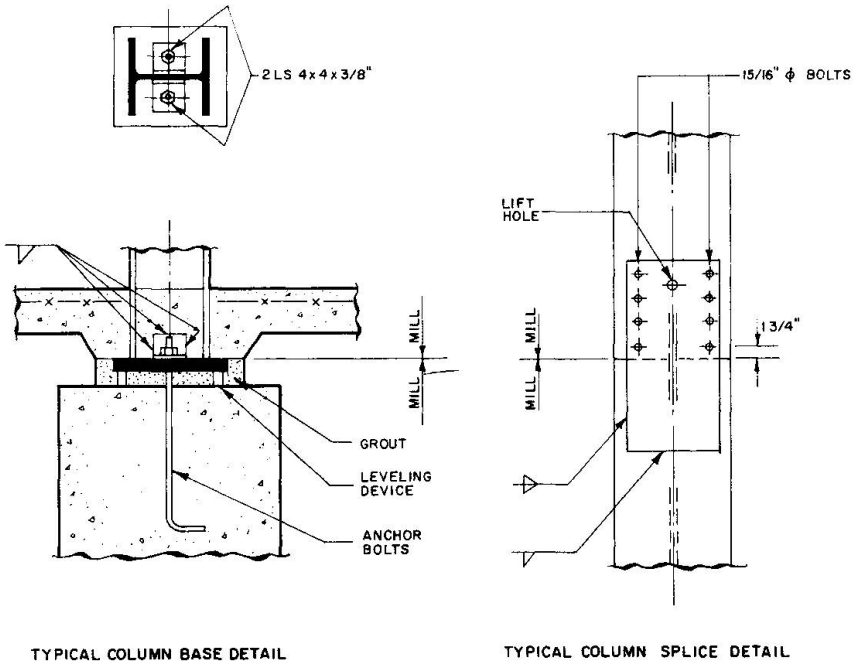

Fig.7 Typical Steel Column Details

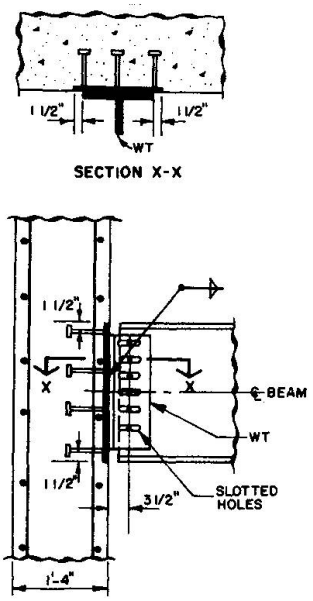

Fig.8 Typical Connection of Steel Beam to Concrete Core Wall

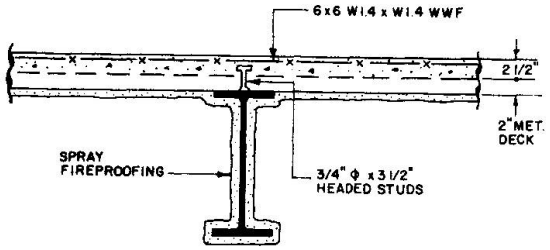

Fig.9 Typical Floor Construction Outside Core

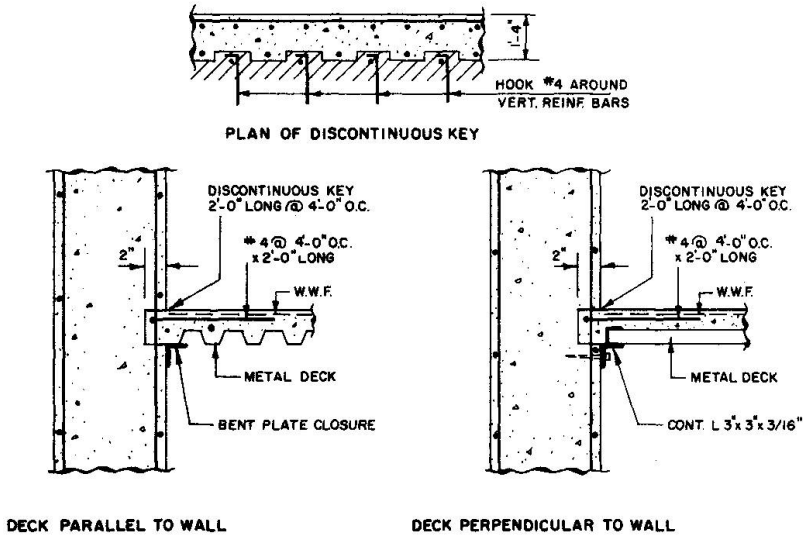

Fig.10 Typical Connection of Floor Slab to Core Wall

Ductility in support regions of continuous composite beams

Ductilité dans les zones d'appuis des poutres mixtes continues

Duktilität im Auflagerbereich von durchlaufenden Verbundträgern

Alan KEMP
Prof. of Civil Eng.
Univ. of the Witwatersrand
Johannesburg, South Africa

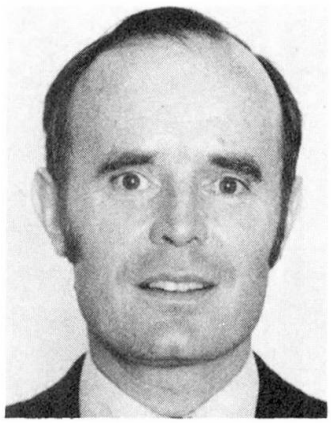

Alan Kemp. born 1940, got his BSc and MSc at the University of the Witwatersrand and his PhD from Cambridge University. He was group consulting engineer of Dorman Long (Africa) and Manufacturing Manager of Dorbyl Rolling Stock before taking the Chair of Structural Engineering, University of the Witwatersrand.

Hennie DE CLERCQ
Director
Van Wyk & Louw
Johannesburg, South Africa

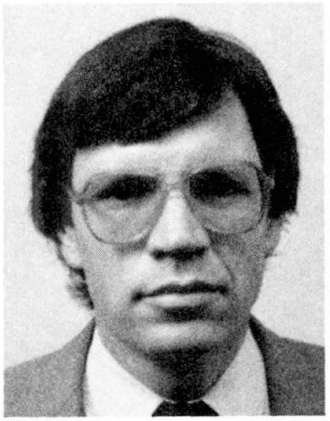

Hennie de Clercq, 39, has a BSc from the University of Pretoria and a PhD from UC Berkeley. He was previously Director of the South African Institute of Steel Construction and is now a consulting engineer.

SUMMARY

Two solutions are investigated for improving the ductility of support regions of continuous composite beams to permit plastic design without uneconomic prescriptions due to possible local web and flange buckling. The behaviour is assessed in three beam tests and compared with theoretical predictions. The economic implications are evaluated by comparitive cost studies. The benefits of a compositely-continuous, simply-supported beam are described.

RÉSUMÉ

Deux solutions sont recherchées pour augmenter la ductilité et la stabilité des zones d'appuis des poutres mixtes dans le but d'assurer la plastification totale de la section – donc d'éviter le voilement de l'aile ou de l'âme – sans avoir recours à des dispositifs trop coûteux. Le comportement de ces zones d'appuis est évalué à l'aide de trois essais de poutres et de leur comparaison avec les prévisions théoriques. Des études de comparaison de coûts permettent de prévoir les implications économiques de ces découvertes. Les gains qu'on obtiendrait avec des poutres mixtes continues, par rapport au poutres simples, sont estimés.

ZUSAMMENFASSUNG

Zwei Lösungen zur Verbesserung der Duktilität im Auflagerbereich von durchlaufenden Verbundträgern werden untersucht, damit plastische Berechnungsmethoden angewendet werden können, ohne dass unwirtschaftliche Vorschriften aufgrund des möglichen, lokalen Flansch- und Stegbeulens auferlegt werden. Das Verhalten wird mit 3 Balken-Tests belegt und mit theoretischen Voraussagen verglichen. Die wirtschaftlichen Folgen werden durch Kostenvergleiche bewertet. Die Vorteile eines einfach gelagerten, durchlaufenden Verbundträgers werden beschrieben.

1. INTRODUCTION

It is well established that continuous composite beams provide an efficient and economic solution in building structures, particularly if they are designed to develop their plastic moment capacities in both sagging (positive moment) and hogging (negative moment) regions. However, it is also recognised that in order to develop the plastic collapse mechanism in such continuous beams a large amount of redistribution of moment is necessary between the support and midspan regions. This implies a requirement for adequate ductility in hogging moment regions as reflected by the plastic plateau in representative moment-rotation curves (Fig.1). This requirement is particularly demanding in the case of composite beams.

Local buckling as described subsequently and, to a lesser extent, lateral buckling of the steel section critically influence the ability of composite beams in support regions to maintain their moment capacity during the hinge rotations which are necessary to develop a collapse mechanism. These modes of failure are particularly important in limiting the ductility because of the concurrent axial compressive force applied to the steel beam which balances the tension force in the longitudinal reinforcement in the slab. The applicability of simple plastic theory to continuous composite beams has been reviewed by Johnson [1] and assessed in quantitative terms by Johnson and Hope-Gill [2].

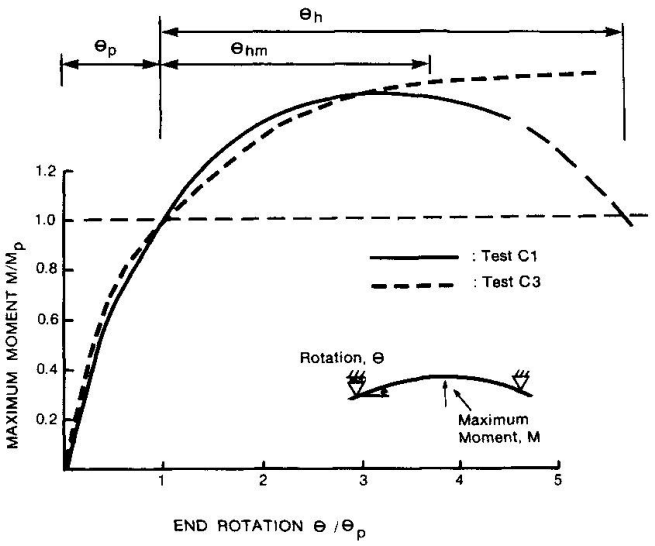

Fig. 1 Moment-rotation curves

Two solutions for improving ductility are described; the first incorporates the use of inclined stiffeners and the second involves designing and detailing a composite beam so that it is simply-supported prior to the concrete achieving its characteristic strength and continuous subsequently. The project was directed towards solving a hypothetical design problem and the cost implications are also evaluated and discussed.

2. THEORETICAL CONSIDERATIONS

2.1 Ductility

The two-span continuous beam illustrated in Fig. 2a provides the terms of reference in this paper for considering ductility, local buckling and cost comparisons. The limiting elastic and ultimate bending moment diagrams are shown in Fig. 2b and are based on the following assumptions:

- Ratio of flexural regidities (EI) in hogging (cracked) to sagging regions = 0,4
- Ratio of plastic moment capacities in hogging to sagging bending = 0,7

Once the moment at the support reaches its ultimate capacity, $M'_e = M'_p$ in the idealised elastic bending-moment diagram, a redistribution of moment is required

from support to midspan region in order to develop the ultimate bending-moment diagram. This redistribution can be achieved if a sufficiently long, plastic-moment plateau exists in the relationship shown in Fig. 1 between support moment and rotation at the end of the hogging moment region (length L_h in Fig. 2). This ductility is normally assessed by the rotation capacity, R, which is defined as follows with reference to Fig. 1:

$$R = \frac{\Theta_h}{\Theta_p} \quad \text{or} \quad R_m = \frac{\Theta_{hm}}{\Theta_p}$$

2,2 Local Buckling

The inverted simply-supported beam arrangement shown in Fig. 3 forms the basis of the experiments described subsequently and represents the hogging region of length $2L_h$ between points of inflection of the beam shown in Fig. 2. Local buckling of the compression flange is the most significant cause of strain-weakening behaviour in continuous beams. Following the proposals of Lay and Galambos [3] , the local buckle is assumed to develop when the length of the yielded region of the flange (L_p in Fig.3) extends sufficiently far to accommodate the full wave-length of the buckle. Kemp [4] has rearranged the formulations and assumptions of Lay and Galambos [3,5] Southward [6] and Stowell [7] to give the following formulae which can be solved iteratively to give the ratio of yielded to half-span length $\ell_f = L_{pf}/L_h$, at the onset of local flange buckling in regions of moment gradient:

$$\left(\frac{b}{t_f}\right)^2 = \frac{4}{3\varepsilon_b - n_1\left(\frac{\pi t_f}{\ell_f L}\right)^2} \qquad (1a)$$

in which (b/t_f) is the ratio of flange width to thickness, $n_1 = 1$ for no web restraint (coincident web buckling) or $= 2$ for web providing restraint and ε_b is the longitudinal strain at buckling in the compression flange at the centre of the buckled length, given by:

$$\varepsilon_b = \varepsilon_y \{s + 0{,}5e\ell_f / (1-\ell_f)\} \qquad (1b)$$

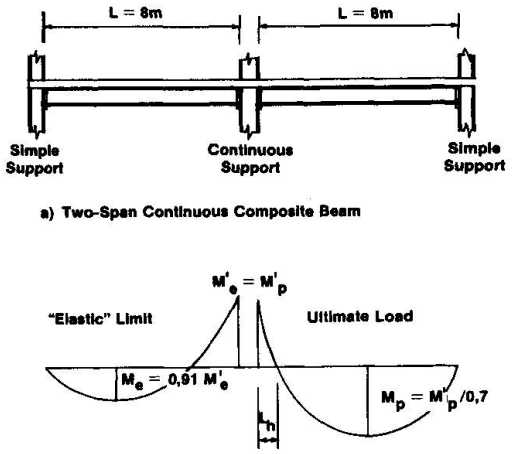

Fig. 2 Illustrative beam arrangement.

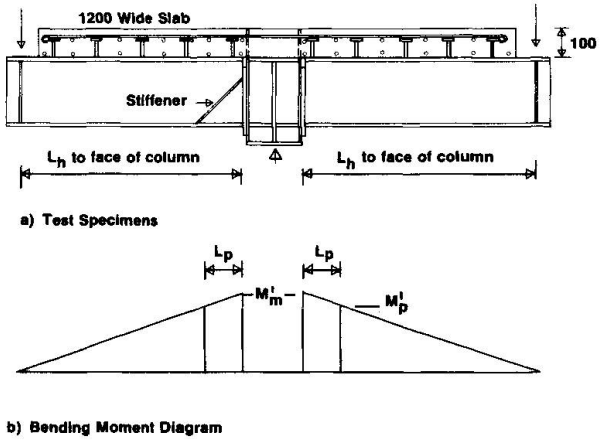

Test	C1	C2	C3
Size of steel section	305x102x25	305x165x41	305x102x25
Area of longit. reinforc.	470mm²	470mm²	940mm²
No. of studs/half-span	5	5	9
Detail of beam end plate at column connection (Grade 8,8 Bolts)	Rigid Continuous	Rigid Continuous	Flexible No tension transfer

Fig. 3 Test specimens

in which ε_y is the yield strain, s is the ratio of strain at the onset of strain-hardening to yield strain and e is the ratio of modulus of elasticity to strain-hardening modulus.

Web buckling is predicted to occur [8] when the ratio of yielded to half-span length, $\ell_w = L_{pw}/L_h$, extends far enough to satisfy the following relationship:

$$\ell_w = 27 \frac{t_w}{L_h} \{(2n_{wc}^2 - 1) - \sqrt{(2n_{wc}^2 - 1)^2 - 1}\}^{0.5} \sqrt{240/f_y} \qquad (2)$$

provided $h_{wc} > 27\, t_w \sqrt{240/f_{sd}}$

in which $n_{wc} = h_{wc}/27t_w \sqrt{240/f_y}$, h_{wc} is the clear depth of web in compression, t_w is the web thickness and f_y is the yield stress.

Kemp [8] has identified in tests on plain steel beams that local flange buckling may be initiated under the conditions defined by Eqs. 1, but may not develop due to strain compatibility constraints across the flange, which introduce inhibiting forces. These are released by the onset of web buckling or lateral torsional buckling. A combined mode of local flange buckling and web buckling may therefore be expected to occur when the ratio of yielded to half-span length, $\ell_b = L_p/L_h$, is equal to the larger of ℓ_f (Eqs. 1 with $n_1 = 1$ for no web restraint) or ℓ_w (Eq. 2). This model has been shown [8] to compare favourably with test results, using the following simplified relationship between rotation capacity at maximum moment and plastic length ratio:

$$R_m = \frac{\theta_{hm}}{\theta_p} = \frac{h_w}{2h_{wc}} \ell_b \left(2s - 1 + \frac{e\ell_b}{1-\ell_b}\right) \qquad (3)$$

3. COMPOSITELY-CONTINUOUS, SIMPLY-SUPPORTED BEAMS

Code requirements to avoid local buckling of the web of continuous composite beams often lead to uneconomic steel sections due to the extended depth in compression which is required to balance the tension force in the longitudinal reinforcement. The need for such limitation has also been demonstrated in tests on plain steel sections [8] .

The authors decided to investigate the implications of applying to building structures the concept of "compositely-continuous, simply-supported beams", which was suggested by Fried [9] for bridges in Australia. These beams possess simple, welded end-plates for connection to the column with no provision for continuity of the top, tension flange but the facility for compression force to be transmitted in bearing from the compression flange and web, with the possible need for shim plates to allow for fabrication tolerances and erection clearances. Such a beam will behave as simply-supported prior to the concrete achieving its strength and continuous when the longitudinal slab reinforcement becomes effective. This procedure effectively upgrades the resistance of a simply-supported beam by using the longitudinal reinforcement provided over the support, which may only be the minimum amount required to control cracking. The reinforcement should be staggered and extend far enough to allow for both elastic and plastic positions of the point of inflection. This arrangement was studied experimentally and assessed in terms of relative cost.

3.1 Experimental Results

Three beams, C1 to C3, were tested in the arrangement shown in Fig. 3 in order to assess the ductility requirements further. These specimens were intended to represent the hogging region of the two-span continuous beam of Fig. 2 and were

deliberately chosen to reflect relatively slender sections. The details of the test specimens are given in Fig. 3 and Table 1. Beams C1 and C2 possess conventional rigid end-plate connections appropriate to a continuous beam, whereas beam C3 is a compositely-continuous, simply-supported beam as described above with sufficient longitudinal reinforcement to give approximately the same moment capacity as beam C1.

The relationship between moment at the face of the column and the relative rotation between the column and end of the beam is shown in Fig. 1 for beams C1 and C3. Whereas C1 failed in combined local buckling of web and flange at a rotation capacity of 3,5, specimen C3 exhibited significantly larger rotations and the test was stopped due to failure of the slab in horizontal shear. Beam C1 just satisfied the intention in the South African code [10] of $R_m > 3$. Beam C3 more than met this requirement due to the greater flexibility in the simply-supported end connection. Furthermore local buckling was less likely in this case due to the smaller proportion of web depth in compression.

The observed plastic rotations, Θ_{hm} in Fig. 1, are recorded in Table 1 for the beam and end connection to the column, as well as for the beam alone. It is apparent that the rotation capacity is approximately doubled by the flexibility of the end connection. This beneficial effect is difficult to quantify for designs in general and has partly been allowed for in the relatively low rotation capacity required for plastic design (eg. $R_m \geq 3$). The plastic rotations predicted using the theoretical models of Eqs. 1 to 3 are given in the last line of Table 1 and compare favourably with the observed behaviour. The plastic rotations are described rather than the rotation capacities due to the difficulty in consistently identifying EI and thus Θ_p in the test beams due to large rotations in the end connection and variable amounts of concrete cracking. The beneficial effects of the diagonal stiffener (Fig. 3) which inhibits local buckling of the flange and web can be seen in the results of beam C2. Investigations are proceeding on how to quantify this benefit.

Test		C1	C2		C3
flange slenderness b/t_f		15,4	16,5		15,3
flange yield stress		378	341		378
flange length ratio L/t_f (Eq. 1a)		141	101		141
web slenderness n_{wc} (Eq. 2)		1,23	1,28		0,3
web yield stress		412	359		412
diagonal stiffener (Fig. 3)		NO	NO	YES	NO
Plastic rotation $\Theta_{hm} \times 10^{-3}$	observed : beam & end connection	22,6	29,9	47,2	>34,3*
	observed : beam only	12,0	14,8	23,0	> 9,7*
	predicted : beam only	12,8	16,6	n.a.	18,8

(*: beam C3 did not fail in web & flange buckling)

Table 1 Local buckling characteristics

3.2 Cost Implications

In order to determine how the requirements for ductility of the hogging moment region influence the cost of construction, the structure of a four storey building with beams spaced at 3m and supported on three rows of columns as shown in Fig. 2a was designed for clear beam spans L of 8, 10 and 12m. For each value of beam span, three different joint details were considered : simply-supported,

compositely-continuous, and fully-continuous. At the two exterior columns the beams were assumed to be simply-supported. These structures were designed for each of two assumptions: steel beams propped until concrete has hardened, and steel beams unpropped from the start. The assumption was made that before hardening of the concrete the top flange of the steel beam is fully-restrained against lateral torsional buckling. Various steelwork contractors were asked to price each of the design variations.

The results of this study are shown in Table 2, where the cost/m² of the 8m span, simply-supported, propped beam construction was taken as unity. The cost/m² of floor relates only to those aspects which are not common to all beams: the steel beams with connections, shear connectors, reinforcing in the hogging moment region, and the cost of erection. The cost or nuisance effect of propping was not taken into account, the former is minor and the latter difficult to assess in general terms.

Span L of beam	8m	10m	12m
Simply-supported beams, propped:			
section	305x102x33 I	406x140x46 I	406x178x60 I
no. of stud connectors	32	24	64
cost/m² of floor	1,00	1,13	1,40
Compositely-continuous beams, propped:			
section	305x102x29 I	406x140x39 I	406x178x54 I
no. of stud connectors	22	27	34
mass of reinforcement (kg)	10,6	11,5	23,3
cost/m² of floor	0,94	1,11	1,31
Fully-continuous beams:			
section	305x102x29 I	356x171x45 I	406x178x54 I
no. of stud connectors	20	26	32
mass of reinforcement (kg)	3,5	5,4	7,8
cost/m² of floor	1,02	1,31	1,41
Simply -supported beams, unpropped:			
section	406x140x39 I	406x140x46 I	406x178x160 I
no. of stud connectors	20	24	64
cost/m² of floor	1,11	1,13	1,40

Table 2 Summary of design solutions

Table 2 shows compositely-continuous propped beams to be the least-cost solution for each of the three spans, assuming the cost of propping to be negligible. The question as to the performance of unpropped, compositely-continuous beams is answered by the fact that the steel sections would be the same as the simply-supported, unpropped beams for which the temporary criterion of supporting wet concrete and construction loads was found to be the limiting condition for the spans and loading under consideration. Propping (at low cost) is thus a requirement for the success of compositely-continuous beams in this study, in which the construction loads were 52% of the final value of dead plus live load. Further investigations, the results of which are not quoted in this paper, indicated that for certain realistic but lower values of the ratio of dead to live load, unpropped compositely-continuous beams may be used without having to pay any

penalty in the weight of the steel section.

Fully-continuous beams proved in this study to be uneconomical, although the uncertainty of the cost of propping is avoided through the fact that deletion of the propping was found not to affect the choice of the steel section. A striking observation is that in the 10m span case a heavier section had to be chosen than for the compositely-continuous counterpart, in order to satisfy the codified web buckling provisions.

It needs to be said that partial interaction between steel and concrete was assumed where the strength of a full-interaction beam exceeded requirements, thus saving on the number of shear connectors needed. Furthermore, limitations in the range of available steel sections led on occasions to slightly unrepresentative results.

4. DISCUSSION

This study, including the experimental work, showed that local web buckling is significant in the design of continuous composite beams, although solutions have been proposed, [11] which make no reference to these ductility requirements. It is further clear that satisfying the ductility requirements in continuous beams has cost implications, as relatively slender sections are not suitable for plastic design. The compositely-continuous beam as described above, is however, an economic way of providing continuity without ductility problems, provided either that the beams are propped until the concrete has hardened, or that the live loads are relatively high in comparison with the construction loads. The improved ductility of a compositely-continuous beam over a fully-continuous member with the same moment of resistance is due to the fact that less web depth is under compression, and these beams exhibit considerably larger rotations within the end connection between the beam and the column. This is illustrated by the observed rotations in beam C3 in Fig. 1.

Taking the importance of speed of construction into account, the unpropped simply-supported beam remains a viable alternative. There are, however, good reasons to favour compositely-continuous beams:

- they are less expensive (up to 6% in this evaluation);
- cracking has been experienced in the support regions of simply-supported beams [12] and reinforcing is recommended; thus the only remaining requirement to create compositely-continuous conditions is to ensure contact between the compression region of the beam and the column face, which contact need not be extremely tight for the unloaded beam;
- the deflection and propensity for objectionable vibrations of the floors will be reduced with continuous construction.

5. CONCLUSIONS

Codes for plastically-designed continuous composite beams should contain prescriptions on web slenderness in hogging regions which allow for the depth of web in compression. These provisions will often increase the cost of the steelwork. The use of the compositely-continuous beams is shown to satisfy these ductility requirements and provide an economic solution which merits further attention.

6. ACKNOWLEDGMENTS

This research was supported by the South African Institute of Steel Construction and the South African Iron and Steel Corporation. Dorbyl Structural Engineering fabricated the beams used in the tests and Mr. J. Dyer assisted with the tests.

REFERENCES

1. JOHNSON R.P., Research on Steel-Concrete Composite Beams. Journal of the Structural Division, ASCE, Vol. 96, March 1970, 445-459

2. JOHNSON R.P. and HOPE-GILL M.C., Applicability of Simple Plastic Theory to Continuous Composite Beams. Proceedings, Institution of Civil Engineers, London, Part 2, Vol 61, March 1976, 127-143

3. LAY M.G. and GALAMBOS T.V., Inelastic Steel Beams under Uniform Moment. Journal of the Structural Division, ASCE, Vol. 91, Dec. 1965, 67-93.

4. KEMP A.R., Interaction of Plastic Local and Lateral Buckling. Paper provisionally accepted for publication, Journal of Structural Division, ASCE.

5. LAY M.G. and GALAMBOS T.V., Inelastic Beams under Moment Gradient. Journal of the Structural Division, ASCE, Vol 93, Feb. 1967, 381-399.

6. SOUTHWARD R.E., Local Buckling in Universal Sections. Internal Report, University of Cambridge Engineering Department, 1969.

7. STOWELL E.Z., Compressive Strength of Flanges. Technical Note No. 2020, National Advisory Committee for Aeronautics 1950.

8. KEMP A.R., Local Buckling of Webs and Flanges in Plastic Design to SABS 0162:1984. Paper submitted to the Civil Engineer in South Africa.

9. FRIED A., New Type of Continuous Composite Steel and Concrete Bridge. Acier-Stahl-Steel, Nov 1974, 482.

10. KEMP A.R., Commentary on Chapter 12: Plastic Design, SABS 0162-1984. South African Institute of Steel Construction.

11. LE MESSURIER W.J., Plastic Composite Design Cuts Steel Tonnage in Johns Manville's New H/O Building. Architectural Record, Sept 1977, 127, 128.

12. CHIEN E. and RITCHIE J., Design and Construction of Composite Floor Systems. Canadian Institute of Steel Construction, 1984.

Continuous Composite Beams for Buildings

Poutres mixtes continues dans le bâtiment

Durchlaufende Verbundträger für Hochbauten

R.P. JOHNSON
Professor of Civil Engineering
University of Warwick
Coventry, United Kingdom

Roger Johnson graduated at Cambridge, then worked in industry before becoming a university lecturer. He has been active in research on composite structures since 1960, and has been contributing since 1968 to the preparation of codes of practice.

SUMMARY

The treatments in the first draft of Eurocode 4 of the classification of steel cross sections, lateral torsional buckling, and partial shear connection are shown to have much influence on the conception and design of continuous composite beams. Further research on lateral torsional buckling and on the stiffening of steel webs is needed, to enable design methods to be improved and costs to be reduced.

RÉSUMÉ

Le déversement et la connection partielle ont une très grande influence sur la conception et le dimensionnement des poutres mixtes continues dans la version préliminaire de l'Eurocode 4. Dans le but d'améliorer les méthodes de calcul et de réduire les coûts de construction, il est nécessaire d'entreprendre des recherches sur le déversement et sur les raidisseurs d'âme.

ZUSAMMENFASSUNG

Die im ersten Entwurf des Eurocodes 4 bearbeitete Klassifizierung von Stahl-Querschnitten, das Torsionsdrillknicken und die Teilverdübelungen haben erwiesenermassen grossen Einfluss auf den Entwurf und die Ausführung von durchlaufenden Verbundträgern. Weitere Untersuchungen in Bezug auf das Torsionsdrillknicken und die Stegversteifungen sind zur Verbesserung der Berechnungsmethoden und zur Reduzierung der Kosten erforderlich.

1. INTRODUCTION

One of the first decisions that has to be made in the design of a composite floor structure for a building, with or without steel sheeting, is whether to use simply-supported or continuous beams.

The advantages of continuity are:
- the structure can be made shallower or its deflections reduced, or both:
- the susceptibility of the structure to vibration should be reduced;
- close control of the width of cracks in the slab near internal supports becomes possible without the use of joints in the slab; and
- the weight of steel in the beams can be reduced.

The apparent disadvantages (with comments on them) are:
- the beam-to-column joints become more expensive, unless the beams are designed to pass either side of the columns;
- if end-plate joints are used, the steel frame is more sensitive to inaccuracies of fabrication;
- erection of the frame may be more difficult; but when erected, it needs less temporary bracing; and
- there may be an increase in the design bending moments in some columns; but the influence of this on the weight of steel in columns is rarely significant.

It appears that in many structures, the use of continuity should save money. Except in respect of lateral buckling, nearly all the necessary research has been done; much of it before 1967, when continuous composite beams were first treated in a British Code of Practice (CP 117: Part 2, for bridges); but in 1985 there is still no British code for continuous beams in buildings, which partly explains why they are so rarely used in the U.K. They were fully treated in the European Model Code of 1981 [1], and its scope was extended in the draft Eurocode 4 [2] to include composite frames.

Another problem of continuity is that at present, design takes longer, partly because designers get so little relevant experience. The remedy lies with computers. The development of software for this purpose is likely to accelerate as soon as Eurocode 4 is finalised.

The object of this paper is to discuss the implications of some of the clauses of draft Eurocode 4 relevant to continuous beams, with reference to:
- the influence of the classification of steel cross sections;
- design for lateral torsional buckling; and
- partial shear connection.

The scope of the paper is limited to fully continuous composite beams in frames braced against sidesway, using rolled steel sections. Semi-rigid joints are not considered, nor is the use of elastic-plastic analysis of the structure, as these are subjects for current research.

2. CLASSIFICATION OF CROSS SECTIONS OF COMPOSITE BEAMS

2.1 The four Classes of Eurocodes 3 and 4

In these and other recent codes, account is taken of local buckling of steelwork by placing each steel web and compression flange into one of four classes: Class 1, Plastic; Class 2, Compact; Class 3, Semi-compact; and Class 4, Slender. The methods of analysis given in Eurocode 4 for a continuous beam are determined by the classes of its critical cross sections, which for this purpose can be assumed to be sections at each internal support and near the centre of each span.

Plastic hinge analysis of the structure is allowed when all relevant sections are in Class 1, and plastic analysis can be used for the resistance in bending (or bending and shear) of sections in Class 1 or 2. Elastic analysis can be used without

restriction. The limiting slendernesses proposed in draft Eurocode 4 are given in Table 1. Those for Classes 1 and 2 are 10% to 25% lower than their counterparts in draft Eurocode 3 [3], for reasons explained elsewhere [4]. In Table 1:

b_o is the overall breadth of a flange of mean thickness t,
d is the depth between fillets of a web of thickness w,
αd is the depth of the web in compression, and
ϵ takes account of the specified yield strength of the steel, with values:
1.0 for steel Fe 360, with yield strength 235 N/mm^2,
0.814 for steel Fe 510, with yield strength 355 N/mm^2.

		Class 1	Class 2	Class 3
Flanges,	b_o/t	16ϵ	20ϵ	30ϵ
Webs,	d/w	$30\epsilon/\alpha$	$33\epsilon/\alpha$	As in EC3

Table 1 Maximum b_o/t and d/w ratios for steel sections in composite beams

2.2 Steel compression flanges

Any steel flange that is attached to a concrete slab by shear connection in accordance with EC3 is assumed to be in Class 1. The class of other flanges depends only on the specified yield strength of the steel. Guidance is given in Table 2 on the classification of the flanges of the European standard sections IPE, IPE-A, and HEA [5] and of the British UB sections, in terms of the overall depth of the section, h.

Steel	Class 1		Class 2	
Fe 360	IPE,	all	IPE,	all
	IPE-A,	$h \geq 330$ mm	IPE-A,	all
	HEA,	$h \geq 390$ mm	HEA,	$h \geq 310$ mm
	UB	nearly all	UB,	all
Fe 510	IPE,	$h \geq 190$ mm	IPE,	all
	IPE-A,	$h \geq 600$ mm	IPE-A,	$h \geq 330$ mm
	HEA,	$h \geq 490$ mm	HEA,	$h \geq 390$ mm
	UB,	heavier end of each size range	UB,	nearly all

Table 2 Classification of flanges of rolled steel sections

2.3 Steel webs

To demonstrate that a web is in Class 1 or Class 2, the depth of the web in compression is determined from the position of the plastic neutral axis of the composite section: so that no account need be taken of the modular ratio or of the effects of sequential construction of the concrete slab. If the depth exceeds the limit for Class 2, the web will normally be in Class 3 if the steel member is a rolled section.

For midspan cross sections of composite T-beams for buildings, the plastic neutral axis is usually in the slab or steel top flange, so the section is in Class 1. Even in L-beams, the depth of web in compression is rarely enough to put the section into Class 2.

At an internal support, the class of the section depends on the amount of

longitudinal reinforcement in the slab. This is shown by the following example. An internal span of length 12 m of a T-beam consists of a slab 120 mm thick and more than 3.0 m wide, composite with an IPE 550 steel section, for which the web has a depth between fillets of 468 mm and a thickness of 11.1 mm (d/w = 42.2). The corresponding UB section is a 533 x 210 UB 109, with d = 476.5 mm, w = 11.6 mm, and d/w = 41.1. If the section is in Class 1 or Class 2, the effective breadth of the concrete flange is given by Eurocode 4 as L/4, or 3.0 m. Let there be r% of longitudinal reinforcement at an internal support (i.e., an area of 36r cm^2), with a design yield strength of 425/1.15 = 370 N/mm^2.

When the section reaches its plastic moment of resistance in hogging bending, the net compressive force in the web equals the tensile force to cause yield of the reinforcement, so that the proportion of the depth of the web in compression, α, increases with r. Maximum values of r for the web to be just in Classes 1 and 2 are given in Table 3, for steels Fe 360 and Fe 510.

	Class 1	Class 2
Fe 360	r = 0.39%, α = 0.71	r = 0.52%, α = 0.78
Fe 510	r = 0.22%, α = 0.58	r = 0.38% α = 0.64

Table 3. Influence of reinforcement ratios on class of cross section

The signficance of these results is that the four values of r all lie within the practical range. The lightest slab reinforcement possible is that required for crack-width control, which could be less than 0.2% if half or more of the overall depth of the slab is taken up with profiled steel sheeting. The section would then be in Class 1, as are the sections at midspan, so plastic hinge analysis could be used.

If the designer sought to take maximum advantage of continuity because the span/depth ratio was high, a reinforcement ratio exceeding 0.8% might be considered, which would put the composite section well into Class 3, with consequences for design that are now considered.

2.4 Design of a beam with one or more sections in Class 3

In beams with critical sections in Classes 1 and 2 only, plastic behaviour can occur without buckling. Such beams are more tolerant of the effects of sequence of construction, unforeseen load distribution, shrinkage of concrete, and temperature differences than are beams with sections in Classes 3 or 4. The boundary between Class 2 and Class 3 also corresponds roughly to the transition from beams for buildings to beams for bridges. For these reasons there is in both Eurocodes 3 and 4 a marked increase in the complexity of design methods, when even one section of a continuous beam is moved from Class 2 into Class 3. The main requirements for Class 3 composite beams that differ from those for Class 2 are now outlined.

(1) The classification of a web depends on the depth of the web in compression as given by elastic analysis *for the load case considered*, and so is not independent of loading or of the sequence of construction.

(2) If continuous beams are analysed using uncracked flexural stiffnesses, redistribution of moments from internal supports is allowed up to 30% when these sections are in Class 2: but none is allowed for Class 3 unless the midspan sections are designed elastically, as if in Class 3, even though they are likely to be in Class 1. The reason is that when regions near internal supports remain elastic (as Class 3 sections must do), a midspan region is likely to shed bending moment to them before it can reach its plastic moment of resistance.

(3) It can no longer be assumed in design that all load is carried by the composite

member when unpropped construction is used.

(4) The secondary (hyperstatic) effects of shrinkage of concrete have to be considered.

(5) Elastic analysis of the section is used, with a more accurate but less simple evaluation of effective width. It may be necessary to use different modular ratios for live and for dead loading, and so to keep the effects of these loads distinct in calculations.

(6) No provision is made in Eurocode 4 for the use of partial shear connection in members with sections in Classes 3 or 4, because of the lack of relevant research.

The consequences for design are obvious. The entrance fee to Class 3 is high!

For a continuous beam of equal spans, the most critical sections are at the penultimate supports. Often, one would like to use a steel beam of constant section, probably just in Class 2, and to stiffen these two regions while keeping them in Class 2. It is clear from Table 3 that there is little scope for doing this by increasing the longitudinal reinforcement in the slab, unless:

- a bottom-flange plate of equivalent area is also added (which may be visually unacceptable), or
- the web is made less slender, so that the increased depth in compression is still in Class 2.

If the vertical shear is high, it is to be expected that vertical stiffeners would improve the stability of the web: but their spacing would have to be less than its depth, because local buckles in regions of moment gradient are of short wavelength. A cheaper alternative would be to provide a longitudinal stiffener just below mid-depth of the web (Fig. 1). These have been shown in tests [6] to be most effective in delaying web buckling until after much plastic rotation has occurred. No design methods for such stiffeners, related to the classification of the web, are given in the draft Eurocodes because further research on them is needed.

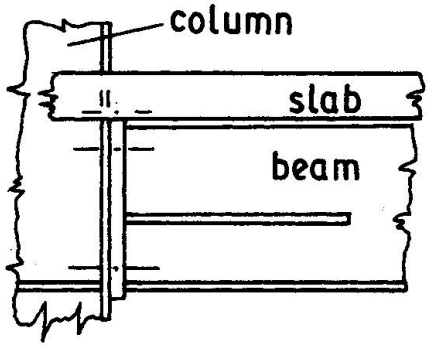

Fig. 1 Longitudinal stiffener

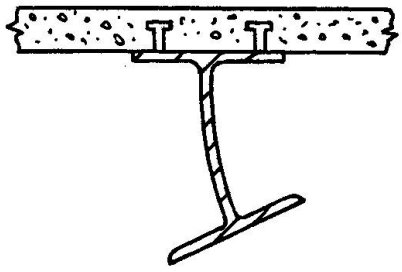

Fig. 2 Lateral buckling

3. LATERAL BUCKLING OF BOTTOM FLANGES NEAR INTERNAL SUPPORTS

3.1 Eurocode 4

This form of buckling involves lateral and torsional displacement of a bottom flange in a region of steep moment gradient. Most rolled sections used for composite beams are not susceptible, so a quick method is needed for identifying those which are. Design methods given for all-steel beams can be used, but are likely to be over-conservative, because most of them, including that of Eurocode 3, are based on theory in which the top (tension) flange of the steel member is assumed to be free to twist about a longitudinal axis and to deflect sideways, so that buckling can occur without distortion of the cross section. None of these assumptions is true for composite beams. The slab cannot deflect sideways and provides stiff resistance

to twisting, so that the buckling is *distortional* and involves bending of the web, which provides vertical, lateral, and torsional restraint to the bottom flange (Fig. 2). It is stated in Eurocode 4 which are the IPE and HE steel sections that can be assumed not to need permanent bracing against lateral buckling. These exemptions are based on the rules for continuous torsional restraint given in Eurocode 3, modified to allow for distortion of the section, and checked by a parametric study done during drafting of the Netherlands code of practice of 1983. They are conservative, in that the steel top flange is still assumed to be free to deflect laterally. They apply to members in Fe 510 or weaker steel, supported at both ends, and connected to a concrete slab not less than 100 mm thick.

When elastic analysis of the structure is used, all IPE and HE sections qualify (Table 4). The list in Eurocode 4 of sections that qualify when plastic hinge analysis is used is misleading, because lateral buckling rarely governs. The webs of many of the sections that qualify are found to be in Class 2, when account is taken of the reinforcement in the slab. For example, typical calculations show that even with lightly reinforced slabs, the level of the plastic neutral axis of the composite section in hogging bending is usually such that $0.6 < \alpha < 0.7$, where α is as in Table 1. If α is taken as 0.65, the slenderness limits for Class 1 webs become:

$$\left.\begin{aligned} d/w &> 46.1 \quad \text{when} \quad f_y = 235\ \text{N/mm}^2 \\ d/w &> 37.6 \quad \text{when} \quad f_y = 355\ \text{N/mm}^2. \end{aligned}\right\} \qquad (1)$$

These limits are shown in Fig. 3, together with the ranges of values of d and w for UB sections (horizontal lines), and for IPE-A and IPE sections (dashed lines).

Steel	Plastic hinge analysis (governed by local buckling)	Elastic analysis (governed by lateral buckling)
Fe 360	IPE, all IPE-A, $d \leq 300$ mm HEA, $d \leq 700$ mm UB, most with $d \leq 550$ mm	IPE, all IPE-A, all HEA, all UB, all
Fe 510	IPE, $d \leq 300$ mm IPE-A, none HEA, $d \leq 490$ mm UB, few, see Figure 3	IPE, all IPE-A in Class 2, $d \leq 300$ mm IPE-A in Class 3, all HEA, all UB, most with $d \leq 550$ mm

Table 4 Sections unlikely to require bracing against lateral buckling

3.2 Other steel sections that should not need lateral bracing

Exemptions for other types of steel section are now discussed. The writer studied this subject by means of parametric numerical analyses for elastic critical stresses for distortional lateral buckling of bottom flanges of fixed-ended composite T-beams [7]. It was found that for floor slabs of typical stiffness, the only significant parameter was the depth/thickness ratio (d/w) of the steel web.

It was assumed that the relationship between the critical stress and the true buckling stress was given by the Perry-Robertson equation that is used in the British Bridge Code (BS 5400) for other forms of lateral buckling. The equivalent lateral-torsional slenderness was found to be

$$\lambda = 3.08\ (d/w)^{0.7}\ . \qquad (2)$$

In the Bridge Code, this form of buckling is neglected when

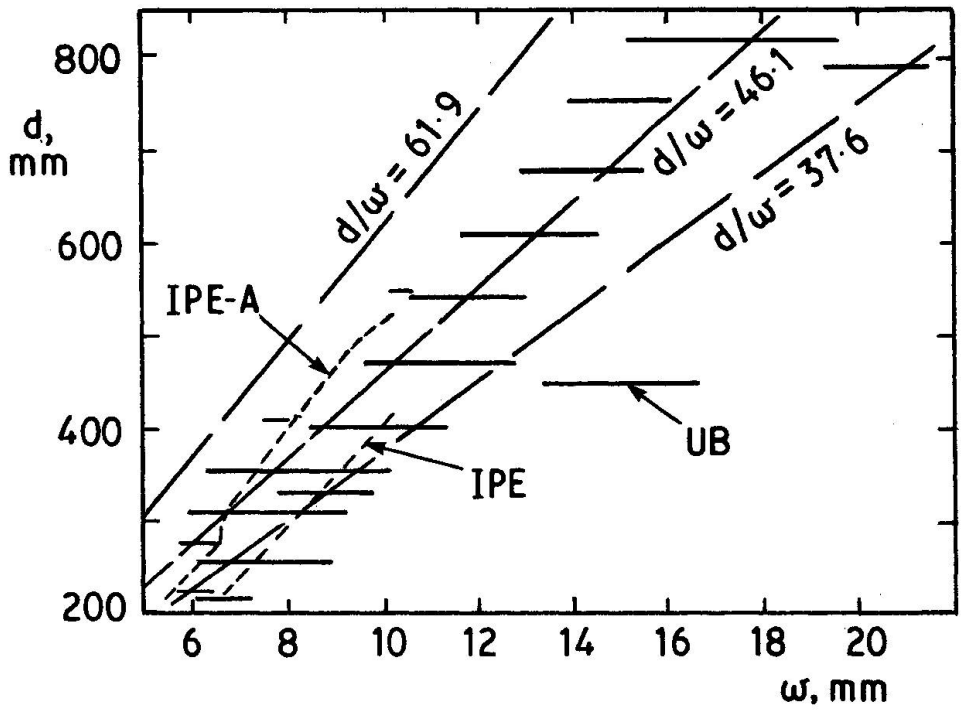

Fig. 3. Limiting slendernesses for web

$\lambda_{LT}(f_y/355)^{1/2} \leq 45$, with the yield strength f_y in N/mm² units. From equation (2) this gives

$$d/w \leq 46.1\,(355/f_y)^{0.714} \qquad (3)$$

which is:

$$\left.\begin{aligned} d/w &\leq 61.9 \quad \text{when} \quad f_y = 235\ \text{N/mm}^2 \\ d/w &\leq 46.1 \quad \text{when} \quad f_y = 355\ \text{N/mm}^2\ . \end{aligned}\right\} \qquad (4)$$

These results take account of the use of plastic analysis of sections at each internal support, but not of the use of plastic hinge theory, so they are relevant to sections in Class 2, and conservative for Class 3. The limits (4) are shown in Fig. 3. They confirm the recommendation in Eurocode 4 that all IPE and HE sections qualify, and give the results for IPE-A and UB sections shown in column 2 of Table 4.

4. PARTIAL SHEAR CONNECTION

The design methods of Eurocode 4 for partial shear connection in continuous composite beams [8] are developed from those given in the Model Code [1]. They are applicable to beams with all critical cross sections in Classes 1 or 2. They often enable only 50% of full shear connection to be used, which simplifies detailing when profiled steel sheeting is used.

The methods are explained with reference to stud shear connectors and a propped cantilever subjected to uniformly distributed load (Fig. 4). The relevant levels of load per unit length are:

w, the design ultimate load, for which the number N of uniformly-spaced studs is to be calculated;
w_f, the ultimate load calculated from plastic hinge analysis of the composite member, for which N_f uniformly-spaced studs would be needed; and
w_a, the ultimate load from plastic hinge analysis of the steel beam alone.

Connectors are classified as "ductile" or "stiff". Welded studs of the usual sizes are ductile, provided that the specified cylinder strength of the concrete does not exceed

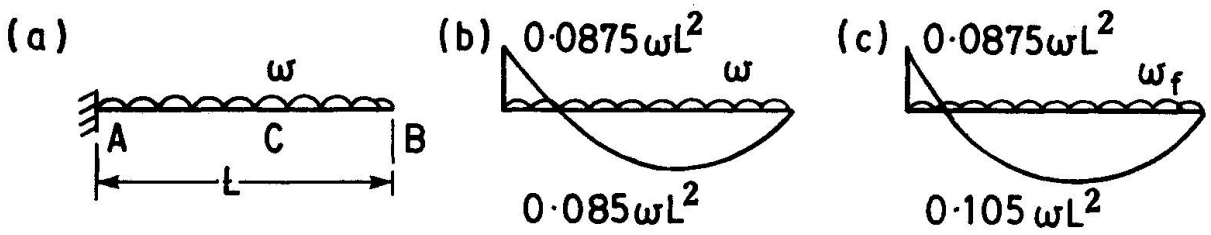

Fig. 4. Propped cantilever in Class 2

30 N/mm². This limit takes account of the reduced strain capacity of stronger concrete. Most bar-type connectors are stiff.

The principal design equations are:

- for ductile connectors, $N/N_f = (w - w_a)/(w_f - w_a)$, but ≥ 0.5, (5)
- for stiff connectors, $N/N_f = w/w_f$, but ≥ 0.5. (6)

As an example, it is assumed that the cross section at A (Fig. 4(a)) is in Class 2. Elastic analysis of a uniform member with 30% redistribution to midspan gives the design moments of Fig. 4(b). A member is designed with full-interaction bending resistance at A, M_a, equal to the required value $0.0875\ wL^2$; a sagging resistance at C, $M_c = 1.2\ M_a$; and resistance of the steel beam alone, $M_s = 0.9\ M_a$.

Plastic hinge analyses give $w_f = 1.163\ w$, Fig. 4(c), and $w_a = 0.918\ w$. Equation (5) then gives $N/N_f = 0.33$, so 50% shear connection is provided.

The savings in shear connection are due mainly to the fact that when the structure is analysed elastically, there is usually surplus flexural resistance at midspan, even when redistribution is used.

5. CLOSURE

Accounts have been given of the treatment in the draft Eurocode 4 of three aspects of the design of continuous composite beams for buildings, and of their expected implications in practice. These show why "the limiting slendernesses given for Class 2 are the most significant numbers in the code" [4]. The use and calibration of these methods in trial designs should enable them and their presentation to be further improved.

REFERENCES

1. Joint Committee IABSE-CEB-FIP-CECM, Model Code for composite structures, Construction Press, 1981.
2. Eurocode 4, Composite steel and concrete structures, 1st draft, Commission of the European Communities, October 1984.
3. Eurocode 3, Steel structures, 3rd draft, Commission of the European Communities, July 1983.
4. JOHNSON, R.P., Eurocode 4, Composite steel and concrete structures, Session B, IABSE Symposium, Steel in Buildings, Luxembourg, Sept. 1985.
5. International structural steelwork handbook, British Constructional Steelwork Association, March 1983.
6. CLIMENHAGA, J.J. and JOHNSON, R.P., Local buckling in continuous composite beams, Struct. Engr, 50, 367-74, Sept. 1972.
7. JOHNSON, R.P. and BRADFORD, M.A., Distortional lateral buckling of unstiffened composite bridge girders, Instability and Plastic Collapse of Steel Structures (ed. L.J. Morris), 569-580, Granada, 1983.
8. BUITENKAMP, H.S. and STARK, J., Collapse model for continuous composite beams, Bouwen mit Staal, 36, 28-33, July 1976.

Traglastbemessung für durchlaufende Verbundträger im Hochbau

Limit State Design for Continuous Composite Beams

Méthodes de dimensionnement des poutres mixtes continues

Helmut BODE
Professor Dr.-Ing.
Universität Kaiserslautern
Kaiserslautern, BR Deutschland

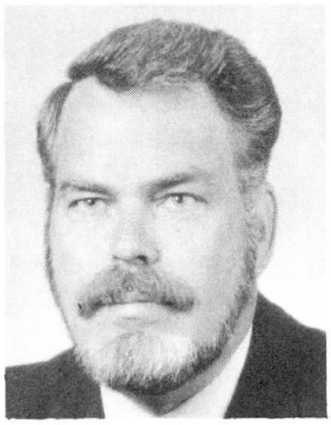

Dr. H. Bode, geboren 1940 in Dresden, studierte an der TH Hannover, war danach einige Jahre in der Praxis tätig und promovierte 1974 an der Ruhr-Universität Bochum. Seit 1980 ist Dr. Bode Professor für Stahlbau an der Universität Kaiserslautern. Einen besonderen Forschungsschwerpunkt unter seiner Leitung stellen Stahlverbundkonstruktionen dar.

Wolfgang FICHTER
Dipl.-Ing.
Universität Kaiserslautern
Kaiserslautern, BR Deutschland

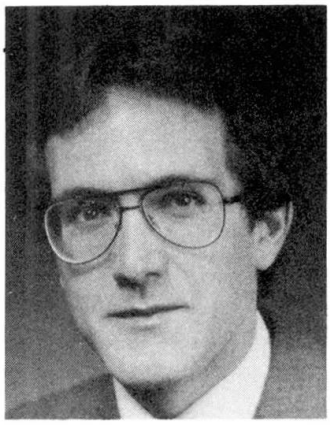

W. Fichter, geboren 1954, studierte an der Universität Stuttgart. Nach einjähriger Tätigkeit in einem Ingenieurbüro wurde er wissenschaftlicher Mitarbeiter an der Universität Kaiserslautern. Seine wissenschaftlichen Arbeiten betreffen Verbundkonstruktionen, insbesondere durchlaufende Verbundträger für den Hoch- und Industriebau.

ZUSAMMENFASSUNG

Der Beitrag betrifft die Bemessung von durchlaufenden Verbundträgern unter ruhender Belastung. Auf der Basis von Verbundträgerversuchen und genauen Berechnungen werden Ergebnisse zur Traglastberechnung, zum Versagensverhalten sowie zum Gebrauchszustand mitgeteilt. Auf den Eurocode 4 und andere Bemessungshilfen wird Bezug genommen.

SUMMARY

This paper deals with the design of continuous composite girders for buildings under static loading conditions. Based on experimental research and accurate calculations results are presented concerning load carrying capacity, failure mechanism and behaviour under service loadings. The Eurocode 4 and other design aids are taken into regard.

RÉSUMÉ

Cet article traite du dimensionnement des poutres mixtes continues sous charges statiques. Des modèles de calcul simples de l'état ultime de ruine et de l'état limite d'utilisation sont comparés à des résultats d'essais et à des modèles «exacts». Ces méthodes simplifiées sont tirées de l'Eurocode 4 et d'autres règlements.

1. EINLEITUNG

Dieser Beitrag betrifft durchlaufende Verbundträger für den Stahlhoch- und Industriebau unter vorwiegend ruhender Belastung. Die Stahlträgerquerschnitte sollen kompakt sein, so daß ein vorzeitiges örtliches Beulen im Steg oder im Untergurt ausgeschlossen ist.

Die uns bekannten Vorschriften und Empfehlungen, z. B. [1] bis [3], lassen bei der Tragfähigkeitsberechnung grundsätzlich zwei Methoden zu, und zwar

- die elastische Schnittgrößenermittlung (im Zustand I oder II) mit plastischer Querschnittsbemessung, und
- die Fließgelenktheorie (plastic design) als vereinfachtes Traglastverfahren mit voller Momentenumlagerung.

Die Fließgelenktheorie wird dadurch einfach, daß man dem Anwender den Gültigkeitsbereich genau vorschreibt (der Hinweis auf "geeignete Träger" [7], [8] genügt nicht). Zusätzlich sind bestimmte Nachweise im Gebrauchszustand erforderlich (z. B. die Rißbreitenbeschränkung).

Werden die Schnittgrößen mit Hilfe der Elastizitätstheorie berechnet, läßt sich die Tragfähigkeit des Verbundträgers in der Regel nicht ausnutzen. Auch können wirtschaftliche Bauweisen, die von der Umlagerung der Momente von der Stütze ins Feld "leben", benachteiligt werden. Aber mit Hilfe der allgemein zur Verfügung stehenden Computer-Programme sind die Nachweise unproblematisch. Sehr weitgehend aufbereitete Bemessungshilfen enthält übrigens [4].

Zu beiden Nachweisarten enthält der folgende Beitrag einige kurze Anmerkungen auf der Basis von Versuchsergebnissen und genauen Vergleichsberechnungen.

2. ZUR FLIESSGELENKTHEORIE

2.1 Plastische Rotation im Feld

Für einen einfachen Zweifeldträger, der im kleineren Feld mit einer konzentrierten Einzellast belastet ist, sind in Bild 1 die Ergebnisse der genauen Traglastberechnung und nach der Fließgelenktheorie dargestellt. Wie man an diesem einfa-

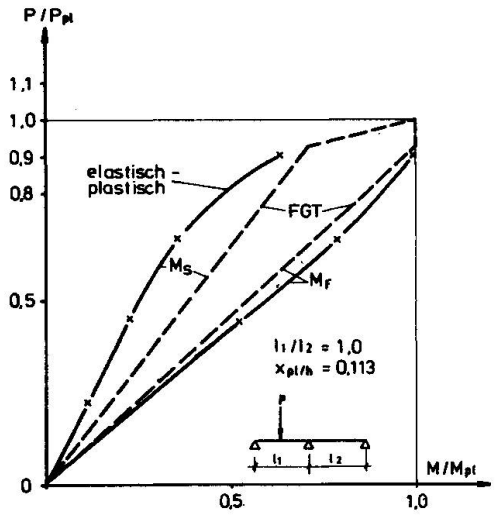

Bild 1: Biegemomente am Zweifeldträger mit Einzellast (Beispiel)

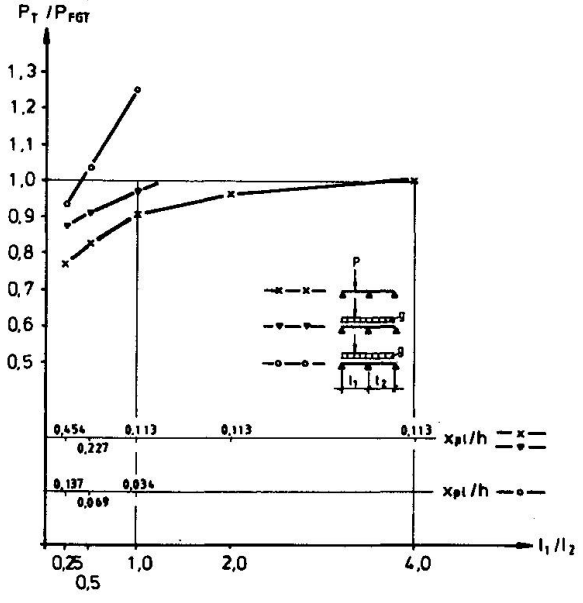

Bild 2: Traglasten für unterschiedliche Werte ℓ_1/ℓ_2 und x_{pl}/h

chen Beispiel leicht erkennt, wird im Feld zwar die Biegetragfähigkeit $M_{pl,F}$ erreicht, aber der Feldbereich ist nicht ausreichend verformbar, um die Resttragfähigkeit an der Stütze ausnutzen zu können: hier liefert die Fließgelenktheorie eine zu optimistische Traglast P_{pl}.

Einen wesentlichen Parameter zur Beurteilung der Rotationskapazität eines Verbundträgers im Bereich positiver Momente stellt die Nullinienlage x_{pl} im Vergleich zur Gesamthöhe h dar: liegt die Nullinie hoch genug, ist der Querschnitt duktil. Auf Ansourian [5], [6] geht die Forderung zurück, der Baustahl an der Trägerunterseite soll den Verfestigungsbereich erreichen, bevor der Beton an der Oberkante auf Druck versagt. Mit den Grenzdehnungen -3,5 ‰ und +20 ‰ ergibt sich der Wert x = 0,15 h. Diese Nullinienlage wird in etwa auch von Ansourian genannt und im Eurocode IV [2] zur Berücksichtigung konzentrierter Einzellasten gefordert.

Ansourian stellt allerdings auch fest, daß die Nullinie zur Erzielung der erforderlichen Rotation für die ungünstigste Kombination von Spannweiten und Lasten etwas höher liegen sollte. Er definiert dazu einen "ductility parameter" χ, der das Verhältnis der mindestens erforderlichen Nullinienlage zur wirklich vorhandenen wiedergibt, und fordert $\chi \geq 1{,}3 \div 1{,}4$. Wir kommen durch folgende einfache Überlegung zu einem ähnlichen Ergebnis:

$$x \leq 0{,}15\ h \qquad (1)$$

$$x_{pl} \approx 0{,}8\ x \qquad (2)$$

$$x_{pl} \leq 0{,}12\ h \qquad (3)$$

Einige typische Verhältnisse haben wir im Bild 2 dargestellt. Sie gelten für das Stahlprofil IPE 400 aus St 37/52 und einen Beton mit β_w = 25/55. Die mitwirkende Betongurtbreite beträgt $0{,}8 \cdot \ell_1 \cdot 1/3$ im Feld und $0{,}6 \cdot b_{mF}$ an der Stütze. Daher kommt es, daß der an sich konstante Querschnitt mit dem Stützweitenverhältnis ℓ_1/ℓ_2 veränderlich ist, so daß sich auch die Lage der Nullinie ändert. Berücksichtigt man nur Querschnitte, die Bedingung (3) erfüllen, und stellt man zusätzlich zur Einzellast auch das Eigengewicht in Rechnung, so sind die mit der Fließgelenktheorie berechneten Traglasten P_{FGT} ausreichend sicher: gegenüber [1] bis [3] läßt sich der Anwendungsbereich der Fließgelenktheorie damit erweitern.

2.2 Plastische Rotation an der Stütze

Ein einfaches Beispiel für einen Zweifeld-Verbundträger, bei dem das erste Fließgelenk an der Innenstütze auftritt, enthält Bild 3. Wenn die Verformbarkeit des Stützquerschnitts weder durch örtliche Instabilität noch durch eine Dehnung der oberen Bewehrung begrenzt ist, ist eine vollständige Momentenumlagerung ins Feld möglich: die Fließgelenktheorie liefert sichere Ergebnisse. Die Traglast im Versuch sowie nach der genauen Berechnung liefert sogar etwa 10 % höhere Werte, da die Stahlträgerdehnungen den Verfestigungsbereich erreichen (was im Versuch auftritt und in der genauen elastisch-plastischen Berechnung daher berücksichtigt wird).

Traglasten für Gleichlast, aber für unterschiedliche Feldweiten und damit unterschiedliche Nullinienlagen $x_{pl/h}$ enthält Bild 4. Die obere Kurve (gerechnet für 8 % Dehnungsbegrenzung, d. h. praktisch ohne) läßt erkennen, daß die Fließgelenktheorie in allen Fällen sichere Ergebnisse liefert. Da über der Stütze eine geringe obere Bewehrung vorhanden ist und mitgerechnet wird, wird die plastische Rotation an der Stütze alternativ auf die Dehnung von 10 ‰ in der Bewehrungsfaser begrenzt. Die so berechnete zweite Kurve im Bild 4 liegt viel niedriger (bei etwa 90 %) und läßt erkennen, daß die Dehnungsbegrenzung keine volle Momentenumlagerung in das Feld zuläßt. Ein höherer Bewehrungsgrad würde diese Traglasten q_T zwar anheben, die volle Umlagerung wäre aber ebenso wenig möglich.

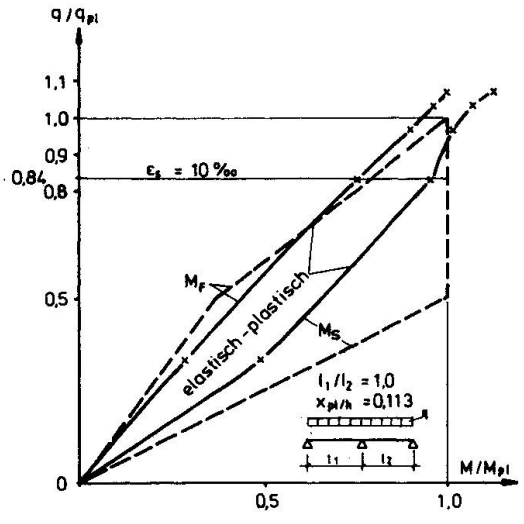

Bild 3: Biegemomente am Zweifeldträger mit Gleichlast (Beispiel)

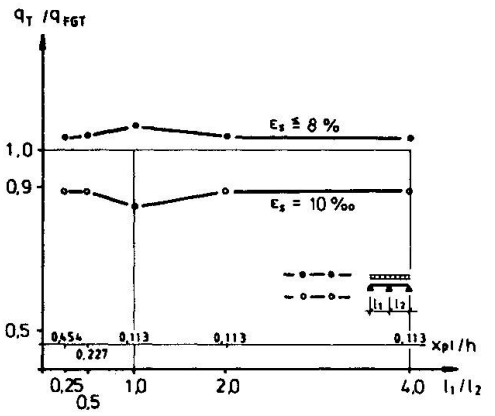

Bild 4: Traglasten für unterschiedliche Werte ℓ_1/ℓ_2 und x_{pl}/h

Bei unseren Versuchen haben wir häufig das Reißen der Bewehrungsstäbe erlebt, und zwar insbesondere bei niedrigen Bewehrungsgraden und bei Verwendung von Betonstahlmatten (mit geringer Bruchdehnung). Mit abnehmender Tragfähigkeit fiel dann auch die Prüflast plötzlich ab, aber der Querschnitt konnte weiter verformt werden. Daraus läßt sich ableiten, daß die Bewehrung bei Systemen, die nach der Fließgelenktheorie bemessen werden und die eine plastische Rotation des Stützquerschnitts erfordern, nicht in Rechnung gestellt werden darf (siehe Bild 5 links). Das gilt nicht für den Fall, daß sich das Fließgelenk über der Innenstütze als letztes bildet (siehe Bild 5 rechts).

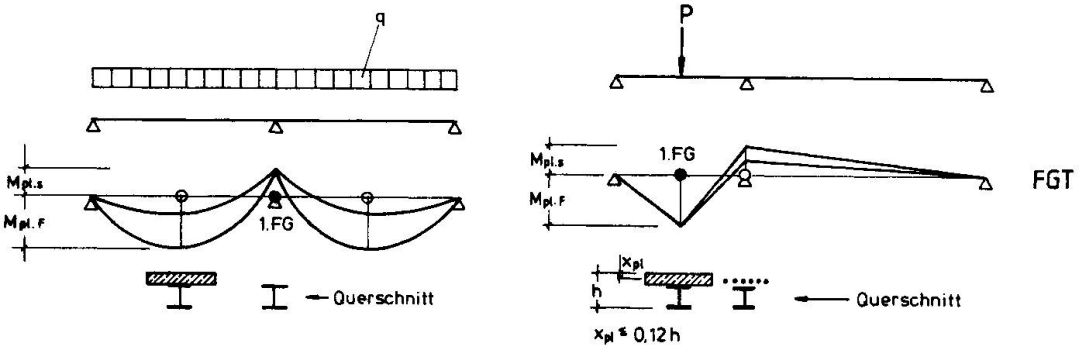

Bild 5: Anforderungen an die Querschnitte bei der Fließgelenktheorie

2.3 Durchbrüche in der Betondecke

Gerade im Industriebau wird es häufig erforderlich, in den Decken, die als Verbundträger-Obergurte mitwirken, größere Öffnungen oder Durchbrüche vorzusehen. Diese schränken die Betongurtbreite örtlich ein, was im Hinblick auf die Fließgelenktheorie insbesondere dann von Nachteil ist, wenn sich das erste Fließgelenk im Feld im Bereich der Öffnung bildet. In diesem Bereich kann dann die plastische Rotation begrenzt sein. Die Nachbarbereiche sind außerdem relativ niedrig beansprucht, so daß die Verformungen insgesamt klein sind (was eine noch größere plastische Rotation erfordert).

Bild 6 zeigt den Einfluß einer Deckenöffnung im Feld 1 auf die Traglast eines Zweifeldträgers. Die Einhaltung der Bedingung nach Gl. (3) ergibt aber nur beim Träger mit Gleichlast sichere Ergebnisse nach der Fließgelenktheorie. Bei Einzellast in einem Feld fällt die tatsächliche Traglast gegenüber der Last nach der Fließgelenktheorie mit abnehmenden ℓ_1/ℓ_2 bis auf ca. 80 % ab. Die Fließgelenktheorie liefert dann Ergebnisse auf der unsicheren Seite.

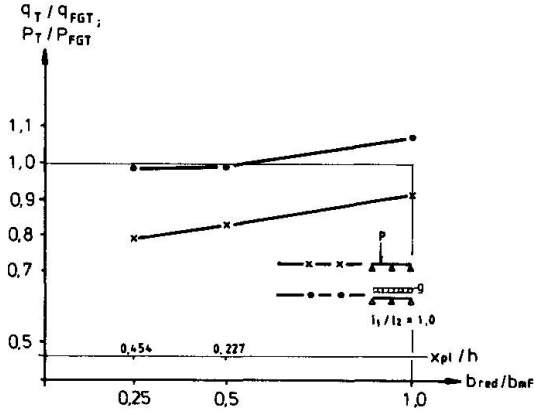

Bild 6: Einfluß von Durchbrücken (Deckenöffnungen)

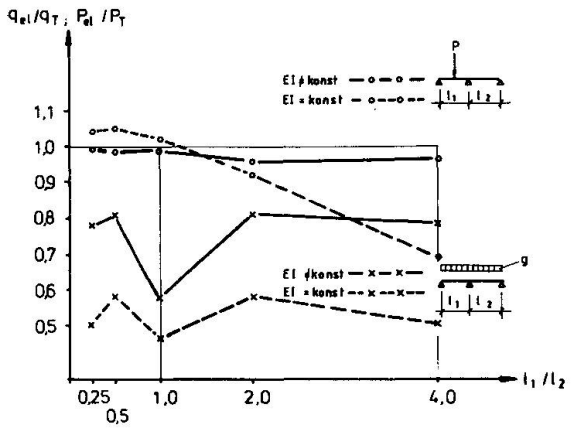

Bild 7: Über elastische Schnittgrößen berechnete Traglasten

3. ZUR ELASTISCHEN SCHNITTGRÖSSENERMITTLUNG

Wir gehen davon aus, daß der entwerfende Ingenieur eine Schnittgrößenberechnung auf der Grundlage der Elastizitätstheorie mit Hilfe vorhandener Computerprogramme durchführt (vergl. aber auch [4]). Es ist dann kein Problem, mit unterschiedlichen Steifigkeiten zu rechnen, die sich daraus ergeben, daß die mitwirkenden Breiten im Feld und an der Stütze ungleich sind, und daß der Betongurt im negativen Momentenbereich gerissen ist. Im Zugbereich wirkt der Beton nur noch zum Teil, einfacher gar nicht mit, und gerade diese Rißbildung im Zustand II liefert die in der Regel gewünschten, reduzierten Stützmomente. Denn anders als im Betonbau tritt diese Steifigkeitseinbuße nur im Bereich der negativen Momente ein.

Bild 7 enthält einige Ergebnisse sowohl für Gleichstreckenlast als auch für Einzellast in einem Feld. Bei Gleichstreckenlast wird die Tragfähigkeit begrenzt durch das aufnehmbare Stützmoment. Ohne Umlagerung liefert die Berechnung mit ungerissenem Beton (EJ = konst.) 50 ÷ 60 %, mit gerissenem Beton (EJ ≠ konst.) im Zustand II 60 ÷ 80 % der genau berechneten Traglast. In diesem Rahmen liegen die möglichen willkürlichen Umlagerungen, auch die des Eurocodes IV mit 20 %. Doch muß man auch hier stärker zwischen Gleichlasten und konzentrierten Einzellasten unterscheiden, wie Bild 7 deutlich zeigt. Denn die genauen Traglasten werden bei konzentrierten Einzellasten erreicht und überschritten, so daß man in aller Regel keine willkürlichen Umlagerungen zulassen darf.

Ein großer Vorteil der elastischen Schnittgrößenermittlung liegt natürlich darin, daß man verschiedene Lastfälle superponieren kann (etwas eingeschränkt im Zustand II), und daß die Tragfähigkeit und Gebrauchszustände am selben System untersucht werden können.

4. STAHLTRÄGER MIT BETONUMMANTELUNG

In den letzten Jahren sind in Deutschland aus Brandschutzgründen häufiger Verbundträger eingesetzt worden, bei denen das Stahlprofil entweder nur zwischen

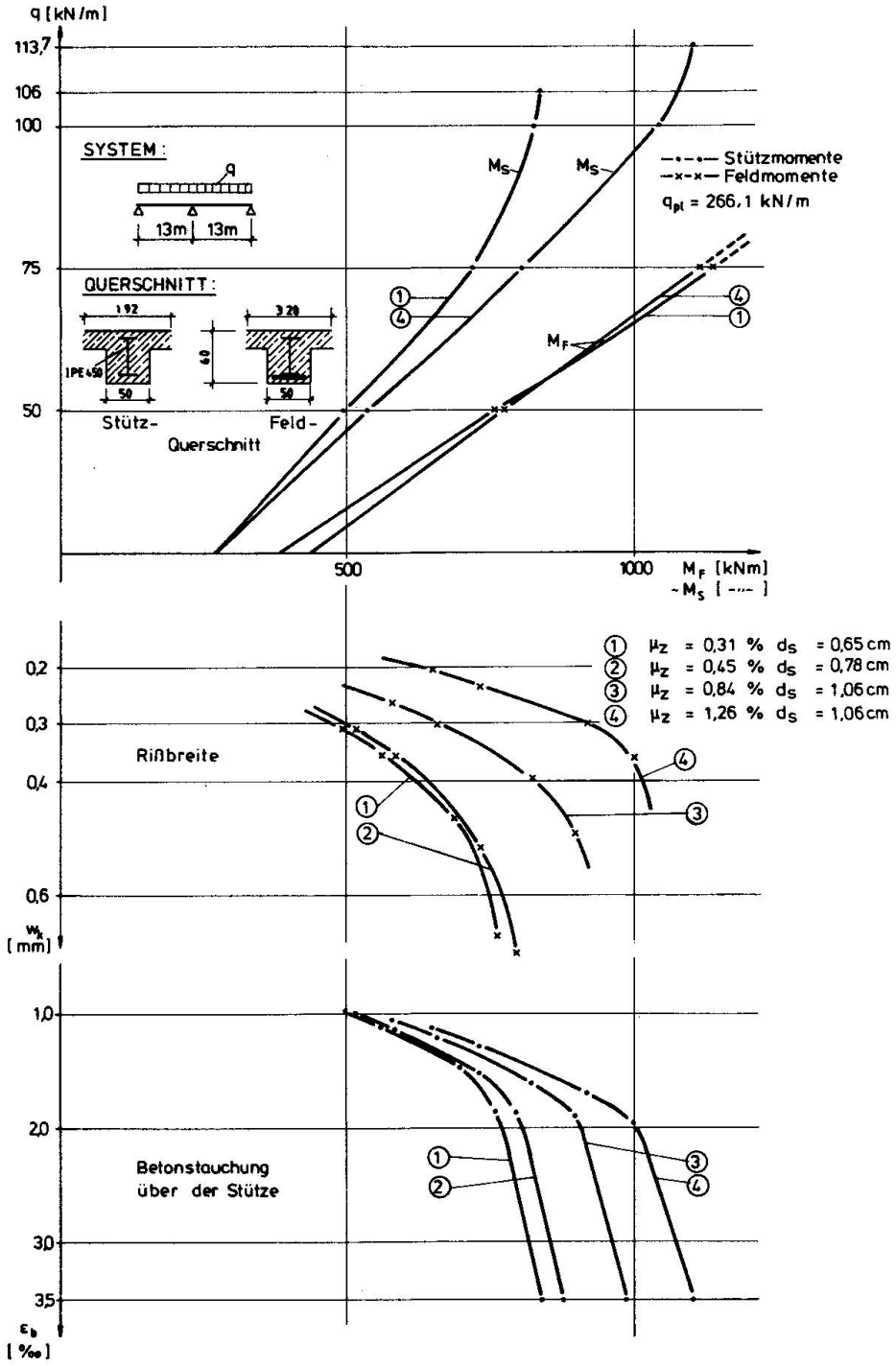

Bild 8: Bemessungdiagramm für einbetonierten Träger

den Trägerflanschen (in den Kammern) ausbetoniert oder ganz einbetoniert war. Wir haben auch mit solchen Trägern eine Reihe von Versuchen durchgeführt [11].

Auf diese Träger läßt sich die Fließgelenktheorie genauso anwenden, allerdings mit Zusatznachweisen im Gebrauchszustand (vergl. Bild 8). Insbesondere die vollständig einbetonierten Träger können höher belastet werden als die nicht einbetonierten, "nackten" Verbundträger, da die Vertikalkraft vom Stahlbetonmantel aufgenommen werden kann, so daß die Biegetragfähigkeit M_{pl} nicht auf $M_{pl,Q}$ abzumindern ist. Außerdem ist örtliches Beulen verhindert, und Kippaussteifungen sind nicht erforderlich.

Die Traglast der Versuche läßt sich mit voller Momentenumlagerung nach der Fließgelenktheorie sehr genau berechnen. Das gilt auch für ungünstige Systeme wie das in Bild 8 dargestellte und berechnete, bei dem der Feldquerschnitt nicht nur wie üblich tragfähiger ist als der Querschnitt über der Stütze, sondern durch eine weitere Untergurtlamelle verstärkt ist. Das erfordert eine besonders große plastische Rotation im negativen Momentenbereich, so daß die dort vorhandene Bewehrung nicht berücksichtigt wird (vergl. Bild 5 links). Auch der Betonmantel, der zwar bewehrt, aber nicht mit dem Stahlträger verdübelt ist, wird im Traglastzustand nicht berücksichtigt, so daß der Querschnitt über der Innenstütze allein aus dem Stahlträger besteht, der gegen Instabilwerden ausreichend ausgesteift ist.

Die Schnittgrößen weichen im Gebrauchszustand jedoch so stark von der Veteilung nach der Fließgelenktheorie ab, daß weitere Nachweise im Gebrauch erforderlich sind, und zwar der Nachweis der Betonstauchung an der Trägerunterkante über der Innenstütze sowie die Rißbreitenbeschränkung (siehe Bild 8). Wir fordern in Deutschland das Einhalten der kritischen Rißbreite von 0,4 mm unter dem dauernd wirkenden Lastanteil (in der Regel 70 % der Gebrauchslast), wenn nicht zusätzliche Anforderungen gestellt werden. Was die Betonstauchung betrifft, schlagen wir vor, die kritische Stauchung von 3 ‰ nicht zu überschreiten. Der Mantelbeton wird zwar nicht für die Tragsicherheit gebraucht, aber er soll die Dauerhaftigkeit und Funktionstüchtigkeit im Gebrauch sicherstellen. Im Gebrauch ist infolge der hohen Druckstauchungen bis 3 ‰ zwar mit Rißbildung zu rechnen, aber unsere Versuche sowie weitere in Bochum unter der Leitung von Roik [9] haben gezeigt, daß diese Stauchung ohne Abplatzungen ertragen wird. Hierzu und zur besseren Einleitung der konzentrierten Auflagerkraft sollte die Bügelbewehrung im Fließgelenk über der Innenstütze verstärkt werden; dadurch wird die Beton duktiler. Das Bemessungsdiagramm in Bild 8 ist gut geeignet, den Gebrauchszustand in dieser Hinsicht zu überprüfen und die zulässige Last gegebenenfalls abzumindern.

5. SCHLUSSBETRACHTUNGEN

Wir sind auf das örtliche Beulen des Stahlträgers und auf das seitliche Ausweichen des Druckgurtes nicht eingegangen, zum einen aus Platz- und Zeitgründen, zum anderen deshalb, weil die Untersuchungen in Kaiserslautern zu diesen Themen noch nicht abgeschlossen sind. Hier haben vor allem Johnson und seine Mitarbeiter wertvolle Beiträge geleistet. Leider fehlen aber gerade im Eurocode IV [2] Hinweise darauf, welche Rotationskapazität bei Verbundträgern tatsächlich angenommen werden kann. Für alle genauen elasto-plastischen Berechnungen wären Krümmungsgrenzwerte κ/κ_{pl} wünschenswert; die b/t-Verhältnisse sind da nicht aussagefähig genug.

Was die Fließgelenktheorie betrifft, so zeigt sich, daß der Anwendungsbereich in der Tat erweitert werden kann. Das liegt zum einen an der zusätzlichen Anforderung an den Feldquerschnitt gemäß Gl. (3) und Bild 5 (rechts), zum anderen aber auch daran, daß in den genauen Berechnungen die Verfestigung des Baustahls rechnerisch berücksichtigt wird (sie tritt in den Versuchen ebenfalls auf), und zwar realistischer, als es im Eurocode III vorgesehen ist.

Auch das in der Schweiz unter der Leitung von Badoux neu bearbeitete, vorzügliche Buch [4] enthält für die Fließgelenktheorie noch einen Gültigkeitsbereich, der die Anwendung auf Gleichstreckenlasten (oder ähnliche) beschränkt.

Wir haben die Fließgelenktheorie auch auf einbetonierte Verbundträger angewendet, die weder im Eurocode IV [2] noch in den deutschen Verbundträger-Richtlinien [1] enthalten sind, aber häufig eingesetzt werden. Hier sind die beschriebenen Zusatznachweise und konstruktiven Maßnahmen für den Gebrauchszustand erforderlich.

LITERATURVERZEICHNIS

1. Richtlinien für die Bemessung und Ausführung von Stahlverbundträgern. Ausgabe März 1981. Ergänzende Bestimmungen zu den Richtlinien. Fassung März 1984.
2. Eurocode IV (Entwurf). Oktober 1984.
3. SIA-Norm 161: Stahlbauten. Schweizer Ingenieur- und Architektenverein (SIA), Zürich, 1979.
4. BUCHELI, P., CRISINEL, M., Verbundträger im Hochbau. Schweizerische Zentralstelle für Stahlbau (SZS), Zürich, 1982.
5. ANSOURIAN, P., Beitrag zur plastischen Bemessung von Verbundträgern. Bauingenieur (59) 1984, S. 267-272.
6. ANSOURIAN, P., On the Design of Continuous Composite Beams. Vortrag auf "Joint US-Japan Seminar on Composite Construction", Seattle, July 1984.
7. BODE, H., Verbundträger im Hochbau. Merkblatt 267, Beratungsstelle für Stahlverwendung, Düsseldorf, 1980.
8. ROIK, K., Verbundkonstruktionen. Stahlbau-Handbuch Band 1, Kapitel 11, Stahlbau-Verlags-GmbH, Köln, 1982.
9. ROIK, K., BREIT, M., Untersuchung der Verbundwirkung zwischen Stahlprofil und Beton bei Stützenkonstruktionen. Studiengesellschaft für Anwendungstechnik von Eisen und Stahl e. V., Projekt 51, Düsseldorf, 1984.
10. JOHNSON, R. P., Composite Structures of Steel and Concrete, Vol. 1, Crosby Lockwood Staples, London, 1975.
11. BODE, H., FICHTER, W., Untersuchung einbetonierter Stahl-Verbundträger für den Hochbau. Versuchsbericht, Universität Kaiserslautern, 1984 (unveröffentlicht).

Abschließend möchten die Autoren der Studiengesellschaft für Anwendungstechnik von Eisen und Stahl sowie der AIF (Arbeitsgemeinschaft industrieller Forschungsvereinigungen) einen herzlichen Dank sagen; ihre Unterstützung und Förderung hat diese Forschungsarbeiten erst ermöglicht.

Design Practice, Standards and Research Trends for SRC Buildings in Japan

Tendance japonaise en matière de conception, normes et recherches pour les bâtiments à ossature mixte

Entwurfstechnik, Normen und Forschungsentwicklungen für Stahl-Betonverbundkonstruktionen in Japan

Minoru WAKABAYASHI
Professor
DPRI, Kyoto University
Kyoto, Japan

Minoru Wakabayashi, born 1921 received Bachelor's degree 1946, Doctor's degree 1957 from the University of Tokyo, has been working on earthquake resistant design of steel, reinforced concrete and composite structures.

SUMMARY

This paper first reviews recent trends in the design and construction of steel reinforced concrete (SRC) buildings in Japan, taking into account relevant aspects such as physical, constructional and economic characteristics, as well as the experience of designers. Design specifications and research developments in Japan are then briefly discussed.

RÉSUMÉ

L'article présente la tendance japonaise en matière de conception et de construction des bâtiments à ossature mixte, prenant en considération des aspects importants tels que les caractéristiques physiques, mécaniques et économiques; l'expérience des ingénieurs est aussi prise en compte. La tendance des Normes et des recherches est brièvement esquissée.

ZUSAMMENFASSUNG

In diesem Artikel wird die Entwicklung von Entwurf und Ausführung von Verbundkonstruktionen in Japan aufgezeigt, wobei bedeutende Gesichtspunkte wie physikalische, bauliche und wirtschaftliche Eigenschaften sowie Erfahrungen von Konstrukteuren berücksichtigt werden. Ferner werden Konstruktionsrichtlinien und Forschungsentwicklungen in Japan kurz diskutiert.

1. INTRODUCTION

A structural system consisting of concrete encased columns and beams, which is called steel reinforced concrete (SRC), has been used in Japan, mainly for tall-building construction, since the Kanto Earthquake in 1923 (1). It is nowadays widely applied for mid-rise and high-rise buildings.

The paper discusses the charactiristics of the SRC system and the reasons for its wide use in Japan, and briefly reviews design standards and recent research trends.

2. RECENT CONSTRUCTION OF SRC BUILDINGS

2.1 Amount of SRC Building Construction

The total gross floor area of building structures constructed in Japan in the last 5 years is about 160 million m^2, the proportions for individual structural systems being as follows : SRC = 8% ; reinforced concrete (RC) = 21% ; steel (S) = 24% ; and timber = 46%. With regard to the total number of buildings, the share of the SRC system is only 0.4%. It should be pointed out, in this respect, that the gross floor area for an SRC building is usually quite large. Thus, the SRC system is often adopted in tall-building construction so that SRC buildings comprise about 50% of the buildings taller than 6 stories, as shown in Fig. 1. Investigation of the use of SRC buildings shows that offices account for 30%, and apartment houses for 60%, with the latter figure tending recently to increase.

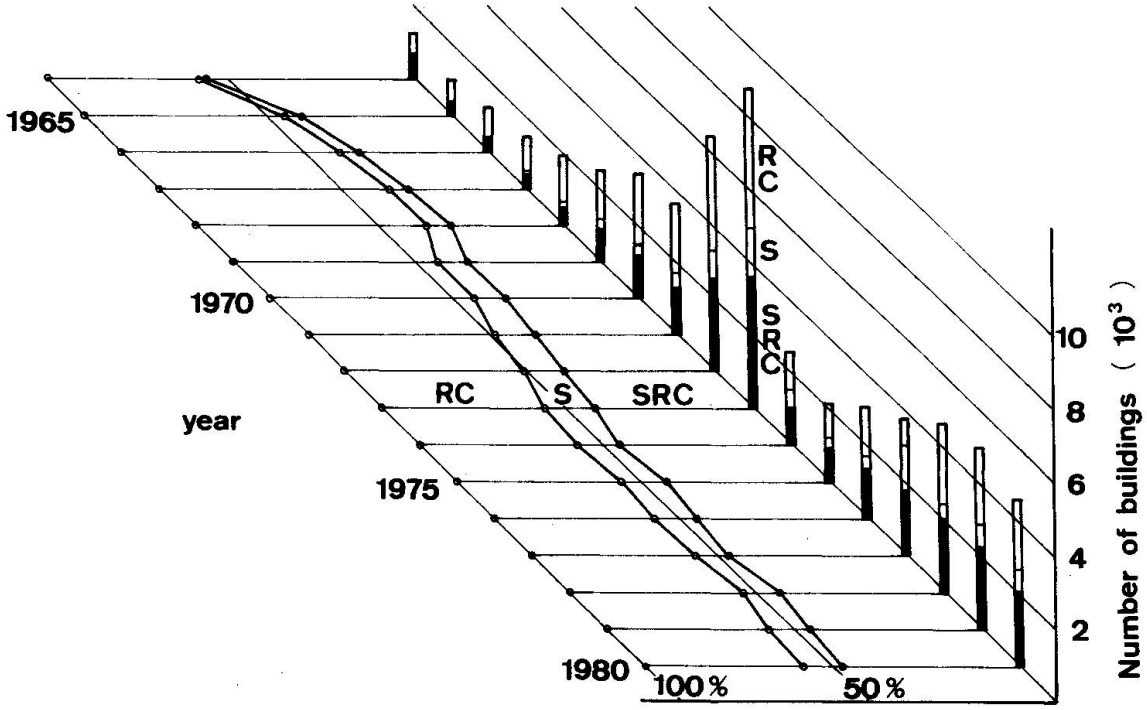

Fig. 1 Variations in the number of buildings taller than six stories with various types of construction systems every year.

2.2 Characteristics of SRC System

2.2.1 General Characteristics

The SRC structural system has several merits which are counted as reasons why the SRC system is selected.

Advantages of the SRC system over a reinforced concrete structural system are as follows:

1. Large ductility.
2. Large amounts of steel can be arranged in a limited area of cross section.
3. A steel skeleton can be used as a support of construction work.

Advantages over a steel structural system are as follows:

1. Great resistance to fire.
2. Concrete working as fireproof material can carry the load.
3. High rigidity.
4. Strong against buckling.
5. High dampening.

Therefore, as SRC system is effectively applied in the following situations:

1. When the reinforced concrete system is not adequate from the viewpoint of earthquake resisting ability, since the building is tall and the stresses in the lower story are large.
2. When the relative story deflection becomes excessively large if the steel system is applied, because of small rigidity.
3. When the span is too large and thus the floor area carried by a column is too large for the reinforced concrete system.
4. When the reinforced concrete system may not provide sufficient strength, and the steel system may suffer from vibration because of a large span.
5. When the reinforced concrete system is not adequate because a brittle type of shear failure may occur due to a mixed existence of short columns, although the building is low.
6. When torsional deformation and/or concentration of deformation is expected because the shape of the building and/or distribution of rigidity is not well balanced in the plan and/or along the height of the building.
7. When a smooth transfer of stresses is desired in the middle portion of a building of which the upper portion is constructed by the steel system and lower portion around the foundation is constructed by the reinforced concrete system.

2.2.2 Designers' Views of the SRC System

Designers' views on individual structural systems are one of the important factors, when a specific system is selected in the course of the design. Table 1 shows the results of an investigation of designers views on the performance of individual structural systems (2). Designers consider the SRC system as follows : the earthquake resisting capacity and the construction efficiency of the SRC system are between those of the reinforced concrete and the steel systems, living comfort is excellent, but structural details are more complicated than for the other two systems. As indicated in Table 1, the reinforced concrete and the SRC systems are often used for buildings such as houses and hospitals which reguire high dwelling performance, while the steel system is suited to buildings such as factories in which the work enviroment is more important than the dwelling performance.

2.2.3 Mechanical Characteristics

One of the most important mechanical features of the SRC system is its high ductility. Shear failure, often seen in reinforced concrete members and connections, does not often occur in the SRC system, and even if it occurs, the failure is not very brittle.

Figure 2 shows hysteresis loops of SRC and RC specimens subjected to cyclic shear with a constant axial thrust equal to 0 or 30% of the ultimate axial strength. It is observed that the SRC member shows larger ductility and more stable, spindle-shaped hysteresis loops than the RC member. These characteristics are also observed in the behavior of an SRC beam-to-column connection

		RC	SRC	S
earthquake resisting capacity	strength/weight ratio	C	B	A
	ductility	C	B	A
dwelling performance disaster prevention	rigidity	A	A	C
	sound insulation	A	A	C
	fire resistance	A	A	C
construction	term of works	C	B	A
design	details	simple	complex	fairly complex

A : excellent B : good C : passable

Table 1 Performance of structural systems in view of structural planning

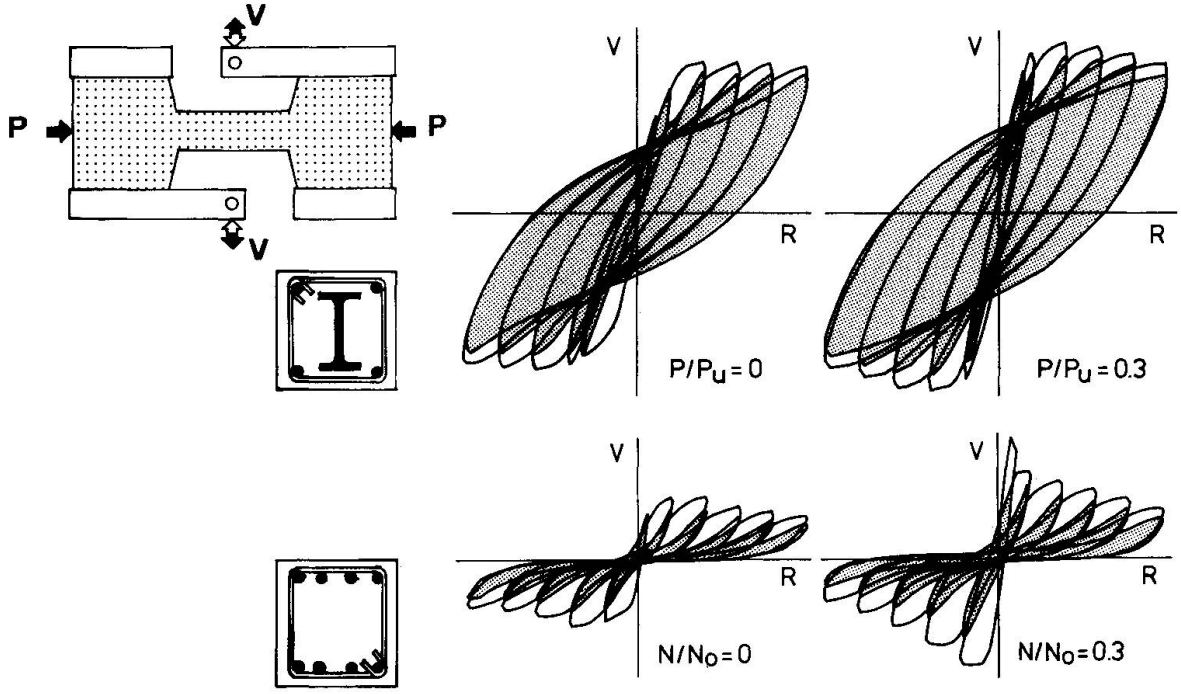

Fig. 2 Shear force-deformation relationships for columns under constant axial force and repeated shear and bending

failing in shear, shown in Fig. 3, where large ductility and energy dissipation capacity are obtained, even though the connection panel fails in shear.

If the axial thrust becomes large, reduced ductility is also observed in the behavior of an SRC beam-column failing in flexure; however, the reduction is not so severe as in the case of an RC beam-columns. This is mainly because the local buckling of plate elements of the concrete encased steel is rarer than the buckling of the longitudinal reinforcing bars. Once concrete crushing occurs, an RC member loses its integrity, while the steel itself behaves as an integral body, and thus the failure advances rather moderately in the case of an SRC member.

2.2.4 Construction Characteristics

Tabel 2 shows the evaluation of construction efficiency of general office buildings with various heights and structural systems. Overall evaluation reveals that the steel system is most efficient in general since form work is not used, and also that the SRC system becomes more efficient than the RC system as the height increases.

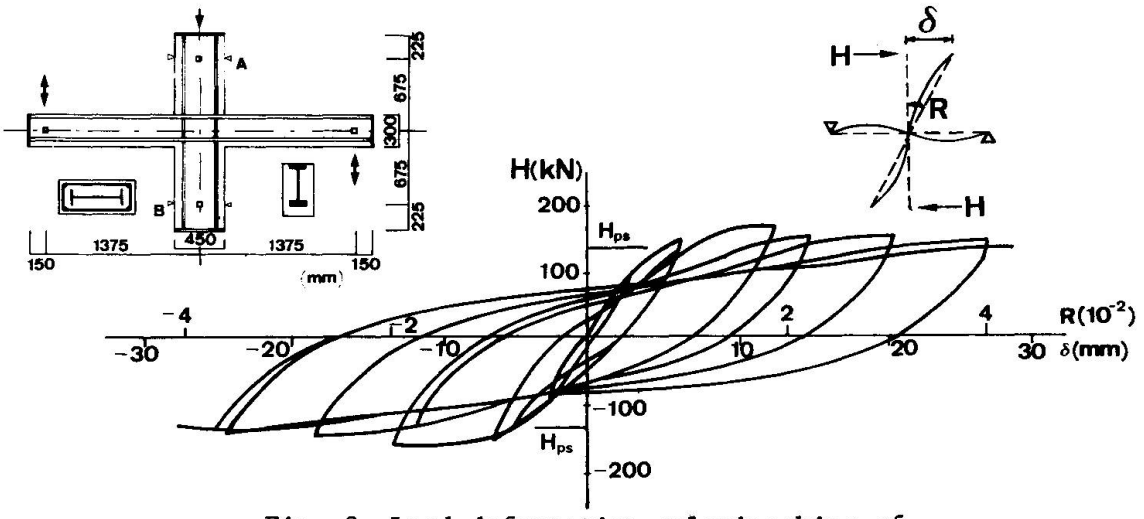

Fig. 3 Load-deformation relationships of an SRC beam-to-column connection

height	low-rise H < 25m			medium-rise 25 < H <45m			high-rise 45m < H		
structural system	RC	SRC	S	RC	SRC	S	RC	SRC	S
general construction planning	B	C	B	C	B	A	C	B	A
planning of work progress	B	C	A	C	B	A	C	B	A
quality control	B	C	B	B	C	A	C	C	A
labor management	C	C	B	C	B	A	C	B	A
neighboring environmental pollution	B	C	C	B	C	C	C	C	C
safety supervision	B	C	B	C	C	B	C	C	B
synthetic assessment	B	C	A	C	B	A	C	B	A

A : excellent B : good C : passable

Table 2 Construction efficiency of general office buildings

2.2.5 Economic Characteristics

Unit cost of the structural component of a building is obtained by summing the quantities of concrete, forms, reinforcing bars and steel per unit floor area, multiplied by the corresponding unit costs. However, the unit cost is itself a function of total quantity of steel, and thus the unit cost rises with the increase in the amount of steel. The amount of steel per unit area of an SRC building increases with the increase in the number of stories, while the amount of concrete decreases, and the amount of reinforcing bars remains unchanged. Therefore, as the building becomes taller, the amount of steel can be replaced by cheaper reinforcing bars in the case of the SRC system, and thus tall SRC buildings are sometimes cheaper than tall steel buildings.

2.3 Reasons for the Selection of the SRC System

Table 3 shows the results of investigation by quenstionnaires on the reasons why the SRC system is selected in real construction practice. In addition to the reasons explained above in Sec. 2.2, there is an important administrative reason. The administrative authorities guide the structural designer, so that buildings taller than 7 to 8 stories are as a rule constructed by steel or SRC systems. This guidence is from the viewpoint of safety against earthquakes. Therefore, it can be said from the data in Table 3 that in more than 2/3 of the cases, the reasons for the selection of the SRC system are related to earthquake resisting capacity. Table 4 indicates the criteria for the selection of the structural system for office buildings. The SRC system is often used for the construction of mid-rise to high-rise buildings, i.e., 7-to 15-story buildings.

reasons	%
administrative reason (such as height limit)	36
to increase earthquake resisting capacity	34
to make the beam span longer	11
because of great importance of the building	8
to cut down the construction cost	4
to make the dwelling performance higher	2
no answer	4

Table 3 Reasons of selecting SRC structural system

	span length	< 10m	< 15m	> 15m
number of stories	1 - 6	RC	SRC	S
	7 - 15	SRC	SRC	S
	> 15	S	S	S

Table 4 Criteria for the selection of structural systems (Office buildings)

3. DESIGN STANDARDS

The first edition of the design standards for SRC systems in Japan was published by the Architectural Institute of Japan (AIJ) in 1958, based on the results of extensive experimental investigations carried out in the 1950's (3). Until the publication of the standards, SRC systems had been designed either as steel or reinforced concrete systems, or by superposition method. However, the first edition adopted the last method, that is superposed strength method : the strength of an SRC member is given as the sum of the strengths of the steel and the reiforced concrete components.

The design standards for reinforced concrete systems were revised, based on the experiences in the Tokachi-Oki Earthquake in 1968, and the SRC standards were revised accordingly in 1975 (4). The main purpose of the revision was to prevent brittle shear failure in beam-columns.

In 1981, the Building Standards Act was revised to require the calculation of the story shear strength of the building for the check of earthquake resistance, except for small buildings. The SRC standards are now being revised to include provisions for the calculation of the ultimate story shear strength.

4. RESEARCH ACTIVITIES

Figure 4 shows the change in the total number of research papers on SRC systems, which have been published in the Transactions of AIJ and the Abstracts of the Annual Congress of AIJ. Also shown is the breakdown according to

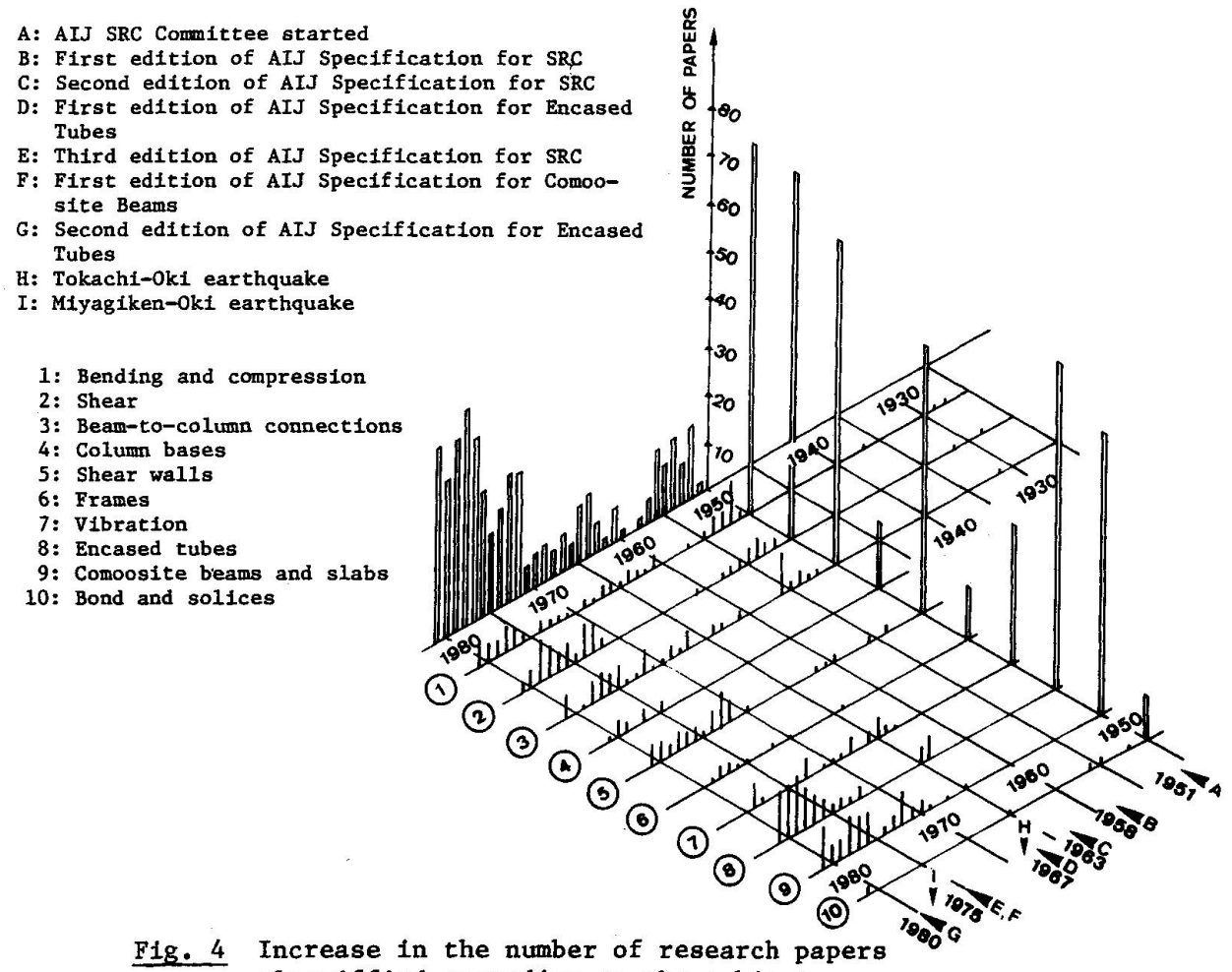

Fig. 4 Increase in the number of research papers classiffied according to the subject

subjects. In the 1950's, most research dealt with the behavior of SRC members with open-web steel composed of angles under compression, bending or shear, and SRC beam-to-column connections under shear. The number of papers decreased for a while in the 1960's because of the publication of the design standards. In the 1970's, the number of papers has again increased and the research objectivs have broadened : not only the SRC system but also general composite systems have recently been studied. New methods of construction have also been proposed.

5. CONCLUDING REMARKS

The SRC system has been very widely used in Japan. For the future success of this system there is a need for rationalisation of the system to make the best use of the mechanical, economic and constructional advantages. Such rationalisation also needs to be incorporated into the design standards.

REFERENCES

(1) M. Wakabayashi, " Recent Japanese Developments in Mixed Structures," Proceedings of the National Structural Engineering Conference, Method of Structural Analysis, ASCE Structural Division Specialty Conference, The University of Wisconsin, August 22-25, 1976 Madison, Wisconsin, Vol. 2 pp. 497-515.
(2) SRC Working Group on the Characteristics of Composite Steel and Reinforced Concrete Structures, " On the Characteristics of SRC Structures - Problems and Review ", Journal of AIJ, Vol. 97, No. 1201, Dec. 1982, pp. 76-82, and Vol. 98, No. 1202, Jan. 1983, pp. 88-97 (in Japanese).
(3) Wakabayashi, M. " Standards for the Design of Concrete Encased-Steel and Concrete-Filled Tubular Structures in Japan," Proc. US-Japan Seminar on Composite structures and Mixed Structural Systems, Gihodo Shuppan, 1980, pp. 69-84.
(4) Architectural Institute of Japan, " AIJ Standard for Structural Calculation of Steel-Reinforced Concrete Structures," 3rd Edition, Nov., 1975 (in Japanese).

Composite Floors: Comparisons of Performance Testing and Methods of Analysis

Dalles mixtes: comparaison des méthodes d'essais et d'analyses

Verbunddecken: Vergleich der Versuche mit den Berechnungsmethoden

Howard D. WRIGHT
Lecturer
University College
Cardiff, United Kingdom

Howard Wright, born 1952, obtained his degree at Sheffield University, Britain. He has worked for the Electricity Board and the Boots Co P.L.C. as a structural engineer before joining the lecturing staff at University College, Cardiff in 1982.

H. Roy EVANS
Prof. of Struct. Engineering
University College
Cardiff, United Kingdom

Roy Evans, born 1942, obtained his degree at University College, Swansea. Following a period with Freeman Fox and Partners he joined the staff of University College, Cardiff in 1969, where he is now Professor of Structural Engineering and Head of the Department of Civil and Structural Engineering.

Philip W. HARDING
Director
Alpha Eng. Services Ltd
Cheddar, United Kingdom

Philip Harding, born 1956, obtained his degree at University College, Cardiff and has spent 3 years working towards a Ph. D. He is now a director of Alpha Stud Welding and is currently managing composite floor system construction.

SUMMARY

Profiled steel sheeting may be used as both permanent formwork and tension reinforcement to concrete slabs, the composite action being provided by embossments to the surface of the steel sheet. Current design is based on performance testing of representative slabs to obtain empirical factors which may then be used in analysis for differing span and load conditions of the same profiled steel sheet and embossment. This paper presents the results of a series of performance tests on a British manufactured composite steel deck and compare the results of the various methods of analysis.

RÉSUMÉ

Les tôles profilées sont utilisées à la fois comme coffrage permanent et comme armature de la dalle, l'effet mixte étant assuré par les bosses à la surface de la tôle. Les méthodes de calcul courantes, basées sur des essais de dalles types, utilisent des coefficients de correction empiriques, pour tenir compte des conditions particulières de charge, de portée, etc., pour chaque modèle de tôle. Cet article présente les résultats d'essais conduits sur une tôle, produite en Grande-Bretagne, et compare les résultats obtenus avec différentes méthodes d'analyses.

ZUSAMMENFASSUNG

Profilierte Stahlbleche werden als bleibende Schalung und Zugbewehrung für Betondecken verwendet, wobei die Verbundwirkung durch die Oberflächengestaltung des Stahlblechs erzielt wird. Die gegenwärtigen Bemessungsmethoden basieren auf Versuchen an repräsentativen Plattenelementen, bei denen Erfahrungswerte ermittelt wurden, welche dann in den Berechnungen für unterschiedliche Spannweiten und Belastungsbedingungen desselben profilierten Stahlblechs und Oberflächengestaltung angewendet werden können. Dieser Vortrag beschreibt eine Reihe von Versuchen einer in England hergestellten Verbundstahldecke und vergleicht die Resultate mit den verschiedenen Berechnungsmethoden.

1. OUTLINE OF THE SYSTEM AND DEVELOPMENT

Profiled steel sheeting has, for many years, been used as permanent formwork to reinforced concrete slabs. As such its use depends on its strength and stiffness when supporting wet concrete and other construction loads, additional conventional reinforcing bars being required to provide strength and stiffness of the flooring decks under working loads.

The presence of the steel sheeting in the tensile area of the resulting slab was first utilised by the Granco Steel Products Co of St. Louis. They patented a product, known as 'Cofar', in 1950 which, by means of hard drawn wires welded to the top of the profiled steel sheeting, enabled shear forces to be transmitted from the concrete into the steel, thereby allowing the sheeting to act as tensile reinforcement. No additional reinforcement of the concrete slab was then required.

The advantages of this system were soon recognised and many more manufacturers commenced production in the sixties. The cost of welding wires to the top of the sheeting was, however, high and alternative shear transfer devices were developed. The most popular method, and the one now used almost universally, is by forming embossments in the surface of the profiled sheet. These regular embossments, which are normally made in the web, act in a similar way to the protrusions on cold deformed reinforcing bars, and provide the necessary shear key between the steel and concrete. The first system that became generally available in Britain was the 'Holorib' system marketed by Richard Lees. This sheeting has a re-entrant profile with embossments to the compression flange (Fig.1). Other

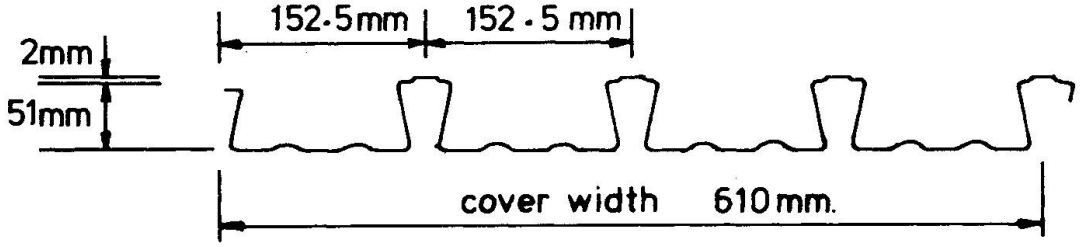

Fig.1 Richard Lees Super Holorib

profiles were introduced to Britain in the seventies from America and Europe and in the early eighties another British manufacturer, Precision Metal Forming, commenced production (Fig.2). The use of the system in Britain has been very limited in comparison to American practice, possibly because of the relatively small size of construction and the more onerous fire regulations. However,

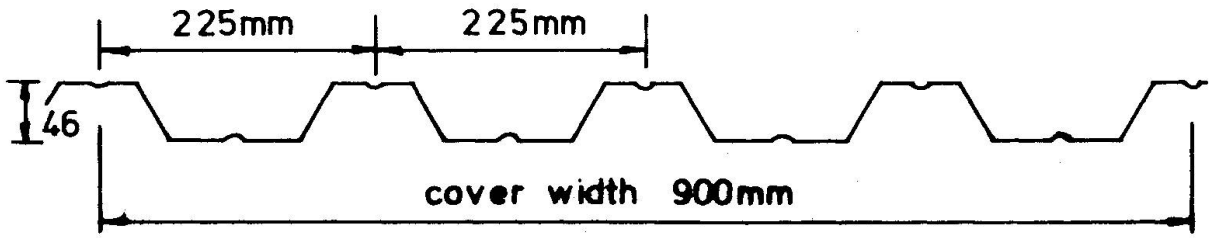

Fig.2 Precision Metal Forming CF 46.

recent large projects in Britain using this system include the National Westminster Tower, Victoria Station redevelopment and the proposed London Bridge City development. There is, currently, widespread interest in its use and development.

2. SHEAR BOND

The structural action of the system under working load relies almost entirely on the shear transfer device: without adequate bond the slab will have no additional strength over its unreinforced capacity. The bond achieved, known as "shear bond", is very dependent on the geometry and frequency of the embossments. Ultimate failure of the slab will occur with a breakdown of shear bond often preceded by tensile cracking at a position defined as the "shear span" (Fig.3).

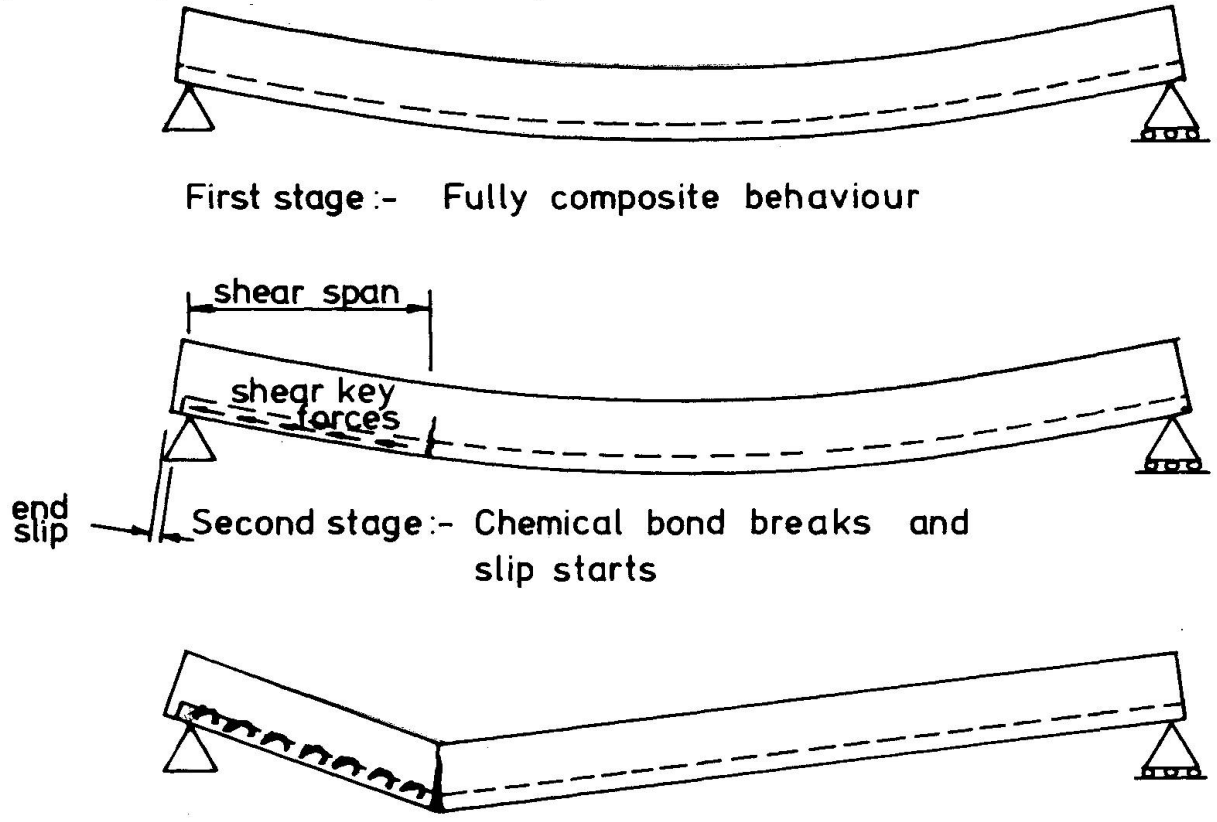

Fig.3

The shear span is normally defined by the distance from the support to the nearest point load or approximately $\frac{1}{4}$ span for a uniformly loaded slab. After initial slip has occurred at the breakdown of shear bond, the concrete slab separates, lifts and rides over the embossments and collapse occurs.

The geometry of embossment can be extremely complex involving many parameters such as embossment height, shape, overall size and orientation. Its effect on the shear bond may also be influenced by the flexibility and geometry of the sheeting itself. Consequently, the prediction the bond capacity of each system is difficult and performance testing has become the recognised alternative.

3. PERFORMANCE TESTING

The system's adoption in America was slightly delayed by the lack of standard test procedures or methods of analysis. Each manufacturer was required to carry out independent tests, often for individual jobs, and it was not until 1967 that the American Iron and Steel Institute initiated a research project at Iowa State University under the direction of Schuster and Ekberg [1]. Further research carried out by both Schuster [2] and Porter and Ekberg [3] led to the linear regression method that forms the basis for the testing requirements included in the new British code of practice; B.S.5950 Pt.4 [4].

The Code requires a minimum of 6 tests to be carried out on representative composite slabs from which a straight line may be drawn (the regression line) relating :

$\frac{V_E}{B_s.d_s.\sqrt{f_{cu}}}$ on the vertical axis to $\frac{A_p}{B_s.L_v.\sqrt{f_{cu}}}$ on the

the horizontal axis, as in Fig.4. This line is then adjusted by a reduction of between 10% and 15%, depending on the number of tests carried out. Two values may be taken from this reduced line; the first value (m_r) represents the slope and the second value (k_r) represents the intercept (Fig.4). These values of the

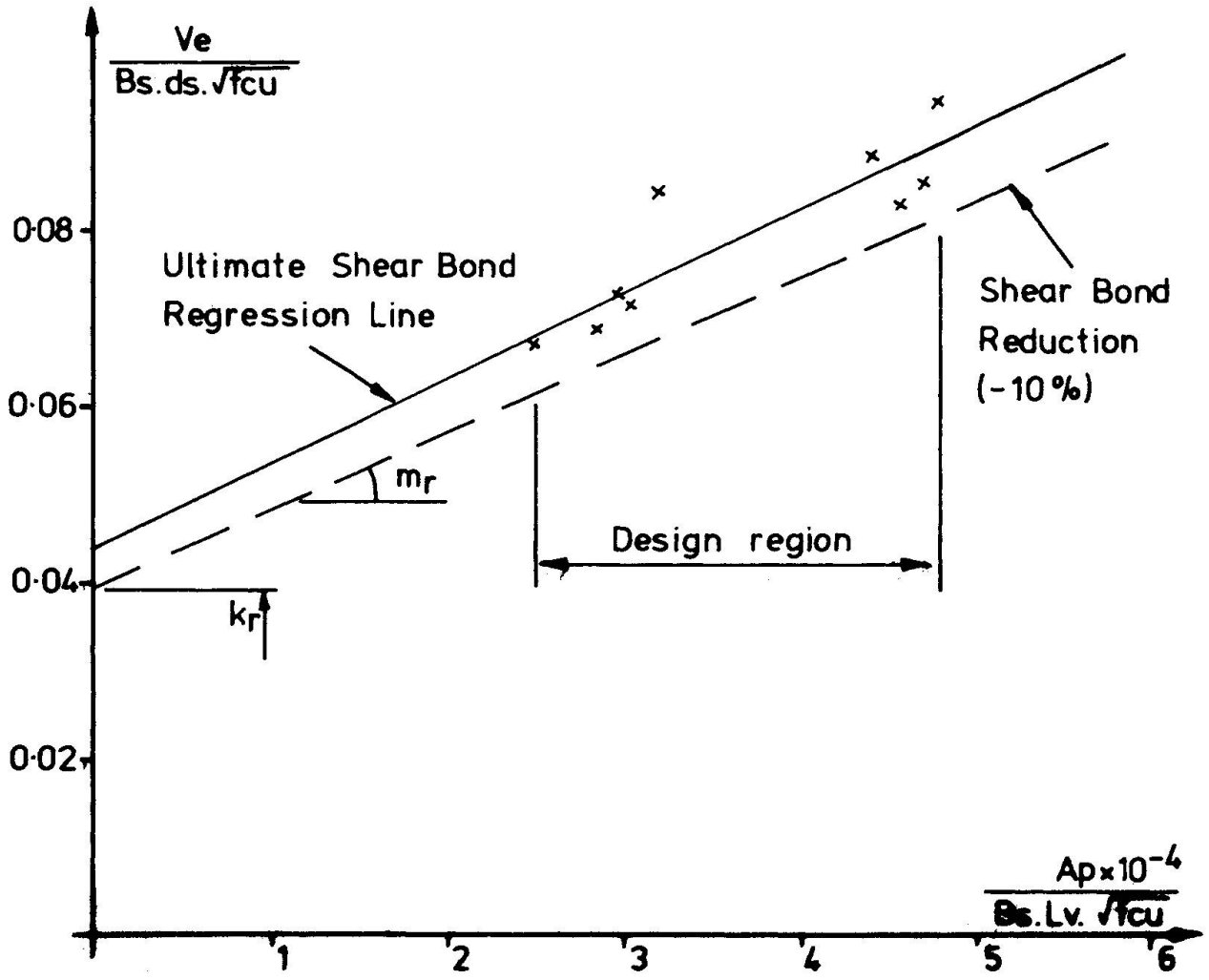

Fig.4

m and k factors may then be used subsequently to determine the strength and stiffness when the same sheet is used for different spans and with different concrete thicknesses.

The Code requires a complex preliminary procedure, involving the application of some 10,000 load cycles around the design load attained in each test. This preliminary cyling ensures that any chemical bond between concrete and steel has been destroyed before the slab is loaded to collapse so that a true value of embossment capacity is measured.

4. CARDIFF TESTS

The introduction of the CF 46 composite flooring system in 1982 preceded the final introduction of the new British Code by nearly a year. The manufacturers, Precision Metal Forming, required confirmation, not only of the new system's potential, but also of its compliance with the proposed Code. At that time, the draft version of the Code was available as the European Convention for Structural Steelwork Committee 11 report [5]. A series of tests based on this Code were carried out on the CF 46 system in the summer of 1982.

In all, twelve tests were carried out on production specimens. In addition to the measurements taken to satisfy the requirements of the Code, steel strains at mid-span and end slip between concrete and steel were measured.

The following conclusions were reached on the basis of the detailed test observations :

a) The shear transfer device in the form of a 3mm high chevron embossment provided considerable shear bond. In many tests, the strain gauges recorded yield strains in the steel sheet before ultimate failure. Extremely high load-carrying capacities were measured; generally the failure loads exceeded the required design loads by a factor of 5.

b) The use of cyclic loading to break the chemical bond may not be strictly necessary. One of the tests was carried out without preliminary cycling and a value of failure load similar to that obtained for specimens that had been cycled was obtained.

c) The height of the embossment is of vital importance. Two tests were carried out on sheets where the embossment height had been reduced from 3mm to 2mm. Both showed a reduction of approximately 50% in load capacity.

d) Variation in concrete strength, beyond a certain required minimum, does not affect the ultimate load capacity. Concrete grades ranged from 25 N/mm^2 to 55 N/mm^2 and similar load capacities were recorded in each case.

5. METHODS OF ANALYSIS

The regression line and reduction line allows the determination of slab capacity for varying spans and concrete thicknesses without recourse to further testing. The regression formula :

$$\frac{V_u . s}{bd} = \frac{m_r \rho d}{L'} + k_r \sqrt{f_{cu}} \qquad \text{(Porter and Ekberg [3])}$$

utilises two unknown quantities m_r and k_r which are often thought to represent the mechanical bond and chemical bond, respectively, between steel and concrete. This is, however, not accurate and the two factors in fact have no physical meaning.

Seleim and Schuster [6] presented a further formula in 1982 in which the thickness of the sheeting was included, thus further reducing the number of tests required.

$$\frac{V_u}{bd} = \frac{k_1 t}{L'} + \frac{k_2}{L'} + k_3 t + k_4 \qquad \text{(Seleim and Schuster [6])}$$

This formula increases the number of unknowns and proves very complex to use as computer statistical packages are required. Again the unknown factors have no physical meaning.

The reliance on testing to provide certain factors for use in further analysis appears to be inevitable. However, Parasannam and Luttrell have recently proposed a design method which completely removes the requirement for testing [7]. The formula is based on an elastic analysis with four modification factors, one of these factors being determined empirically from a large number of test results obtained from Luttrell's comprehensive studies over many years.

$$M_t = \frac{k_3}{k_1+k_2} m_f - k_4.s \qquad \text{(Parasannam and Luttrell [7])}$$

The factors used in the Parasannam and Luttrell formula do have some physical meaning, although their accuracy is dependent on whether the previous test results are entirely representative.

6. COMPARISON OF RESULTS

The results of these methods can be compared to those obtained from the series of tests carried out by the Authors. For this, the 12 tests may be divided into a group of 10, all of which have an embossment depth of 3mm, and a group of two, which have an embossment depth of 2mm. Clearly, the m_r and k_r factors obtained for the 10 test group cannot be applied to the 2 test group and only the Parasannam Luttrell formula can be used for the latter tests.

Table 1 summarizes the results of this comparison, several conclusions may be reached :

a) Both methods of analysis requiring test information give accurate prediction of shear bond capacity.

b) The additional complexity of the Seleim Schuster formula does not appear to achieve additional accuracy.

c) The Parasannam Luttrell formula appears unacceptable for deep embossments but reasonably accurate for shallow embossments. (This is most probably due to the formula being based on previous American testing. Most American decks have very shallow embossments).

TABLE 1

MEAN ERRORS OF METHODS FOR PREDICTING SHEAR BOND CAPACITY			
	PORTER ET AL	SELEIM & SCHUSTER	PARASANNAM & LUTTRELL
10 TEST RESULTS OF PMF CF 46 TRAPEZOIDAL DECK WITH 3mm EMBOSSMENTS	3.6%	4.3%	> 50%
2 TEST RESULTS OF PMF CF 46 TRAPE-ZOIDAL DECK WITH 2mm EMBOSSMENTS	N/A	N/A	12%

7. CONCLUSIONS

The test series and the comparison of methods of analysis shows 3 important facets of this form of construction :

1) The strength of the concrete does not affect the shear bond strength of the system, providing a minimum concrete strength is achieved.

2) The depth of the embossment has a significant effect on the shear bond capacity.

3) The requirement for representative testing appears unavoidable but decks of similar geometry and indentation may be compared by the Parasannam and Luttrell formula.

REFERENCES

1. EKBERG, C.E. Jr. and SCHUSTER, R.M., Floor Systems with Composite Form-Reinforced Concrete Slabs. Final Report. International Association for Bridge and Structural Engineering, 8th Congress, New York, Sept. 1968.

2. SCHUSTER, R.M., Composite Steel-Deck Concrete Floor Systems. Journal of the Structures Division, ASCE, No. ST5, May 1976.

3. PORTER, M.L. and EKBERG, C.E. Jr., Investigation of Cold Formed Steel Deck Reinforced Concrete Floor Slabs. Proceedings of the 1st Speciality Conference on Cold Formed Steel Structures, University of Missouri-Rolla, Mo, 1971.

4. BRITISH STANDARD B.S.5950 : Part 4 : 1982, Structural Use of Steel in Building Part 4. Code of Practice for Design of Floors with Profiled Steel Sheeting.

5. EUROPEAN CONVENTION FOR STRUCTURAL STEELWORK, Document 20, European Recommendations for the Testing of Profiled Metal Sheets, ECCS-XVII-77-2E, April 1977.

6. SELEIM and SCHUSTER, R.M., Composite Floor Slabs. Proceedings of the 6th Speciality Conference on Cold Formed Steel Structures, University of Missouri-Rolla, Mo, 1982.

7. PARASANNAM and LUTTRELL, L. M.Sc. Thesis, West Virginia University, 1984.

Leere Seite
Blank page
Page vide

Efficacité de la connexion dans les planchers mixtes de bâtiment

Wirksamkeit der Verbindung in Verbunddecken

Efficiency of the connection in composite floor

Jean-Marie ARIBERT
Prof. des Universités
INSA
Rennes, France

Jean-Marie Aribert, 44 ans, Ing. et Docteur-es-Sciences, enseigne la Mécanique des Structures à l'Institut National des Sciences Appliquées de Rennes, depuis 1970. Il dirige un laboratoire orienté principalement vers la Construction Métallique. Il est Conseiller Scientifique au CTICM.

Chantha MOUM
Ingénieur d'Etudes
CTICM
Paris, France

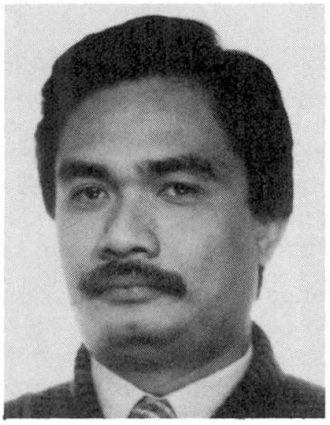

Chantha Moum, né en 1949, obtient son diplôme d'Ingénieur des Arts et Manufactures à l'Ecole Centrale de Paris. Il est Ingénieur d'Etudes au CTICM depuis 1975, et s'occupe, entre autres, des problèmes de structures mixtes acier-béton dans les bâtiments et les ouvrages d'art.

RÉSUMÉ

Cette communication concerne d'une part la définition d'une procédure pour déterminer la limite d'adhérence des dalles collaborantes, d'autre part le développement d'un modèle général de calcul de la connexion de ces dalles avec les poutres. La maîtrise de ces deux aspects permet d'envisager alors un dimensionnement optimal des planchers mixtes de bâtiment.

ZUSAMMENFASSUNG

Dieser Beitrag behandelt einerseits die genaue Darstellung eines Verfahrens, durch das die Haftungsgrenze von Verbundplatten bestimmt werden kann und andererseits die Entwicklung eines generellen Berechnungsmodells für die Verbindung zwischen diesen Platten und den Trägern. Unter Berücksichtigung dieser beiden Aspekte dürfte eine optimale Dimensionierung der Verbunddecken möglich sein.

SUMMARY

The present paper deals with the definition of a procedure for detérmining the limiting adhesive strength of composite slabs on the one hand, and for developing a general calculation model of the connection between these slabs and the beams, on the other hand. The control of both these aspects allows an optimal design of building composite floors.

1. INTRODUCTION

Un système de plancher qui est courant dans le bâtiment, consiste à utiliser des tôles minces nervurées en acier, profilées à froid ; ces tôles reposent sur le réseau des poutres et des solives et servent à la fois d'armatures et de coffrage à la dalle en béton armé, coulée sur place. Pour obtenir une pleine efficacité du système, il est nécessaire de savoir déterminer les possibilités mécaniques de l'action mixte à deux niveaux : celui de l'adhérence du béton avec le bac acier (dalle collaborante), et celui de la connexion de la dalle avec les poutres.

Tout d'abord, on met l'accent sur l'aspect de la dalle collaborante, l'observation amenant à distinguer deux niveaux de charge : l'un correspond au début du glissement, l'autre à la ruine consécutive à une perte complète de l'adhérence. On indique alors comment, avec une sécurité appropriée, il est possible de définir la charge d'utilisation de la dalle, en tenant compte à la fois de la charge de ruine et de celle relevée au début du glissement.

Dans une seconde partie relative à la connexion de la dalle avec les poutres ou solives, on présente, dans ses grandes lignes, un modèle original de calcul non linéaire, applicable jusqu'au stade de la ruine du plancher. Le modèle intègre l'influence du glissement au droit des connecteurs ainsi que celle d'une séparation éventuelle de la dalle et de la poutre en certaines parties de leur interface ; il permet de suivre, au cours d'un chargement croissant, l'évolution des flèches, des efforts sur les connecteurs et des contraintes en section, tout le long de la poutre.

Pour terminer, on donne un exemple d'application au dimensionnement d'un plancher mixte avec une dalle conçue pour être collaborante selon le critère indiqué en première partie ; par comparaison à un dimensionnement conventionnel, l'analyse du comportement exact du plancher à l'aide du modèle exposé dans la deuxième partie, permet de déterminer un dimensionnement optimal conduisant à une économie de matière et de connexion.

2. METHODE POUR LA DETERMINATION DE LA LIMITE D'ADHERENCE TOLE-BETON DES DALLES A BACS COLLABORANTS

2.1 Présentation du système

La collaboration entre la tôle nervurée et le béton, coulé au-dessus, d'une dalle dite "à bac collaborant" (fig. 1) est obtenue grâce aux bossages situés sur les flancs d'onde ou grâce à la forme même du bac en acier. Le concept de collaboration sans aucun glissement est théorique et ne peut constituer un critère d'adhérence significatif pour la dalle. En réalité, à partir d'un certain niveau de chargement, un glissement très faible se produit qui permet aux bossages de jouer leur rôle d'accrochage mécanique entre la tôle et le béton.

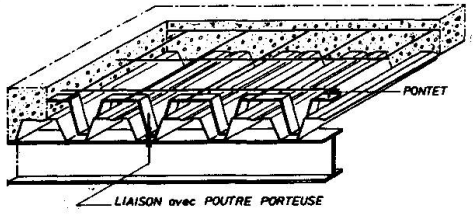

Fig. 1 - Système à bac collaborant

2.2 Comportement des dalles

L'observation expérimentale montre que le comportement des dalles suit, en général, l'allure de la courbe de la figure 2 où l'on peut distinguer trois niveaux de charge :
- la charge P_f de fissuration du béton ;
- la charge P_g de début de glissement ;
- et la charge P_r de ruine de la dalle, obtenue par une perte complète d'adhérence (entraînant nécessairement sa rupture).

A partir des divers essais de laboratoire réalisés en France, il a été possible de tirer les conclusions suivantes :

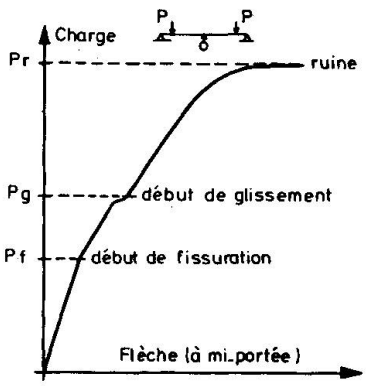

Fig. 2 - Comportement général d'une dalle

- les bossages ou autres systèmes d'accrochage ne jouent pleinement leur rôle qu'à partir de la charge de début de glissement ;
- la différence entre les charges P_r et P_g constitue une information essentielle pour la performance du système d'adhérence d'un profil donné. Au plan de la sécurité, on pourra considérer la dalle comme "ductile" si $(P_r - P_g)$ est important, et comme "fragile" si cette différence est faible ;
- pour un type de dalle et un type de chargement fixés, la charge de ruine est pratiquement inchangée en répétant plusieurs essais, si bien que l'on peut attribuer à P_r un caractère déterministe ;
- en revanche, la charge de début de glissement P_g est assez aléatoire : elle dépend beaucoup de l'état de surface de la tôle et du phénomène de "collage", d'origine physico-chimique, entre la tôle et le béton, suite au coulage du béton.

2.3 Détermination de la contrainte limite d'adhérence à la ruine

Des études ont été réalisées aux Etats-Unis par SCHUSTER [1] sur un grand nombre d'échantillons et elles ont permis d'établir des formulations enveloppes recouvrant toutes les formes de ruine possibles (ruine par cisaillement sans glissement, ruine par flexion, ruine par cisaillement avec glissement, etc...).

En France, les dalles collaborantes sont calculées ou vérifiées en utilisant tous les critères normalement en vigueur pour les structures en béton et celles en acier. En ce qui concerne la détermination des limites d'adhérence, le C.S.T.B. [2], dans le cadre de ses Avis Techniques, propose d'effectuer, pour un type de profil donné, trois essais différents de dalle collaborante, répétés chacun une fois (donc six essais au total) ; les paramètres à faire varier entre ces trois essais sont :
- le pourcentage d'acier ρ constitué par la tôle pour la section de dalle,
- la hauteur totale d de la dalle,
- et la portée de la dalle L expérimentée.

Pour chaque essai, on calcule les contraintes de cisaillement :

$$\tau_g = \frac{T_g}{bZ} \quad \text{et} \quad \tau_r = \frac{T_r}{bZ} \qquad (1)$$

où T_g et T_r sont les efforts tranchants au début du glissement et à la ruine, b la largeur de la dalle expérimentée et Z le bras de levier de la section mixte de la dalle (distance entre la résultante des contraintes de la partie comprimée du béton et la position moyenne de l'armature constituée par le bac).

En s'inspirant des travaux de SCHUSTER, les valeurs obtenues pour la contrainte de ruine τ_r peuvent être lissées à l'aide de la loi de régression linéaire :

$$\tau_r = m \frac{4\rho d}{L} + k \qquad (2)$$

où m et k apparaissent comme deux coefficients spécifiques du type de bac étudié.

2.4 Détermination d'une contrainte limite d'adhérence en service

La limite d'adhérence en service est prise égale à la plus faible des deux valeurs :

$$\frac{\tau_r}{2,175} \quad \text{et} \quad \frac{\tau_g}{1,2} \quad ; \qquad (3)$$

le coefficient 2,175 résulte du produit d'un coefficient de sécurité de 1,5 vis-à-vis de la ruine, propre au matériau, par un coefficient de pondération des charges, de

valeur moyenne 1,45.

Par ailleurs, le coefficient 1,2 affecté à τ_g ne vaut que pour les surcharges statiques; dans le cas de surcharges dynamiques, il est à remplacer par 1,5.

Le critère (3) permet d'obtenir une sécurité relativement homogène, aussi bien pour une dalle "ductile" (fig. 3.a) que pour une dalle "fragile" (fig. 3.b).

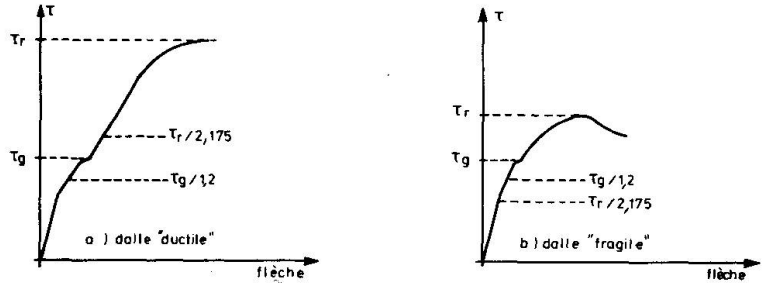

Fig. 3 – Position de la contrainte limite d'adhérence

La figure 4 montre, sur un cas réel, comment a été déterminée la droite de cisaillement limite d'adhérence, pour l'état de service (ici, la droite D_3 et non la droite D_2 affine de la droite de régression D_1 relative à la rupture).

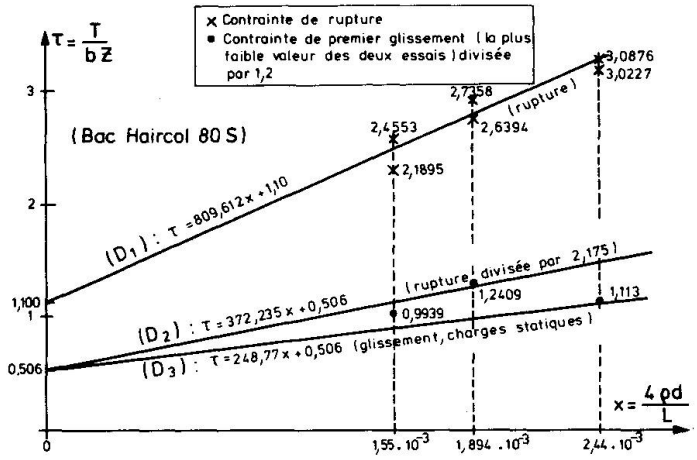

Fig. 4 – Détermination semi-empirique de la limite d'adhérence

3. MODELISATION DE LA CONNEXION DE LA DALLE AVEC LES POUTRES

3.1 Notations

On désigne par (fig. 5) :

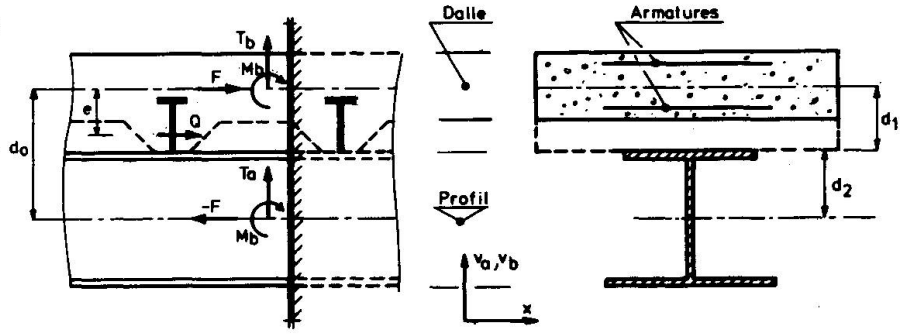

Fig. 5
Géométrie et efforts internes de la poutre mixte

d_0 : la distance entre les fibres moyennes de la dalle et du profil acier ;

d_1 : la distance entre la fibre moyenne et la fibre inférieure de la dalle ;

d_2 : la distance entre la fibre moyenne et la fibre supérieure du profil ;

e : la distance entre la résultante Q des efforts de cisaillement du connecteur et

la fibre moyenne de la dalle ;
F : l'effort normal dans la dalle (avec l'effort - F dans le profil) ;
M, M_a et M_b : les moments fléchissants appliqués respectivement à la section mixte acier-béton, au profil acier seul et à la dalle seule ;
T, T_a et T_b : les efforts tranchants appliqués respectivement à la section mixte, au profil seul et à la dalle seule ;
$v_a(x)$, $v_b(x)$: les déformées transversales par flexion des lignes moyennes respectivement du profil et de la dalle ;
x : l'abscisse d'une section droite quelconque de la poutre ;
$\gamma(x)$: le glissement relatif de l'acier par rapport au béton le long de la connexion :
$\Delta(x) = v_b(x) - v_a(x) \geq 0$: le soulèvement de la dalle par rapport au profil ;
ε_a et ε_b : les allongements linéiques relatifs au niveau des centres de gravité respectivement du profil et de la dalle.

3.2 Equations

Les équations ou relations à la base du modèle sont présentées brièvement ci-après :

3.2.1 Relations de comportement du profil acier et de la dalle. Adoptant comme des inconnues de base la force d'interaction F et les courbures des déformées $v_a(x)$ et $v_b(x)$, les relations de comportement peuvent s'écrire (en variables généralisées) sous la forme :

- pour le profil : $\varepsilon_a = f_a\left(F, \frac{d^2 v_a}{dx^2}\right)$ **(4)**

$$M_a = g_a\left(F, \frac{d^2 v_a}{dx^2}\right) \quad \textbf{(5)}$$

pour la dalle : $\varepsilon_b = f_b\left(F, \frac{d^2 v_b}{dx^2}\right)$ **(6)**

$$M_b = g_b\left(F, \frac{d^2 v_b}{dx^2}\right) . \quad \textbf{(7)}$$

Dans le cas particulier où le comportement local du béton en compression relève d'un diagramme parabole-rectangle et où celui de l'acier est de type élasto-plastique parfait, des expressions analytiques ont pu être données pour les fonctions f_a, g_a, f_b et g_b [3]. Dans le cas général, ces fonctions, relativement complexes, sont déterminées par intégration numérique en section [7].

3.2.2 Equation de compatibilité des déformations
En tout point de l'interface acier-béton (excepté au droit des connecteurs), on peut montrer que l'on doit satisfaire à :

$$\frac{d\gamma}{dx} = \varepsilon_b - \varepsilon_a + d_1 \frac{d^2 v_b}{dx^2} + d_2 \frac{d^2 v_a}{dx^2} \quad \textbf{(8)}$$

3.2.3 Equations d'équilibre en section
L'équilibre en moments de la section mixte exige :

$$M = M_a + M_b + F\, d_0 , \quad \textbf{(9)}$$

et l'équilibre en efforts tranchants :

$$T = T_a + T_b . \quad \textbf{(10)}$$

3.2.4 Equations d'équilibre au droit des connecteurs
Soit i l'indice repérant la position d'un connecteur le long de la poutre (i = 1, m). Au passage de ce connecteur (fig. 6), on a trois équations d'équilibre :
- en résultante selon la direction longitudinale :

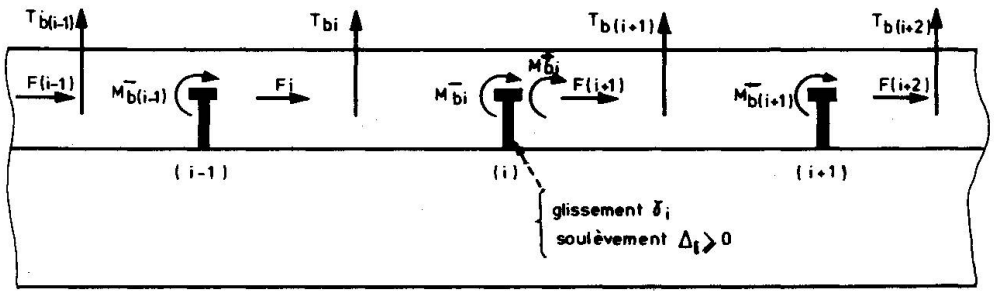

Fig. 6 - Transfert des efforts d'un connecteur à un autre

$$F_{i+1} = F_i - R_g(\gamma_i).\gamma_i \qquad (11)$$

où R_g est la rigidité en cisaillement du connecteur qui est une fonction non linéaire du glissement γ_i ;

- en résultante selon la direction transversale :

$$T_{b(i+1)} = T_{bi} - R_d(\Delta_i).\Delta_i \qquad (12)$$

où R_d est la rigidité à l'arrachement du connecteur qui est une fonction (éventuellement non linéaire) du soulèvement de la dalle Δ_i, avec obligatoirement : $\Delta_i \geqslant 0$;

- enfin, en moment :

$$M^+_{bi} = M^-_{bi} + R_g(\gamma_i) \cdot \gamma_i \cdot e \qquad (13)$$

traduisant une discontinuité du moment flèchissant dans la dalle de part et d'autre du connecteur ; on a également une discontinuité du moment fléchissant dans le profil, mais de signe opposé.

Quelques remarques s'imposent au sujet des trois équations précédentes. Comme l'impliquent les équations (11) et (12), la force d'interaction F_{i+1} et l'effort tranchant $T_{b(i+1)}$ restent constants dans l'intervalle entre deux connecteurs (i) et (i+1). Par ailleurs, la condition de soulèvement $\Delta_i \geqslant 0$, sans laquelle l'équation (12) n'est pas valable, peut être traîtée par une technique itérative de relaxation, consistant à introduire au droit du connecteur (i) une réaction de contact C_i ; ainsi à l'itération (j), l'équation (12) est remplacée par la suivante :

$$T^{(j)}_{b(i+1)} = T^{(j)}_{bi} - R_d(\Delta^{(j-1)}_i) \cdot \Delta^{(j)}_i + C^{(j)}_i$$

avec :

$$C^{(j)}_i = \begin{cases} C^{(j-1)}_i - R_d(\Delta^{(j-1)}).\Delta^{(j-1)}_i & \text{si} \quad \Delta^{(j-1)}_i < 0 \\ 0 & \text{si} \quad \Delta^{(j-1)}_i \geqslant 0 \end{cases}$$

Ce calcul itératif peut être utilisé aussi pour résoudre simultanément la non-linéarité de comportement des connecteurs (rigidités variables $R_g(\gamma_i)$ et $R_d(\Delta_i)$).

Enfin, on signale la facilité d'introduire dans le modèle, en plus des connecteurs réels, un certain nombre de connecteurs virtuels de résistance nulle, ceci dans le but de réduire l'intervalle entre deux connecteurs réels si celui-ci est estimé trop important lors de la résolution numérique. Cette disposition permet de traduire avec une grande précision les variations des rigidités flexionnelles des parties acier et béton tout le long de la poutre, ainsi que de supposer, sans que cela soit restrictif, des variations linéaires des moments M(x), $M_a(x)$ et $M_b(x)$ dans chaque intervalle entre deux connecteurs.

3.2.5 Conditions aux limites

La force d'interaction F doit être nulle aux deux extrémités de la poutre :

$$F_1 = F_{m+1} = 0 \,, \qquad (14)$$

ainsi que, pour la partie béton, les efforts tranchants et moments fléchissants ci-après :

$$T_{b1} = T_{b(m+1)} = M^{-}_{b1} = M^{+}_{bm} = 0 \qquad (15)$$

(il en serait de même pour la partie acier, mais il n'est pas nécessaire de la considérer ici pour la résolution du problème). Aux conditions (14) et (15) s'ajoutent, pour une poutre hyperstatique, des conditions supplémentaires qui correspondent à des valeurs fixées des flèches au droit des appuis intermédiaires, du type $v_{a(i=p)} = 0$.

3.3 Principe de la résolution numérique

3.3.1 Dans le cas où l'on néglige tout soulèvement de la dalle, c'est à dire où : $v_a(x) = v_b(x), \forall\, x$, le problème se trouve relativement simplifié et la résolution peut s'effectuer de manière itérative à l'aide de trois boucles de calcul imbriquées [3]. La boucle la plus interne consiste à trouver la distribution des glissements des différents connecteurs ; la boucle intermédiaire qui enveloppe la précédente, permet de déterminer dans le cas d'une poutre hyperstatique, le diagramme du moment fléchissant M(x), a priori inconnu. Enfin, la boucle externe porte sur la résolution de l'aspect non-linéaire du comportement des matériaux. On trouvera aux références [4], [5] et [6] des comparaisons précises entre les résultats du modèle de calcul et des mesures expérimentales effectuées sur plusieurs types de poutre, isostatiques ou hyperstatiques, qui autorisent à affirmer que le modèle théorique développé est bien représentatif de la réalité physique, jusqu'au stade de la ruine.

3.3.2 Dans le cas plus général où le soulèvement est pris en considération $(\Delta(x) \geqslant 0)$, une formulation tout à fait originale a été développée qui rend, en outre, beaucoup plus efficace la résolution, en supprimant les deux boucles internes de calcul itératif mentionnées en 3.3.1. Pour simplifier, on laissera de côté ici l'aspect hyperstatique, mais on indique comment une détermination directe des déformations de l'ensemble des connecteurs est possible [7]. Au préalable, on notera que l'on peut toujours définir, à partir des relations (4), (5), (6) et (7), des modules d'élasticité équivalents E^{*}_{a} et E^{*}_{b} comme :

$$E^{*}_{a} = M_a / \left(I_a \frac{d^2 v_a}{dx^2}\right) \quad , \quad E^{*}_{b} = M_b / \left(I_b \frac{d^2 v_b}{dx^2}\right) \qquad (16)$$

où I_a et I_b sont les moments d'inertie en flexion élastique du profil et de la dalle. Si l'on convient d'associer à chaque connecteur (i) le vecteur $\{V\}_i$ constitué des inconnues suivantes, de type mixte :

$$\{V\}_i = [\gamma_i, \left(\frac{d\Delta}{dx}\right)_i, \Delta_i, F_i, M^{-}_{bi}, T_{bi}, 1\,]^T , \qquad (17)$$

on peut démontrer, à partir des équations données dans les paragraphes 3.2.1 à 3.2.4, qu'il existe une matrice de transfert $[H]_i^{(i+1)}$, ici de dimensions 7 x 7, permettant de passer du connecteur (i) au connecteur (i+1) :

$$\{V\}_{(i+1)} = [H]_i^{(i+1)} \{V\}_i \, . \qquad (18)$$

Les expressions analytiques des coefficients de cette matrice $[H]_i^{(i+1)}$ ont été déterminées; ces coefficients peuvent être calculés dès l'instant où sont supposées connues les valeurs de $R_g(\gamma_i)$, $R_d(\Delta_i)$, C_i et celles des modules équivalents $E^{*(i+1)}_{a\,i}$ et $E^{*(i+1)}_{b\,i}$ (ces derniers étant pris en valeur moyenne sur l'intervalle entre les deux connecteurs). Effectuant en cascade le produit des différentes matrices élémentaires de transfert, on obtient automatiquement la matrice de transfert $[H]_1^m$ de la poutre entre les connecteurs (1) et (m) :

$$\{V\}_m = [H]^m_{(m-1)} [H]^{(m-1)}_{(m-2)} \ldots\ldots [H]^2_1 \{V\}_1 = [H]^m_1 \{V\}_1 \quad . \qquad (19)$$

Par ailleurs, les conditions aux limites (14) et (15) peuvent s'écrire également :

$$\begin{Bmatrix} F_l \\ M_{bl}^- \\ T_{bl} \end{Bmatrix} = \begin{Bmatrix} 0 \end{Bmatrix} ; \begin{Bmatrix} F_m \\ M_{bm}^- \\ T_{bm} \end{Bmatrix} = \begin{bmatrix} R_g(\gamma_m) & 0 & 0 \\ -R_g(\gamma_m).e & 0 & 0 \\ 0 & 0 & R_d(\Delta_m) \end{bmatrix} \begin{Bmatrix} \gamma_m \\ (\frac{d\Delta}{dx})_m \\ \Delta_m \end{Bmatrix} + \begin{Bmatrix} 0 \\ 0 \\ -C(\Delta_m) \end{Bmatrix} \quad \cdot \quad (20)$$

La relation (19), compte tenu des conditions aux limites (20), conduit à un système de dimension trois qui, par résolution directe, donne le sous-vecteur $[\gamma_1, (\frac{d\Delta}{dx})_1 , \Delta_1]^T$; il suffit ensuite d'utiliser, un intervalle après l'autre, l'équation de transfert élémentaire (18) pour obtenir l'ensemble des inconnues $\{V\}_i$ de tous les connecteurs.

3.3.3 Performances

Un programme de calcul, basé sur le modèle précédent, permet, sur ordinateur CII Honeywell Bull 68 DPS 3 (Système Multics), de résoudre en 200 à 300 secondes, vingt cas de chargement progressif jusqu'à la ruine de la poutre mixte.

4. APPLICATION AU DIMENSIONNEMENT D'UN ENSEMBLE PLANCHER-DALLE

4.1 Caractéristiques du plancher-dalle

- Bac d'acier avec des bossages, d'épaisseur de tôle 0,75 mm et de hauteur d'onde 55 mm ;
- épaisseur totale de la dalle : 12 cm ; poids propre de la dalle : 233 daN/m² ;
- portée L de la dalle (fonction de la position des solives) pouvant varier de 1,60 m à 2,60 m ;
- solives constituées par des I.P.E. 220, de portée 5 m (perpendiculairement à celle de la dalle).

4.2 Dimensionnement de la dalle seule

Portée L de la dalle (m)	Surcharge nominale sur dalle (daN/m²)	Surcharge nominale S sur poutre (daN/m)
1,60	2765	4424
1,80	2154	3877
2,00	1720	3440
2,20	1400	3080
2,40	1130	2712
2,60	*	*

TABLEAU 1 (* flèche de pose excessive du bac seul, dépassant 1/240 de la portée)

En effectuant les vérifications portant sur la résistance en flexion, la limite d'adhérence (conformément au § 2), la limitation des flèches à la pose et en service, on trouve comme surcharge nominale (c'est à dire non pondérée) en fonction de la portée L de la dalle, la valeur indiquée au tableau 1.

4.3 Dimensionnement conventionnel de la poutre mixte

Par dimensionnement conventionnel, on entend le dimensionnement aux différents états limites réglementaires, en supposant qu'il y a connexion complète entre la dalle et la solive. Indépendamment de la portée L de la dalle, la largeur participante de la poutre mixte reste égale à 1,10 m. En adoptant des connecteurs de type goujon, de diamètre 19 mm et de hauteur 100 mm, le calcul conventionnel oblige à utiliser au moins 11 goujons par demi-travée de solive (très exactement : 11,3 goujons à l'état limite de service, et 11,5 goujons à l'état limite ultime). Quant à la surcharge nominale S de la poutre, elle ne peut dépasser 2400 daN/m (en plus du poids mort de l'ensemble dalle-solive, de 506,2 daN/m) ; cette valeur maximale de S est imposée ici par la vérification à l'état limite de service (atteinte de la limite d'élasticité de 240 MPa dans la semelle inférieure de l'I.P.E. 220). Si l'on compare ce dernier résultat par rapport à la courbe S(L) de la dalle seule (Tableau 1), on en déduit que la portée optimale de la dalle serait de 2,40 m ; il faut préciser qu'au delà de cette portée, la flèche de pose pour le bac seul serait excessive.

4.4 Dimensionnement de la poutre mixte à l'aide du modèle numérique

La configuration retenue précédemment avec une connexion à 22 goujons, distribués tout le long de la solive I.P.E. 220 en tenant compte des emplacements des ondes (cf. fig. 8) a été analysée, du point de vue comportement sous une charge répartie croissante, à l'aide du modèle exposé au § 3. Les goujons ont été caractérisés au cisaillement par la relation [4] :

$$Q = 130\,(1 - e^{-0,7|\gamma|})^{0,8}\ , \qquad \text{avec Q en KN et } \gamma \text{ en mm ;}$$

à l'arrachement, faute de données précises, il a semblé raisonnable d'adopter une rigidité $R_d(\Delta)$ constante, de 25 KN/mm. On s'est basé également sur des lois de comportement réalistes des matériaux acier et béton (cf. fig. 7), en tenant compte pour l'acier d'un effet d'écrouissage et pour le béton d'une légère résistance en traction et d'une chute de résistance en compression au delà d'un raccourcissement de 2,8‰ (sans toutefois dépasser 4 ‰ conduisant à la rupture par écrasement). Une nappe d'armatures minimale, imposée d'ailleurs dans les règlements (au moins 1 % de la section de béton), constituée ici de 10 Ø 10 pour la largeur participante de 1,10 m, a été admise dans la dalle, à 33,5 mm de sa face supérieure. Parmi les nombreux résultats fournis par le modèle, on s'est contenté de représenter sous forme de courbes:
- à la figure 7, la variation de la flèche, en milieu de portée de la solive, en fonction de la charge répartie totale p (on notera, compte tenu des coefficients de pondération de charge, que p est à comparer à : 1,5 S + 1,35 x 506 daN/m) ;
- à la figure 8, l'évolution (identique pour chaque demi-portée), en fonction de la charge répartie p, d'une part du glissement γ (x), d'autre part du soulèvement partiel Δ(x).

La ruine du plancher mixte se produit par écrasement du béton, dans la section en milieu de portée, pour la charge p = 5500 daN/m, sans risque particulier de rupture des connecteurs (en cisaillement comme à l'arrachement). Ceci correspondrait donc à une surcharge nominale S de l'ordre de 3200 daN/m, donc supérieure à celle 2400 daN/m de la dalle ; il en résulte que le dimensionnement de l'ensemble plancher-dalle n'est pas réellement optimal (comme le laissait entendre le calcul conventionnel en 4.3), la partie poutre mixte apparaissant surdimensionnée. Aussi deux autres configurations ont-elles été étudiées à l'aide du modèle numérique : l'une avec une connexion seulement à 6 goujons par demi-travée, la solive étant toujours un I.P.E. 220 (les goujons ont été répartis uniformément, à raison d'un goujon toutes les trois ondes); l'autre avec la connexion initiale mais une solive en I.P.E. 200. Dans les deux cas, on peut considérer que l'on obtient un dimensionnement optimal de plancher-dalle, avec d'ailleurs un type différent de ruine ; on pourra comparer au tableau 2, plus en détail, les performances en résistance et déformation des trois configurations étudiées.

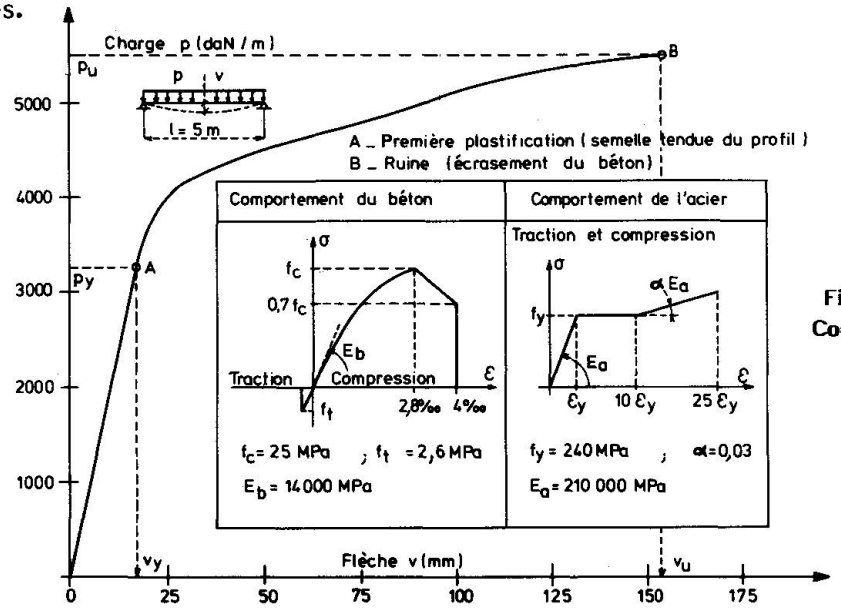

Fig. 7
Courbe "charge-flèche"

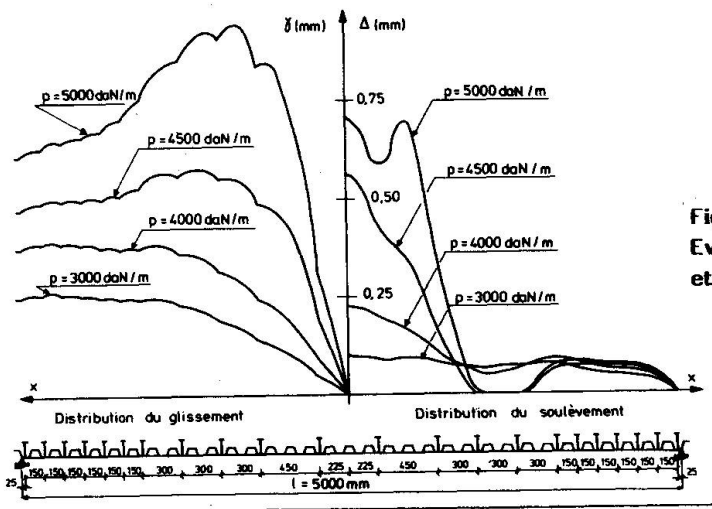

Fig. 8
Evolution des glissements et soulèvements

Type de profil acier	Nombre de connecteurs (demi-travée)	Etat limite élastique		Etat limite ultime					
		Charge p_y (daN/m)	Flèche relative v_y/l	Charge p_u (daN/m)	Surcharge S (daN/m)	Flèche relative v_u/l	Connecteurs: Glissement max. γ(mm)	Connecteurs: Soulèvement max. Δ(mm)	Mode de ruine
IPE 220	11	3250	1/300	5500	3210	1/30	1,4	1,6	Ecrasement du béton
IPE 220	6	3000	1/270	4500	2540	1/50	2,0	0,5	Cisaillement d'un connecteur
IPE 200	11	2750	1/270	4250	2380	1/40	0,8	0,9	Rupture dans le profil

TABLEAU 2 - Comparaison de trois configurations différentes

5. CONCLUSION

Une approche rationnelle a été proposée pour la détermination, par le calcul, d'un dimensionnement optimal des planchers mixtes à bac collaborant. Un exemple a été traité, qui ne peut être qu'indicatif en l'absence de certaines données expérimentales. Toutefois, l'étude systématique du problème, à des fins économiques, est désormais envisageable, sous réserve de disposer de connaissances précises sur le comportement des types de connecteurs utilisés en présence d'un bac (comportement au cisaillement, à l'arrachement et sous la sollicitation combinée "cisaillement-arrachement").

6. BIBLIOGRAPHIE

1. R. SCHUSTER, "Strength and behavior of cold rolled steel deck reinforced concrete floor slab" - Iowa State University (U.S.A.) - Ph. D. Thesis - 1970 -
2. Centre Scientifique et Technique du Bâtiment - Paris -
3. J.M. ARIBERT et A.G. LABIB, "Modèle de calcul élasto-plastique de poutres mixtes à connexion partielle" - Revue Construction Métallique, n° 4 - 1982 -
4. J.M. ARIBERT, A.G. LABIB et J.C. RIVAL, "Etude numérique et expérimentale de l'influence d'une connexion partielle sur le comportement de poutres mixtes"- Journées A.F.P.C. - Thème I - 15-16 mars 1983 - Paris -
5. J.M. ARIBERT, J. BROZZETTI et Ch. MOUM " Etude d'une poutre mixte de pont à âme élancée" - Journées A.F.P.C. - Thème I - 15-16 mars 1983 - Paris -
6. J.M. ARIBERT, " Modélisation de la connexion dans les poutres mixtes acier-béton"- Actes du Colloque National Génie Civil et Recherche - Tome II - Ministère de l'Industrie et de la Recherche - 16-17 juin 1983 - Paris -
7. J.M. ARIBERT et K. ABDEL AZIZ, "Calcul des poutres mixtes jusqu'à l'état ultime avec un effet de soulèvement à l'interface acier-béton" - Revue Construction Métallique (à paraître en 1985) -

Composite Steel-Concrete Components: Current State of the Art and Future Possibilities

Eléments structuraux mixtes acier-béton: progrès récents et futurs

Stahl-Beton Verbundteile: gegenwärtige Erkenntnisse und Zukunftsaussichten

W. KLINGSCH
Prof. Dr. Ing.
University Wuppertal
Wuppertal, Fed. Rep. Germany

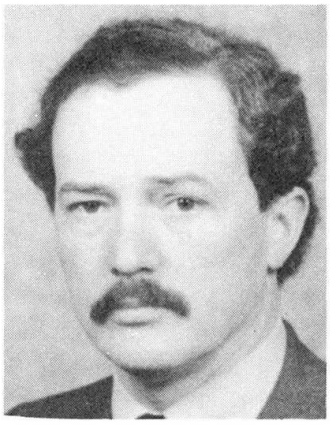

Wolfram Klingsch, born 1944, Dipl.-Ing. degree in 1970, doctor's degree in 1975. Activities as scientist, lecturer and consulting engineer. Since 1982 he hold the chair of building materials technology and fire safety at Bergische University Wuppertal; director of material testing station and institute of constructional engineering.

J.B. SCHLEICH
Department Manager
ARBED-Recherches
Luxembourg

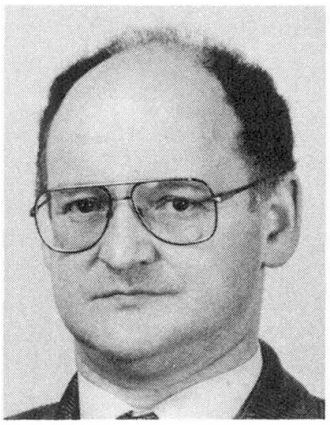

J.B. Schleich, born 1942, got his civil engineering degree at the Univ. of Liège, where he was involved for two years in teaching and research. He then got active for eleven years in the constructional steelwork industry in Luxembourg. He is now responsible for the research on steel construction at ARBED's Research Centre, Luxembourg. President of the ECCS in 1985.

SUMMARY

The paper gives a survey of the most commonly used composite cross-section types, deals with architectural and practical points of view, and shows the future possibilities of the newly developed thermo-mechanical numerical computer codes and of new material technologies.

RÉSUMÉ

Cette contribution donne un aperçu sur les sections mixtes les plus usuelles, traite de points de vue d'architecture et de la pratique, et indique les perspectives d'avenir concernant les nouveaux programmes de calcul thermo-mécaniques et numériques ainsi que les nouvelles technologies à venir dans le domaine des matériaux.

ZUSAMMENFASSUNG

Dieser Text gibt eine Übersicht von den gebräuchlichsten Verbundquerschnitten, behandelt architektonische und praktische Gesichtspunkte, und beleuchtet zusätzlich die Zukunftsaussichten der neuen thermo-mechanischen, numerischen DV-Programme sowie der neu zu erwartenden Materialtechnologien.

1. Introduction

The base principle of composite steel-concrete constructions consists in combining ideally advantageous characteristics of both materials steel and concrete. Ductility, high-tension-strength and easy prefabrication are procured by the steel component; high compressive strength and low thermal diffusibility ($\lambda/c.\rho$) are supplied by the concrete component. In a composite cross section these single parameters don't just add, but activate new additional effects like high stiffness for slender members, high rotation capacity, higher load bearing capacity etc. Therefore composite steel-concrete structural elements are coming into favour for all typical building applications.
The possibility of using visible steel as load bearing component, even for fire resistant structural elements, opens new and trendsetting aspects for architectural design concepts (fig. 1).

2. Present time acquirements

2.1. Slabs

Steel-concrete composite slabs are commonly based on a cold rolled profiled steel sheet supporting the concrete deck. Using special shaped steel sheets, no additional reinforcement is required as well for normal temperature load bearing capacity as under fire load [1]. Quick and easy setting up of such slabs, due to concreting without additional supports, to easy beam connections and to a steel sheet surface ready for use allow very economic applications.

2.2. Beams

Hot rolled steel profils acting as shear connected beams with a concrete or a composite slab are well known structural elements. High load bearing capacity, high bending stiffness, easy prefabrication and a practically always given feasibility explain why this type of composite element is nowadays so largely involved in the field of industrial and office buildings.

A new technology [2,3] for fireproof elements allows to do definitively without cladding of the steel surfaces by concreting between the profile flanges (fig. 2). The lower flange remains as an unprotected visible steel surface. In industrial buildings this is of the highest advantage for making connections by welding at any time not only during the construction procedure but also later for constructional modifications.

Concrete filled beams of this type, but without shear connections to the concrete plate reach higher load bearing capacity than simple steel beams by activating the concrete filling in the compression zone. The same advantage exists for this type of composite beam when used as cantilever, where negative bending moments become the predominant load effect. For fire design the proportional loss of load bearing capacity from the unprotected steel flange, must be compensated by reinforcing bars (fig. 3) or steel strips welded to the web.

These numerous advantages undoubtedly are leading to a dominating application of this type of composite beams in case of fire resistance requirements.

2.3. Columns

Three basic types of cross-section design (fig. 4, 5, 6) lead to the standard steel-concrete composite columns:

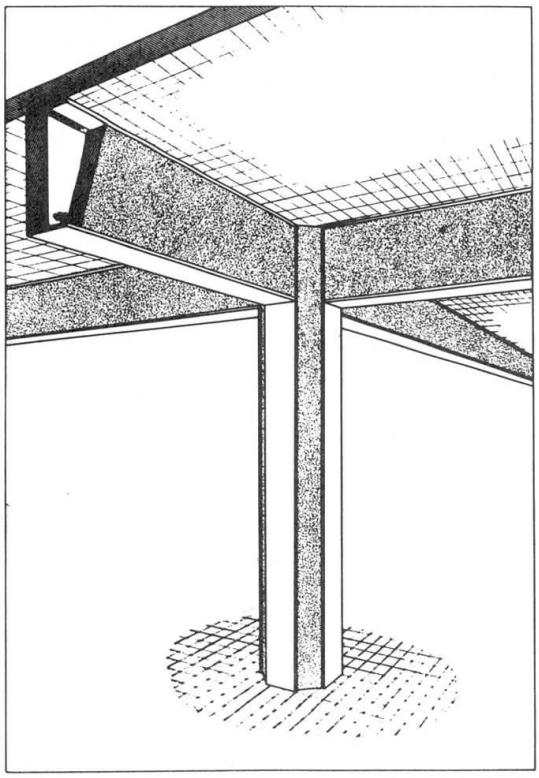

Fig. 1 Octagonal composite column supporting four composite beams, high fire resistance and visible steel

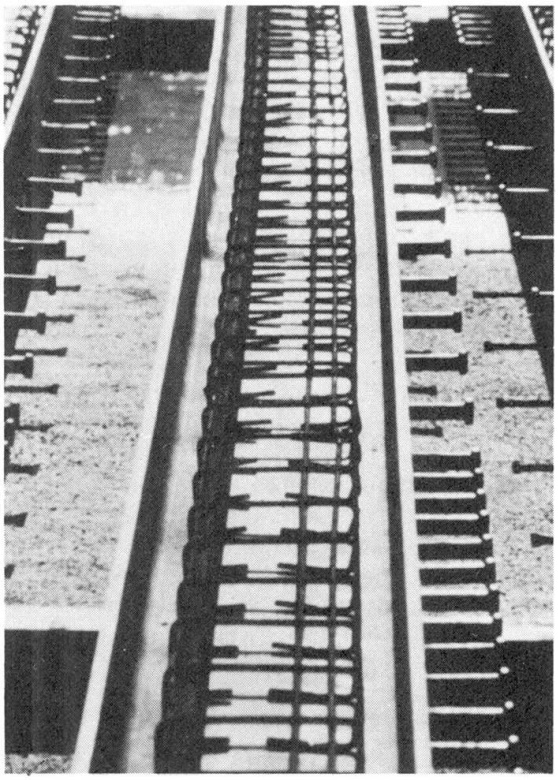

Fig. 2 AF 90 beams before concreting: Office building Magnus Müller, Delmenhorst W-Germany, 1982

Fig. 3 Design diagram for AF composite beams [7] using HE-AA profiles of ARBED (β_y/β_c = 355/35 N/mm²).(Hatched part: $f_q \leqq L/300$ at ambient temperature

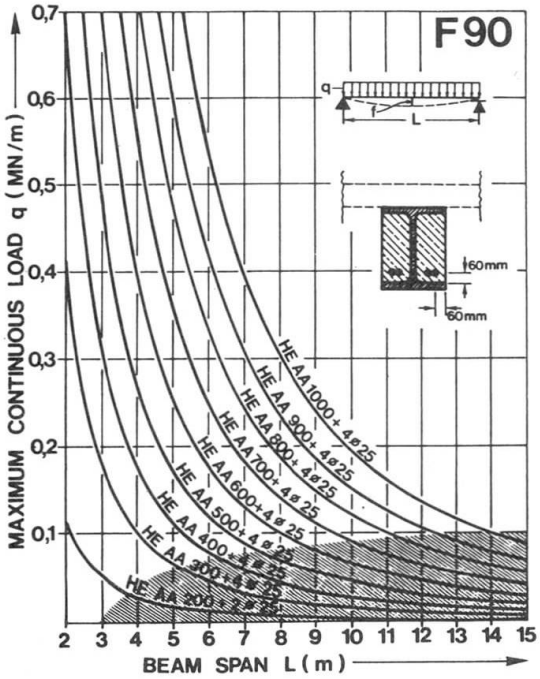

Fig. 4 Hollow section composite columns (openings for concrete filling): Office building, Bielefeld, W-Germany, 1980

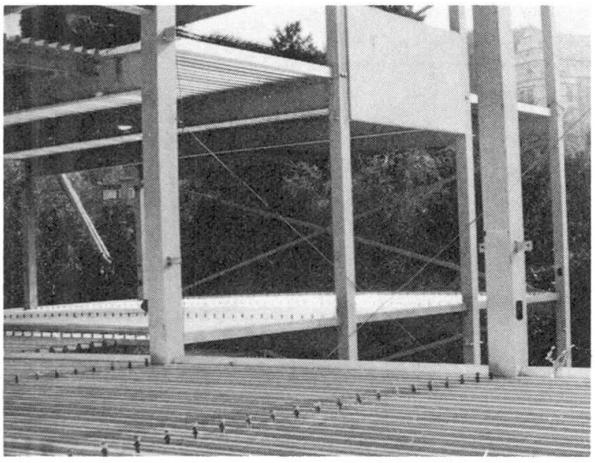

-hollow sections filled with concrete [4],
-hot rolled profiles concreted between the flanges [2,3],
-hot rolled profiles completely encased in concrete [5].

Under normal temperature conditions load bearing behaviour and hence design procedures are uniform for all these types of composite columns. But every type has different fire behaviour characteristics. The reason is the different location and consequently the different heating behaviour of the steel component. Columns with higher percentage of unprotected steel, show reduction in load bearing capacity sooner than those with steel completely protected by the concrete component.

For fire design the uniform service load calculation concept must be modified and adapted to each different cross section type.

All the mentioned column types can be designed for high fire resistance times [6]. The key for this, is the realistic consideration of the internal interaction between the cross section components. A credible fire design therefore must be based on numerical methods. Service load tables for normal temperature conditions and ultimate load tables attached to fire resistance classes have been calculated in this way (fig. 7,8,9).

2.4. Structures

The creation of complete steel-concrete composite structures indicates a new tendency in building technology, especially in industrial and office buildings. The advantages are numerous: prefabrication, easy fitting (fig. 10), reduced erection time and hence, lower financial costs.

In fire design the step from the single member calculation to the global structural analysis should activate additional economic advantages for instance given by the frame stiffening of columns or the bending moment rearrangement possible with continuous beams. Two options are offered: higher fire safety with the benefit of less fire damage on one hand, or lower building costs for a well defined fire safety on the other hand.

3. Future possibilities

New fields of application for composite structural elements can be expected in the very next future by new developments in material technology and structural analysis [7, 8].

Numerical simulations of the component interaction together with combinations of the well known basic cross-section types lead to improved shapes for beams and columns (fig. 11). Experimental results confirmed the reliability of this new design procedure. This improved cross-section design enhanced as well load bearing capacity as fire resistance.

New developments in material technology open new fields of applications for composite elements. Improved light weight concrete with no tendency towards explosive spalling, promotes the application of composite beams in light frame structures. Consequently industrial halls could be covered by a fire proof composite roof structure with visible steel surfaces and increased load bearing capacity. New high temperature resistant cements will improve the design of hollow section composite columns with unprotected steel surface, high slenderness and high fire resistance. Heat absorbing concrete for encased steel profiles and rolled profiles of the highest steel quality can be combined in order to conceive high load bearing columns for long fire resistance times.

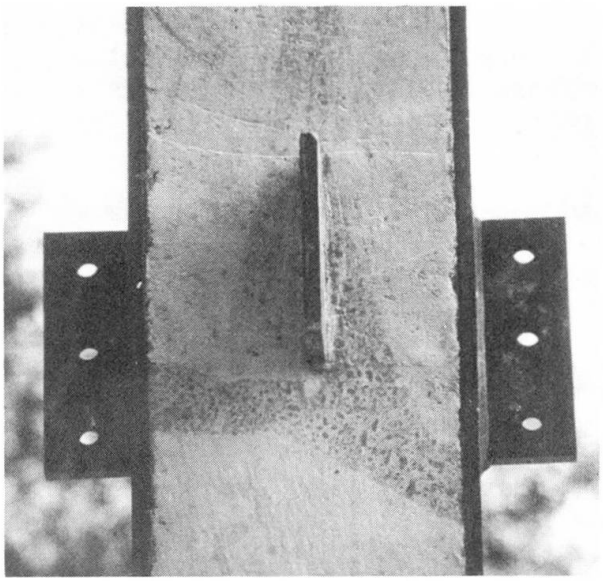

Fig. 5 AF 90 column with gussets for beam connection: Office building TRADE ARBED, Cologne, W-Germany, 1980

Fig. 6 Composite columns with encased hot rolled H-profiles and steel shear heads: Office building LE FOYER, Luxembourg, 1982

Fig. 7 Influence of load level η and cross section size a on failure time t_u of composite columns on concrete filled hollow sections

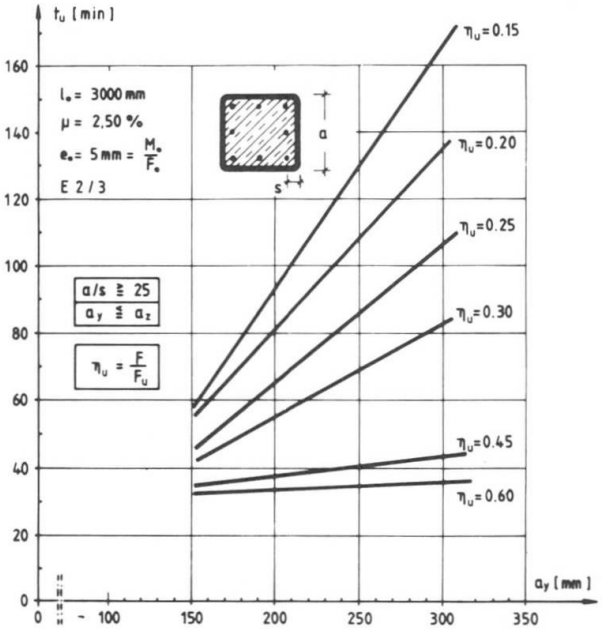

Fig. 8 F 120-design diagram for AF columns, American wide flange shapes W 10''x 10'' to 40''x 18'' concreted between flanges (β_y/β_c = 355/45 N/mm²)

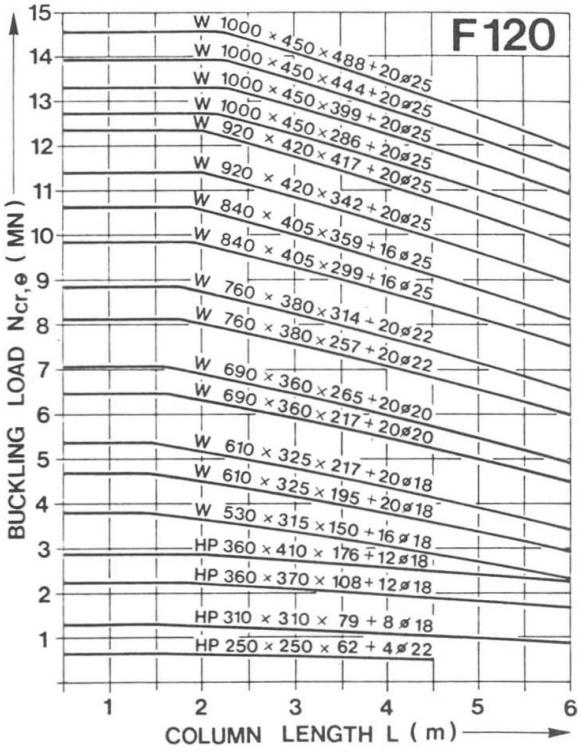

Composite structural elements composed of rolled H-profiles either completely embeded in concrete or concreted between the flanges, could be prefabricated in a more economical way by using the adequate steel-fibre concrete technology; by this the high labour cost involving stirrup reinforcement can be dropped.

A wide application of composite construction elements in engineering, presumes the availability of good prepared design tables, graphes - not only for service load design but also for fire engineering. Such informations are already available or will be worked up in function of running research projects (fig. 12). But cross-section improvement discussed above will remain an individual analysis, which cannot be completely solved by practical design tools; for fire design the problems are similar f.i. for columns with normal force and bending moment interaction. It's a new generation of computer programmes developed for computer aided calculation and design and running on micro computers, which will support this tendency of wider application. Using these programmes, calculation and design of single construction members could be done easily by consulting engineers. Complete structures could even be analysed in order to activate the advantage of construction member interaction, so leading to a more economic design of the structural elements. Especially for fire design this is of fundamental importance (fig. 13).

The high rotative capacity of composite steel-concrete beams and columns notifies a high seismic resistance of these structural members.
Japanese investigations in this field clearly indicate wide and important applications in civil engineering. The combination of seismic resistance and fire safety in addition to the well known traditional advantages of composite steel-concrete structural elements, will activate a new trendsetting technology for buildings in seismic areas.
The above mentioned new aspects of prefabrication and material development can support this tendency.

B I B L I O G R A P H Y

[1] ECCS, TC3 - Calculation of the Fire Resistance of Composite Concrete Slabs with Profiled Steel Sheet Exposed to the Standard Fire - Brussels, 1984.

[2] JUNGBLUTH O., FEYEREISEN H., OBEREGGE O. -Verbundprofilkonstruktionen mit erhöhter Feuerwiderstandsdauer - Bauingenieur 55, 1980.

[3] SCHLEICH J.B., LAHODA E., LICKES J.P., HUTMACHER H., - A new technology in fireproof steel construction - Acier, Stahl, Steel, 3/1983.

[4] KLINGSCH W., K.-G. Würker, R. Martin-Bullmann,- Brandverhalten von Hohlprofil- Verbundstützen - Stahlbau, 10/1984.

[5] KLINGSCH W., BODE H.G., FINSTERLE A. - Brandverhalten von Verbundstützen aus vollständig einbetonierten Walzprofilen - Bauingenieur 59, 1984.

[6] SCHLEICH J.B. - Fire Safety Design of Composite Columns - International Conference "Fire Safe Steel Construction; Practical Design", Luxembourg, April 1984.

[7] DOTREPPE J.Cl., FRANSSEN J.M., SCHLEICH J.B. - Computer Aided Fire Resistance for Steel and Composite Structures - Acier, Stahl, Steel, 3/1984.

[8] SCHLEICH J.B. - Neuentwicklungen auf dem Gebiet des feuerwiderstandsfähigen Verbundbaus auf der Basis von Walzträgern - Fachtagung, "Stahlbau für Hochschullehrer", Köln, 21.- 23. März 1985.

t_u min	L_o	PROFILE HE	d_2 mm	HD	d_2	remarks
30	≤6000	≥100A	≥50	≥210 . 210 . 46	≥40	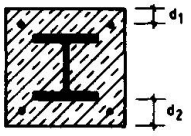 cover d_1 according to reinforced concrete colums
		≥100B	≥40	≥260 . ≥260 . 73		
	≤8000	≥100B	≥40	≥310 . 310 . 97		
60	≤6000	≥100A	≥50	≥360 . 360 . 134		
		≥100B	≥40	≥400 . 400 . 187		
	≤8000	≥100B	≥40			
90	≤4500	≥100B	≥50	≥210 . 210 . 87		
		≥200B	≥40	≥260 . 260 . 101		
		≥100M	≥40	≥310 . 310 . 130		
	≤6000	≥200B	≥50	≥360 . 360 . 148		
		≥120M	≥50	≥400 . 400 . 187		
	≤8000	≥180M	≥40	≥210 . 210 . 100		
120	≤4000	≥120M	≥50	≥260 . 260 . 149		
				≥310 . 310 . 158		
	≤8000	≥180M	≥40	≥360 . 360 . 196		
				≥400 . 400 . 187		

Reinforcement:
μ ≤3 % for t_u ≤ 90'
μ ≤1 % for tu ≥ 120'

Fig. 9 Fire design diagram, minimum steel profiles encased in concrete without load reduction (L_o : real column length)

Fig. 10 AF 30/120 construction system composed of composite columns and beams

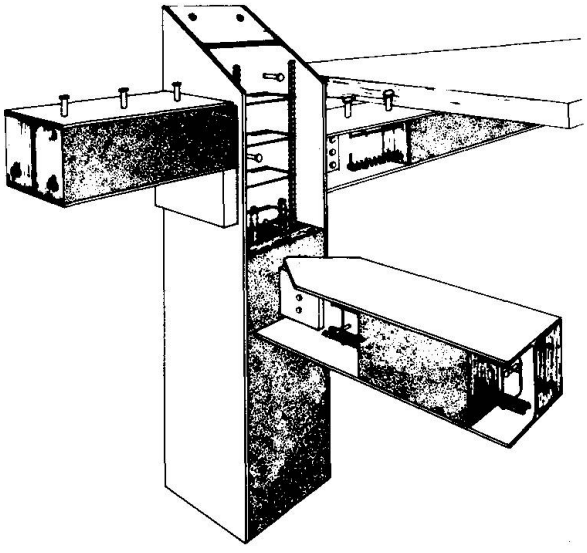

Fig. 11
Special composite cross sections

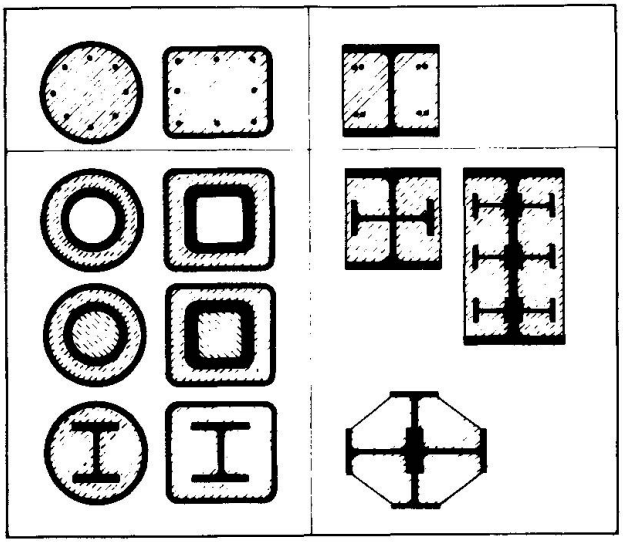

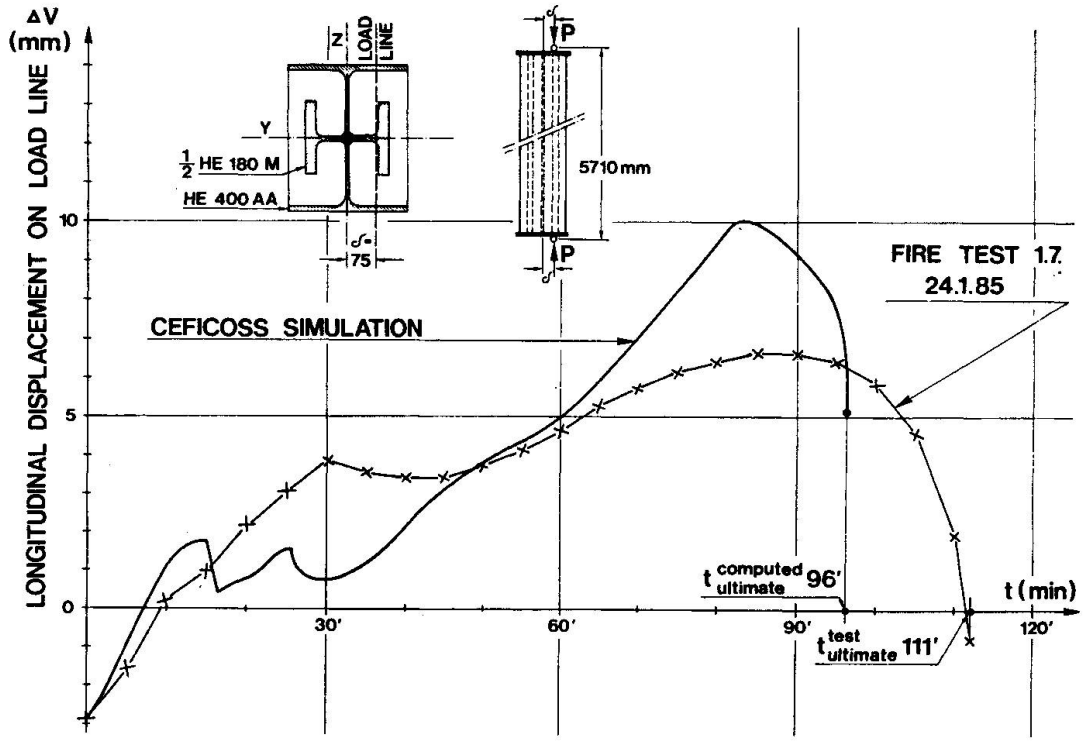

Fig. 12 Calculated [8] and measured longitudinal displacements of a composite AF column, supporting a eccentric load

Fig. 13 Different column-beam interaction possibilities in AF 30/180 construction system: pure shear connection and mixed hear-bending moment connection [8]

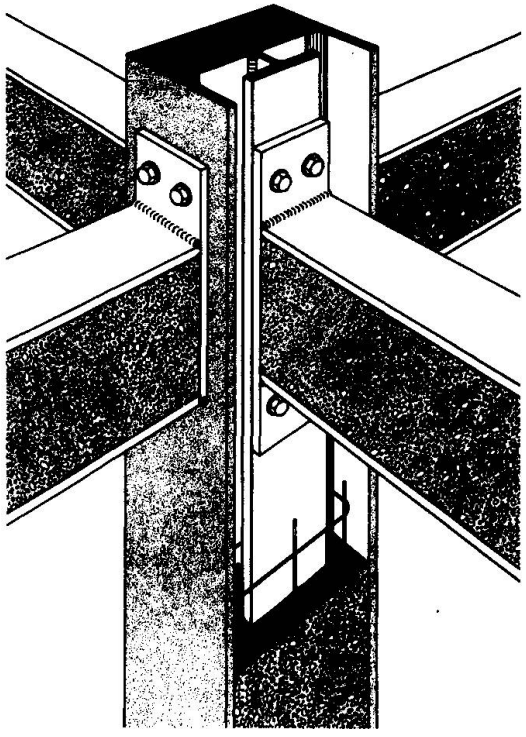

Connections Using Cast Steel T-Stubs in Composite Structures

Assemblages utilisant des souches en forme de T pour les structures mixtes

Verwendung von Gussstahl T-Stücken in Verbundtragwerken

Toshio SAEKI
Senior Res. Eng.
Kajima Corp.
Tokyo, Japan

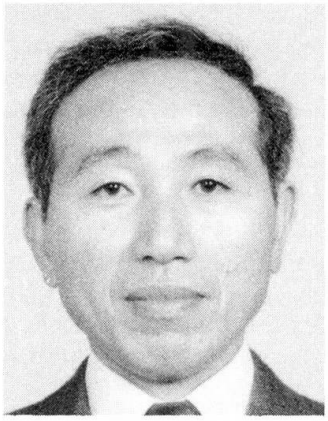

Toshio Saeki, born in 1942, received his Master's Degree in Eng. from Waseda Univ., Tokyo. Since 1965, he has carried out research on the structural behaviour of connections in steel structures at Institute of Kajima Corp.

Ben KATO
Professor
Tokyo Univ.
Tokyo, Japan

Kuniaki SATO
Manager
Kajima Corp.
Tokyo, Japan

Kozo TOYAMA
Assist. Head
Kajima Corp.
Tokyo, Japan

Satoshi BESSHO
Senior Res. Eng.
Kajima Corp.
Tokyo, Japan

SUMMARY

The aim of this study is to investigate the structural behaviour under seismic loading of beam-to-column connections in composite structures, in which steel beams are connected to concrete-encased steel columns by high-strength bolts using cast steel T-stubs. For this purpose, lateral load tests were conducted on beam-to-column subassemblages of this composite structure and the ultimate flexural strength of the connections was investigated both experimentally and theoretically.

RÉSUMÉ

Le but de l'étude présentée ici est d'examiner le comportement sous charges sismiques d'assemblages poutres-colonnes dans les constructions mixtes; la poutre en acier est liée à travers le béton de la colonne par une souche en forme de T, en acier moulé et par des boulons HR. Ce type d'assemblage a été testé, avec des charges latérales, et la résistance ultime à la flexion a été déterminée expérimentalement et par calcul.

ZUSAMMENFASSUNG

Das Ziel dieser Studie ist die Untersuchung des Tragverhaltens einer Träger-Stützen Verbindung in einer Verbundkonstruktion unter seismischer Belastung. Dabei werden die Stahlträger mit den ausbetonierten Stahlstützen mittels hochfester Schrauben unter Verwendung von Gussstahl T-Stücken verbunden. An Träger-Stützen Elementen des Verbundtragwerks wurden Biegeversuche durchgeführt, und die Traglast dieser Verbindung wurde experimentell und theoretisch ermittelt.

1. INTRODUCTION

Composite structures have been applied lately not only to low- and middle-rise buildings but also high-rise buildings for the advantages of structural rationality and economy in building construction in Japan.

A composite structure system, which consists of concrete encased steel column and steel or composite beam, has been developed. The most distinctive feature of this system is that the high-strength bolted T-stub connection method using cast steel attachments called HISPLIT is adopted in the connection of steel beam and steel member of the column. HISPLIT is an improved version of ordinary T-stubs; the thickness of T-stub flange is tapered from stub center to edges, and thus the prying force due to the flexural deflection of the T-stub flange is minimized. It has been confirmed experimentally that the structural properties of the HISPLIT connection in steel frames well enable it to fulfil the function of a moment resisting rigid connection. However, an out-of-plane bending force acts on the flange of the H-shaped steel column because the lateral stiffener plates in the steel column are generally eliminated in the HISPLIT connection system, and so the resisting capacity of the flange of the H-shaped column controls the strength and rigidity of the connection considerably.

Previous to the application of the HISPLIT connection system to the composite structure, the tension test was carried out to investigate the fundamental behaviour of beam flange-to-column connection being covered by concrete and the theoretical prediction method of the pull-out strength of the connection based on the test results has been suggested in Ref. [1].

This paper investigates experimentally the structural behaviour of beam-to-column connection of this composite structure under seismic loading. It also presents the prediction method of ultimate flexural strength of such connection and compares this prediction with the results of the experiments.

2. OUTLINE OF THE COMPOSITE STRUCTURE SYSTEM

An outline of the system is shown in Fig.1. The steel column is rolled H-shaped steel of considerably small cross section compared with the size of concrete encasement. By means of this small section the restraining effect of the covering concrete on the structural properties of the connection is enhanced; moreover greater productivity and cost-saving can be achieved. To increase the restraining effect, tie-bars are used in addition to ordinary square hoops in the column. Floor slab comprising a corrugated metal deck and concrete, is connected to the beam by means of stud connectors to form a composite beam. The steel column and steel beam are connected by high-strength bolts using HISPLIT.

This system, known as the KAJIMA MIXED-STRUCTURE SYSTEM, or KM system, has already been used in more than 50 low-rise and middle-rise buildings and has contributed greatly to cutting construction time and costs.

3. LATERAL LOAD TEST OF BEAM-TO-COLUMN SUBASSEMBLAGE

3.1 Test method

Lateral load test was performed using full-scale beam-to-column subassemblage specimens as shown in Fig.2 to observe the structural behaviour of beam-to-column connections in KM system under seismic loading. As shown in Table 1, in three specimens the beam was connected to the strong-axis of the column (strong-axis specimens), and in another to the weak-axis (weak-axis specimen). In the test of strong-axis specimens, the kind of beams and the method of reinforcement of the connection were chosen as the experimental parameters.

All specimens were designed so that their maximum strength could be determined from the ultimate flexural strength of the connection, which was calculated using Eqs. 1, 2, 3 and 4 proposed in Ref. [1].

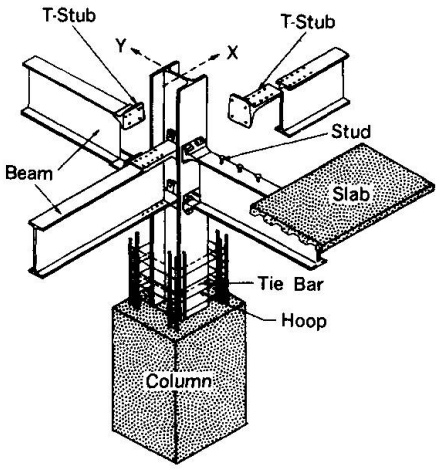

Fig. 1 KM system

Specimen No.	Beam	Reinforcement of joint panel
CX-O	Composite beam	Hoops and tie-bars
SX-O	Steel beam	Hoops and tie-bars
CX-P	Composite beam	Plates
CY-O	Composite beam	Hoops and tie-bars

Table 1 List of Test Specimen

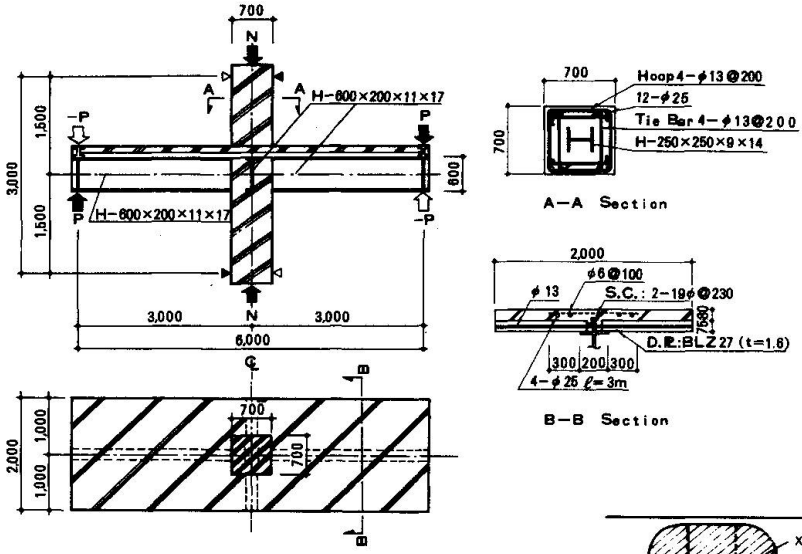

Fig. 2 Test Specimen

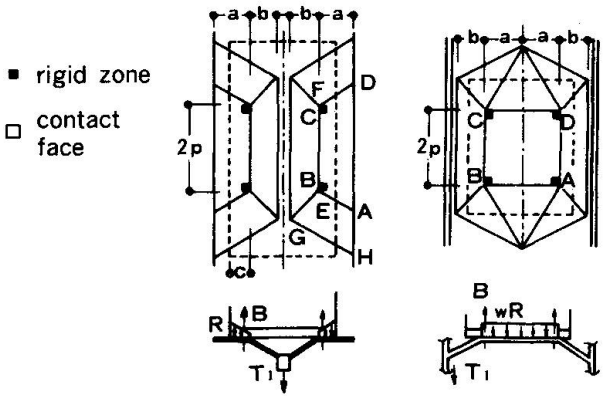

(a) Flange (b) Web

Fig. 3 Collapse Mechanism of Steel Column

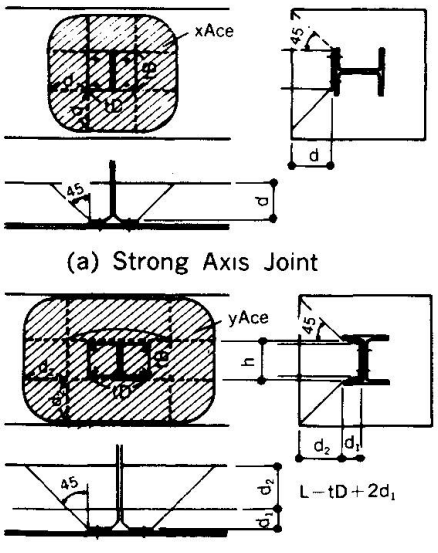

(b) Weak Axis Joint

Fig. 4 Projected Area

$$ {}_jM_u = T_y \cdot j_b \tag{1} $$

$$ T_y = T_s + T_c \tag{2} $$

in which ${}_jM_u$ is the ultimate flexural strength of the connection, T_y is the pull-out strength of the beam flange-to-column connection being covered by concrete, T_s is the yield strength of the connection between the steel column and steel beam, and T_c is the pull-out strength of the covering concrete. T_s and T_c are given by following equations, respectively (see Figs.3 and 4).

For strong-axis specimens,

$$ \left.\begin{aligned} {}_xT_s &= \frac{4}{b}\left(2p + \sqrt{16a\cdot b + 7\,b^2}\right) m_p \\ {}_xT_c &= 32.7\ {}_xA_{ce}\sqrt{f_c'},\quad {}_xA_{ce} = d\,[2\,({}_tD + {}_tB) + d\,] \end{aligned}\right\} \tag{3} $$

and for week-axis specimen,

$$ \left.\begin{aligned} {}_yT_s &= \frac{8}{b}\left(p + \sqrt{4a\cdot b + 3\,b^2}\right) m_p \\ {}_yT_c &= 32.7\,{}_yA_{ce}\sqrt{f_c'} \\ {}_yA_{ce} &= d_2\,[2\,(L + h) + d_2] + L\cdot h - {}_tD\cdot{}_tB,\quad L = {}_tD + 2\,d_1 \end{aligned}\right\} \tag{4} $$

in which m_p is the full plastic moment per unit width of steel column flange, and A_{ce} is effective projected area on concrete surface when cone failure is presumed to occur in the concrete part of the column.

Details of beam-to-column connections are shown in Fig.5 and outlines of HISPLIT used are shown in Fig.6. The mechanical properties of the steel, reinforcements and concrete are shown in Table 2. The high-strength bolts are of F10T grade and are 22 mm in diameter specified by Japanese Industrial Standards. These were tightened to a specified pretension of 221.5 kN. In the specimens with composite beam, CX-0,CX-P, and CY-0, concrete slab of 2 m in width was attached to the steel beam along its entire length with stud connectors. Two rows of studs of 19 mm in diameter were welded to the beam flange with a space of 230 mm along the length of beam.

Constant axial load of 0.3 N_y, where N_y is the axial yield load, was applied to the column. And a couple of reverse transverse load P was repeatedly applied at beam ends.

3.2 Test results

3.2.1 Load-deflection curves of subassemblage

The relationship between load on the beam ends P and deflection at the loading point δ is shown in Fig.7. Predicted values of the ultimate flexural strength of the connection calculated using Eqs. 1, 2, 3 and 4 are shown in terms of transverse load at beam ends P_u' and by chain lines in the figure. Each beam in the three strong-axis specimens did not yield up to its maximum load. Accordingly it can be seen that the maximum strength of these specimens was governed by the strength of the connection as predicted. However, these maximum loads were 30~40 % greater than the predicted values P_u'. The reason for this will be explained that the concrete of the beam end will restrain the rotation of the beam.

The load-deflection curves of CX-0 and CX-P with composite beams were quite similar; they showed stable softening-type up to the maximum loads, but after that they gradually changed into hardening-type and load carrying capacity tended to decrease. Specimen SX-0, with steel-only beam, exhibited about 40 % less elastic rigidity and maximum strength almost 25 % less than the above two specimens. However, it maintained a hysteresis curves of softening-type throughout testing.

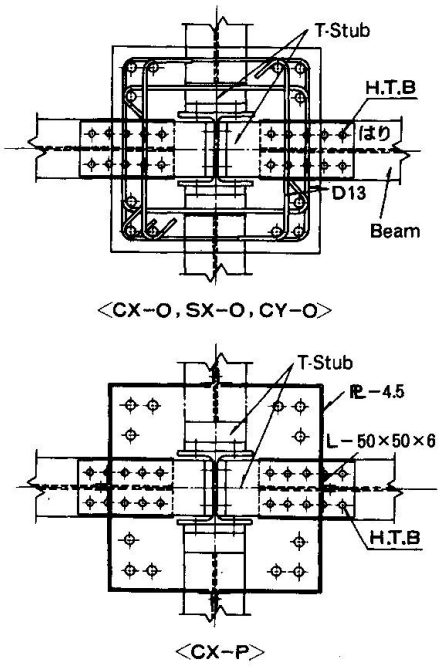

Fig. 5 Details of Beam-to-Column Connections

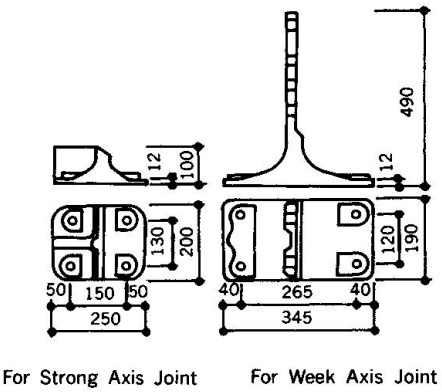

Fig. 6 HISPLIT

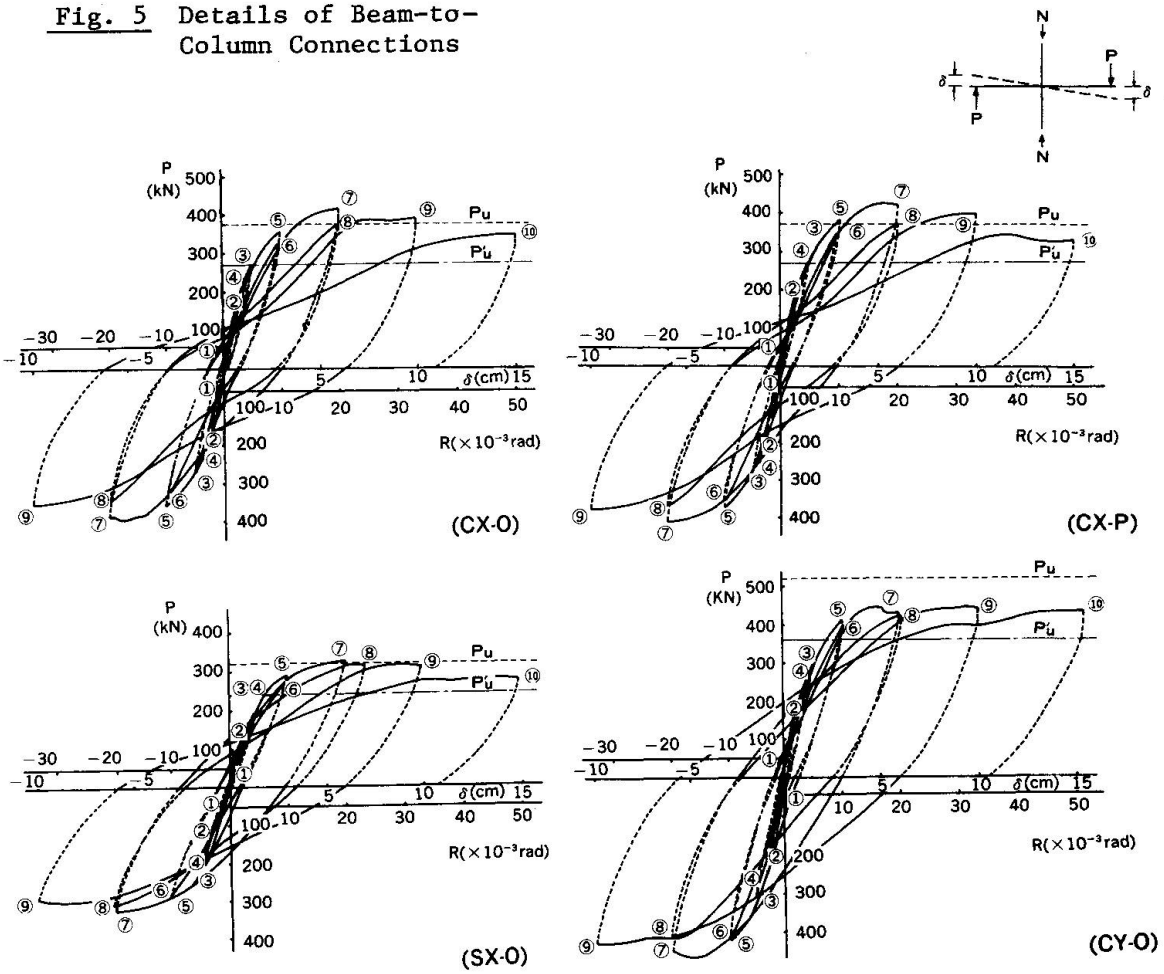

Fig. 7 P-δ Relationship of Subassemblages

In weak-axis specimen CY-0, the local buckling occured in the beam flanges at about $\delta = \pm 5$ cm. However, the buckling load was about 25 % greater than P'_u of this specimen, and the hysteresis curve depicted spindle-type even after buckling.

3.2.2 Pull-out deformation of beam flange-to-column connection

The relationship between load P and pull-out deformation Δ_j of the beam flange-to-column connection is shown in Fig.8. The Δ_j of the three strong-axis specimens were very small at 1 mm or less up to about half of each maximum load. However, at each maximum load, Δ_j increased to 3.2~5.4 mm, which occupied 40~45 % of the deflection at loading point δ, and is thus the most important factor in δ. Furthermore, Δ_j tends to increase rapidly after maximum load. In the light of these observations, it can be seen that all of beam-to-column connections of the three strong-axis specimens yielded at each maximum load.

On the other hand, in the specimen CY-0 the beam end was embedded more deeply in the column than CX-0, so that Δ_j of CY-0 was as a whole smaller; and CY-0 was less damaged around the connection throughout testing.

3.2.3 Behaviour of joint panel

The relationship between load P and shear deflection angle γ of the joint panel is shown in Fig.9. In both specimens SX-0 and CX-0, whose joint panels are reinforced with square hoops and tie-bars, shear yield of steel web panels was observed, but yield of hoops and tie-bars were not observed at each maximum load. Therefore, the concrete panels of these specimens seem to have some reserve strength at each maximum load. In specimen CX-P, whose joint panel is encased in plates instead of the square hoops and tie-bars, the shear yield load of steel web panel and rigidity were greater than that of specimen CX-0 and SX-0. Therefore, it can be said that shear properties of the joint panel encased by plates are superior or equivalent to that of the joint panel reinforced with square hoops and tie-bars. As regards specimen CY-0, its joint panels showed stable behaviour up to its maximum load.

4. ANALYSIS OF THE ULTIMATE STRENGTH OF THE CONNECTION

From the test results described in the previous chapter, it was found that the maximum loads in the strong-axis specimens were governed by the flexural strength of the connection, but the maximum loads in these specimens far exceeded that calculated on the basis of pull-out strength of beam flange-to-column connection. So, the ultimate flextural strength of the beam-to-column connection is analysed theoretically using following assumptions.

—— Ultimate flexural strength of the connection can be predicted by summing the resistant moment on the basis of the pulling-out strength of beam flange-to-column connection given by Eq. 2 and the additional that on the basis of the bearing strength of the concrete encasing beam end.

—— The bearing stress acts evenly along the whole embedded length of beam flange under compression which is embedded in the column ; and the force acts at the center of the embedded length as a concentrated load.

A moment resisting model of beam- to-column connection based on above assumptions is shown in Fig.10. Considering the moment equilibrium at the column steel surface of the connection, Eq. 5 is introduced.

$$T_y \cdot j_b = M_b + \frac{1}{2} Q_b (D_c - {}_sD_c) - \frac{1}{4} P_n (D_c - {}_sD_c) \qquad (5)$$

in which M_b is the bending moment of the beam at the column surface ($=P \cdot l_b$), l_b is the length of beam, Q_b is shear force in beam ($= P$), and P_n is total bearing force which is expressed by Eq. 6.

Materials	Thickness or diameter (mm)	Yield stress (MPa)	Tensile strength (MPa)	Conpressive strength (MPa)
Steel Plates	4.5	276	431	
	9	281	473	
	11	344	518	
	14	265	482	
	17	294	463	
Reinforcements	13ϕ	364	520	
	25ϕ	357	533	
Concrete				25

Table 2 Mechanical Properties of Materials

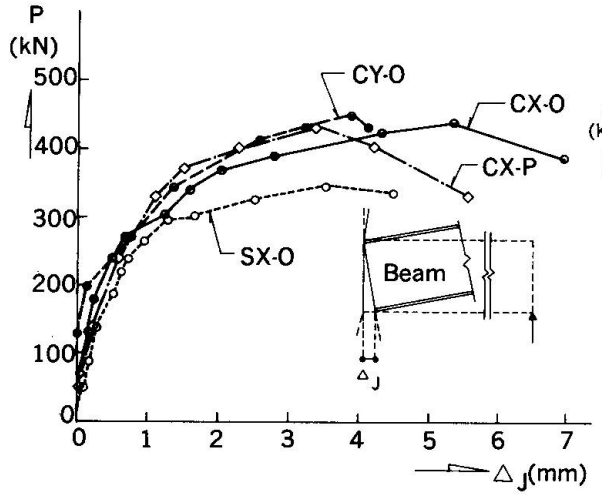

Fig. 8 P-Δ_J Relationship of Beam Flange-to-Column Connection

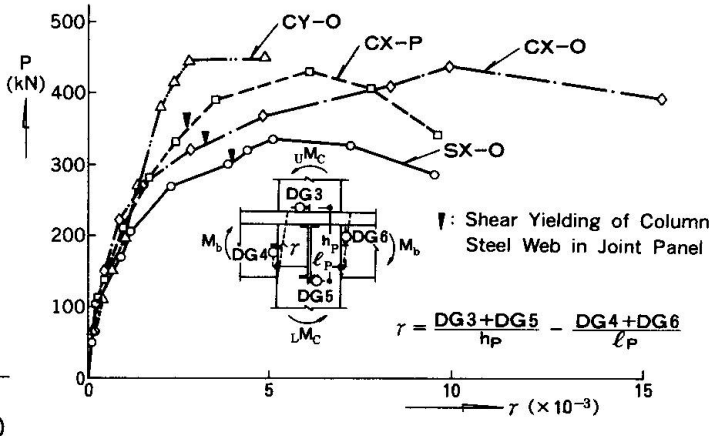

Fig. 9 P-γ Relationship of Joint Panel

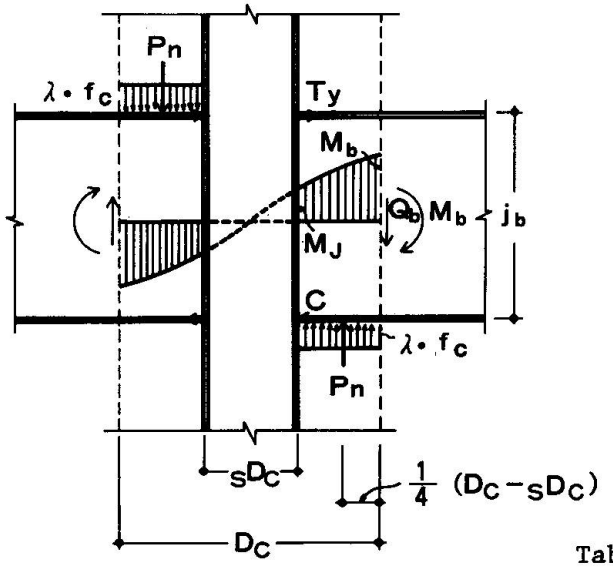

Fig. 10 Moment Resisting Model of Beam-to-Column Connections

Specimen No.	ePmax (kN)	Pu (kN)	Pu/ePmax (%)
CX-O	409.1	366.9	89.7
SX-O	328.6	321.8	97.9
CX-P	418.9	366.9	87.6
CY-O	446.9	515.5	115.4

e^P_{max} = experimental maximum load

Table 3 Comparison of Ultimate Strength between Predictions and Test Results

$$P_n = \frac{1}{2}(D_c - {}_sD_c) \cdot b \cdot \lambda \cdot f_c \qquad (6)$$

in which f_c is compressive strength of concrete, λ =ratio of the bearing stress to F_c. λ varies by the amount of reinforcements in the concrete and by the extent of the area acting bearing force, etc.. However, in this case λ was fixed at 2.0, a value chosen on the basis of Ref. [2]. Therefore, substituting $M_b = P \cdot l_b$, $Q_b = P$ and P_n in Eq. 6 at $\lambda = 2.0$ in Eq. 5, and solving Eq. 5 for the transverse load at the beam ends P, the ultimate load of the connection P_u is given by Eq. 7.

$$P_u = \frac{2}{D_c - {}_sD_c + 2\,l_b}\left[T_y \cdot j_b + \frac{1}{4}(D_c - {}_sD_c)^2 \cdot b \cdot f_c\right] \qquad (7)$$

in which T_y is given by Eqs. 2, 3, and 4.

The prediction values of the ultimate flexural strength of beam-to-column connection of the specimens are calculated by using Eq. 7. These predictions are compared with test results in Table 3 and are shown by broken lines in Fig. 7. They have a good agreement with test results in strong-axis specimens. However, they can not compare with test results in weak-axis specimen, because its maximum load was governed by buckling strength of beam.

5. CONCLUSIONS

The main conclusions obrained by this investigation are as follows:

—— The ultimate flexural strength of beam-to-column connections in strong-axis specimens can be predicted accuratelly by Eq. 7.

—— Beam-to-column connections in this composite structure have a stable restoring characteristics as a moment resisting rigid connection before yielding of them.

—— The rigidity and flexural strength of the composite beam-to-column connection are greater than that of the steel beam-to-column connection.

—— The structural behaviour of the joint panel encased with steel plates is evaluated as the same as that of the joint panel reinforced with square hoops and tie-bars.

From above results, in order to design a beam-to-column connection as a mement resisting rigid connection using KM system, it is desirable that the ultimate flexural strength of the connection as calculated by Eq. 7 exceeds the full-plastic strength of beam. Also it is necessary that the depth of the concrete covering around the connection should be of sufficient depth and that the confining effect of the concrete should be increased by hoops or others.

REFERENCES

1. B. KATO, J. TAGAMI, Beam-to-Column Connection of A Composite Structure. The Second US-Japan Joint Seminar on Composite and Mixed Construction. Seattle, WA, July 1984.
2. M. WAKABAYASHI, K. MINAMI, Y. NISHIMURA, Design Method for Mixed Structures, Part 1, Stress Transfer Mechanism of Exterior Joints. Disaster Prevention Research Institute Annuals of Kyoto Univ.. No.26B-1. 1984.

Composite Steel-Concrete Connections in Stub-Girder Floor System

Connection par goujons des poutres mixtes de planchers

Schubverbindungen von Stahlträgern mit Betondecken mittels Stahlprofilstücken

M.U. HOSAIN
Professor
University of Saskatchewan
Saskatoon, SK, Canada

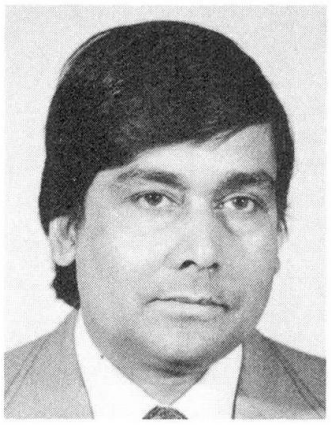

M.U. Hosain, born in Calcutta, received his M.Sc. and Ph.D. degrees in Canada. After two years with consulting firms, he joined University of Saskatchewan in 1969. His research interests are in the areas of steel structures and computer aided design and analysis.

K.T. LEUNG
Graduate Student
University of Saskatchewan
Saskatoon, SK, Canada

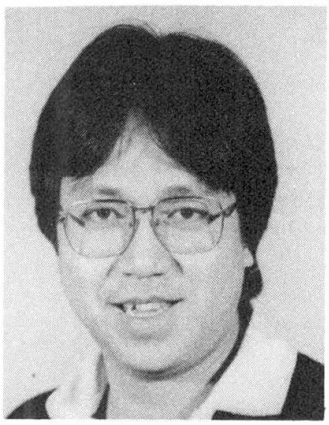

Kwan-tak Leung, who was born in Hong Kong in 1954, received his B.E. and M.Sc. degrees from the University of Saskatchewan in 1980 and 1985, respectively. Currently, he is conducting doctoral research on the stub-girder system in the same University.

SUMMARY

The composite connection between the steel stub and the concrete slab is the weakest link in a stub-girder floor system. This paper briefly summarizes the investigations conducted in this area and identifies the specific areas which are in need of further research.

RÉSUMÉ

La connection entre le goujon et la dalle de béton constitue le point faible d'une poutre mixte de plancher. Cet article résume les recherches faites sur cette question et montre les problèmes qui devront faire l'objet de futures investigations.

ZUSAMMENFASSUNG

Die Verbundverbindung zwischen Stahlstückdübel und Betonplatten ist das schwächste Glied in einem Stahlträger-Betondecken-Verbundsystem. Dieser Beitrag fasst die Untersuchungen auf diesem Gebiet kurz zusammen und zeigt die speziellen Gebiete auf, in denen weitere Forschungen nötig sind.

1. INTRODUCTION

The use of stub-girder floor system was first reported by Joseph Colaco [5] in 1971. As shown in Fig. 1, a stub-girder consists of a steel beam and a reinforced concrete slab separated by a series of short rolled steel sections called 'stubs'. The inherent openings between the girders and the concrete slab lend the system its unique ability to integrate with mechanical, electrical, sprinkler and ceiling systems.

The stub-girder system has been used in numerous buildings in North America [4,10] but an established design method is still lacking. One area which requires further investigation is the shear failure mechanism at the stub-concrete slab interface which is probably the weakest link in a stub-girder system. Recent tests and studies on stub-girder systems or partial assemblages have provided valuable answers but much more work is needed. The over-all problem is much too involved and complicated. It would require comprehensive testing and theoretical analysis not only by a handful of researchers in North America but also by others in Europe and elsehwere. Thus, the main objective of this paper is to briefly summarize the research projects that have been completed thus far and identify the specific areas which would require further investigation.

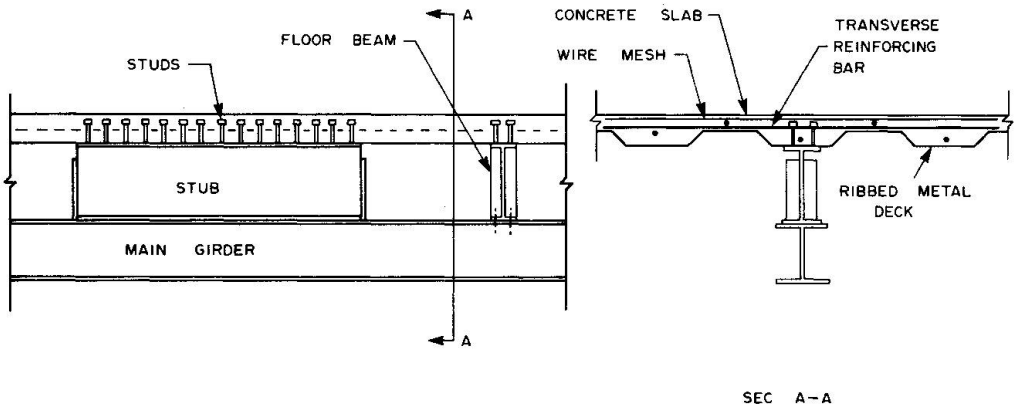

Fig. 1 Stub-Girder Floor System

2. PROPRIETARY RESEARCH

Early investigations on the stub-girder system were proprietary in nature [10].

In 1972, Colaco [5] reported the results of load tests on a stub-girder which was similar to those used in One Allen Center in Houston, Texas. The load test, which was conducted at the test facilities of Granco Steel Products Company in St. Louis, was designed to simulate the actual loading condition of the floor system. A factor of safety of 2.2 on the design load was obtained for the test. Failure was triggered by web crippling at the exterior end of one of the end stubs, followed by the crushing of the concrete slab "at the edge of the first stub piece approximately 7 ft.-0 in. from the support".

Prior to the construction of the First International Building in Dallas, the

consulting structural engineers (Ellisor & Tanner, Inc.) conducted load tests on two full size specimens [9]. The first test was carried out in December 1971 by Inryco Research and Development Company [12] at the University of Wisconsin, Milwaukee. The observed ultimate load exceeded 2.54 times the design load. On completion of the test, stress flaking was observed "on the web of the south spacer and on the weld between this spacer and W14x48 girder. In addition, one of the welds which attached a web stiffener to this spacer was broken". The second test was conducted in January, 1972 by H.H. Robertson Co. of Ambridge, Pennsylvania. The design ultimate load was 1.7 times the service load. The test report [18] stated that: "Prior to failure, two loud noises occurred and at 1.86 times the design load, failure occurred in the stud cluster adjacent to the west support causing loss of composite interaction".

3. NON-PROPRIETARY RESEARCH

The first non-proprietary investigation of stub-girders was started in 1977 at the University of Saskatchewan by the senior author and graduate student W.K. Lam. The M.Sc. thesis project involved tests on ten small size stub-girders. Seven specimens had solid concrete slabs as shown in Fig. 2. In the other three, the slab was placed on ribbed metal deck. Results of this study [14] indicated the susceptibility of stub-girders to longitudinal shear failure. This is due to the shorter length of concrete slab available for shear transfer, the presence of prying forces and the use of ribbed metal deck. This mode of failure was next reported by Buckner et al. [2] in an 8 metre stub-girder with a solid slab. Based on test results, Buckner et al. proposed a method of estimating the transverse reinforcement required and recommended that at least half of this reinforcement should be placed in the bottom half of the slab. However, a stub-girder invariably utilizes a ribbed metal deck which prevents the placement of transverse reinforcement in the bottom half of the slab.

Fig. 2 Test Set-up Used for Small Size Stub-Girders

A research project on stub-girders was carried out at the University of Alberta and reported by Bjorhovde and Zimmerman [1,22]. The research consisted of push-off tests of five full-scale stub assemblages, followed by a theoretical evaluation and testing of a full-scale stub-girder. The stub asemblages failed in a "shear and compression" mode at loads below the design level. Failure of the full-scale stub-girder was caused by a combination of stud shear and stud pull-out at the end stubs. The observed ultimate load exceeded the design ultimate load by 34%. Measured horizontal shear forces were not reported for the test, but the estimated value at failure was 1820 kN based on an elastic Vierendeel analysis proposed by the researchers. This would produce an average shear force per stud of only 61 kN at failure, well below the factored shear resistance of 97 kN, determined in accordance with CAN3-S16.1-M78 [21]. The researchers recommended further evaluation of concrete slab reinforcement requirements.

Concurrently another program was instituted at the University of Saskatchewan and reported by Gosselin and Hosain [7]. The research project involved the testing of two full size stub-girders with slabs on ribbed metal decks. As the first phase of a continuing investigation, this study considered the special case of stub-concrete connections with headed studs arranged in a single line. In both beams, failure was caused by the longitudinal splitting of the concrete slab over the end stubs. The average ultimate shear load per stud was determined to be 26.7 kN for Specimen 1 and 33 kN for Specimen 2. The maximum capacity per stud that can be developed in shear, based on CAN3-S16.1-M78 for conventional composite design, is 64.2 kN for the high strength concrete used. The placement of lateral reinforcement in both tests was ineffective in resisting concrete splitting and shearing [8]. Though the transverse reinforcement area supplied was sufficient to satisfy the CSA requirement (transverse reinforcement ratio = 0.005), the configuration of the metal deck prevented placement in the bottom of the slab as required by the CSA.

In the second phase [13] of the above research program, three full size specimens (K-1, K-2 and K-3), conforming to a typical office floor loading and layout, were tested to failure. The main experimental parameter was the difference in the amount and configuration of the transverse slab reinforcement. The observed ultimate load on the stub-girders exceeded the design ultimate load by 45%, 14% and 21% respectively for K-1, K-2 and K-3. The specimens were very stiff and would meet normal deflection requirements under service loads. In all cases, failure involved crushing of the slab over the interior end of the end stub accompanied by a shear/splitting failure in the slab over the length of the end stub. Straight transverse reinforcing bars in addition to temperature and shrinkage reinforcement, had little effect on the stub-girder capacity. The incorporation of a wide concrete flute along the slab centreline, together with the use of bent transverse reinforcing bars significantly increased the ultimate capacity and improved the ductility of the stub-girder. The average shear load per stud at failure was calculated to be 62.0 kN, 50.7 kN and 51.7 kN for specimens K-1, K-2 and K-3 respectively compared to an ideal value of approximately 97 kN [21] based on the shear failure of the stud itself. In one of the three specimens, the fillet welds along the interior end of the end stub showed signs of distress just prior to the attainment of elastic limit load and required repair work.

The third phase of the research project involved the testing of one full size specimen (K-4) and three full size partial assemblages [11]. Specimen K-4 was

identical to specimen K-3 except that the headed studs were welded through the metal deck. Fig. 3 shows the test set-up used for the full scale test. Specimen K-4 exhibited a 6% higher ultimate load than that of specimen K-3. The increase may be attributed to the weld-thru-deck installation used for the headed studs. The failure mode involved crushing of the slab over the end stub as shown in Fig. 4. The average shear load per stud at failure was 54.48 kN.

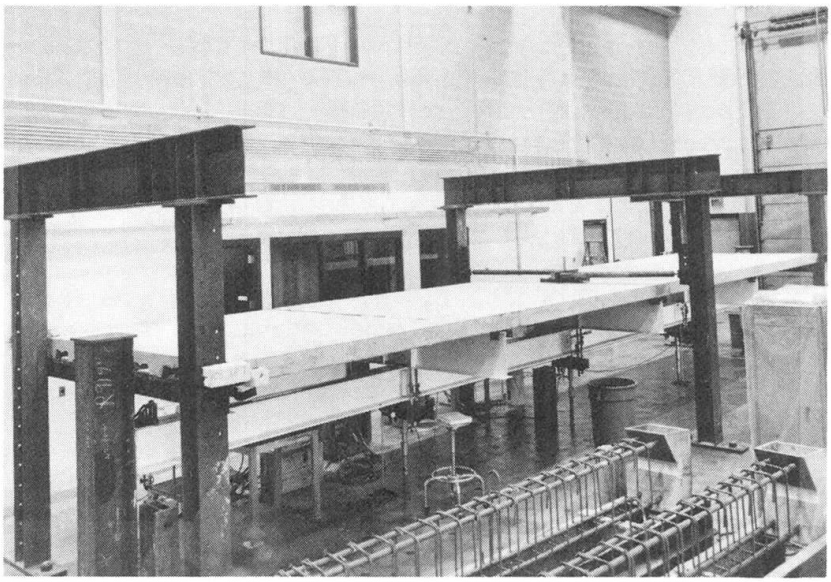

Fig. 3 Test Set-up Used for Full Size Tests

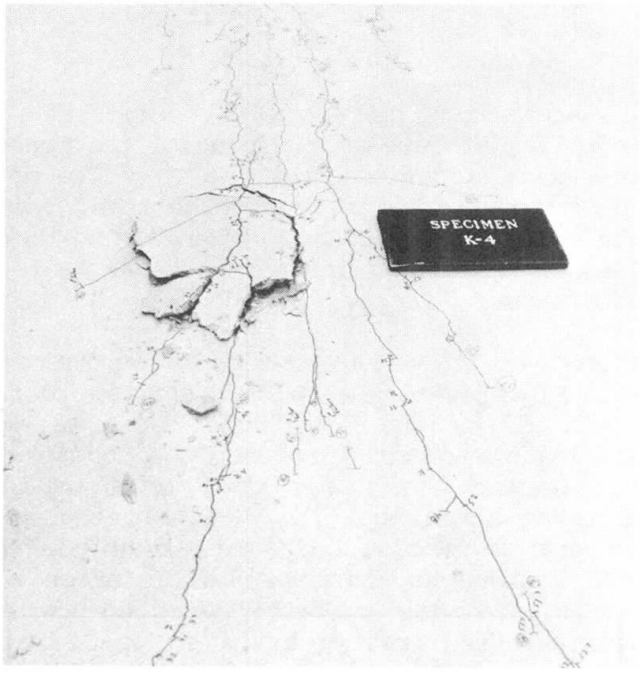

Fig. 4 Concrete Failure

Push-off tests on the three partial assemblages (T-1, T-2 and T-3) reproduced failure patterns similar to that observed in specimen K-4. Once again, straight transverse reinforcement in addition to the wire mesh had only marginal effect on the stub-girder capacity although the bent bars were more effective. Specimen T-3 with the bent transverse bars recorded a 12% increase in ultimate strength compared to specimen T-2 which did not have additional transverse bars. The ribbed metal deck, clear cover and longitudinal reinforcement prevented the placement of the reinforcement in the bottom half of the slab where it may be more effective.

The above-mentioned full scale tests were all carried out on isolated stub-girders. It has recently been reported [17] that an isolated stub-girder is more susceptible to longitudinal shear failure than a girder in a stub-girder system. Researchers at the Louisiana State University reached this conclusion after conducting experiments on an isolated stub-girder model and on a scale model of a two-bay stub-girder floor system.

As part of a M.Sc. thesis project, T.W.K. Chan [3] carried out push-off tests on 42 stub-slab assemblages to simulate the behaviour observed in the full-size tests of stub-girders. This investigation led to the formulation of a set of simple and practical design criteria for 13 mm headed studs.

Two recent developments, although not directly related to the behavior of steel-concrete composite connections, confirmed the versatility of the stub-girder floor system. The first is related to the dynamic response of the system. While the Nova building was under construction in Calgary, researchers from the University of Alberta instrumented two full bays of the sixth floor with accelerometers. Test results [15] revealed very low level of vibrations and the stub-girder system received very high recommendations from the investigators. The second development involves the first successful use of stub-girders as part of a rigid frame system. This feat was recently accomplished in a four story building in Mexico City [20].

4. CONCLUDING REMARKS

In summary, two critical areas can be readily identified. Firstly, the stub-girder is susceptible to failure due to crushing of the concrete slab over the interior end of the end stub (location 1 in Fig. 5). Use of a wide centre concrete flute over the stubs together with transverse reinforcement placed at a lower level would likely remedy the problem. There is a lack of consensus among researchers on this issue [13, 19]. There is a definite need for further investigation in this general area.

The second critical area concerns the fillet welds along the interior end of the end stubs (location 2 in Fig. 5). These welds are prone to fracture due to excessive prying forces. In all of the full scale tests carried out at the University of Saskatchewan, loads were not placed on the concrete slab but were applied through the floor beams. This was done to simulate the loading condition likely to exist in an actual building. Some researchers [6] are of the opinion that observed prying forces could have been due to the loading system used. However, weld failure at this critical location was reported in full scale test [12] where loading was in fact placed on the concrete slab. The presence of prying forces was first observed in small size stub-girder tests where loads were also applied on the concrete slab [14].

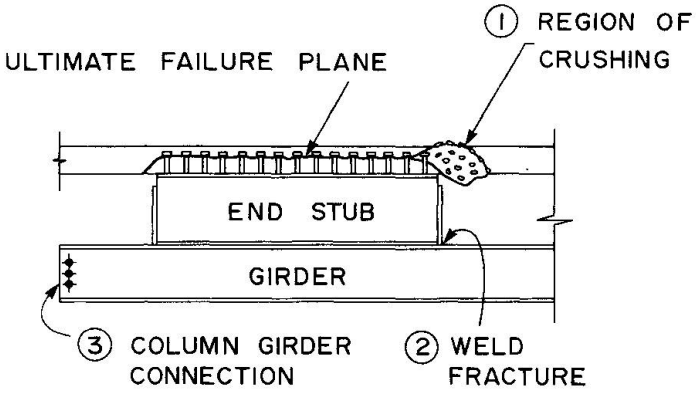

Fig. 5 Critical Areas

Mills [16] reported a third critical area, i.e. the connection between the column and the stub-girder (location 3 in Fig. 5). Slotted holes, loosely fastened bolts etc. have been used to eliminate unwanted bending in the columns. The concrete slab may require additional crack control reinforcing bars [4]. However, a rational way to solve this problem and at the same time achieve an overall construction saving is to modify the end details completely. The junior author is presently working on this project with technical assistance from the Canadian Institute of Steel Construction. Results of forthcoming full scale tests and analytical study are expected to answer some important questions and hopefully lead to the development of some specific design criteria.

ACKNOWLEDGEMENTS

The authors would like to thank the Canadian Institute of Steel Construction and the Bethlehem Steel Company for the information which they provided. The assistance of Heather Larson, who typed the manuscript, is gratefully acknowledged.

REFERENCES

1. BJORHOVDE, R. and ZIMMERMAN, T.J., Some Aspects of Stub-Girder Design, Engineering Journal, AISC Vol. 17, 1980, No. 3, pp. 54-69.
2. BUCKNER, C.D., DEVILLE, D.J., McKEE D.C., Shear Strength of Slabs in Stub-Girders, Journal of Structural Division, ASCE, Vol. 107, No. ST2, Feb. 1981, pp. 273-280.
3. CHAN, T.W.K., REZANSOFF, T. and HOSAIN, M.U., Behaviour of Headed Shear Studs in Stub-Girder Stub Assemblages, Proceedings of the 1984 CSCE Annual Conference, Halifax, Nova Scotia, May 20-25, 1984, pp. 309-326.
4. CHIEN, E.Y.L. and RITCHIE, J.K., Design and Construction of Composite Floor Systems, Published by the Canadian Institute of Steel Construction, Toronto, Canada, September, 1984.
5. COLACO, J.P., A Stub-Girder System for High-Rise Buildings, AISC Engineering Journal, July, 1972, pp. 89-95.

6. CREED, M.W., Analysis and Testing of Stub-girders in a Building Structure, M.Sc. Thesis, Dept. of Civil Engineering, North Carolina State University, Raleigh, 1984.
7. GOSSELIN, G.C., and HOSAIN, M.U., Failure of Stub-Girders due to Longitudinal Shear, IABSE Periodica P-74, May, 1984.
8. GOSSELIN GUY, REZANSOFF T. and HOSAIN, M.U., Shear Failure Characteristics of Stub-Girders, Structural Engineering Report No. 20, September, 1980, University of Saskatchewan, Saskatoon, Canada.
9. GUNNIN, BILL L., The First International Building in Dallas, Texas, Acier Stahl Steel No. 3, 1976.
10. HOSAIN, M.U. and KULLMAN, R.B., Stub-Girder: An Innovative Structural Floor System for Highrise Buildings, Proceedings of the 3rd International Conference on Tall Buildings, Hon Kong and Guangzhou, December 10-15, 1984.
11. HOSAIN, M.U., and TSE, C., Failure Mechanisms of Stub-Girders, Proceedings of the 5th ASCE EMD Specialty Conference, Laramie, Wyoming, August 1-3, 1984.
12. INRYCO, INC., Report of Composite Girder Test, Project No. 1063, December 15, 1971.
13. KULLMAN, R.B. and HOSAIN, M.U., Shear Capacity of Stub-Girders: Full Scale Tests, ASCE Journal of Structural Engineering, Vol. III, No. 1, January 1985, pp. 56-75.
14. LAM, Y.W., REZANSOFF, T. and HOSAIN, M.U., An Experimental Investigation of Stub-Girders. Proceedings of the International Symposium on Behaviour of Building Systems and Building Components, Vanderbilt University, Nashville, Tennessee, March 8-9, 1979, pp. 365-384.
15. MATTHEWS, C.M., MONTGOMERY, C.J. and MURRAY, D.W., Designing Floor Systems for Dynamic Response, Structural Engineering Report No. 106, Dept. of Civil Engineering, University of Alberta, Edmonton, Canada, Oct. 1982.
16. MILLS, R.W., 401 West Georgia, Vancouver, B.C., Proceedings, Canadian Structural Engineering Conference, February, 1984, CISC, 300-201 Consumers Road, Willowdale, Ontario, Canada, M2J 4G8.
17. NADASKAY, A.J. and BUCKNER, C.D., A Scale Model Test of Stub-Girder Systems, Louisiana State University, 1983.
18. Pittsburg Testing Laboratory Report No. PG-6742, Built-Up Composite Girder Test-Project 201192131, January 11, 1972.
19. RITCHIE, J.K. and CHIEN, E.Y.L., Current Canadian Structural Research - Some Practical Aspects, Presented at the 3rd International Colloquium, Structural Stability Research Council, Toronto, Canada, May 9-11, 1983.
20. ROMERO, E.M., Continuous Stub-Girder Structural System for Buildings: A Case Stury, University of Mexico, February, 1983.
21. Steel Structures for Buildings - Limit States Design, Canadian Standards Association Standard No. CAN3-S16.1-M78, Rexdale, Ontario, Dec. 1978.
22. ZIMMERMAN, T.J.E. and BJORHOVDE, R., Analysis and Design of Stub-Girders, Structural Engineering Report No. 90, University of Alberta, Edmonton, Canada, March, 1981.

Neue Stahlbetonverbundkonstruktionen in der UdSSR

New Composite Steel-Reinforced Concrete Constructions in the USSR

Nouvelles structures mixtes acier-béton armé en URSS

N.N. STRELETZKI
Professor
Melnikow-Institut
Moskau, UdSSR

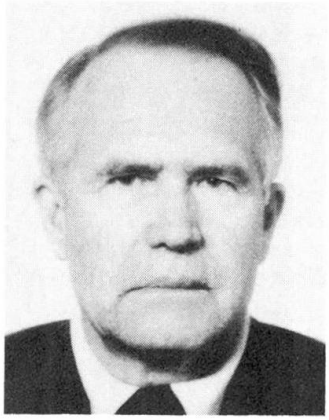

N.N. Streletzki wurde 1921 geboren. 1947 hat er das Moskauer Bauinstitut absolviert. Er führt Lehr- und Forschungsarbeit und spezialisiert sich auf den Metallbau, Stahlbetonverbundkonstruktionen und die Theorie der Grenzzustände. Er ist Abteilungsleiter für Ingenieurbauten.

Ju.S. MARTINOW
Kand. techn. Wissenschaften
Polytechnische Hochschule
Minsk, UdSSR

Ju.S. Martinow wurde 1937 geboren. 1961 hat er die Polytechnische Hochschule in Belorussien (UdSSR) absolviert. Er spezialisiert sich auf theoretische und experimentelle Untersuchungen der Stahlbetonverbundkonstruktionen. Er ist Kathederleiter für Metall- und Holzkonstruktionen.

E.I. CHAJUTIN
Kand. techn. Wissenschaften
Polytechnische Hochschule
Minsk, UdSSR

E.I. Chajutin wurde 1953 geboren. Er hat die Polytechnische Hochschule in Belorussien (UdSSR) absolviert. Er spezialisiert sich auf Stahlbetonverbundkonstruktionen der Industriegebäude. Er ist Kathederlehrer für Metall- und Holzkonstruktionen.

ZUSAMMENFASSUNG

Der Vortrag beschreibt neue Konstruktionen für Eisenbahnbrücken, Autobahnbrücken und Überdachungen, bei welchen eine vorgefertigte Stahlbetonplatte mit Stahlträgern oder Fachwerken durch HV-Schrauben oder Schweissverbindung verbunden wurden. Ferner werden eine neue Verbunddeckenkonstruktion unter sehr starken Belastungen und Versuchsergebnisse aufgezeigt.

SUMMARY

The report describes new forms of construction of railway and highway bridges, building roofs using high-strength bolts and welded connections of reinforced concrete plates to steel beams or trusses without cast-in-place processes, as well as a new structure of composite steel-reinforced concrete floors subjected to extremely heavy loads. Some experimental results are given.

RÉSUMÉ

Ce rapport décrit de nouvelles structures mixtes acier-béton (ponts-rails, ponts-routes, toitures de bâtiments) dont la dalle est préfabriquée et liée à la charpente métallique par boulonnage HR ou soudure. Un exemple de plancher construit selon ce principe, et supportant de très fortes charges est présenté. Des résultats de recherches sont donnés.

1. TRADITIONELLE KONSTRUKTIONEN

In der UdSSR finden eine breite Verwendung Stahlbetonverbundkonstruktionen als stählerne Vollwandträger oder Fachwerkbinder, die zur Mitwirkung mit einer vorgefertigten Stahlbetonplatte vereinigt sind. Die bevorzugte Verwendung vorgefertigter (anstatt monolithischer) Platten wird erklärt: durch die Notwendigkeit den Arbeitsaufwand an der Baustelle höchstmöglich zu vermindern, durch einen hohen Grad der Vereinheitlichung, Typisierung und Standardisierung der Konstruktionen, durch eine genügende Anzahl der Werke für Herstellung vorgefertigter Stahlbetonkonstruktionen und rauhe klimatische Verhältnisse am grösseren Teil des Landes.

Die Vereinigung einer vorgefertigten Stahlbetonplatte mit Stahlträgern oder Stahlbindern wird gewöhnlich durch steife Stützen erreicht, die in den Plattenfenstern und -fugen mit feinkörnigem Beton vergossen werden [1]. Zwischen dem Stahlobergurt und der Platte wird eine Ausfüllung aus demselben Material gemacht, die eine Korrosion des Obergurts vorbeugt und einen vertikalen Druck des Stahlbetons auf den Stahl überträgt. Die Mängel dieses Verfahrens bestehen in einem bedeutenden Arbeitsaufwand und Gütekontrollschwierigkeiten bei dem Vermörteln einer grossen Anzahl kleiner Räume; die Schwierigkeiten erhöhen sich stark in einer kalten Jahreszeit; die Sicherungs- und Gütekontrolle der Ausfüllung stellt eine besondere Schwierigkeit dar; bei mehrmaligen wiederholten Belastungen kommen nach einigen Jahren der Ausnutzung Zerstörungen der Verbindungsfugen vor.

2. NEUE KONSTRUKTIONEN FÜR EISENBAHNBRÜCKEN

In letzter Zeit erschienen neue Lösungen des Problems der Vereinigung einer vorgefertigten Stahlbetonplatte mit Stahlträgern oder Stahlbindern, die keine obengenannte Mängel haben[1].

Die in der UdSSR verwendeten Verbundtragwerke der Eisenbahnbrücken sind durch zwei Stahlträger gekennzeichnet, die einen 2,0...2,3 m-Achsenabstand haben, durch einen gleichbleibenden Querschnitt der Stahlobergurte und durch die Einrichtung der Stahlbetonlängsrippen über den Stahlträgern, um einen konstruktiv annehmbaren Querschnitt der Untergurte zu bekommen, da die Höhe der Stahlträger zur

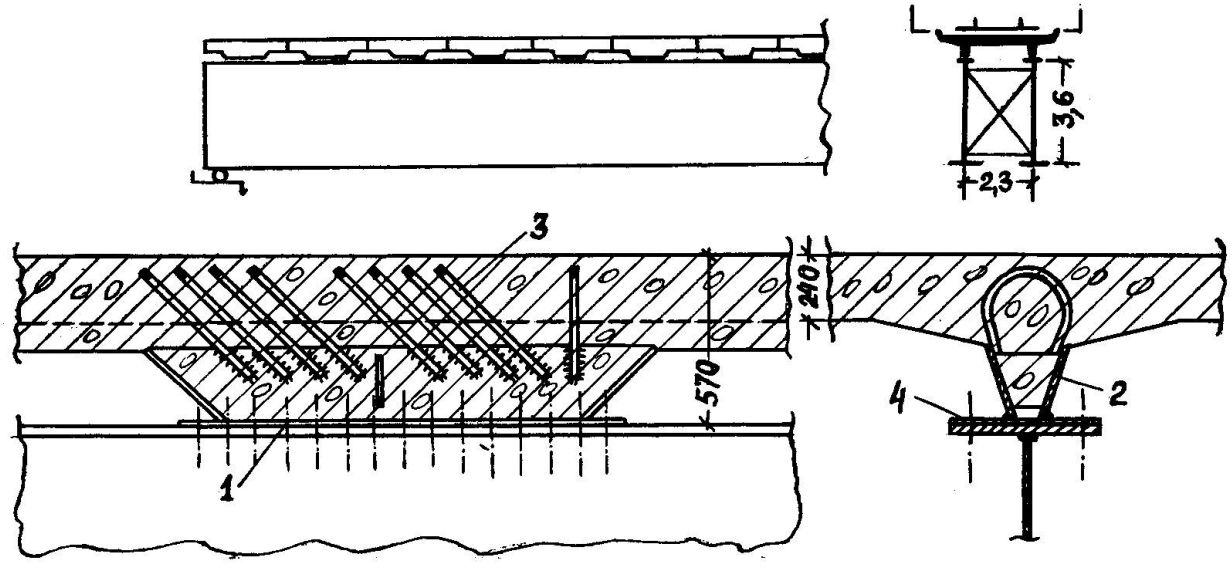

Fig. 1. Eisenbahnbrückenkonstruktion

Erreichung dieses Zwecks ungenügend ist. Die Vereinigung einer vorgefertigten Stahlbetonplatte mit Stahlträgern (Fig. 1) in diesen Tragwerken wird durch HV-Reibschraubenverbindungen (1), Einlegeteile (2) in Längsrippen und geneigte Schlaufenanker (3) realisiert.

Die Blöcke einer vorgefertigten Stahlbetonplatte werden in metallischen Schalungsformen gefertigt, die gleichzeitig als Lehrgerüst für eine genaue Anordnung der Einlegeteile dienen. Jeder Block hat zwei Einlegeteile, je einen über jedem Stahlträger. In Zwischenräumen der Einlegeteile gibt es eine für das Anstreichen genügende Spalt. Die Vereinigung ist absolut trocken, die Ausfüllung und das Vermörteln werden nicht verwendet.

Da die Trägerobergurte keine ideele Form haben können (Pilzförmigkeits- und Verkantungstoleranze werden mit vielen Millimeter gemessen), bilden sich zwischen den Horizontalen der Einlegeteile und den Trägerobergurten bei dem Aufstellen eines Stahlbetonblocks auf Stahlträger vorläufige Spalten aus. Diese Spalten werden durch das Aufziehen der HV-Schrauben vollkommen beseitigt, wozu Horizontale (4) der Einlegeteile möglichst schlank gemacht werden - mit einer minimalen Dicke und maximal möglichen Flanschüberhängen. Zur Sicherung eines mühelosen Aufstellens der HV-Schrauben ohne Lochausbohren bei der Montage sollen Lochdurchmesser in Horizontalen der Einlegeteile und in Trägerobergurten um 6 mm grösser als der Bolzendurchmesser sein. Die Erfahrung zeigt, dass eine solche Durchmesserdifferenz bei möglichst zufälliger Nichtübereinstimmung vereinigender Konstruktionen im Grundriss ganz genügend ist.

Die Querfugen zwischen Plattenblöcken werden in zwei Varianten verwendet: traditionelle (mit dem Schweissen der Anschlussbewehrung und dem Vermörteln) und vorgepresste geklebte bei glatten Blockstirnwänden. Das Vermörteln der Querfugen ist technisch wesentlich leichter als das Vermörteln steifer Stützen und die Fertigung der Ausfüllung.

3. KONSTRUKTIONEN FÜR AUTOBAHNBRÜCKEN

Traditionelle Stahlbetonverbundstützweiten der Autobahnbrücken haben zwei Stahlhauptträger mit einem Achsenabstand von 6,4... ...7,6 m und einem Längsträger dazwischen, der sich auf Querverbände stützt und die Felder einer vorgefertigten Stahlbetonplatte um halb so gross macht. Die Platte ist fast eben, sie vereinigt sich durch steife Stützen mit einer Stahlkonstruktion und hat über dem Längsträger eine Längsfuge. In dieser Fuge entstehen bei mehrmals wiederholten Belastungen besonders oft Zerstörungen.

Es wurde mit der Verwendung einer neuen Konstruktion der Verbundtragwerke für Autobahnbrücken begonnen - ohne Längsträger, mit Stahlbetonquerrippen für 6,4...7,6 m- Stützweiten. Die Platte entfernt sich dabei von Obergurten der Hauptträger, was eine trockene Vereinigung mit HV-Schrauben und Einlegeteilen ermöglicht und den Stahlverbrauch wegen der vergrösserten Konstruktionshöhe vermindert. Eine Stahlersparnis bekommt man auch durch das Nichtvorhandensein des Längsträgers und die Erleichterung der Querverbände. Es wird sich die betriebsnichtsichere Plattenlängsfuge beseitigt. Die vorgefertigte Stahlbetonplatte bildet sich aus Zweikonsolblöcken mit einer Masse von 8...10 t, die im Stahllehrgerüst gefertigt sind und in zwei Varianten bestehen: gerippte (mit zwei Rippen) aus normalem Stahlbeton oder vorgespannte T-förmige (mit einer Rippe). Da die Stahlbetonrippe anders angeordnet sind und

die Obergurtdicke veränderlich ist, was für Autobahnbrücken (besonders für durchlaufende) typisch ist, kann die Konstruktion nach der Fig. 1 für die trockene Vereinigung des Stahls und des Betons nicht gebraucht werden. Für die Gewährleistung einer sicheren Montierbarkeit und einer hohen Qualität werden in der neuen Konstruktion der Autobahnbrücken (Fig. 2) Paarwinkel (1) verwendet, die in beiden Schenkeln Bohrlöcher eines erweiterten Durchmessers für HV-Schrauben haben. Bei einer veränderlichen Dicke des Stahlobergurtes entspricht die Winkelmarkenzahl der Dickenzahl. Die Winkelmarken zeichnen sich durch die verschiedene Höheanordnung der Bohrlöcher in vertikalen Winkelschenkeln aus. Das sichert die Anordnung der Stahlbetonplatte in derselben Ebene über die ganze Länge des Tragwerks.

Bei einer Stahlbetonplatte aus Blöcken mit zwei Rippen hat jeder Block zwei Einlegeteile (4), die zwischen Blockrippen über Stahlträgern liegen und im Hauptteil der Platte mit steifen Stützen (6) und in Rippen- mit schlanken zylindrischen Stützen (6) befestigt sind. Durch einen Einlegeteil wird vor allem die Schubkraft T aus der Stahlkonstruktion an die Stahlbetonplatte übertragen. Da die Platte vom Stahlobergurt für eine Höhe "h" entfernt ist, entsteht ein bedeutendes Moment $Th = M_s + M_b$. Das Moment M_s wird durch einen Stahlträger aufgenommen, und das Moment M_b - durch eine Stahlbetonplatte. Dementsprechend ist die HV-Flanschenverbindung (7) auf die Schubkraft T und das Moment M_s zu berechnen, die über einen Einlegeteil an den Stahlträger übertragen werden, und die schlanken zylindrischen Stützen - auf die Übertragung an die Stahlbetonplatte des Moments M_b. Die steifen Stützen werden nur auf die Übertragung der Schubkraft T geprüft. Bei der Festigkeitsberechnung einer Stahlbetonplatte werden Biegemomente berücksichtigt, die aus dem Moment M_s in Querschnitten in der Nähe von äusseren Rippenkanten in der begrenzten Plattenbreite entstehen.

Ein HV-Schraubenreibbefestigen der Stahlbetonplattenblöcke an die Stahlträgerobergurte sofort nach dem Aufstellen eines jeden Blocks erhöht heftig die Stabilität der Stahlträger bis zur Zeit des Einschlusses der Stahlbetonplatte in die Arbeit.

4. DECKENKONSTRUKTIONEN

Im industriellen und gesellschaftlichen Bauen der UdSSR haben sich

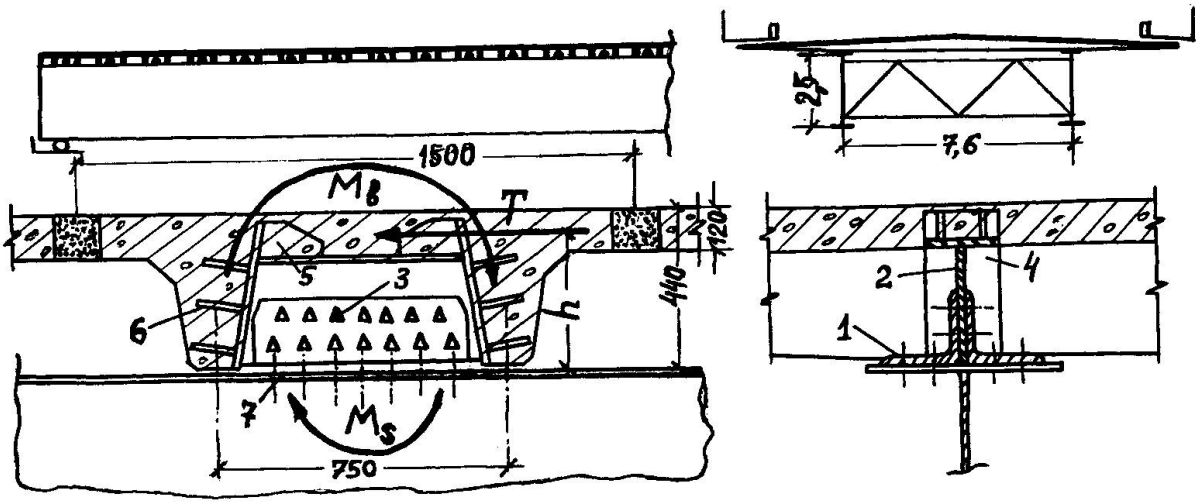

Fig. 2. Autobahnbrückenkonstruktion

Verbunddecken und Verbundzwischendecken gut bewährt. Hier werden Prinzipien der Vereinigung industrieller Konstruktionselemente effektiv ausgenutzt, die eine weite Verwendung im Massenbau finden.

Die weiteste Verwendung fanden Deckensysteme aus Stahlbindern mit einer 24...36 m- Spannweite und aus vorgefertigten 3x6, 3x12 m - Stahlbetonplatten. Die Mitwirkung der Deckenelemente wird durch Verbindungsteile in Fugen zwischen Platten und deren nachfolgendem Vermörteln gesichert. Die vieljährige Erfahrung bei der Verwendung vorgefertigt-monolithischen Stahlbetonverbunddecken zeigte, dass der Stahlverbrauch zu 25% sinken kann [2]. Der Mangel dieser Systeme besteht in einer Erschwerung der Bau- und Montagearbeiten, was vom Vermörteln der Verbindungsfugen "Stahl-Beton" abhängt.

Die neulichen experimentell-teorethischen Untersuchungen im Polytechnischen Institut in Belorussien und im Forschungsinstitut für Baukonstruktionen ergaben eine neue Form der Stahlbetonverbunddecken. Sie sieht die Vereinigung einer vorgefertigten Stahlbetonplatte mit Stahlbindern durch das Montageschweissen der Einlegeteile der Standardplatten vor, die bei Decken ohne Sicherung der Mitwirkung des Stahlbetons und des Stahls verwendet werden (Fig. 3, a, b). Der Vorzug dieser Konstruktionen gegenüber vorgefertigt-monolithischen Konstruktionen besteht in der Bewahrung traditioneller Aufbautechnologie vollvorgefertigter Decken und in der Benutzung handelsüblicher Stahlbetonplatten. Das erlaubt den Bauarbeitsaufwand wesentlich zu erniedrigen und den Nutzeffekt der Stahlbetonverbunddecken im Rahmen der in der UdSSR gültigen Nomenklatur vereinheitlichter Bauelemente der Gebäude zu erhöhen.

Im Polytechnischen Institut in Belorussien wurde eine universelle

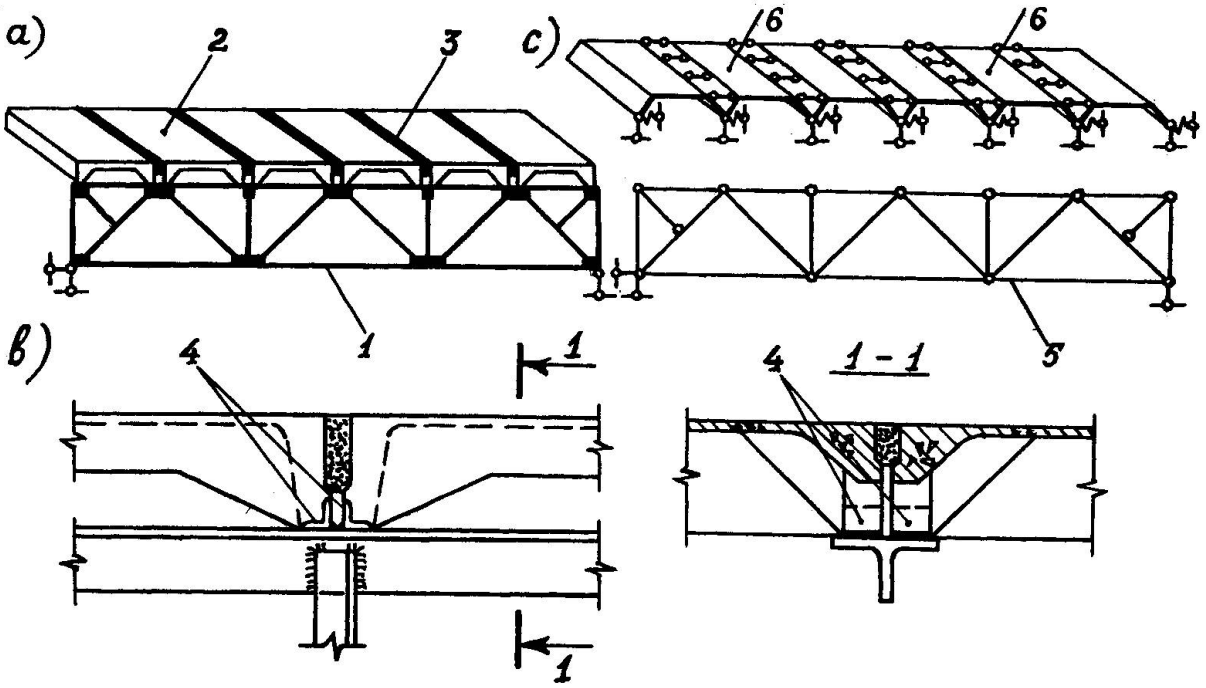

Fig. 3. Verbunddecke: a - Konstruktion; b - Platte-Binder-Verbindungsknoten; c - Berechnungsschema; 1 - Binder; 2 - Platte; 3 - Vergussbeton; 4 - Einlegeteile; 5, 6 - Randsuperelemente "Binder" und "Platte".

Methodik der räumlichen Berechnung vorgefertigter und vorgefertigt-monolithischer Stahlbetonverbunddecken erarbeitet [3]. Ihre Grundlage bildet die Methode der finiten Elemente. Eine Decke teilt sich in Knoten oder Fugen der Vereinigung von Stahlbindern und Stahlbetonplatten in zwei Gruppen der finiten Superelemente: "Binder" und "Platten" (Fig. 3, c). Die Methodik berücksichtigt konstruktive und technologische Besonderheiten der Decke: das Vereinigungsverfahren der Binder und Platten, deren Montagefolge, die Nachgiebigkeit der Verbindungsknoten (Fugen) u.s.w. Die Methodik ist für ER-Einrichtungen geeignet. Sie bekam eine experimentelle Bestätigung durch Versuche mit einem grossformatigen Stahlbetonverbunddeckenfragment (Massstab 1:3) mit einer Schweissverbindung (Fig. 4). Die erfüllten Berechnungen und Versuche haben gezeigt, dass in dieser Decke die Entlastung des Stahlbinderobergurts im Ausnutzungsstadium 75...78% beträgt und im ganzen Änderungsbereich rechnerischer Belastung konstant bleibt. Die Verringerung des Metallverbrauchs beträgt daraus im Durchschnitt 10-15%. Das kommt also von der Verminderung des Binderobergurtquerschnitts vor.

5. ZWISCHENDECKEN UNTER SEHR SCHWEREN BELASTUNGEN

Die Zwischendecken im industriellen und gesellschaftlichen Bauen, die grosse (bis zu 200 kN/m^2) Belastungen aus technologischer Ausrüstung aufnehmen können, sind noch ein effektives Anwendungsgebiet für Stahlbetonverbundkonstruktionen. Die erarbeitete konstruktive Lösung stellt Stahlträger als ein- oder (bei Belastungen über 100 kN/m^2) zweiwandige T-Stahlprofile dar, die mit Längssteifrippen verstärkt sind, die durch spezielle Schubverbindungen (Fig. 5) zur Mitwirkung mit einem vorgefertigten oder vorgefertigt-monolithischen Stahlbetonbelag vereinigt werden.

Wie die Versuche gezeigt haben, ergibt eine solche Querschnittsform bei der Berechnung auf die Aufnahme der Schubkräfte Voraussetzungen zur Berücksichtigung der Haftung zwischen Beton zum Vermörteln und dem in seinem Bereich liegenden Stegoberteil. Die

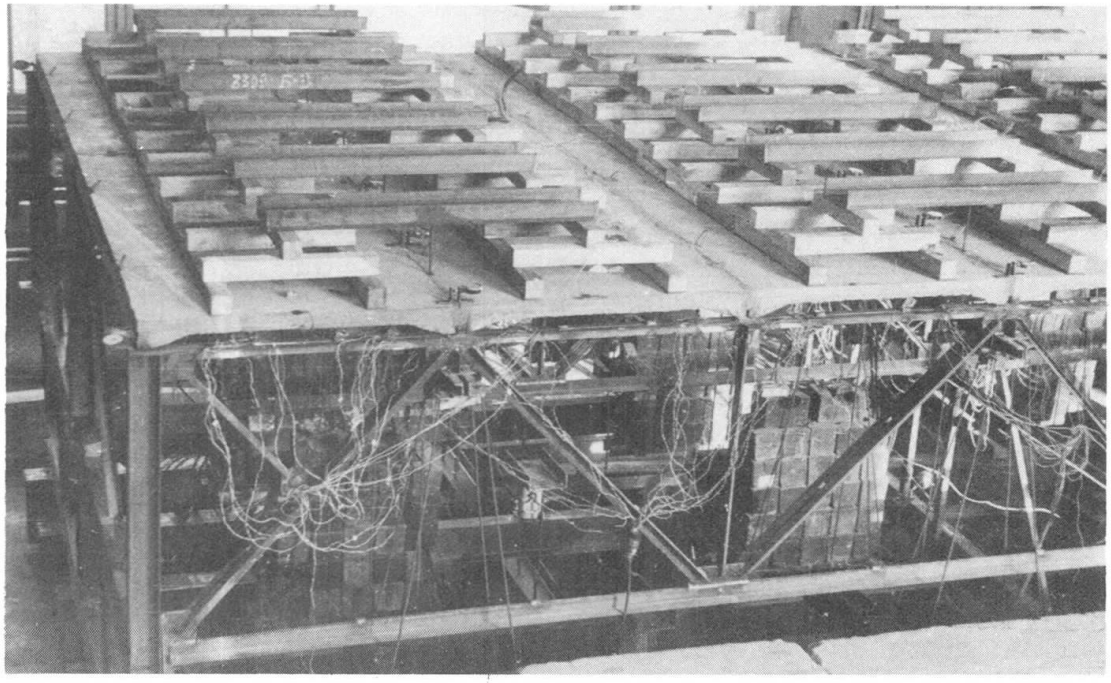

Fig. 4. Versuche mit einem Stahlbetonverbundfragment

versuchsweise ermittelte, rechnerische Haftungskraft kann bei 1 MPa angenommen werden.

Es ist bemerkenswert, dass die Verbundzwischendeckenkonstruktionen eine Reihe von Besonderheiten im Unterschied zu gleichen Brückentragwerksystemen haben. Dazu gehören unbedingt: relativ nicht grosse (8...15 m) Trägerfelder, die Benutzung der Stahlbetonrippenplatten mit entfalteten Rippen und verhältnismässig dünnen Flanschen und der dominierende Einfluss der Querkräfte in allgemeiner Bilanz der Krafteeinwirkungen.

Die teorethischen Untersuchungen mit Berücksichtigung elastoplastischer Betoneigenschaften, Laborversuche mit grossformatigen Modellen und der Naturversuch mit einem Zwischendeckenfragment eines Industriegebäudes haben gezeigt, dass in Verbundzwischendecken die Stahlbetonplatte sich nicht über den ganzen Querschnitt (wie gewöhnlich bei Brückentragwerken) zerstört: der Beton zersplittert in maximal beanspruchten Fibern. Das ermöglichte Kriterien rechnerischer Festigkeitsgrenzzustände zu begründen, wofür entweder die Erscheinung plastischer Verformungen im Trägerstahluntergurt oder der rechnerische Grenzwert der maximalen Faserverformung des Belagbetons gehalten wird. Auf Grundlage dieser Kriterien wurden rechnerische Hauptlastfälle bestimmt, die entweder eine elastische Arbeit der Querschnittselemente oder die Entwicklung plastischer Teilverformungen in maximal beanspruchten Plattenbereichen voraussetzen [4].

Das zweite kennzeichnende Merkmal einer Verbundzwischendecken ist das hohe Niveau der Querkräfte. Gewöhnlich wird die Berechnung einer Verbundkonstruktion auf Schubspannungen mit der Annahme durchgeführt, dass deren Aufnahme nur durch einen Stahlsteg gesichert ist. Dieser Standpunkt kann nur bei Trägern des Brückenbaus begründet gelten, wo die geringe Dicke der Stahlbetonplatte die Übergabe darin der Schubspannungen ausschliesst und wo wegen der grossen Querschnittshöhe die Stegdicke gewöhnlich aus Bedingungen der örtlichen Stabilität bestimmt wird. In angeführter Zwischendeckenkonstruktion ist die Stegdicke mit der Querschnittsbeanspru-

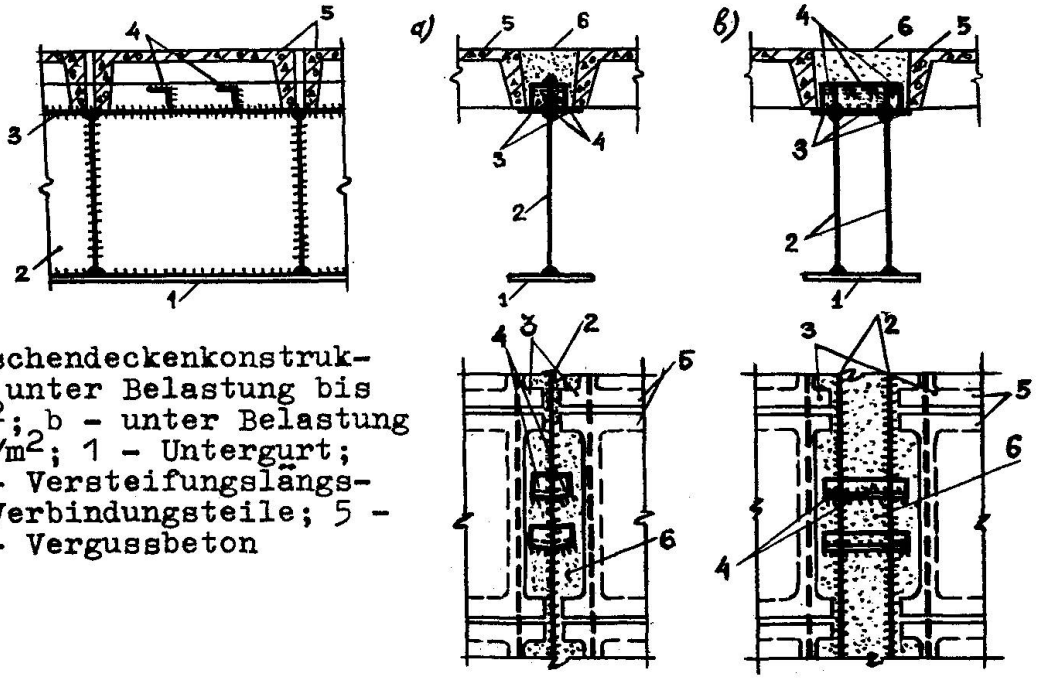

Fig. 5. Zwischendeckenkonstruktionen: a - unter Belastung bis zu 100 kN/m^2; b - unter Belastung über 100 kN/m^2; 1 - Untergurt; 2- Steg; 3 - Versteifungslängsrippe; 4 - Verbindungsteile; 5 - Platten; 6 - Vergussbeton

chung auf Schub an der Stütze begrenzt, und der mächtige Stahlbetonteil macht Voraussetzungen für die Teilquerkraftübergabe an den Beton.

Wie teorethische und experimentelle Untersuchungen gezeigt haben, arbeitet der Stahlbetonteil aktiv mit, indem er bis zu 30% der Querkraft aufnimmt, die im vereinigten Querschnitt wirkt. Am intensivsten wird dabei die Querkraft durch eine Längsrippe aufgenommen, die mit Stirnrippen vorgefertigter Platten und dem Vergussbeton gebildet ist. Es wurde 2 Kriterien der Grenzzustände der Stahlbetonverbundträger bei der Querkraftbeanspruchung bestimmt:

- das Erreichen eines Schubspannungsgrenzwertes im Stahlsteg eines Verbundquerschnitts;
- das Erreichen eines Schubspannungsgrenzwertes im Plattenrippenbeton in der Höhe eines Stützenoberteils, der durch die rechnerische Betonzugfestigkeit ausgedrückt ist.

Auf Grund dieser Kriterien wurde eine technische Berechnungsmethodik erarbeitet.

LITERATURVERZEICHNIS

I. СТРЕЛЕЦКИЙ Н.Н. Сталежелезобетонные пролетные строения мостов. Изд. "Транспорт", Москва, 1981.

2. МАРТЫНОВ Ю.С., ШАТИЛО А.И. Сталежелезобетонные конструкции покрытий и перекрытий в промышленном строительстве БССР. – Строительство и архитектура Белоруссии, 1982, № 3, с.37–38.

3. МАРТЫНОВ Ю.С., АЛЕКСАНДРОВИЧ А.С. К вопросу о методике статического расчета сталежелезобетонных решетчатых покрытий с объединением на сварке. –Техника, технология, организация и экономика строительства: Строительная механика и строительные конструкции, 1984, вып.10, с.98–102.

4. МАРТЫНОВ Ю.С., ХАЮТИН Е.И. Особенности проверки прочности объединенных балок с развитой железобетонной частью. – Техника, технология, организация и экономика строительства: Строительная механика и строительные конструкции, 1984, вып.10, с.103–107.

Local Buckling of Concrete Filled Steel Square Tubular Columns

Voilement local de colonnes mixtes en tubes carrés remplis de béton

Örtliche Beulen von betongefüllten, quadratischen Hohlprofilstützen

Chiaki MATSUI
Professor
Kyushu University
Fukuoka-Shi, Japan

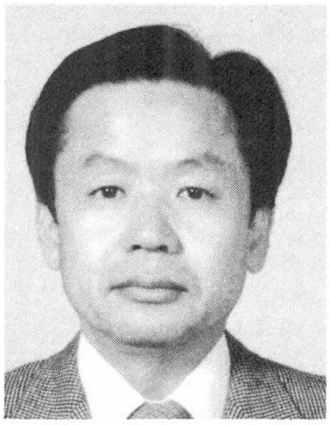

Chiaki Matsui, born 1937, graduated from the Department of Architecture, Kyoto University in 1962, received a doctorate in engineering at Kyoto University in 1971. He has worked at Kyushu University since 1968 and has been a professor since 1980. His researches have been concerned with strength and behaviour of steel and composite structures.

SUMMARY

This paper presents a new limiting value of the width-to-thickness ratio for plate elements of concrete filled steel square tubular columns. The new value is derived from the comparison of the post buckling behavior of concrete filled tubular members with that of hollow tubular members from the viewpoint of equivalent energy absorption capacity. The post buckling behavior is obtained on the basis of plastic limit analysis for collapse mechanisms due to local buckling of tubes. The proposed value is about 1.5 times of that currently used for steel structures.

RÉSUMÉ

Cet article présente une nouvelle valeur du rapport épaisseur/largeur des faces des colonnes formées de tubes carrés remplis de béton. Cette nouvelle valeur est tirée de la comparaison entre le comportement au voilement des tubes creux et celui de ces mêmes tubes remplis de béton, en considérant l'énergie d'absorption. Le comportement post-critique est obtenu en analysant le mécanisme plastique du voilement local des tubes. La valeur proposée est d'environ 1,5 fois supérieure à celle utilisée couramment en construction métallique.

ZUSAMMENFASSUNG

Dieser Beitrag beschreibt einen neuen begrenzenden Wert des Breite/Dicke-Verhältnisses von Plattenelementen bei betongefüllten, quadratischen Hohlprofilstützen. Der neue Wert wird abgeleitet aus dem Vergleich des Beulverhaltens im überkritischen Bereich von betongefüllten Hohlprofilelementen mit demjenigen von Hohlprofilelementen unter dem Gesichtspunkt eines gleichwertigen Energieaufnahme-Vermögens. Das Beulverhalten im überkritischen Bereich, auf der Basis einer plastischen Grenzanalyse für den Bruchmechanismus, verursacht durch ein örtliches Beulen der Hohlprofile. Der vorgeschlagene Wert ist ungefähr 1,5fach grösser als der gegenwärtig bei Stahlbauten angewandte.

1. INTRODUCTION

Strength and behavior of concrete filled steel tubular members have been investigated in Europe, U.S.A. and Japan, and it becomes known that there are many advantages to be gained by combining the properties of steel hollow sections with those of concrete to form a composite column. It is recognized that the load carrying capacity and deformation capacity of these columns are both satisfactory in comparison with those of steel tubular columns or ordinaly reinforced concrete columns.

However, in the design of concrete filled tubular columns, the limiting width-to-thickness ratio of plate elements of a composite column is usually used with the same value as for hollow sections. The ratio is about 50 for mild steel square tubes based on the allowable stress design method in Japan. Other countries have basically adopted the same values. It seems too conservative for concrete filled tubular columns.

This paper presents the results of analyses for plastic collapse mechanisms of tubular columns filled with and without concrete and gives a new limiting value. This value is derived from the comparison of the post buckling behaviors of concrete filled tubular members with those of hollow tubular members from the viewpoint of equivalent energy absorption capacity of the members. The proposed value is about 1.5 times of that currently used for steel structures. This conclusion enables us to construct ductile and low cost building frames by using concrete filled steel tubular columns.

2. EFFECT OF FILLED CONCRETE

The effect of filled concrete on the behavior of frames with steel square tubular columns is discussed. Figure 1 shows the behavior of two frames under constant vertical and varying horizontal loads [1]. Frame A is composed of hollow tubular columns and Frame B is composed of concrete filled tubular columns. The same steel tubular columns and wide flange beams in size and property are used for two frames. The width-to-thickness ratio B/t of the tube is about 47. The limiting value specified in the AIJ design standard for steel structures [2] is $d/t \leq 232/\sqrt{F}$ for square and rectangular tubes of uniform thickness (Fig. 2). Where F is defined as the basic value used in determining allowable stresses and the specified minimum yield point 23.5 KN/cm^2 ($t \leq 40$ mm) is used for mild steel. Using the actual yield stress of the tubes 32.4 KN/cm^2 instead of the specified value, d/t becomes about 41. The radius of the section corner r is nearly equal to plate thickness t, then the limiting value B/t for the tubes becomes 45. The ratio of the tubes is a little over the limiting one. The beam-to-column connections of the frames are designed in order to have enough strength to transfer the stresses from the beams to the columns.

The restoring force of Frame A decreases rather rapidly at the occurrence of web local buckling after flange local buckling of the tubes. However, when the tubes are filled with concrete, the restoring force is strengthened due to the concrete and the behavior is markedly improved, especially in the post local buckling range. The main reasons for the improvement in post buckling behavior are as follows:

1° Collapse mechanism of a concrete filled tube due to local buckling is different from that of a hollow tube.
2° In concrete filled tubes, a part of or all of compression force sustained by the tube can be transfered to the concrete after the occurrence of local buckling.

The reason 1° will be mentioned in the next section in reference to the analyses for post buckling behavior of tubes.

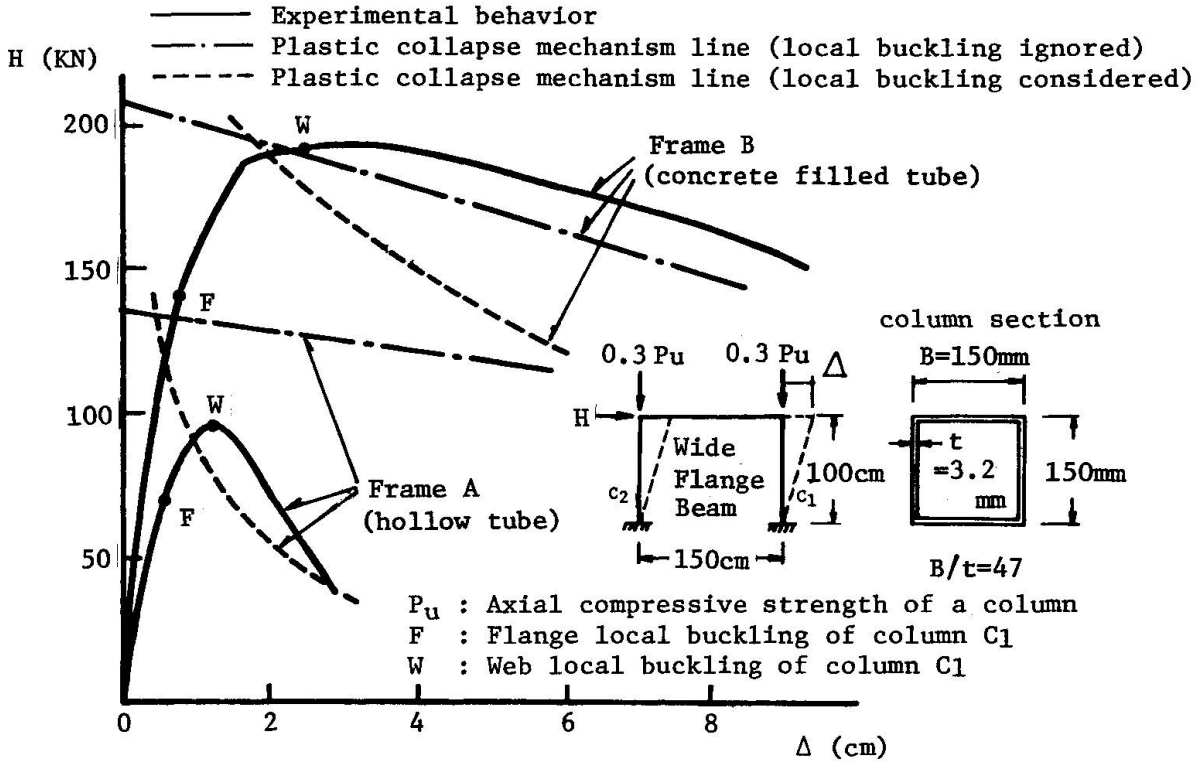

Fig. 1 Behavior of Frames

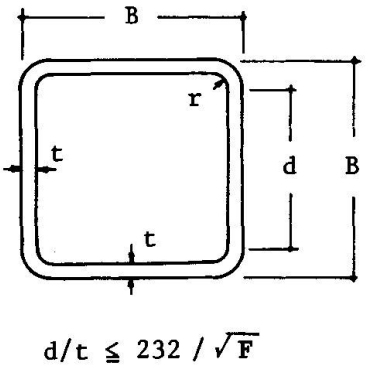

Fig. 2 Shape of Tube

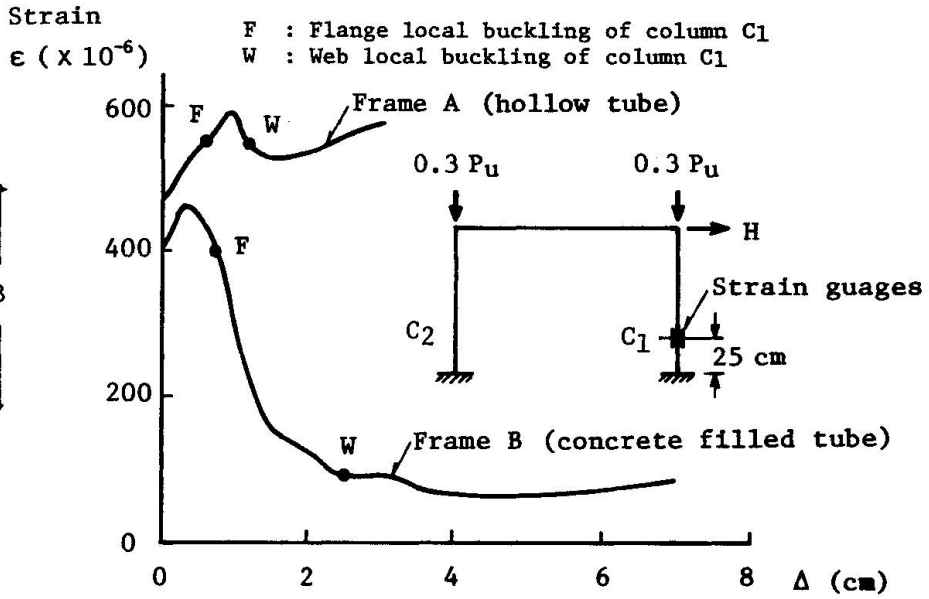

Fig. 3 Change of Average Compressive Strain in Steel Tube

Figure 3 shows an example of supporting bases for 2°. It represents the relationship between average compressive strain of the tube and sidesway displacement of the frame. The strains were measured by two strain gauges at points 25 cm apart from the column end. In Frame B, rapid reduction in strain is observed after the occurrence of local buckling near the column end. From this figure, it is recognized that when the axial rigidity of a tube decreases as a result of the appearance of local buckling in the tube, the compressive force in the tube transfers to the concrete under the condition of constant column axial load.

3. ALLOWABLE COMPRESSIVE LOAD ON A COMPOSITE COLUMN

In the case that the value of constant compressive axial load applied to a composite column exceeds the maximum compressive strength of the concrete, the steel tube must sustain a part of it. The compressive load which a tube must sustain can be obtained from the following manner. In the design of composite columns, allowable compressive load P is recommended in the AIJ standard for Structural Calculation for Steel Reinforced Concrete Structures [3] as follow:

$$P \leqq \frac{1}{3} \cdot {}_cA \cdot F_c + \frac{2}{3} \cdot {}_sA \cdot \sigma_y \qquad (1)$$

where ${}_cA$ and ${}_sA$ are areas of concrete and steel, respectively, F_c compressive strength of concrete and σ_y yield stress of steel. Eq. (1) has been proposed on the basis of the experimental data and it guarantees for a column the deformation capacity of 0.01 rotation angle under cyclic plastic bending moment. It is assumed that the compressive strength of the concrete is equal to ${}_cA \cdot F_c$ and the compressive load P' which a tube must sustain is expressed as $P' = P - {}_cA \cdot F_c$. By substituting Eq. (1) for the equation of P' and expressing yield load of a tube $P_y = {}_sA \cdot \sigma_y$, the following equation can be obtained.

$$\frac{P'}{P_y} = \frac{2}{3} \cdot \left\{ 1 - \frac{F_c}{4\sigma_y} \cdot \frac{(B/t - 2)^2}{(B/t - 1)} \right\} \qquad (2)$$

Figure 4 shows Eq. (2) for three values of a parameter σ_y/F_c which cover the ordinary range of material strengths. From this figure, it is recognized that a tube does not need to sustain compressive force after the occurrence of local buckling under the condition of $B/t > 50$. In this case all compressive load sustained by a tube is able to be transfered to the concrete.

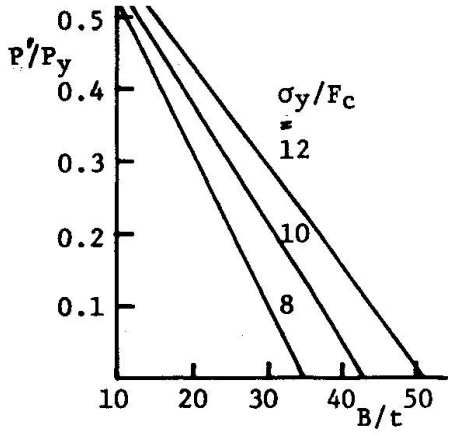

Fig. 4 Axial Force of Steel Tube

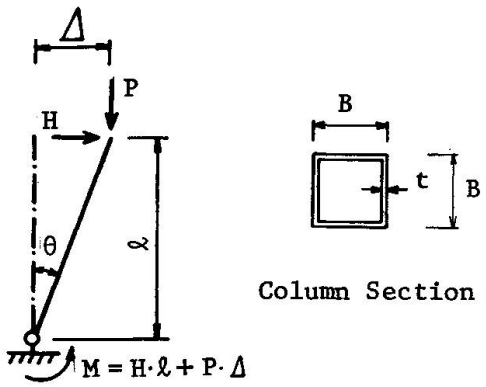

Fig. 5 Analytical Model of a Column

4. PLASTIC COLLAPSE MECHANISM DUE TO LOCAL BUCKLING

The post buckling behavior of steel hollow square tubular columns has been investigated on the base of plastic limit analysis [4]. The same technique can be applied to the analysis for tubes filled with concrete. The deformed configuration of a cantilever column at the post local buckling state is idealized as shown in Fig. 5. The local buckling mechanism is assumed as shown in Fig. 6.

The buckling mode of a tube filled with concrete differs from that of a hollow tube (Fig. 6(d)). In the case of a concrete filled tube, plate elements deform only outside of a section and plastic hinge lines form at the edges of the compression flange as shown in Figs. 6(a), (b), (c). M - θ relation of a model can

be obtained by applying the principle of virtual velocities, and it can be written as follows:

$$M = -P \cdot (\eta - 0.5) \cdot d + D_p / \dot{\theta} \qquad (3)$$

where M denotes the applied moment at the plastic hinge, P the constant vertical load, ηd the distance between compressive flange and neutral axis, d the web depth, $\dot{\theta}$ the virtual angular velocity of the plastic hinge, and D_p the rate of internal energy dissipation. The prime assumptions to estimate the value of D_p are as follows, 1) plate elements are in state of the plane stresses, 2) the material has a rigid-perfectly-plastic characteristic conforming to the yield condition of von Mises. 3) Plastic axial deformation at hinge lines is ignored. 4) Effect of shear force is ignored. The value of D_p is dependent on 3 variables ψ, η and θ (see Figs. 6(a), (b)) that define the form of the local buckling mechanism, and therefore the resisting moment M in Eq. (3) is also dependent on them. Based on the plastic upper bound theorem, the minimum resisting moment among the values computed by Eq. (3) gives a correct solution. Minimum moment is obtained by changing the values of η, ψ for a given value of θ.

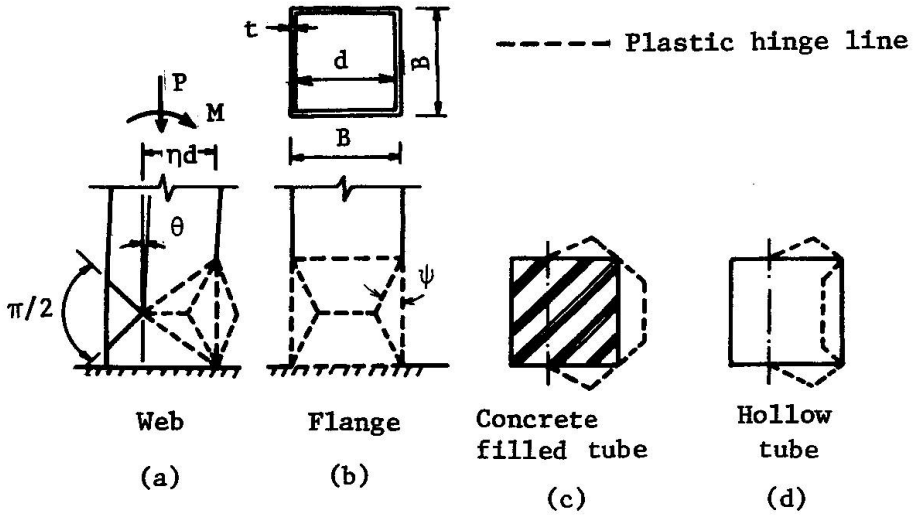

Fig. 6 Collapse Mechanism due to Local Buckling

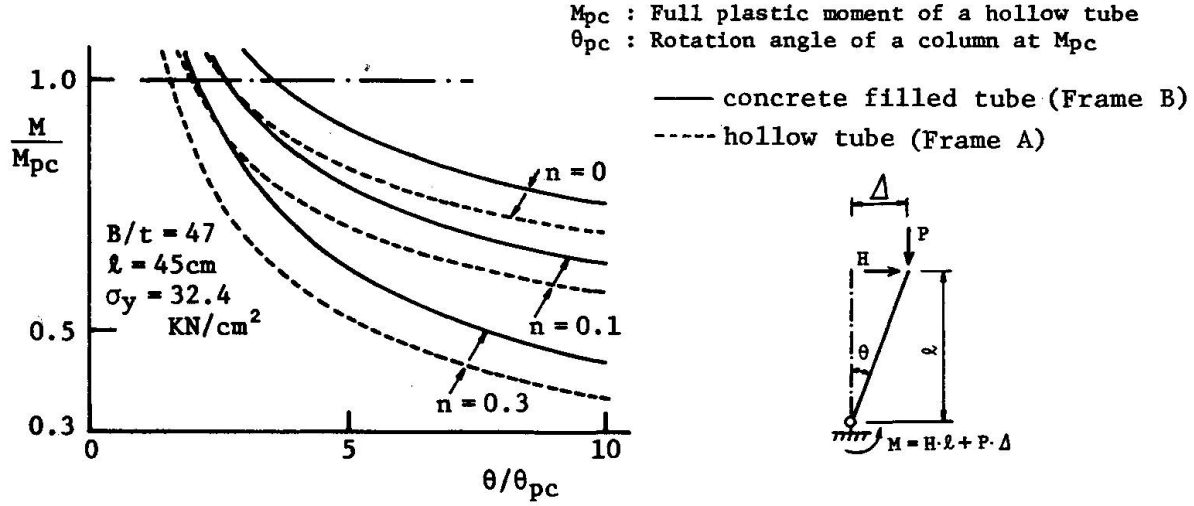

Fig. 7 Post Buckling Behavior of Columns

Figure 7 shows the numerical results for the columns of the frames shown in Fig. 1. The columns are analyzed as a cantilever of 45 cm in length which represents the distance from the inflection point of a column at the collapse mechanism state to the end of the column. There are no remarkable differences in the behavior of two columns having the same axial load ratio n. However, in the case of Frame B, the compressive load in a tube is transfered to the concrete after the occurrence of local buckling. Then, the behavior of a concrete filled column of $n = 0$ should be compared with that of a hollow column of $n \neq 0$. It is recognized that there are remarkable differences in the behavior of the two columns. By using the numerical results, the plastic collapse mechanism lines considered local buckling for two frames are shown in Fig. 1. In the mechanism line of Frame B, the ultimate bending strength of the concrete is calculated under the assumption that compressive stress distribution is rectangular with the constant value of compressive strength F_c and all of the vertical load P is applied to the concrete. The bending strength of a composite column is assumed to be expressed by the superposition of the strength of the tube and the conrete.

5. LIMITING VALUE OF WIDTH-TO-THICKNESS RATIO

Based on the above mentioned considerations, a new limiting value of width-to-thickness ratio for concrete filled steel square tube columns can be derived in the following manner. First, a hollow tube with $B/t = 50$ is selected as a standard member made of mild steel in strength and behavior. $M - \theta$ relations of the model with local buckling mechanism shown in Fig. 6(d) are analyzed under the several values of n by the method of analysis mensioned in section 4. The axial compressive load ratio n as a standard value must be decided. It may be selected in considering the values in the actual columns of building frames. In this study, $n = 0.1$ is chosen as a standard value. The behavior of a column with $B/t = 50$ and $n = 0.1$ is defined as a standard one which is demanded for steel framed structures having minimum strength and deformation capacity (Fig. 8).

Second, $M - \theta$ relations of the models shown in Fig. 6(c) with several values of $B/t > 50$ are analyzed under $n = 0$. The numerical results are shown in Fig. 9. Then, the standard behavior of a hollow tube is compared with that of a concrete filled tube in the view point of equal energy absorption capacity at the same displacement θ / θ_{pc}. Changing the value of $\theta / \theta_{pc} = 5, 7.5, 10$, the energy

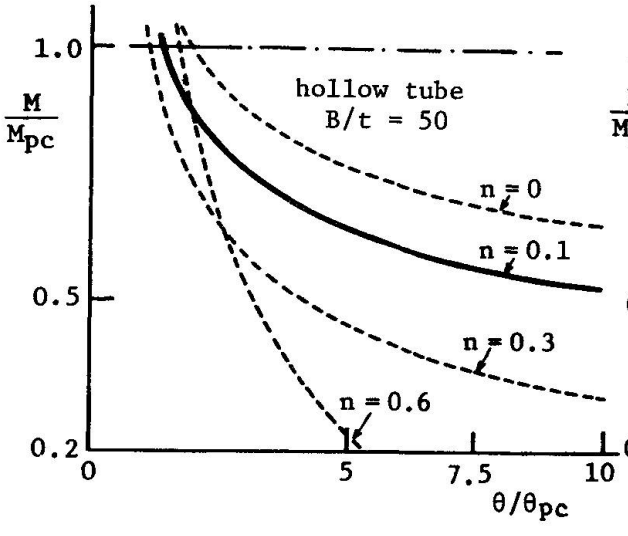

Fig. 8 Behavior of Hollow Tubes

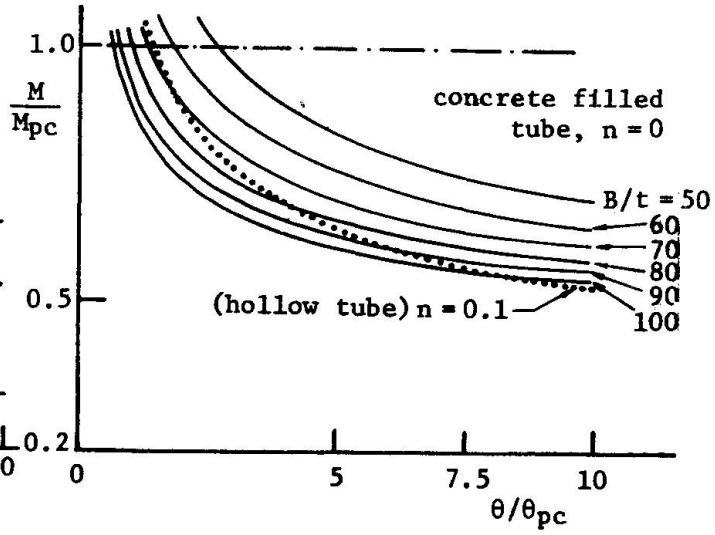

Fig. 9 Behavior of Concrete Filled Tubes

absorption capacity of two columns is compared in Fig. 10. In the figure, the value of 1.0 in the ordinate means that the two columns have equal energy absorption capacity. From this figure, a new limiting value 75 is found conservatively for mild steel tubes with $\sigma_y = 23.5$ KN/cm^2. It is 1.5 times of that for hollow tubular columns. The new values for other grades of steel are obtained by the same method. The numerical results show that the same rate for mild steel may be used for high strength steel.

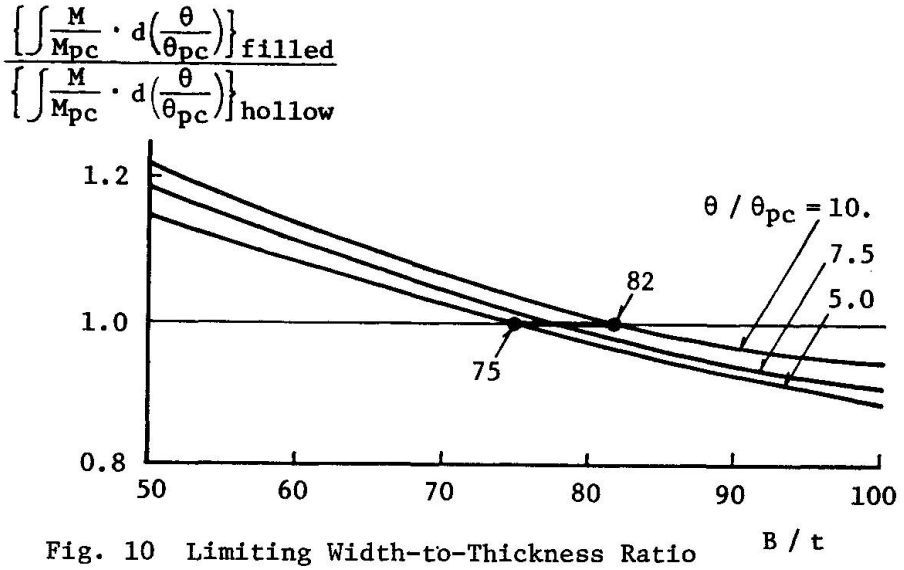

Fig. 10 Limiting Width-to-Thickness Ratio

Figure 11 shows the behavior of the frames composed of the concrete filled steel tubular columns with B/t = 68 (d/t = 64) [5]. The actual yield point of the tubes is 28.8 KN/cm^2, the limiting value of d/t becomes about 43. Then the value of d/t = 64 is 1.5 times of the limiting value. From the figure, it is observed that the frame can be expected to behave in ductile manner and attain the mechanism line ignored local buckling. This fact supports that a proposed limit value is reasonable to be used in the design of concrete filled columns.

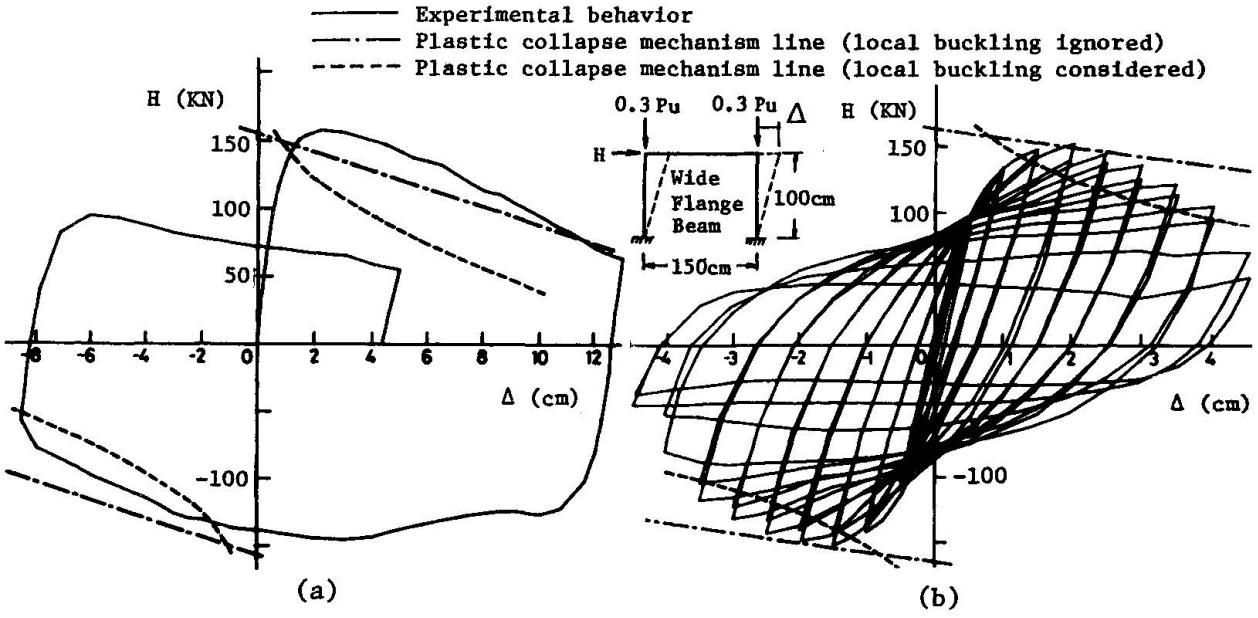

Fig. 11 Behavior of Frames Composed of Columns with B/t = 68

6. CONCLUSION

A new limiting value of the width-to-thickness ratio of plate elements of concrete filled steel square tubular columns is proposed on the basis of the numerical results obtained by plastic limit analysis. It is about 1.5 times of that for hollow tubular columns.

ACKNOWLEGEMENT

I wish to express thanks to Messers. A. KAWANO and K. TSUDA, research assistants of Kyushu University, for discussion in preparation of this manuscript.

REFERENCE

1. MATSUI C. and IKEZAKI M., Elastic Plastic Behavior of Frames with Concrete Filled Steel Square tubular Columns under Vertical and Horizontal Loads, Abstracts of the Annual Congress of AIJ, Sept. 1981, pp. 2123-2124.
2. Architectural Institute of Japan, Design Standard for Steel Structures, June 1970.
3. Architectural Institute of Japan, Standard for Structural Calculation of Steel Reinforced Concrete Structures, Nov. 1975.
4. MATSUI C., MORINO S. and TSUDA K., Inelastic Behavior of Steel Beam-Columns of Box Section under the Constant Vertical and Horizontal Loads, Proc. 8th WCEE, San Francisco, July 1984, Vol. 6, pp. 153-160.
5. MATSUI C. and SHIIBA K., An Experimental Study on Horizontal Strength and Deformation Capacity of Frames with Concrete Filled Steel Tubular Columns, Abstract of the Annual Congress of AIJ, Oct. 1984, pp. 2729-2730.

Seismic Behavior of Steel Beam-to-Column Connection

Comportement sismique d'assemblages poutres-colonnes

Seismisches Verhalten von Stützen-Träger Anschlüssen

Hiroshi OSANO
Research Associate
Tokyo Denki Univ.
Saitama, Japan

Hiroshi Osano, born 1955, graduated from Tokyo Denki Univ. in 1977.

Masami NAKAO
Prof. Dr.
Tokyo Denki Univ.
Saitama, Japan

Masami Nakao, born 1939, received his engineering degree at the University of Tokyo, Japan. After ten years as research associate, lecturer and associate professor at the University of Tokyo, he was appointed to the faculty of Tokyo Denki University.

Sanzo UNNO
Prof. Dr.
Tokyo Denki Univ.
Tokyo, Japan

Sanzo Unno, born 1912, graduated from Kyoto University in 1942. As chief of the Architectural Design Department of Yawata Iron and Steel Company he supervised numerous projects. He consulted for steel rib fabrication for the Society of Steel Buildings of Japan.

Takeo NAKA
Prof. Emeritus, Dr.
Univ. of Tokyo
Tokyo, Japan

Takeo Naka, born 1907, received his engineering degree at the University of Tokyo. For twenty three years he was professor at the University of Tokyo and for fifteen years he was professor at Tokyo Denki University.

SUMMARY

Tests on the seismic behavior of beam-to-column connections composed of H-shaped column and composite beams are reported. Methods to evaluate strength, ductility and energy absorption are presented, which utilize an enlargement model of the panel region due to the reinforcing effect of concrete slab and empirical formulas derived from test results of beam-to-column connections composed of normal steel beams. A model to evaluate restoring force characteristics of beam-to-column connections under repeated loading is also proposed.

RÉSUMÉ

Des essais du comportement sismique d'assemblages poutres-colonnes composés d'une poutre mixte et d'une colonne en H sont rapportées. Des méthodes d'évaluation de la résistance, de la ductilité et de la capacité d'absorption d'énergie en sont tirés; ces méthodes utilisent un modèle de panneaux – renforcés par l'effet de la dalle de béton – dérivé de celui utilisé pour ces mêmes assemblages, mais pour des structures métalliques pures. Un modèle de comportement de ces assemblages sous charges répétitives est donné.

ZUSAMMENFASSUNG

Tests über das seismische Verhalten von Stützen-Träger Anschlüssen, bestehend aus H-Profil Stütze und Verbundträger werden dargestellt. Methoden zur Bewertung der Festigkeit, der Dehnbarkeit und des Energieaufnahmevermögens werden vorgestellt, die sich im Plattenbereich ein Modell zunutze machen, welches aus der armierenden Wirkung der Betonplatte und aus empirischen Formeln, hergeleitet aus Testresultaten von Stützen-Träger Anschlüssen mit reinen Stahlträgern, basiert. Ein Modell zur Ermittlung der Umlagerungskräftecharakteristiken von Stützen-Träger Anschlüssen unter zyklischer Belastung wird ebenfalls vorgeschlagen.

1. INTRODUCTION

In the present design of steel buildings, reinforced concrete slabs with steel deck-plate are commonly used and usually connected to steel beams using shear-connectors to combine parallel frames under seismic loading. Hence, it is necessary to treat the beams as composite beams in the evaluation process of restoring force characteristics of beam-to-column connections as well as beams themselves. However, recent researches on the beam-to-column connections deal with those composed of bare steel beams and no paper has reported on the influence of the reinforced concrete slab of composite beams on the strength and the deformation capacity of steel beam-to-column connections subjected to seismic loading.

As this problem is very important in the seismic design of steel buildings, study on the behavior of steel beam-to-column connections was executed through experiments of 11 specimens of frame subassemblage composed of H-shaped column subjected to strong axis bending and composite beams.

2. OUTLINE OF EXPERIMENTS

2.1 Frame Subassemblage

Specimens designed represent a model of frame subassemblage around inner column subjected to strong axis bending. Configuration of specimens is shown in figure 1. Cross-sections of beams and columns are listed in table 1. The values of relative yield strength of panel-zone to those of adjoining members,"cRpy" and "sRpy", are also shown in table 1. Those are considered to be the key parameter on the evaluations of strength, deformation capacity and energy absorption of beam-to-column connections and are named as "panel yield ratio". Series of specimens are named as (Z0, A0, B0, B'0, C0, D0) in descending order of panel yield ratio. Mechanical properties of steel plates are shown in table 2.

2.2 Reinforced Concrete Slab with Steel Deck-plate

Five types of reinforced concrete slab with steel deck-plate are planned as shown in figures 2a-e. In the cases of type-I, type-III and type-IV, deformed

Table 1 Test Specimens

Specimen	Column	Beam	Slab type	Material group	$_cR_{py}$	$_sR_{py}$	
Z0-I	H-300x300x22x22	H-350x175x9x12	I	2	1.13	0.80	m
A0-I	H-300x300x16x16	H-350x175x9x12	I	1	0.63	0.62	m
B0-I	H-300x305x16x16	H-450x200x9x16	I	3	0.52	0.47	m
B0-IV	ditto	ditto	IV	3	0.57	0.47	m
B'0-I	H-250x250x12x16	H-350x175x9x12	I	2	0.56	0.40	c
B'0-III	ditto	ditto	III	2	0.56	0.40	c
B'1-I	ditto	ditto	I	2	0.49	0.80	m
C0-I	H-250x250x 9x16	H-350x175x9x12	I	1	0.33	0.33	c
C0-IIW	ditto	ditto	IIW	1	0.51	0.33	c
C0-IIS	ditto	ditto	IIS	1	0.28	0.33	c
D0-I	H-234x234x 6x12	H-339x170x6x12	I	3	0.25	0.25	c

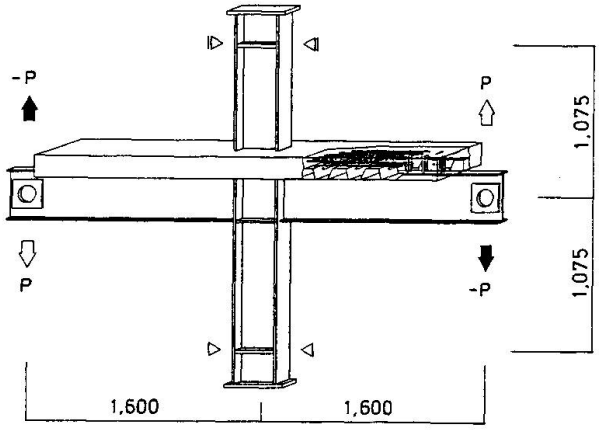

Fig.1 Configuration of Specimen

Table 2 Mechanical Properties of Materials

Group	thickness	σ_y MPa	σ_B MPa	ε_{st} (%)	elong. (%)	E_{st} MPa
1	9	401.	547.	1.95	22.1	3730.
	12	366.	524.	1.81	20.4	4350.
	16	348.	505.	1.99	23.0	4350.
2	9	366.	528.	2.28	22.7	4220.
	12	351.	529.	2.03	23.8	4890.
	16	329.	518.	1.56	26.0	4290.
	22	321.	517.	1.38	28.1	4970.
3	6	433.	528.	2.34	19.6	3460.
	9	434.	554.	2.59	22.2	3980.
	12	379.	513.	2.27	26.4	3580.
	16	354.	503.	2.07	28.4	4080.

bars (D10) are arranged at intervals of 200 millimeters in parallel with steel beam and deformed bars (D13) are arranged at intervals of 230 millimeters in each groove of deck-plate in the perpendicular direction to beam. Welded wire fabrics (D10) are arranged at 35 millimeters below surface to prevent surface cracks of concrete. In the case of type-II, reinforcing bars (ϕ4) are arranged at intervals of 900 millimeters in the perpendicular direction to grooves of deck-plate and deformed bars (D13) are arranged in each groove of deck-plate. Welded wire fabrics (ϕ5) are arranged at 35 millimeters below surface. Type-IIS has the same reinforcement with type-II, however, grooves of deck-plate were set in parallel with steel beam. In the case of type-I and type-IV, stud-connectors are disposed in double rows to beam flange at intervals of 120 millimeters to satisfy the condition of "fully composite beam". In the case of type-II, stud-connectors are disposed in a row to beam flange at intervals of 120 millimeters to make "partially composite beam". In the case of type-III, stud-connectors are disposed in a row to beam flange at intervals of 230 millimeters.

Width of slab, 100 millimeters except for the case of type-IV, is nearly equal to the calculated effective width according to the "Design Standard for Concrete Structures" of the Architectural Institute of Japan.

The hollows surrounded by web and flanges of column are filled up with concrete and no diaphragm is set at the surface level of concrete slab. The influence of the reinforced concrete slab of composite beams on the local deformation of column flanges is to be observed.

Designed type of concrete is normal weight concrete of required strength 20.6 MPa and required slump 18 cm. Measured compressive strength were 23.0 MPa (used for A0-I, C0-I, C0-II and C0-IIS) , 24.5 MPa (used for Z0-I, B'0-I, B'0-III and B'1-I) and 27.6 MPa (used for B0-I, B0-IV and D0-I).

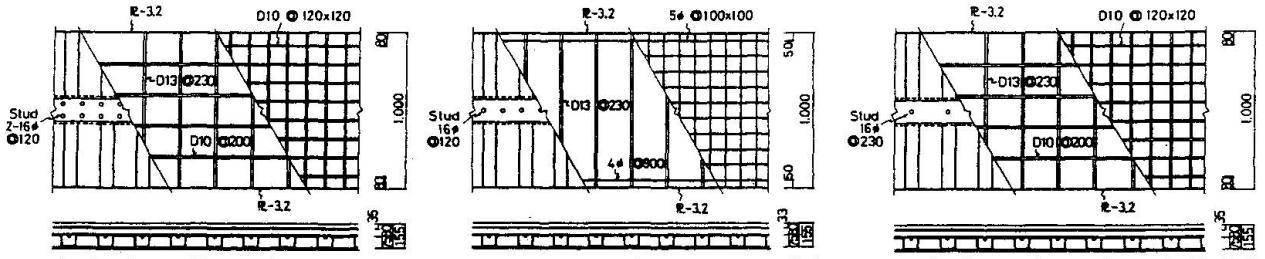

Fig.2 Details of Concrete Slab

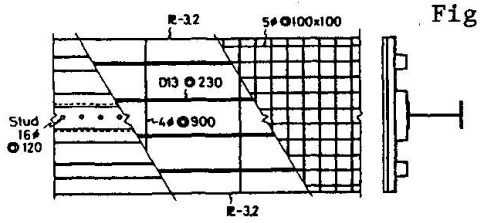

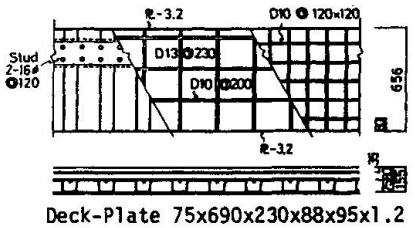

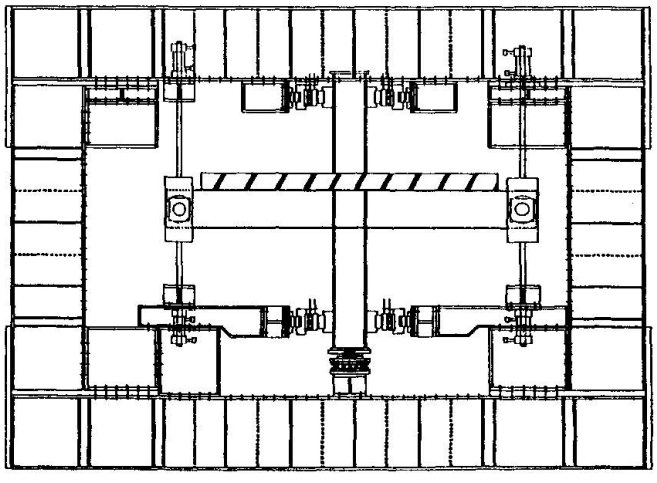

Fig.3 Loading Apparatus

2.3 Loading

Loads to simulate horizontal loading on frame are applied to beam ends in the opposite directions as shown in figure 1 in a loading apparatus shown in figure 3. Applied loads are monotonic for some specimens (marked "m" in table 1) and cyclic for the others (marked "c" in table 1).

3. RESTORING FORCE CHARACTERISTICS

3.1 Frame Subassemblage

Figure 4 illustrates relations between load and deflection of standard specimens. Vertical axis represents the ratio of load to calculated yield strength of column or steel beam whichever is smaller, while horizontal axis represents the ratio of deformation to calculated yield deformation at the yielding of column or steel beam whichever is smaller. Ultimate strength of frame subassemblage is larger than Ppm when sRpy is larger than 0.62.

Relations between deformation capacity of frame subassemblage and panel yield ratio of bare steel beam-to-column connection (sRpy) when shear deformation of panel-zone became twenty times the yield shear deformation are shown in figure 5 with test results of beam-to-column connections composed of bare steel beams [1]. The empirical formula in figure 5 is one derived from regression analysis on the test results of beam-to-column connections composed of bare steel beams. The results of beam-to-column connections with composite beams have resemblance to those of beam-to-column connections composed of bare steel beams. The deformation capacity of frame subassemblage can be estimated by the empirical formula in figure 5.

3.2 Beam-to-Column Connections

Monotonized restoring force characteristics of beam-to-column connections are shown in figures 6a-c. Vertical axis represents the ratio of load to calculated yield strength of beam-to-column connections composed of bare steel beams, while horizontal axis represents the ratio of shear deformation of panel-zone to calculated yield shear deformation. Dotted lines in figures 6a-e show the test results of beam-to-column connections of the same configuration with bare steel beams. The reinforcing effect of steel beam-to-column connections by the reinforced concrete slab of composite beam is illustrated.

A model to take the effect of concrete slab into consideration is proposed in figure 7. In this model, the strength of panel-zone is considered to increase by the enlargement of nominal volume of panel-zone ($V_{pc} \rightarrow V_{pc}'$) as shown in figure 7. Volumes of panel-zone are defined as

$$V_{pc} = d_b \cdot d_c \cdot t_p \qquad V_{pc}' = d_b' \cdot d_c \cdot t_p$$

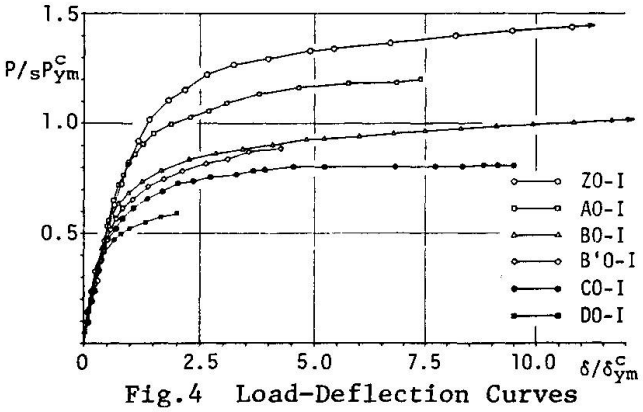

Fig.4 Load-Deflection Curves

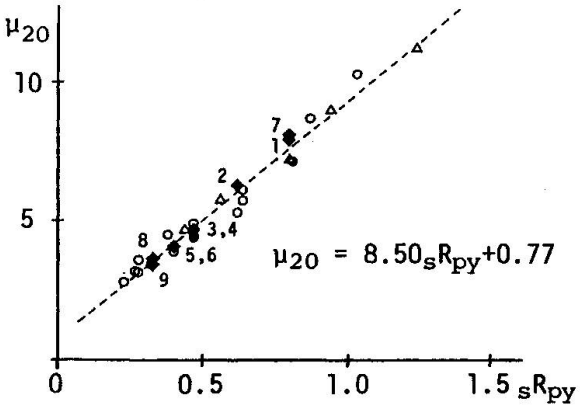

Fig.5 μ_{20} - sRpy Relation

in which, d_b=beam depth, d_c= column depth, t_p = thickness of panel-zone, d_b' = distance between center of the distributed compressive stress and center of thickness of lower flange in composite beam.

Relations between ultimate strength of panel and panel yield ratio of bare steel beam-to-column connection (sRpy) are shown in figure 8. Relations between strength of panel-zone and panel yield ratio (sRpy) when shear deformation of panel-zone became twenty times the yield shear deformation are shown in figure 9. The other data shown in figures 8 and 9 are test results of beam-to-column connections composed of bare steel beams. The empirical formulas in figures 8 and 9 are those derived from regression analyses on the test results of beam-to-column connections composed of bare steel beams. Shiftings to the estimated

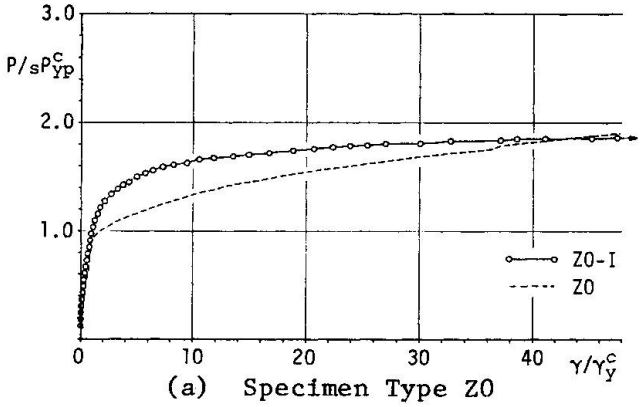

(a) Specimen Type Z0

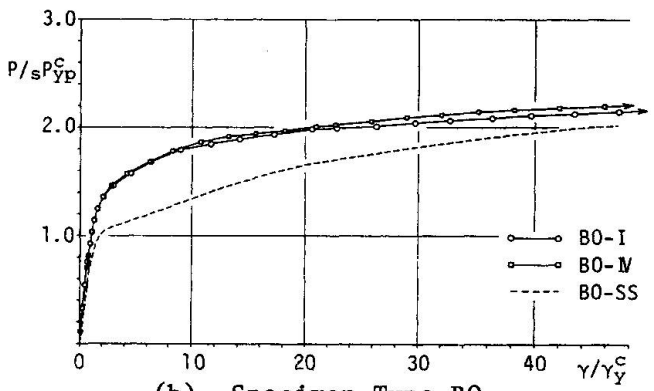

(b) Specimen Type B0

Fig.6 Monotonized Restoring Force Characteristics of Panel Compared with those of Steel Specimens

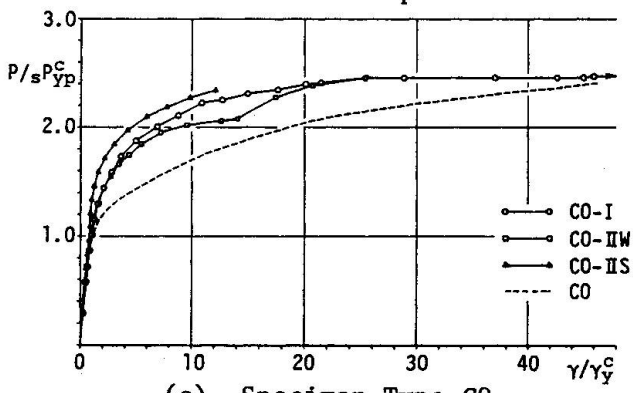

(c) Specimen Type C0

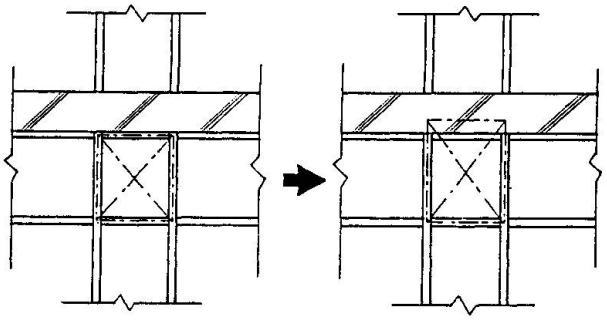

Fig.7 Enlargement of Panel Region

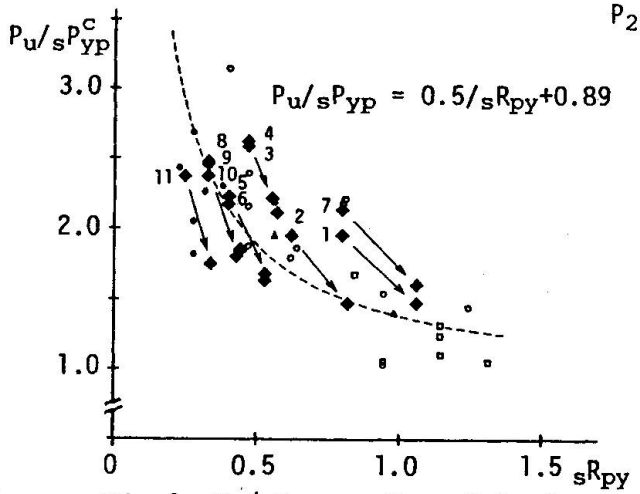

Fig.8 Pu/sPyp - sRpy Relation

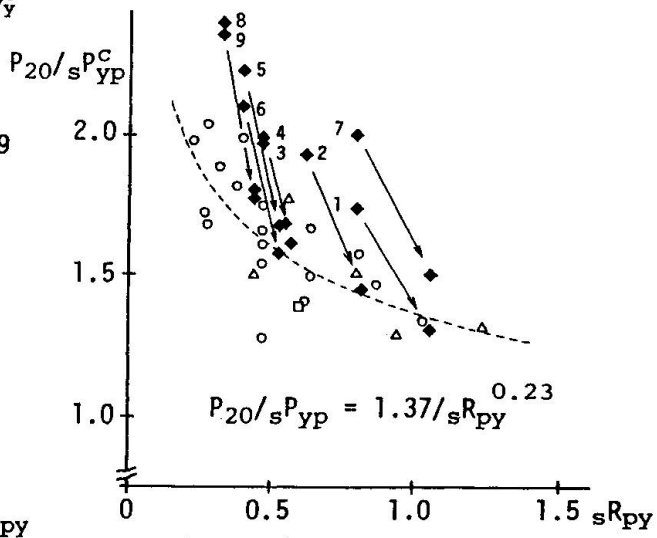

Fig.9 P_{20}/sPyp - sRpy Relation

results of yield strength of enlarged panel-zone are indicated by arrows. The strength of panel-zone can be evaluated by making use of the enlargement model of panel-zone (figure 7) and empirical formula in figure 8 or 9.

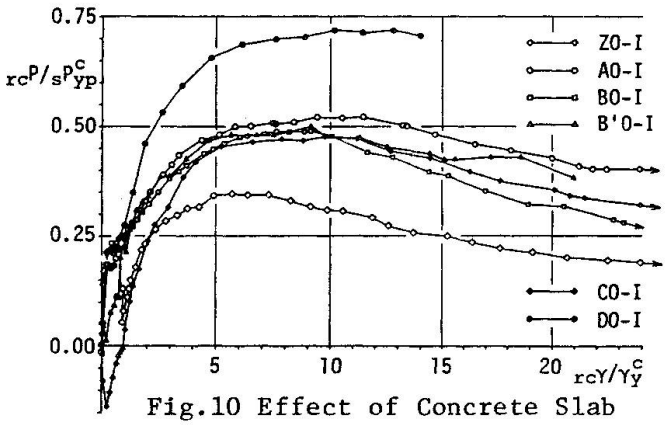

Fig.10 Effect of Concrete Slab

The differences between restoring force of beam-to-column connections with composite beams and that of beam-to-column connections composed of bare steel beams are plotted in figure 10, which can be regarded as the reinforcing effect of concrete slab of composite beam. Restoring force characteristics of each specimen due to the reinforcing effect by concrete slab has the same feature except for the following two cases: when the ultimate strength is larger than 1.3Pmy; when panel yield ratio is smaller than 0.25.

Restoring force characteristics of reinforcing effect by concrete slab tend as follows: rcP/sPyp is nearly equal 0.25 when shear deformation of panel-zone arrives at the yield value; rcP/sPyp is nearly equal 0.48 when shear deformation of panel-zone is between four times and eleven times the yield shear deformation; rcP/sPyp decreases after shear deformation of panel-zone exceeds eleven times the yield shear deformation.

A model to evaluate restoring force characteristics of beam-to-column connections with composite beams under repeated loading is proposed as follows.

1) Restoring force of beam-to-column connections with composite beams comprises two components: restoring force of beam-to-column connections composed of bare steel beams and column (steel part); reinforcing effect of beam-to-column connections by concrete slab (R.C. part).

2) Restoring force characteristics of steel part can be evaluated by the model proposed by NAKAO [2].

3) Skeleton restoring force model of R.C. part is shown in figure 11b. Parameters in figure 11b were determined from test results in figure 10 as follows.
rcPy = 0.25sPyp , rcPu = minimum (0.48sPyp , 0.80 (Ppm-sPpy))
$_{rc}\gamma 1 = \gamma_{yp}$, $_{rc}\gamma 2 = 5\gamma_{yp}$, $_{rc}\gamma 3 = 11\gamma_{yp}$, $_{rc}\gamma 4 = 48.2\gamma_{yp}$

4) Restoring force of steel part under negative or positive loading is influenced by the preceding restoring force of R.C. part positive or negative respectively as illustrated in figure 11c. In this figure, a_i = maximum restoring force of R.C. part at loop i, b_i = the difference between skeleton restoring force shown in figure 11a and restoring force of steel part when shear deformation of panel-zone becomes maximum in loop i, Δ_i = drop of restoring force of steel part at loop i, i = number of loop odd for positive loading and even for negative loading.

5) Restoring force characteristics model of R.C. part under repeated loading is shown in figure 11d. In this figure, rc cr = shear deformation of panel-zone when crack due to bending moment appears at surface of concrete slab.

Samples of restoring force characteristics of beam-to-column connections with composite beams under repeated loading evaluated by the model mentioned above are illustrated and compared with test results in figures 12a,b. Estimated curves and test curves are in considerable coincidence.

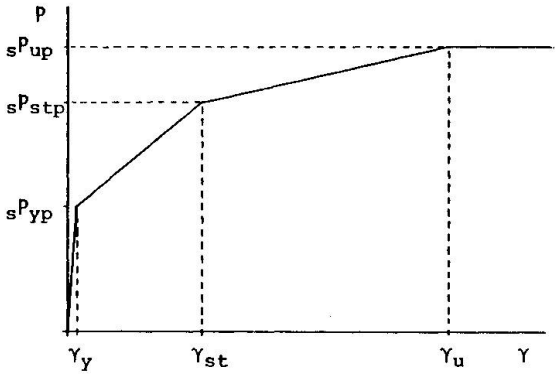

(a) Steel Part

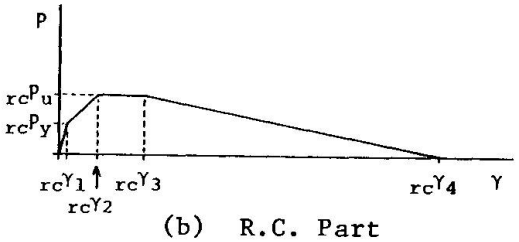

(b) R.C. Part

Fig.11 Restoring Force Characteristics Model

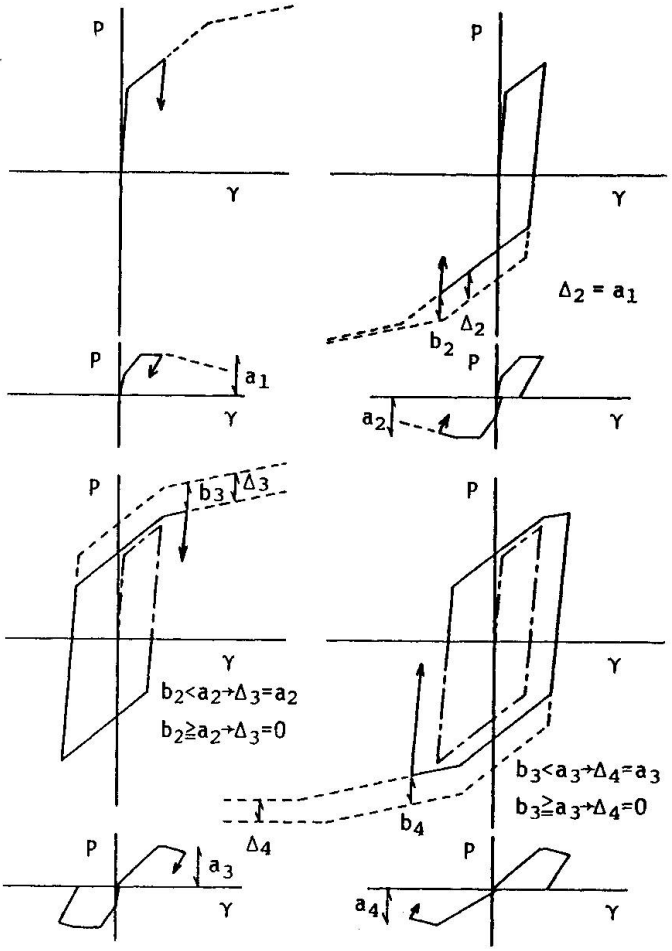

(c) Steel Part in Negative or Positive Loading influenced by the Restoring Force of R.C. Part Positive or Negative respectively

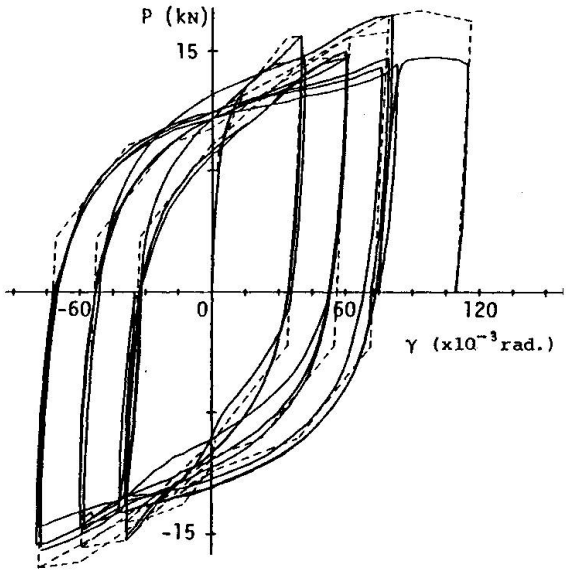

Fig.12a Evaluation of Hysteretic Loops Compared with Test Results (type C0)

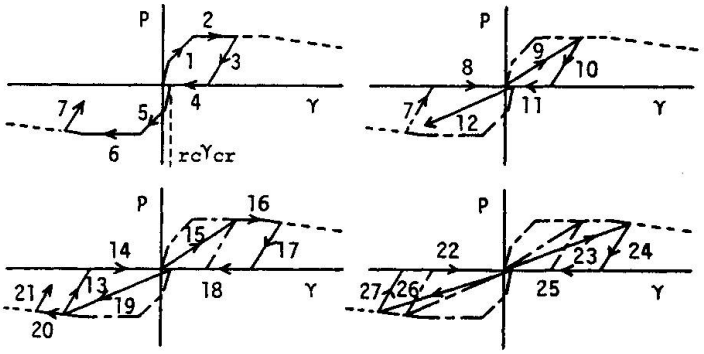

(d) Slip Modeling of R.C. Part due to Crack

4. ENERGY ABSORPTION

Relation between energy absorption of frame subassemblage and panel yield ratio (sRpy) are plotted in figure 13 with test results of beam-to-column connections composed of bare steel beams. The empirical formula in figure 13 is one derived from regression analysis on the test results of beam-to-column connections composed of bare steel beams. Shiftings to the estimated results of panel yield

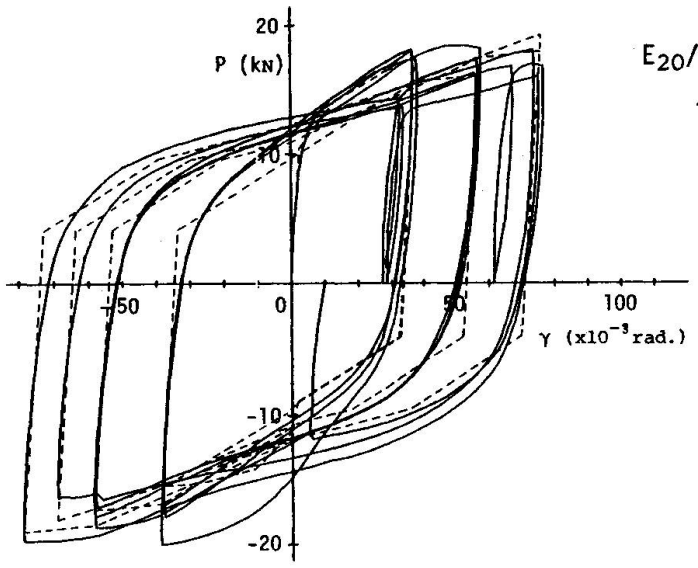

Fig.12b Evaluation of Hysteretic Loops Compared with Test Results (type B'0)

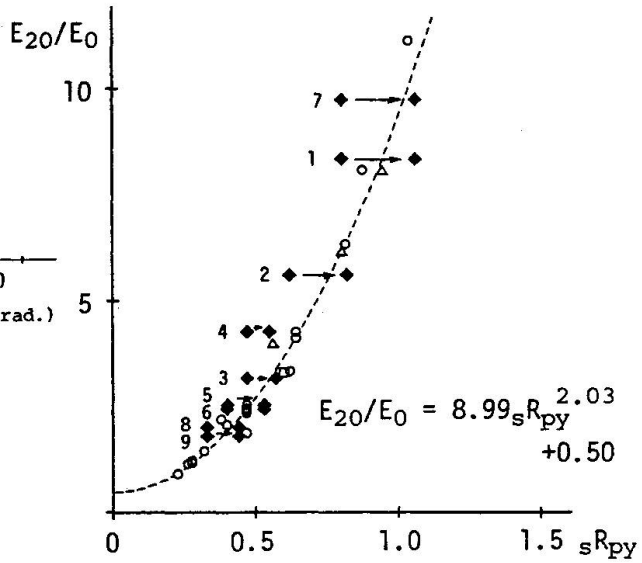

Fig.13 E_{20}/E_0 - sRpy Relation

ratio of enlarged panel-zone are indicated by arrows. The energy absorption of frame subassemblage can also be evaluated by the enlargement model of panel-zone and empirical formula in figure 13.

5. CONCLUSION

Through experiments of frame subassemblage composed of H-shaped column and composite beams, the followings are clarified on the seismic behavior of steel beam-to-column connections with composite beams.

1) Reinforcing effect by concrete slab of composite beams improve the restoring force of beam-to-column connections within the maximum practical shear deformation (i.e. twenty times the yield shear deformation).

2) Strength, deformation capacity and energy absorption can be estimated by making use of the model in figure 7 and empirical formulas in the figures 5,8 and 9.

3) Restoring force characteristics of beam-to-column connections under repeated loading can be evaluated by the model proposed through figures 11a-d.

4) No diaphragm will be required to prevent local deformation of column flange if the hollows surrounded by column web and flanges are filled with concrete.

SYMBOLS

$cRpy = sPyp / Pym$ $sRpy = sPyp / sPym$ $\mu_{20} = \delta_{20} / \delta_{ym}$ $E_0 = sPym \cdot \delta_{ym}$

sPyp = Yield strength of panel-zone.
sPym = Yield strength of column or steel beam, whichever is smaller.
Pym = Yield strength of column or composite beam, whichever is smaller.
sPpm = Full plastic strength of column or steel beam, whichever is smaller.

REFERENCES

1. T.NAKA, M.NAKAO, H.OSANO, "Contribution of the Restoring Force Characteristics of Steel Beam-to-Column Connections to the Aseismic Behavior of Frame", 27th National Symposium on Bridge and Structural Engineering, Feb., 1981

2. B.KATO and M.NAKAO, "A Proposal to Evaluate the Restoring Force Characteristics of Steel Beam-to-Column Connections Composed of H-shapes Subjected to Strong Axis Bending", Proceedings of A.I.J. Extra, Oct., 1976.

Théorie non linéaire des poutres mixtes

Nicht-lineare Theorie von Verbundbalken

Non-Linear Theory of Composite Beams

Luc LACHANCE
Professeur titulaire
Université Laval
Québec, PQ, Canada

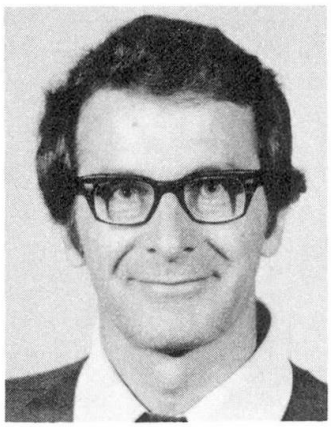

Luc Lachance obtient son diplôme d'ingénieur civil de l'Université Laval en 1958. Boursier Athlone en 1958–60, il obtient un MSc de l'Imperial College, Londres. En 1973, il obtient un doctorat de l'Université Laval. Il est l'auteur d'une vingtaine d'articles scientifiques dans le domaine du béton armé.

André PICARD
Professeur titulaire
Université Laval
Québec, PQ, Canada

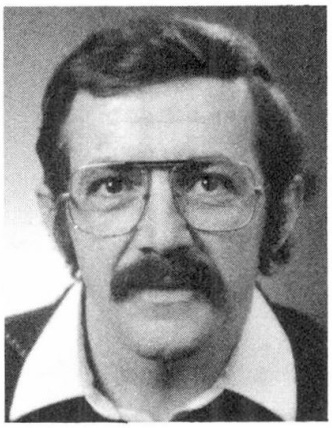

André Picard obtient son diplôme d'ingénieur civil et sa maîtrise de l'Université Laval en 1967 et 1969, et son PhD de l'Université de Londres en 1971. Il est l'auteur d'une vingtaine d'articles scientifiques et des volumes «Béton Précontraint» et «Calcul aux états limites des charpentes d'acier».

Yvon MICHAUD
Etudiant gradué
Université Laval
Québec, PQ, Canada

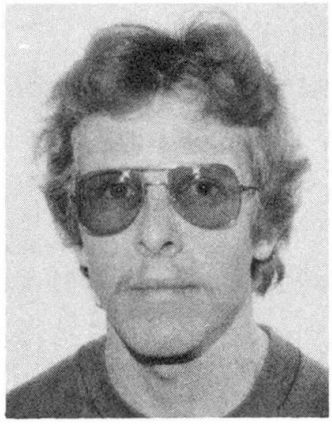

Yvon Michaud obtient son diplôme d'ingénieur civil et sa maîtrise de l'Université Laval en 1982 et 1984. Présentement, il poursuit ses études dans le domaine des poteaux mixtes en vue d'obtenir un doctorat.

RÉSUMÉ

Une théorie non linéaire des sections mixtes, tenant compte rigoureusement des courbes contrainte-déformation des matériaux, est utilisé pour vérifier les moments et les flèches à la rupture de huit poutres mixtes mises à l'essai. En modifiant raisonnablement la courbe de comportement du béton mesurée sur des cylindres de contrôle, il est possible d'obtenir un moment théorique identique au moment expérimental, et une flèche environ 10% plus faible.

ZUSAMMENFASSUNG

Eine nicht-lineare Theorie für Verbundquerschnitte, welche die Spannungs-Dehnungsdiagramme der Materialien streng berücksichtigt, wird angewandt, um die Momente und Durchbiegungen zum Zeitpunkt des Bruchs im Versuch mit 8 Verbundträgern nachzuweisen. Durch die angemessene Anpassung der Spannungs-Dehnungskurve des Betons, bestimmt am Prüfzylinder, ist es möglich, eine Übereinstimmung des theoretischen und experimentell bestimmten Momentes und eine 10% kleinere Durchbiegung zu erhalten.

SUMMARY

A composite section non-linear theory which takes into account actual concrete and steel stress-strain curves is used to predict ultimate moments and deflections of eight composite beams. By adequately adjusting the concrete stress-strain curve measured on control cylinders, we obtain theoretical moments identical to experimental ones, and deflections about 10% smaller.

1. INTRODUCTION

Ce sont des évènements tels que les tremblements de terre qui ont permis de constater la supériorité des bâtiments utilisant des pièces composites sur les bâtiments en acier ou en béton armé [8, 14]. Ces constatations stimulèrent l'intérêt des chercheurs pour les pièces mixtes (aussi appelées pièces composites) constituées de profilés d'acier enrobés entièrement de béton, renforcés ou non par des barres d'armature longitudinales et des étriers transversaux.

Dans un récent rapport, "Planning and Design of Tall Building" [2], un groupe de chercheurs de plusieurs pays ont fait le point sur tout ce qui concerne la construction de bâtiments multi-étagés. Il est question entre autres des poutres mixtes qui, selon ces chercheurs, constituent dans bien des cas un très bon choix, même dans les régions non-sujettes aux tremblements de terre.

La présente étude sur les poutres composites est le début d'une série de recherches qui s'effectueront à l'Université Laval dans le domaine des constructions mixtes. Les résultats obtenus sur une poutre mixte rectangulaire en flexion serviront de base pour étudier la composante de flexion d'un poteau mixte.

Si on fait exception des études faites au Japon [14, 15], peu de recherches ont été effectuées sur les poutres composites. Les chercheurs qui se sont intéressés à ces poutres avaient pour objectif de démontrer que le béton collabore avec l'acier du profilé lors de la flexion. Une fois que l'action composite fut démontrée, il ne semble pas qu'il y ait eu beaucoup d'autres recherches sur les poutres mixtes.

2. ETUDE THEORIQUE

Dans cet article, nous utiliserons une méthode d'analyse théorique des poutres ou poteaux mixtes, mise au point par Lachance [3, 5] et Lachance and Hays [4], qui tient compte de la non-linéarité des matériaux constituant la pièce mixte. Cette théorie permet de connaître la distribution des contraintes dans une section quelconque composée de trois matériaux et travaillant en flexion biaxiale. Avec cette théorie, nous pouvons analyser aussi bien une poutre mixte fléchie uniaxialement, qu'un poteau mixte soumis à de la flexion composée biaxiale. Nous étudierons principalement, à l'aide de cette théorie, le moment de flexion et la flèche à la rupture.

Nous pouvons connaître le moment de flexion et la courbure d'une section en fixant la déformation unitaire d'une fibre d'un des matériaux constituant la pièce. Le nombre de tronçons de la courbe moment-courbure est relié directement à la déformation maximale de chacun des matériaux lors du chargement de la poutre. Pour bien comprendre comment est divisée cette courbe, prenons un cas rencontré fréquemment avec les poutres mixtes, ou la rupture survient lorsque le béton atteint sa déformation relative ultime. A ce moment, les barres longitudinales inférieures ont atteint depuis un certain temps la limite élastique, sans cependant

parvenir à l'écrouissage de l'acier. Il en est de même pour le profilé dont les fibres inférieures ont atteint la limite élastique. Par conséquent, la courbe moment-courbure possède six tronçons différents (réf. 6), chacun se terminant lorsqu'un des trois matériaux entre dans une nouvelle phase de comportement. Lorsqu'on connaît les coordonnées du début et de la fin de chaque tronçon de la courbe moment-courbure, nous calculons un certain nombre de points intermédiaires, de façon à pouvoir faire une approximation polynômiale valable pour chacun des tronçons.

Si on veut connaître la flèche en un point quelconque d'une poutre, on utilise la théorie de la poutre conjuguée, selon laquelle la flèche en un point de la poutre est égale au moment fléchissant en ce même point, produit par un chargement fictif M/EI. La courbe moment-courbure est utilisée pour déterminer ce chargement fictif, puisque M/EI est égal à la courbure, aussi bien dans le domaine linéaire que non linéaire.

3. ETUDE EXPERIMENTALE

Le but premier des essais est de vérifier expérimentalement si on peut prédire de façon adéquate le comportement en flexion des pièces mixtes, en utilisant une théorie non linéaire qui fait appel à l'hypothese selon laquelle le comportement du béton dans la zone en compression des poutres fléchies suit une relation similaire au béton du cylindre de contrôle en compression.

Les mesures effectuées lors des essais sur les poutres permettront de vérifier ces hypothèses, afin de pouvoir les corriger, s'il y a lieu, dans la théorie non linéaire.

Quatorze poutres ayant une longueur de 4100 mm et une section rectangulaire de 250x300 mm, ont été fabriquées en laboratoire [6]. La figure 1 illustre l'arrangement de l'armature à l'intérieur des poutres. Un profilé d'acier M100x19 (ayant une profondeur nominale de 100 mm et une masse linéique de 19 kN/m), d'une longueur de 4060 mm, fut placé au centre du coffrage, son axe fort coincidant avec l'axe fort de la poutre. Quatre barres d'armature no. 15, d'une longueur de 4060 mm chacune, furent disposées aux quatre coins de la section et entourées par 34 étriers fermés no. 15 uniformément répartis le long de la poutre. Le pourcentage d'armature longitudinale, i.e. le profilé et les quatre barres, est de 4,3%.

Des quatorze poutres fabriquées, huit ont été conçues pour être fléchies par rapport à l'axe fort et les six autres par rapport à l'axe faible. Tel que rapporté par Michaud [6], la technique de fabrication des poutres fut légèrement différente selon l'essai effectué. Afin de ne pas confondre les deux séries de poutres, celles qui ont été fabriquées pour être fléchies par rapport à l'axe fort sont dénommées type A, et les autres type B. Les poutres de type B ont été fabriquées pour étudier la composante de flexion par rapport à l'axe faible des poteaux mixtes. Dans le présent article, il n'est question que des poutres de type A.

Pour limiter le glissement entre le béton et le profilé d'acier on a utilisé des goujons ou des plaques d'acier dans certaines des huit poutres de la série A. Sur quatre profilés, nous avons soudé

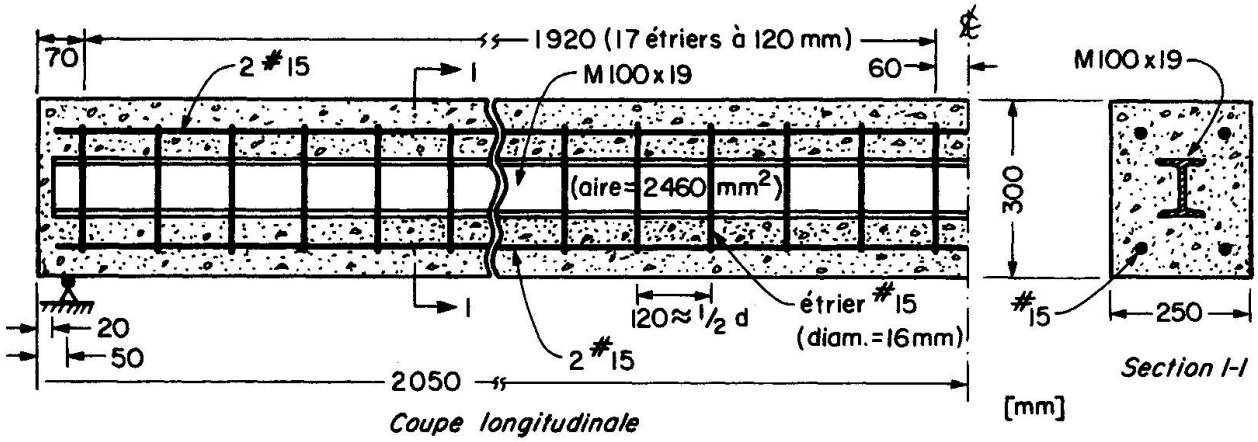

Fig. 1 — Armature des poutres composites.

Tableau 1. Comparaison entre les valeurs expérimentales et les valeurs théoriques pour différentes courbes contrainte-déformation du béton

Déformation unitaire ultime	Moment ultime		Rapport	Flèche ultime		Rapport
	Expérimental	Théorique	col.(3)/col.(2)	Expérimentale	Théorique	col.(6)/col.(5)
10^{-3}	kN-m	kN-m		mm	mm	
(1)	(2)	(3)	(4)	(5)	(6)	(7)
3,0	Valeur moyenne de la 1re coulée: 126,5	113,14	0,89	Valeur moyenne de la 1re coulée: 48,2	30,02	0,62
4,5		124,02	0,98		40,21	0,83
5,0		126,17	1,00		42,69	0,89
5,5		127,90	1,01		44,95	0,93
3,0	Valeur moyenne de la 2me coulée: 120,3	112,02	0,93	Valeur moyenne de la 2me coulée: 47,8	29,55	0,62
4,5		122,66	1,02		39,17	0,82
5,0		124,46	1,03		41,28	0,86
5,5		125,91	1,05		43,21	0,90

des goujons sur l'âme. Sur deux profilés, dont un n'ayant pas de goujons, une plaque d'acier a été soudée à chaque extrémité, dans le but d'empêcher le glissement global du profilé.

Pour fléchir les poutres on a appliqué une charge concentrée à la mi-portée. Pour la mesure des flèches on a utilisé quatre potentiomètres linéaires, appelés aussi déflectomètres électroniques, disposés dans la zone centrale de la poutre. Les déformations unitaires du profilé d'acier ont été mesurées par huit jauges électriques collées sur les ailes du profilé, à la section centrale de la poutre. Les déformations unitaires moyennes ont permis de calculer la position de l'axe neutre et la courbure de la section d'acier. Des jauges électriques, servant à mesurer les déformations unitaires du béton, ont été collées à la mi-portée des poutres à 20 mm et 80 mm de la fibre supérieure, de chaque côté de la poutre. Ces jauges ont permis de calculer la déformation unitaire des fibres supérieures, ainsi que la position de l'axe neutre et la courbure de la section.

Trois cylindres de 150x300 mm ont été prélevés pour chacune des poutres, afin de déterminer la résistance en compression du béton. La courbe contrainte-déformation est obtenue grâce à un déflectomètre électronique installé sur le cylindre. La charge appliquée et la déformation sont automatiquement enregistrées par le système d'acquisition des données. La résistance en traction du béton est obtenue par un essai brésilien sur trois cylindres de 100x200 mm pour chaque poutre.

Lors de la commande des barres d'armature servant à la fabrication des poutres, nous avons exigé que toutes les barres proviennent du même lot. Il en a été de même pour les profilés. La courbe contrainte-déformation de l'acier est mesurée sur des éprouvettes en traction et on suppose que cette courbe est identique en compression. De plus, on a admis que le module d'élasticité de l'acier est égal à 200000 MPa.

4. COMPARAISON DES RESULTATS THEORIQUES ET EXPERIMENTAUX

Si on compare les valeurs théoriques du moment de flexion ultime et de la flèche à la rupture, avec les valeurs moyennes de ces paramètres obtenues expérimentalement, on constate que la théorie sous-estime d'environ 10% le moment ultime et d'environ 38% la flèche à la rupture des poutres mises à l'essai. Ces résultats théoriques sont obtenus en utilisant, pour l'analyse non linéaire, la courbe contrainte-déformation du béton obtenue à partir des cylindres de contrôle. Cependant, nous savons que le taux de déformation, le gradient de déformation et le confinement par l'armature modifient de façon significative le comportement du béton en compression, de sorte que la courbe contrainte-déformation, mesurée sur des cylindres en compression uniforme, peut être différente de celle d'une fibre en compression d'une poutre fléchie.

4.1 Comportement du béton en fonction du taux de déformation

Rüsch [9] a étudié l'influence de la vitesse de chargement sur la courbe contrainte-déformation du béton. Ses résultats montrent qu'après avoir atteint 30% de la contrainte ultime, plus le taux

de déformation est lent, plus la déformation unitaire est grande pour une même charge et plus la contrainte ultime supportée par le béton est faible.

Sargin [10] conclut, à la suite de ses essais, qu'en diminuant le taux de déformation, on augmente la déformation unitaire ultime, tandis qu'on diminue la contrainte correspondante et le module d'élasticité initial.

4.2 Comportement du béton soumis a un gradient de déformation

Plusieurs chercheurs ont voulu déterminer l'influence d'un gradient de déformation sur la courbe contrainte-déformation du béton. Cet intérêt vient du fait qu'on avait noté que le béton en flexion se rupture à des déformations unitaires plus grandes que le béton en compression uniforme.

Sturman et al. [12] ont trouvé qu'un gradient de déformation en flexion a pour effet de retarder la propagation des fissures dans le béton. Par une approche combinant l'expérimentation et une méthode statistique, ils ont trouvé que la contrainte maximale en flexion est 20% plus élevée et correspond à une déformation unitaire 50% plus grande que la valeur trouvée en compression uniforme. D'après leurs résultats, la courbe contrainte-déformation du béton dans une poutre en flexion, est similaire à la courbe trouvée à l'aide d'un prisme chargé excentriquement.

Les recherches pour déterminer l'effet du gradient de déformation n'ont pas donné les mêmes résultats d'un chercheur à l'autre, de sorte qu'il est difficile à l'heure actuelle de déterminer la courbe contrainte-déformation du béton dans une poutre, à partir de la courbe obtenue en compression uniforme.

4.3 Comportement du béton confiné par l'armature

Plusieurs chercheurs ont tenté de calculer ou de mesurer l'effet de confinement du béton causé par l'armature transversale et longitudinale, à l'intérieur des poutres et des poteaux. Priestley et al. [7] qui ont mesuré l'effet du confinement dans des poteaux de béton, armés de spires hélicoidales, ont démontré que la résistance du béton augmente grandement et que sa déformation ultime est trois à cinq fois plus grande. Ahmad et Shah [1] qui ont fait le même genre d'essais ont obtenu un béton jusqu'à 25% plus résistant, avec une déformation ultime deux à trois fois plus grande, selon la distance entre les spires.

Szulczynski et Sozen [13] ont fait des essais sur des prismes de béton armé transversalement par des étriers rectangulaires et soumis à une compression uniforme. Leurs résultats indiquent que la ductilité du béton est considérablement accrue par la présence d'étriers.

Soliman et Yu [11] sont d'avis que l'effet de confinement par les étriers dans une pièce de béton en flexion est différente et plus difficile à déterminer que dans une pièce en compression uniforme. Dans une pièce en flexion, les déformations latérales sont plus importantes dans les fibres extrêmes en compression et

pratiquement nulles près de l'axe neutre. Conséquemment, l'effet du confinement latéral est irrégulier sur la profondeur en compression.

4.4 Modification des courbes contrainte-déformation du béton

En tenant compte des résultats des principaux travaux de recherche, nous avons été en mesure de modifier de façon réaliste les courbes contrainte-déformation mesurées sur les cylindres de béton.

Dans le tableau 1 , on compare les résultats théoriques avec les résultats expérimentaux moyens. Pour les poutres de la première coulée, l'erreur sur le moment ultime théorique, qui est de -11% en utilisant sans modification la courbe contrainte-déformation du béton mesurée sur des cylindres, devient nulle si on utilise la courbe modifiée avec une déformation unitaire ultime égale à 0,005, tandis que l'erreur correspondante sur la flèche à la rupture passe de -38% à -11%. Pour la deuxième coulée, les mêmes comparaisons montrent que l'erreur sur le moment ultime est réduite de -7% à +3%, tandis que l'erreur sur la flèche à la rupture passe de -38% à -14%.

Il est donc possible d'obtenir de bons résultats en modifiant la courbe contrainte-déformation du béton mesurée sur des cylindres en compression uniaxiale. Cependant, l'état actuel des connaissances sur le comportement du béton ne permet pas d'effectuer avec précision ces modifications.

5. CONCLUSIONS

Huit poutres ont été mises à l'essai, dont quatre avec goujons ou plaques soudés sur le profilé d'acier dans le but de limiter son glissement à l'intérieur de la poutre de béton. Les essais de flexion de ces huit poutres mixtes et l'analyse théorique non linéaire ont permis d'obtenir les renseignements suivants:

1. Le comportement global des poutres mixtes ne fut aucunement influencé par les modifications que nous avons apportées à certains profilés dans le but d'en limiter le glissement dans la poutre (addition de goujons ou plaques).

2. Les recherches rapportées par plusieurs auteurs et les essais sur les cylindres de béton ont permis de modifier raisonnablement la courbe contrainte-déformation du béton obtenue de l'essai standard, de façon à mieux représenter le comportement du béton à l'intérieur de la poutre mixte fléchie.

3. L'utilisation d'une théorie tenant compte de la non-linéarité des contraintes dans les matériaux constituant les poutres mixtes a permis d'obtenir des résultats numériques qui se rapprochent d'une façon satisfaisante des résultats expérimentaux.

6. BIBLIOGRAPHIE

1. AHMAD, S.H., and SHAH, S.P., "Stress-Strain Curves of Concrete Confined by Spiral Reinforcement", Journal of the American Concrete Institute, Proceedings, Vol. 79, No. 6, Nov.-Dec.,

1982, pp.484-490.
2. KHAN, F.R., and RANKINE, J., "Tall Building Systems and Concepts", Monograph of the Council on Tall Buildings and Urban Habitat, ASCE and Council Headquarters of the Fritz Engineering Laboratory, Vol. SC, New York, 1980, pp. 31, 32, 406.
3. LACHANCE, L., "Stress Distribution in Reinforced Concrete Sections Subjected to Biaxial Loading", Journal of the American Concrete Institute, Vol. 77, No. 2, March-April, 1980, pp. 116-123.
4. LACHANCE, L., and HAYS, Clifford O., "Accuracy of Composite Section Nonlinear Solutions", Journal of the Structural Division, ASCE, Vol. 106, No. ST11, Proc. Paper 15801, Nov., 1980, pp. 2203-2219.
5. LACHANCE, L., "Ultimate Strength of Biaxially Loaded Composite Sections", Journal of the Structural Division, ASCE, Vol. 108, No. ST10, Proc. Paper 17420, Oct., 1982, pp. 2313-2329.
6. MICHAUD, Yvon, "Etude théorique et expérimentale de poutres mixtes rectangulaires simplement appuyées soumises à de la flexion uniaxiale selon l'axe majeur", Thèse de maîtrise, Département de génie civil, Université Laval, Québec, Canada, 1984.
7. PRIESTLEY, M.J.N., PARK, R., and LU, F.P.S., "Moment-Curvature Relationships for Prestressed Concrete in Constant Moment Zones", Magazine of Concrete Research, Vol. 23, No. 75-76, June-September, 1971, pp.69-78.
8. PROCTER, A.N., "Composite Construction", The Consulting Engineer, Vol. 33, No. 2, Feb., 1969, pp. 48, 50, 52, 54.
9. RÜSCH, H., "Researches Toward a General Flexural Theory for Structural Concrete", Journal of the American Concrete Institute, Vol. 57, No. 1, July, 1960, pp. 1-28.
10. SARGIN, M., "Stress-Strain Relationships for Concrete and the Analysis of Structural Concrete Sections", Study No. 4, Solid Mechanics Division, University of Waterloo, Waterloo, Ontario, Canada, 1972, 167 pages.
11. SOLIMAN, M.T.M., and YU, C.W., "The Flexural Stress-Strain Relationship of Concrete Confined by Rectangular Transverse Reinforcement", Magazine of Concrete Research, Vol. 19, No. 61, Dec., 1967, pp. 223-238.
12. STURMAN, G.M., SHAH, S.P., and WINTER, G., "Effects of Flexural Strain Gradients on Microcracking and Stress-Strain Behavior of Concrete", Journal of the American Concrete Institute, Vol. 62, No. 7, July, 1965, pp. 805-822.
13. SZULCZYNSKI, T., and SOZEN, M.A., "Load-Deformation Characteristics of Reinforced Concrete Prisms with Rectilinear Transverse Reinforcement", Structural Research Series No. 224, Civil Engineering Studies, University of Illinois, Urbana, September, 1961, 54 pages.
14. WAKABAYASHI, M., NAKA, T., and KATO, B., "Elasto-plastic Behavior of Encased Structures", ASCE-IABSE Proceedings of International Conference on Planning and Design of Tall Buildings, Vol. A, August, 1972, pp. 233-252.
15. WAKABAYASHI, M., "Recent Japanese Developments in Mixed Structures", Proceedings of the National Structural Engineering Conference on Methods of Structural Analysis, ASCE, Vol. 1, 1976, pp. 497-515.

Rational Analysis of Shear in Composite Columns

Etude systématique du cisaillement dans les colonnes mixtes

Beweisfähige Untersuchung des Schubs in Verbundstützen

Koichi MINAMI
Lecturer
Osaka Institute of Technology
Osaka, Japan

Koichi Minami, born 1939, received his Ms degree in 1966 from Kyoto University. His research interests include the shear strength analysis of members, beam-column joints and shear walls in reinforced concrete and composite structures.

Minoru WAKABAYASHI
Professor
DPRI, Kyoto University
Gokasho Uji, Japan

Minoru Wakabayashi, born 1921, graduated from the Architectural Department of the University of Tokyo 1946, received Doctor's degree 1957 from the University of Tokyo. He has been a professor at Disaster Prevention Research Institute since 1964.

SUMMARY

An analytic procedure is developed for calculating the ultimate shear capacity of composite (steel-reinforced concrete) columns. The contributions to member strength of various load carrying mechanisms, such as truss actions, arch actions, and those actions which develop in the steel profile and in the cover concrete and core concrete are evaluated independently and then added according to the superposition method. Closed form equations are obtained to define various regions of the failure interaction curve for combined forces. Theoretical predictions show good agreement with available test data.

RÉSUMÉ

Une procédure analytique est développée pour calculer la résistance ultime à l'effort tranchant d'une colonne mixte (acier et béton armé). Plusieurs modèles sont testés, tels que triangulée de remplacement, effet d'arc, calcul séparé de la résistance des composants (profilé métallique, noyau de béton armé, recouvrement) puis sommation, en vertu du principe de superposition. Des équations précises sont obtenues pour définir les différents domaines des courbes d'interactions donnant les combinaisons d'efforts ultimes.

ZUSAMMENFASSUNG

Ein analytisches Verfahren zur Berechnung der Schubgrenztragfähigkeit von Verbundstützen wird entwickelt. Die Beiträge von verschiedenen Tragmechanismen, wie Fachwerk- und Bogenwirkung sowie internen Wirkung in den Stahlprofilen und im Beton werden unabhängig voneinander ermittelt und anschliessend nach der Überlagerungsmethode zur Festigkeit des Tragelements addiert. Geschlossene Formeln werden erhalten, um verschiedene Bereiche der Bruch-interaktionskurve für kombinierte Lasten zu definieren. Theoretische Voraussagen zeigen eine gute Übereinstimmung mit den Versuchsergebnissen.

1. INTRODUCTION

Most of the design equations provided for estimating the ultimate shear strength of composite structural components were derived empirically, and, therefore, are limited in their applicable range. In fact, there was no formula in which interaction between the axial force, flexural moment and shear force is expressed in a unified manner. These days, we can find studies in which the ultimate shear strength of reinforced concrete and composite structural components is computed based on the concept of the theory of plasticity (1, 2, 3).

Using this concept, the writers developed analytical procedure to estimate the ulimate shear strength of reinforced concrete structural components and proposed relatively simple shear design formulas (4, 5). In this paper, the procedure is extended so that the ultimate shear strength of composite structural components, as shown in Fig. 1, can also be estimated. The basic procedure is explaind, and its effectiveness is demonstrated by comparing the results obtained from this analytical procedure with previous test results.

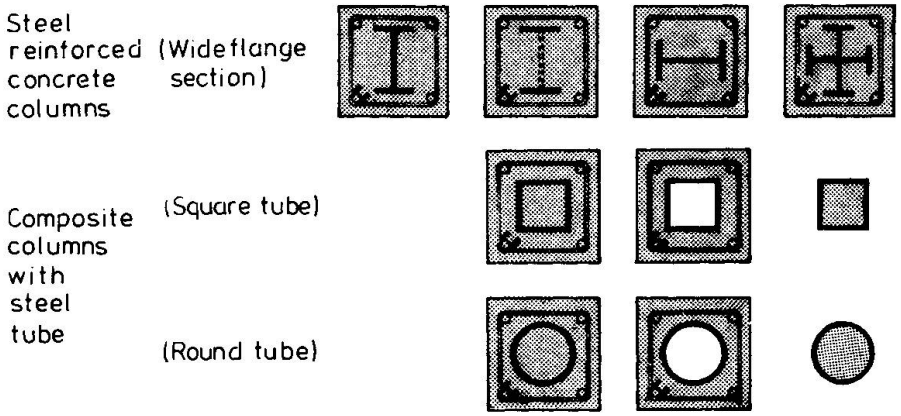

Fig.1 Classification of composite columns

2. SHEAR RESISTING MECHANISM

The writers proposed in Ref. 4 that the shear resistance of a reinforced concrete structural component be taken as the sum of the resistances of two shear resisting mechanisms: that is, the beam mechanism and the arch mechanism. For a composite structural component (a reinforced concrete component with embedded H-shaped steel as shown in Fig. 2), two additional mechanisms are assumed also to contribute to the shear resistance. They are the shear resistance of concrete placed both inside and outside of the steel flanges (Fig. 2(c) and (d)) and the resistance of steel (Fig. 2(e)).

As, in such a composite structural component, the bond strength acting in interfaces between the concrete and steel is small, and the bond stress cannot be significant particularly after the component receives large deformation, the bond is assumed not to contribute to the shear resistance of the component. In Fig. 2, the portion having the effective width of b' is assumed to act as an reinforced concrete component. Here, b' is given as the total width subtracted by the steel flange width, $_fb$. Since the concrete of the remaining part is separated by the steel flanges, the concrete is divided into three portions, each assumed to form its own arch mechanism(theory 1). In the study of Ref. 2, the three portions were treated as one element(theory 2). In composite structural components having usual cross sectional configuration, however, the shear resistance of the concrete having the width of $_fb$ is small as

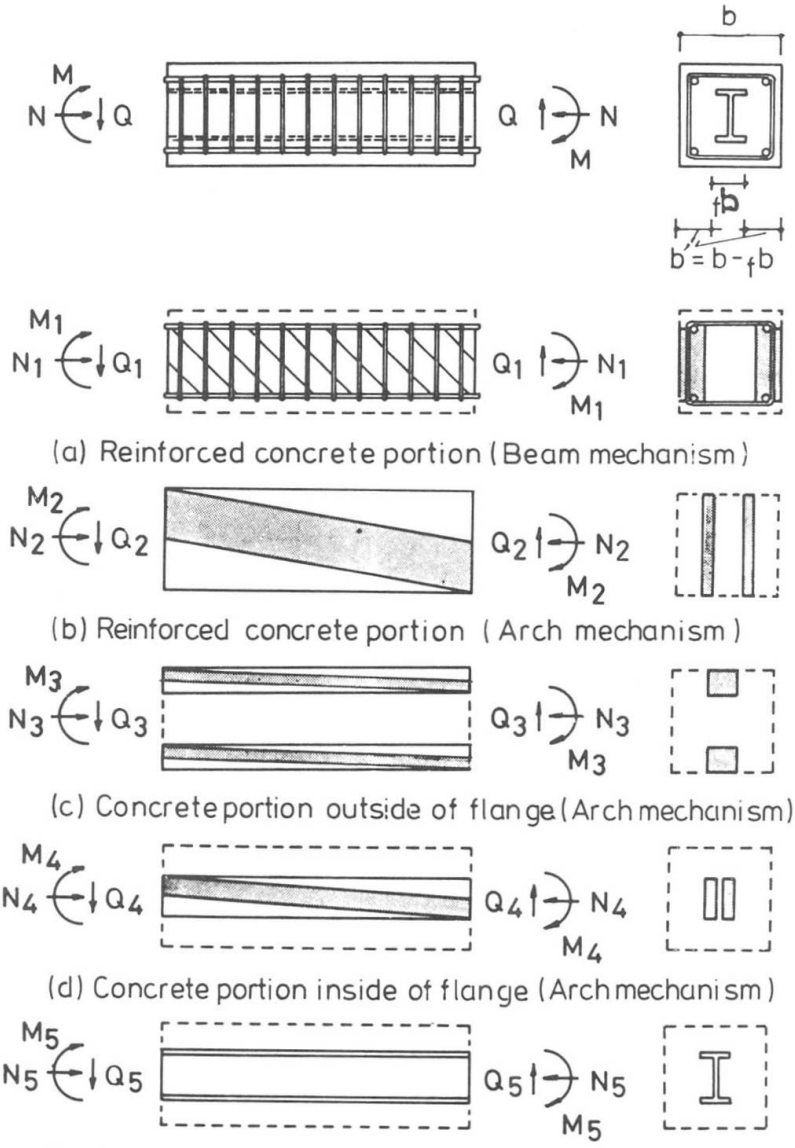

Fig.2 Resistance mechanism of composite columns with wide flange section

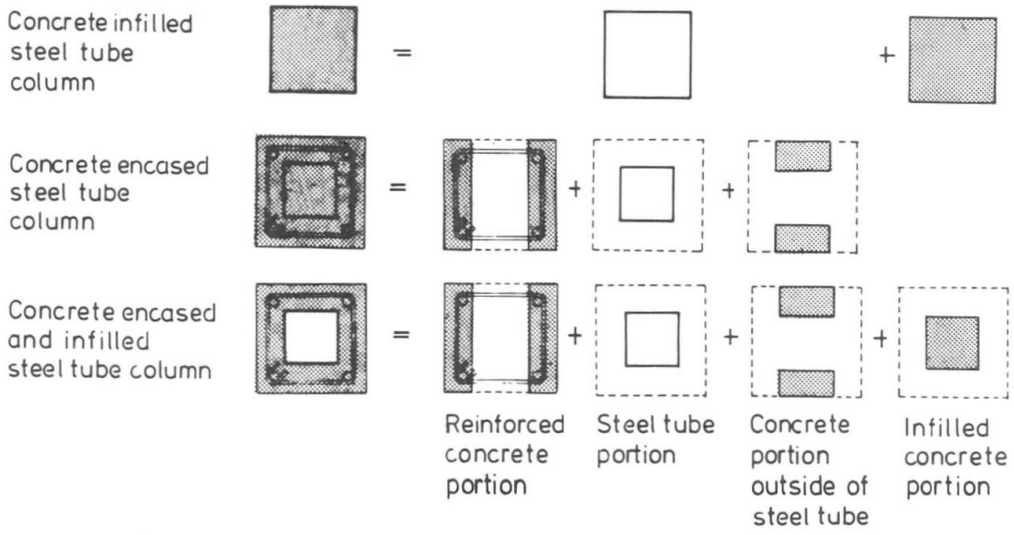

Fig.3 Physical model of stress tranfer of composite columns with steel tube

compared to the resistances of other portions. Then, the neglection of this concrete resistance changes the total shear strength estimate very little.

The same procedure can be applied to other types of composite structural components. Figure 3 shows the resisting mechanisms of a concrete infilled steel tube, a concrete encased steel tube, and a concrete infilled and encased steel tube component.

3. APPLICATION OF STRENGTH SUPERPOSITION CONCEPT

Suppose that the strength combination (M, N, Q) satisfying the statically admissible stress field is determined for individual resisting mechanisms, the total resistance of the composite structural component is given, using the strength superposition concept, as:

$$\begin{aligned} M &= \Sigma Mi \\ N &= \Sigma Ni \\ Q &= \Sigma Qi \end{aligned} \qquad (1)$$

If the inflection point is assumed to be located in the mid-span of the component:

$$M/Q = Mi/Qi = l/2 \qquad (2)$$

Where l is the length of the component.

4. INTERACTION EQUATIONS OF RESISTING MECHANISMS

4.1 Ieteraction Equations of Reinforced Concrete Portion

The interaction of the nondimensionalized axial and shear forces at the reinforced concrete portion is shown in Fig. 4, where the interaction curve comprises seven regions. The interaction equations of those regions is given in Ref. 4, with the reading of b as b'.

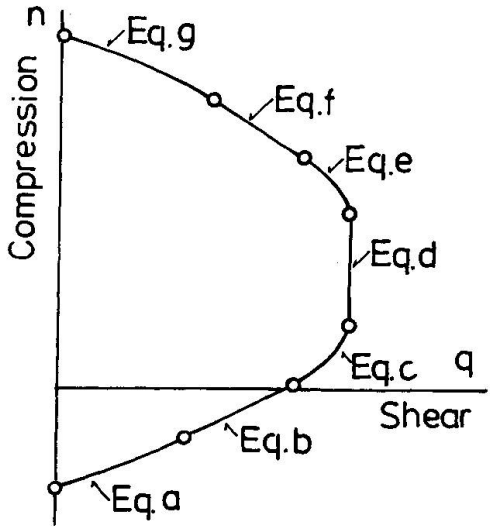

Fig.4 Schematic example of the nondimensionalied axial and shear interaction curves for the reinforced concrete portion

4.2 Interaction Equations of Concrete Portion Having the Steel Flange Width

The interaction equation of the concrete placed inside the steel, the part assumed to form the arch mechanism, can be derived in the same fashion as that of the arch mechanism in the reinforced concrete portion (Fig. 2(b)). On the other hand, the concrete portion outside the steel flanges is assumed to resist only the axial compression since the depth of this portion (measured in the transverse direction) is significantly small relative to its length.

4.3 Interaction Equation of Steel Portion

If the steel stress strain relationship is assumed elasto-plastic, the interaction equation of the steel portion can readily be obtained by employing an appropriate yield criterion.

5. INTERACTION CURVES OF COMPOSITE STRUCTURAL COMPONENT

Nondimensionalized axial and shear force interaction equations of the individual resisting mechanisms can be assumed to form interaction equations of the composite structural component. An example of the interaction curve obtained in this manner is shown in Fig. 5. The interaction curve can be expressed with a series of interaction equations (A-K of Fig. 5), each equation representing certain region of the curve. In Fig. 6, interaction curves drawn by using this analytic procedure are compared with some of the previous test results. In this figure, solid lines and chained lines denote the theoretical strength based on theory 1(concrete is divided into three portions) and the theoretical one based on theory 2(the three portions are treated as one element). The difference between those curves is found to be minimal. The analysis shows that there is a range in which the shear strength becames constant regardless of the value of the axial force.

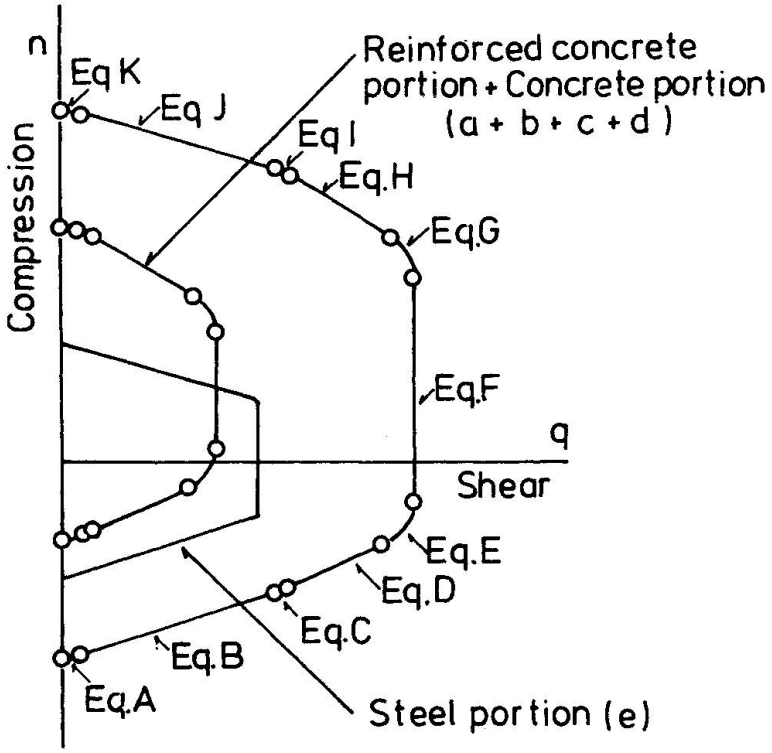

Fig.5 Schematic example of nondimensionalized axial and shear interaction curves

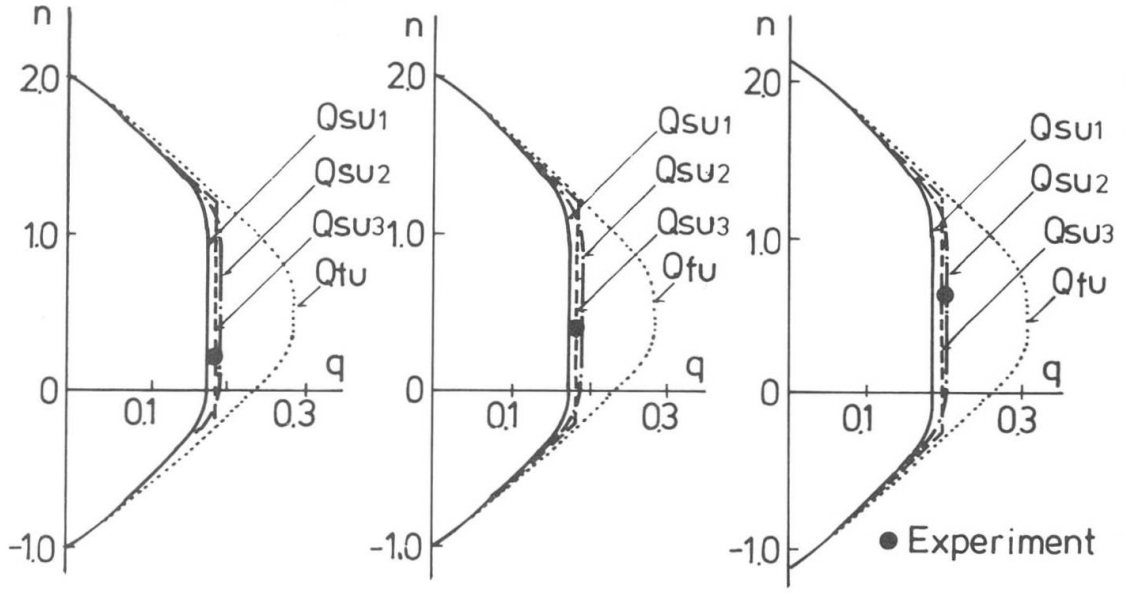

Qfu : Flexural strength
Qsu1 : Shear strength based on theory1 (proposed theory)
Qsu2 : Shear strength based on theory2
Qsu3 : Shear strength obtained by AIJ standard (Ref. 9)

Fig.6 Comparison of theoretical prediction with test results for selected example of composite columns with wide flange section (Ref. 6)

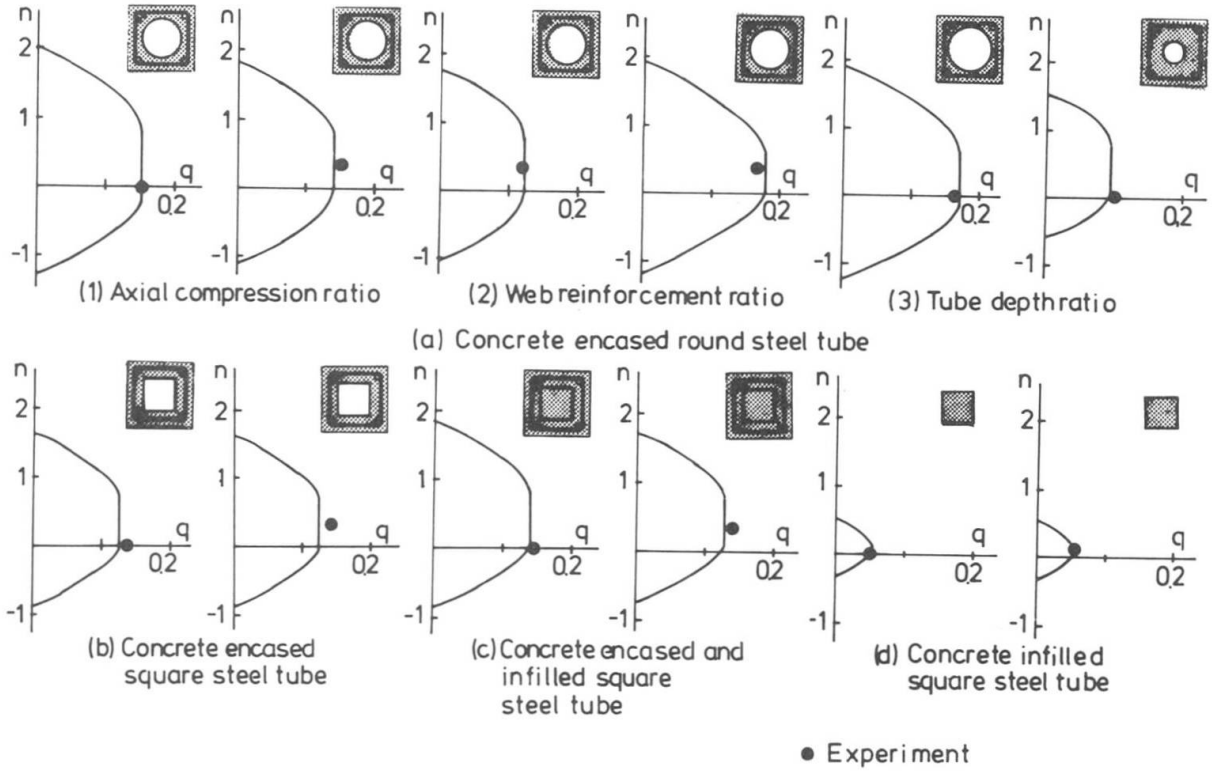

Fig.7 Comparison of theoretical prediction with test results for selected example of composite column with steel tube (Ref. 7)

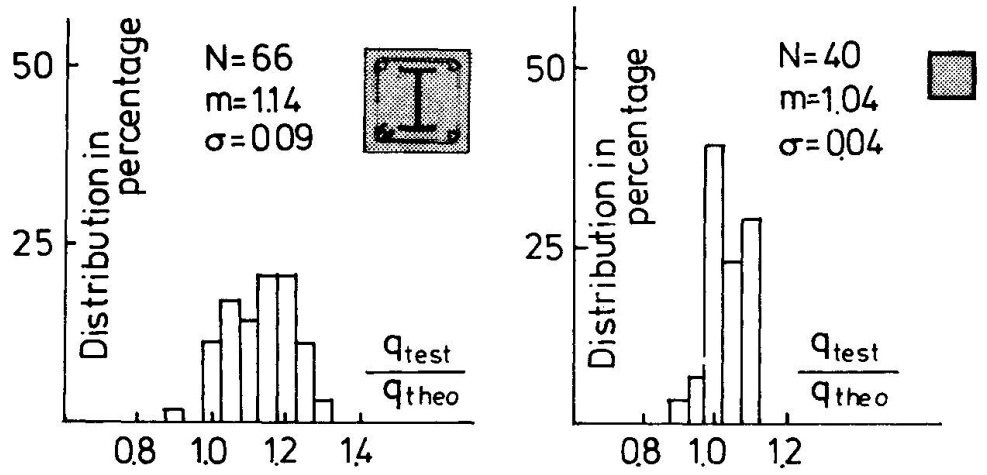

(a) Steel reinforced concrete columns (Ref. 2, 6)

(b) Concrete infilled steel square tube columns (Ref. 8)

Fig.8 Histogram of the ratios of test values to theoretical value

6. COMPARISON BETWEEN THE ANALYTICAL INTERACTION CURVES AND EXPERIMENTAL RESULTS

Figure 7 shows the comparison of analytical interaction curves with results obtained from the test of composite columns with steel tube under load reversal In Fig. 8, the ratio between the analytical estimates and experimental results (66 steel reinforced concrete specimens (Ref. 2, 6) and 40 concrete infilled steel tube specimens (Ref. 8)) is plotted in histograms. Those figures indicate the effectiveness of the analytic procedure proposed in this paper.

7. CONCLUSIONS

The following conclusions can be drawn from this study.

1. The ultimate shear strength of composite structural components can be estimated as the sum of the shear resisting forces of the following four portions: that is, 1) the reinforced concrete portion with the effective width of b' (= b - $_{f}$b), 2) the steel portion, 3) the concrete portion encased by the steel, and 4) the concrete portion outside the steel flanges.

2. The procedure as well as the formula provided by AIJ can estimate the shear strength of previous tests with reasonable accuracy.

ACKNOWLEDGEMENT

The writers wish to thank Dr. M. Nakashima of the Building Research Institute for reviewing the manuscript.

REFERENCE

1. SHOHARA R. and KATO B., Ultimate Strength of Reinforced Concrete Members under Combined Loading, IABSE Colloquium Delft 1981, Final Report, Vol.34,

1981, pp.701-716.

2. KATO B. and SHOHARA R., Strength of Steel-Reinforced Concrete Members, Transactions of AIJ, No.266, April. 1978, pp.19-29.

3. MINAMI K., Limit Analysis of Shear in Reinforced Concrete Members, Proceedings of JCI Colloquium on Shear Analysis of RC Structures, Introductory Report, Sept. 1983, pp.5-28.

4. MINAMI K. and WAKABAYASHI M., Rational Analysis of Shear in Reinforced Concrete Columns, IABSE Colloquium Delft 1981, Final Report, Vol.34, 1981, pp.603-614.

5. WAKABAYASHI M. and MINAMI K., Rational Analysis of Shear in Structural Concrete Columns, Annuals of DPRI, Kyoto University, No.24 B-1, April. 1981, pp.245-277 (in Japanese).

6. MINAMI K. and WAKABAYASHI M., Shear Strength of Steel Reinforced Concrete (SRC) Columns, Preliminary Report of IABSE, Symposium on Design and Safety of Reinforced Concrete Compression Members, Quebec, Aug. 1974, pp.305-313.

7. WAKABAYASHI M., MINAMI K., SASAKI R., and OGAWA H., Experimental Study on Strength of Composite Columns Having Steel Tube, Annuals of DPRI, Kyoto University, No.21 B-1, April. 1978, pp.201-231 (in Japanese).

8. Tomii M. and SAKINO K., Experimental Studies on Concrete Filled Square Steel Tubular Beam-Columns Subjected to Monotonic Shearing Force and Constant Axial Force, Transactions of AIJ, No.281, July, 1979, pp.81-90.

9. Architectural Institute of Japan, AIJ Standard for Structural Calculation of Steel-Reinforced Concrete Structures, 4th Edition (to be publish in 1986).

APPENDIX DESIGN FORMULA OF ULTIMATE SHEAR STRENGTH OF COMPOSITE COLUMNS IN AIJ STANDARD

SRC standard is now being revised, and a new edition will be published in 1986 in which a provision will contain design formula for the ultimate shear strength of composite columns. The shear strength of composite column Qu is considered to be equal to the sum of the strengths of steel portion sQu and that of reinforced concrete portion rcQu and is as follows.

$$
\begin{aligned}
Qu &= sQu + rcQu \\
sQu &= \min(sQfu, sQsu) \\
rcQu &= \min(rcQfu, rcQsu) \\
rcQsu &= \min(rcQsu1, rcQsu2) \\
rcQsu1 &= b \cdot {}_{r}j \cdot (0.075 \cdot F_c \cdot \alpha + 0.5 \cdot p_w \cdot \sigma_{wy}) \\
rcQsu2 &= b \cdot {}_{r}j \cdot (0.15 \cdot F_c \cdot b'/b + p_w \cdot \sigma_{wy})
\end{aligned}
$$

where, the notations are as follows,

- b = width of columns (cm)
- b' = effective width of reinforced concrete portions (cm)
- ${}_{r}j$ = distances between centroids of tension and compression stresses in reinforced concrete (cm)
- F_c = concrete compressive strength (kgf/cm^2)
- α = $4/(rcM/rcQ \cdot {}_{r}d + 1)$ and $(1 \leq \alpha \leq 2)$
- p_w = hoop ratio
- σ_{wy} = yield stress of hoop (kgf/cm^2)

Entwicklung einer neuartigen Stahlprofilblech-Verbunddecke

New Type of Composite Floor of Profiled Steel Sections

Nouveau plafond en construction composite de tôles profilées

H.-D. GLAS
Prof. Dr.-Ing.
Technische Hochschule Leipzig
Leipzig, DDR

H.-E. GOEBEN
Dr.-Ing.
Technische Hochschule Leipzig
Leipzig, DDR

S. KIND
Dr.-Ing.
VEB Metalleichtbaukombinat
Leipzig, DDR

ZUSAMMENFASSUNG

Es wird eine neuartige, in der DDR entwickelte Stahlprofilblech-Verbunddecke vorgestellt. Weiter werden Ergebnisse von fast 100 an der Technischen Hochschule Leipzig und im VEB Metalleichtbaukombinat durchgeführten Versuchen dargestellt und daraus Schlussfolgerungen für die Bemessung gezogen. Insbesondere werden Erkenntnisse diskutiert, die hinsichtlich des Verhaltens solcher Decken über den Stützen (Bereich der negativen Momente) gewonnen werden.

SUMMARY

A new type of composite floor of profiled steel sections, developed in the GDR, is presented. Further, the results of nearly 100 tests performed at the Technische Hochschule Leipzig and the VEB Metalleichtbaukombinat are illustrated and conclusions are drawn regarding design. In particular, the results concerning the behavior of these floors above stanchions (region of negative moments) are discussed.

RÉSUMÉ

On présente un nouveau plafond en construction composite de tôles profilées, développé en RDA. Des résultats de près de 100 essais faits par la Technische Hochschule Leipzig et le VEB Metalleichtbaukombinat sont illustrés et les conséquences pour le dimensionnement en sont tirées. En particulier les conclusions concernant le comportement de tels plafonds sur les appuis (région des moments négatifs) sont discutées.

1. KONSTRUKTIVE LÖSUNG

Bei Stahlprofilblech-Verbunddecken kann der Verbund zwischen Profilblech und Beton auf verschiedene Art konstruktiv realisiert werden, z.B. durch
- spezielle Profilierung des Bleches
- nachträgliche Komplettierung handelsüblicher, aber allein ungeeigneter Stahlprofilbleche
- Endverankerung der Profilbleche am Auflager in der Betonplatte, z.B. durch Kopfbolzendübel.

Es wurde, dem zweiten Weg folgend, der Verbund durch quer zur Profilrichtung aufgeschweißte Verbundbleche oder -winkel realisiert. Diese Variante ist schweißtechnisch besser zu beherrschen als die mehrfach vorgeschlagene Lösung, Bewehrungsstäbe quer auf den Profilblechobergurt aufzuschweißen. Die in Figur 1 dargestellte Verbundsicherung hat bei all ihren technologischen Schwächen die Vorteile, daß Halbzeuge verwendet werden können, die Verbundmittel an die konkrete Beanspruchung anpaßbar sind und mit einer Endverankerung (z.B. durch Kopfbolzendübel) kombiniert werden können.

Diese Verbunddecke wird vom VEB Metalleichtbaukombinat ausgeführt.

Die Brandschutzforderungen werden entsprechend den funktionellen Forderungen entweder durch eine zusätzliche Unterdecke oder durch Zulagebewehrung aus Betonstahl erfüllt. Nähere Angaben sind /1/ zu entnehmen. Die Bemessung erfolgt nach /2/. Weitere veröffentlichte Artikel sind /3/ /4/.

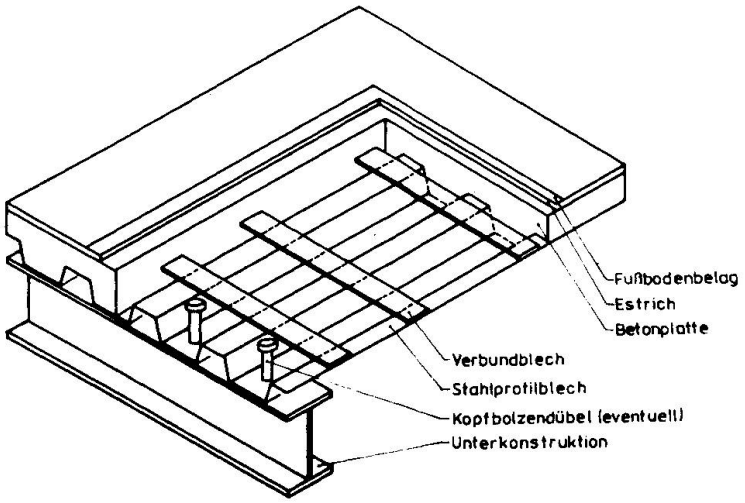

Fig. 1 Deckenaufbau mit Verbundsicherung

2. EINFLUSS DER VERBUNDFUGE AUF DIE TRAGFÄHIGKEIT

2.1 Allgemeines

Die verschiedenen Stahlprofilblech-Verbunddecken unterscheiden sich im wesentlichen durch die Art der Verbundsicherung. Die Ausbildung der Verbundfuge entscheidet darüber, ob das vollplastische Moment erreicht wird.
Es wird der Einfluß unterschiedlicher nichtlinearer Dübelsteifigkeiten, verschiedener Anordnungen der Verdübelungen und der Kombination unterschiedlicher Dübelsteifigkeiten untersucht.

2.2 Berechnung als elastisch verdübelter Träger

2.2.1 Berechnungsmodell

Die Stahlblech-Verbunddecke wird als elastisch verdübelte Rahmenkonstruktion berechnet. Das in Figur 2 dargestellte Berechnungsmodell kann wie folgt charakterisiert werden:
- Die Konstruktion ist diskontinuierlich verdübelt.
- Die Verbundmittel sind durch ihre Federkennlinie gekennzeichnet (elastisch, quasi starr, beliebig gekrümmt).
- Die Schubkräfte können in beliebiger Höhe des Profilbleches eingetragen werden. Bei der gewählten Verbundsicherung erfolgt die Lasteintragung in den Obergurt des Profilbleches.
- Die Stabachse des Profilbleches ist durch die elastische Schwereachse gegeben. Die Verschiebung des Schwerpunktes infolge Teilplastizierung wird in der Regel vernachlässigt.
- Der Betonobergurt ist gekrümmt. Die Stäbe sind dabei abschnittsweise gerade.

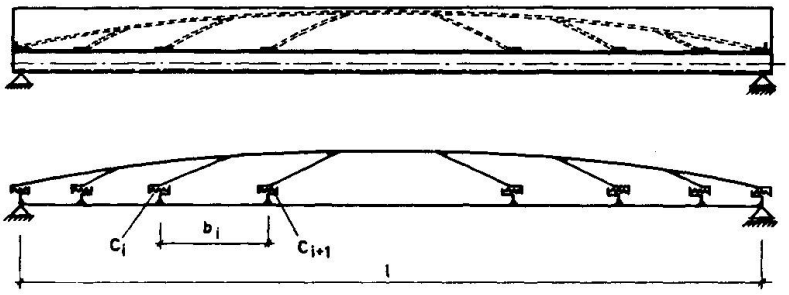

Fig. 2 Berechnungsmodell Einfelddecke

Die Tragfähigkeit gilt als erreicht, wenn von den Versagenskriterien ein Kriterium erreicht wird:
- Das Profilblech wird durch eine Grenzschnittkraftkombination N-M-Q beansprucht.
- Die Spannungen in der Betonplatte sind gleich der vereinbarten Grenzspannung.
- Die aufnehmbare Schubkraft der Verbundfuge ist erreicht.

2.2.2 Verbundmittel

Die Federkennlinie der Verbundmittel wird durch gesonderte Versuche bestimmt und rechnerisch überprüft. Dazu wurden die Verbundbleche als elastisch gestütztes Flächenelement betrachtet, das mit der FEM-Methode berechnet werden kann.
Die dazu benötigten Federkennwerte des Betons wurden näherungsweise über Ausgleichsrechnung aus den Verbundeigenschaften von Betonrippenstählen bestimmt. Grundlage dazu waren die Versuchsergebnisse von Rehm /5/.
Der Einfluß der Verformungen infolge Dauerlast wird nach /6/ über den Ansatz berücksichtigt:

$$s(t) = s(o) \cdot [1 + \varphi(t)] \qquad (1)$$

$$\varphi(t) = (1 + 10t)^{0.08} - 1 \qquad t\ [h] \qquad (2)$$

Die rechnerisch gefundenen Beziehungen wurden an 20 eigenen Detailversuchen überprüft, bei denen Blechdicke und -breite sowie die Art der Befestigung variiert wurden. Es zeigte sich, daß die Befestigung der Verbundbleche einen entscheidenden Einfluß auf die Größe der Relativverschiebungen hat. Je näher die Verbundbleche am Rand des Profilblechobergurtes befestigt sind, um so günstiger ist die Wirkung.

2.2.3 Rechenprogramm

Es wurde ein Rechenprogramm in der Programmiersprache FORTRAN

geschrieben. Die Bearbeitung erfolgte auf der EDVA EC 1022 am Rechenzentrum der TH Leipzig.
Mit Hilfe des Rechenprogrammes können ermittelt werden:
- Schnittkräfte in Profilblech und Betonplatte
- Dübelkräfte und Relativverschiebung in der Verbundfuge
- Durchbiegungen.

Die Ergebnisse werden iterativ verbessert, zuerst die belastungsabhängigen Dübelsteifigkeiten und anschließend die Steifigkeiten von Profilblech und Betonplatte.
Zur Rechenzeit können keine generellen Angaben gemacht werden. Sie ist abhängig von
- Dübelanzahl
- Gleichmäßigkeitsgrad der Dübelauslastung
- Erforderlicher Steifigkeitskorrektur.

Entspricht die Dübelverteilung genau dem Schubkraftbild in der Verbundfuge, so sind nur wenige, manchmal nur ein Iterationsschritt erforderlich. Weicht die Anordnung der Dübel von der Schubkraftverteilung ab, weisen die einzelnen Dübel infolge unterschiedlicher Beanspruchung verschiedene Steifigkeiten auf, so erhöht sich die Anzahl der Berechnungsschritte. Das Rechenprogramm reagiert auch empfindlich auf starke Knicke in der Steifigkeitskennlinie der Dübel.

2.2.4 Versuche

Es wurden 19 Versuchskörper (davon 1 Vorversuch) auf ebener Unterlage aufliegend, hergestellt. Sie wurden nach dem Erhärten entschalt und die erste Woche feucht gehalten, dann ohne weitere Nachbehandlung im Freien gelagert. Die projektierte Betongüte war Bk 25.
Die Prüfkörper (Einfelddecken) hatten eine Länge von 2000 mm (Stützweite 1800 mm). Die Deckendicke betrug 100 mm bis 200 mm. Die Belastung erfolgte bis auf zwei Ausnahmen durch zwei symmetrisch angeordnete Einzellasten im Abstand l_S vom Auflager. Damit liegt das charakteristische Momenten-Schub-Verhältnis

$$MQV = \frac{M}{Q \cdot h_a} = \frac{Q \cdot l_S}{Q \cdot h_a} = \frac{l_S}{h_a} \qquad /-/ \qquad (3)$$

zwischen 1.10 und 7.37. Die Breite der Plattenstreifen beträgt in Abhängigkeit von den verwendeten Profilblechen bei den Vorversuchen 500 mm und bei der Hauptserie 400 mm. Der Versuchsaufbau ist Figur 3 zu entnehmen.
Die Versuchskörper wurden bis zum Versagen stufenweise mit Zwischenentlastung auf eine Vorlast belastet. Die Versuche waren so konzipiert, daß bei den meisten Versuchskörpern die Verbundfuge versagte.
Der Vergleich der rechnerischen Versagenslasten mit den experimentell bestimmten zeigt gute Übereinstimmung. So weichen die Ergebnisse im Mittel 16,8 % nach der sicheren Seite hin ab (Mittelwert 1,168; Standardabweichung 0,143; Variationskoeffizient 0,122).

3. DURCHLAUFENDE DECKEN

3.1 Problemstellung

Bei durchlaufenden Stahlbetondecken ist der Querschnitt über der ersten Innenstütze meist für die Bemessung maßgebend. Bei Stahlprofilblech-Verbunddecken wird dieser Zustand durch die reduzierte Breite der Betonbiegedruckzone verschärft. Der Einfluß dieser reduzierten Breite und der aussteifenden Wirkung des

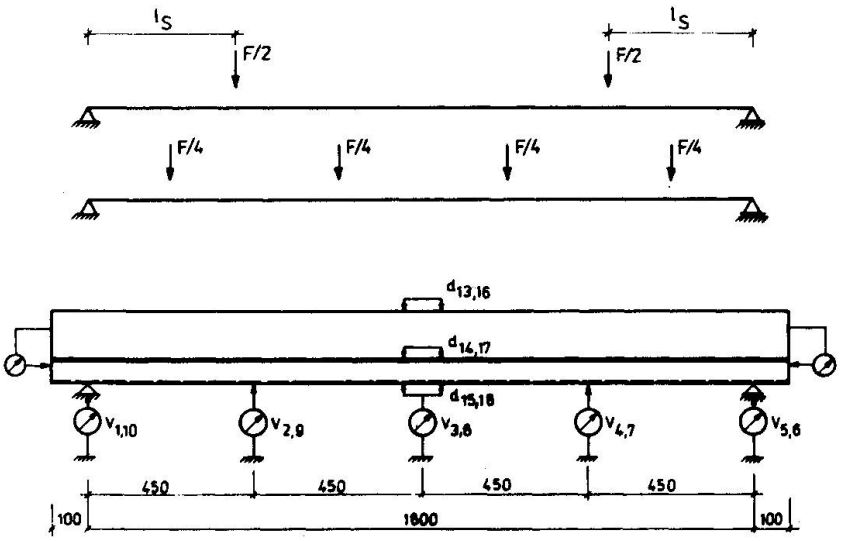

Fig. 3 Versuchsaufbau

Profilbleches auf Trag- und Verformungsverhalten des Querschnittes war zu untersuchen.

3.2 Querschnitt über der Innenstütze

3.2.1 Voraussetzungen und Ansätze

Es wurden folgende Voraussetzungen getroffen:
- Die Querschnitte bleiben eben.
- Der Stahlquerschnitt des Profilblechsteges wirkt voll mit (gilt nur bei geringen Stegblechhöhen).
- Der Druckflansch des Profilbleches wirkt nur teilweise mit (Berücksichtigung des überkritischen Beulens).

Für die Spannungsverteilung in der Betonbiegedruckzone wird der schon von Dilger /7/ verwendete Ansatz verwendet (Figur 4). Die maximale Bruchstauchung wird aus Versuchen von Rüsch bestimmt. Sie ist abhängig von Betongüte und Form der Betonbiegedruckzone. Die Völligkeit der Spannungsverteilung ist im wesentlichen abhängig von Betongüte, Form der Betonbiegedruckzone und vom Belastungsgrad

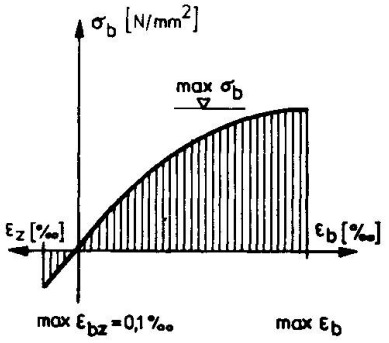

$\sigma_b = \max \sigma_b \left[1-\left(1-\frac{\varepsilon_b}{\max \varepsilon_b}\right)^7\right]$

max ε_b = max ε_b (R_p, Form der Druckzone)

max ε_{bz} = 0,1 ‰

max σ_b = R_p bei Kurzzeitlast

~ 0,8 R_p bei Dauerlast

Fig. 4 Spannungsverteilung über Betonbiegedruck- und -zugzone

(näherungsweise durch die Randstauchung darstellbar). Für den Spannungsverlauf in der Biegedruckzone wird affiner Verlauf vorausgesetzt. Der Ansatz ist gültig für
- Kurzzeit- und Dauerstandsbelastung
- Gebrauchs- und Versagenslast
- beliebige Form der Betonbiegedruckzone.

Mittels der gewählten Spannungsfunktion kann die kammartig geformte Betonbiegedruckzone in eine identische rechteckige überführt werden.

Für die Beschreibung des Trag- und Verformungsverhaltens des Profilblechflansches ist es ausreichend, wenn ein rechteckiges Beulfeld mit den Abmessungen a und b untersucht wird. Dieses ist an den Querrändern starr und an den Längsrändern elastisch eingespannt. Näherungsweise wird gelenkige Lagerung angesetzt (Das Profilblech hebt sich in den unteren Laststufen infolge der grösseren Querdehnzahl vom Beton ab. Damit kann sich die Kante verdrehen, und es kann nicht mehr starre Einspannung angesetzt werden). Für die Vorverformung wird affiner Verlauf vorausgesetzt:

$$w = f \cdot \sin^2 \frac{\pi x}{a} \sin \frac{\pi y}{b} \qquad (4)$$

$$w_o = f_o \cdot \sin^2 \frac{\pi x}{a} \cdot \sin \frac{\pi y}{b} \qquad (5)$$

Mit Hilfe des energetischen Verfahrens nach Galerkin/Bubnow wurden die Differentialgleichungen der biegsamen Platte gelöst. Es ergeben sich Polynome dritten Grades für die Bestimmung der effektiven Profilflanschbreite in Abhängigkeit vom Seitenverhältnis $\alpha = a/b$. Dabei wird α so gewählt, daß $\varphi = b_m/b$ ein Minimum wird.

3.2.2 Ergebnis

Die Auswertung der Beziehungen für $\varphi = b_m/b$ ist in Figur 5 dargestellt. Dabei stellen die Kurven für die Vorverformungen $f_o = (5...25)$ t nur theoretische Grenzwerte dar.

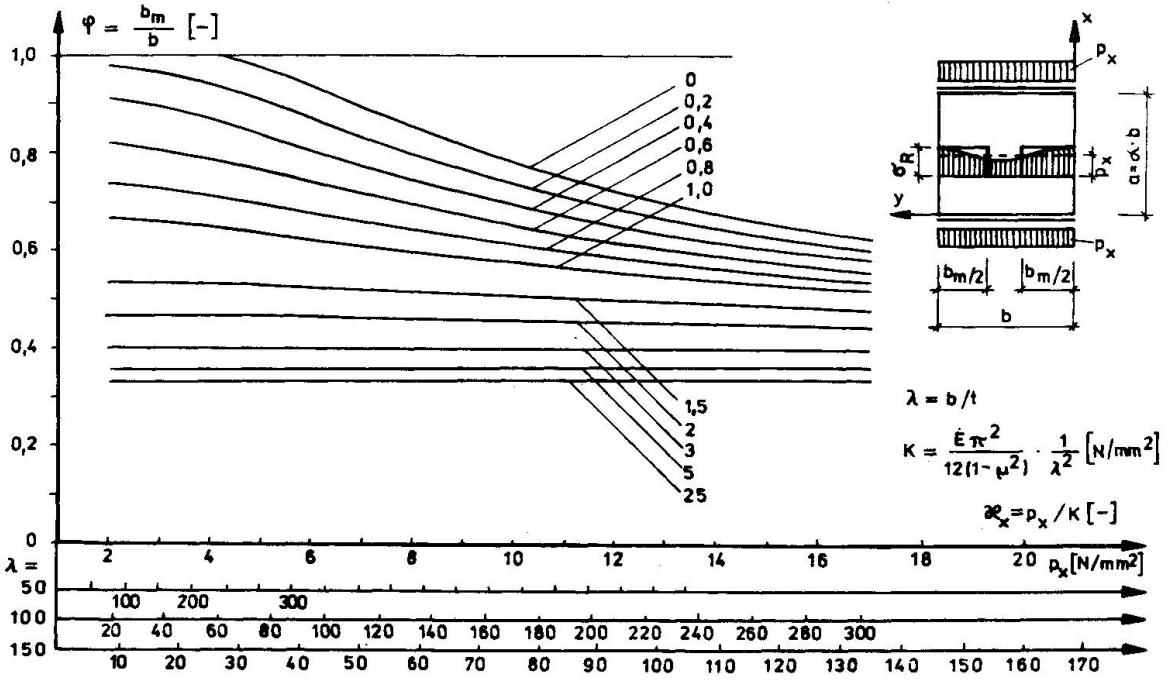

Fig. 5 Mitwirkende Breite des Druckflansches im Verbundzustand

Zur Bestimmung der Vorverformung aus dem Betonierzustand wird ein an den Quer- und Längsrändern gelenkig gelagertes Beulfeld untersucht. Berücksichtigt wurden folgende Einflüsse:
- Vorverformung des unbelasteten Bleches
- Betonierquerlast
- frei verschiebliche bzw. unverschiebliche Längsränder.

Beste Übereinstimmung mit Versuchsergebnissen ergab sich bei der Annahme frei verschieblicher Längsränder und bei Vernachlässigung der Querlast.
Bei der Überlagerung der Spannungen aus Betonier- und Verbundzustand ist das Ergebnis nur noch vom Seitenverhältnis α abhängig. Durch systematisches Einschachteln wird α so bestimmt, daß die mitwirkende Breite ein Minimum wird.
Durch Zusammenfassung der Beziehungen für die Betonbiegedruckzone und das Profilblech ist die Momenten-Krümmungs-Beziehung des Querschnittes bestimmbar. Der Einfluß des Profilbleches auf die Rotationsfähigkeit des Querschnittes sowie auf die zu erwartende Versagenslast ist Figur 6 zu entnehmen.

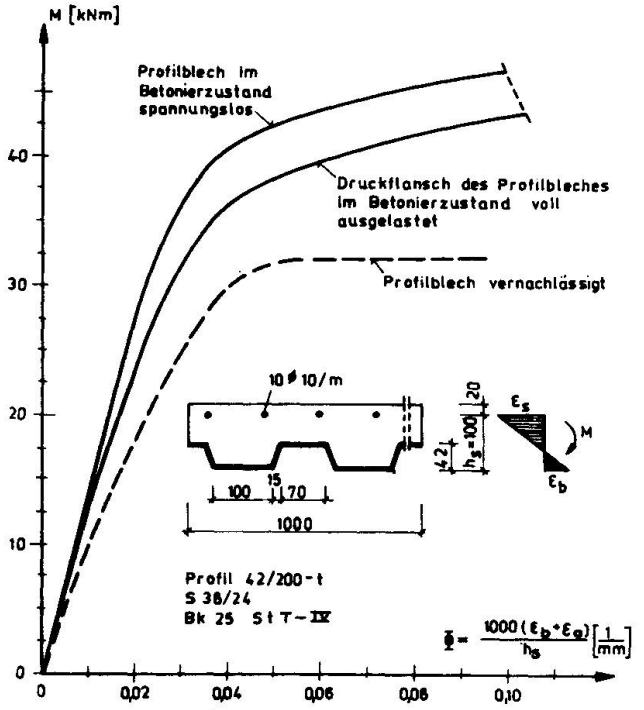

Es wurden 32 Versuchskörper geprüft, bei denen das Profilblech als Druckbewehrung wirkte. Davon versagten 20 durch Biegebruch. Die Nachrechnung dieser Versuche ergab gute Übereinstimmung bei Berücksichtigung des Profilbleches als Druckbewehrung:
- Mittelwert 1.079
- Standardabweichung 0.093
- Variationskoeffizient 0.086

Die bestehende Abweichung ist auch darauf zurückzuführen, daß sich im Beton ein dreiachsiger Spannungszustand aufgebaut hat, der bei der Nachrechnung nicht berücksichtigt wurde. Bei Vernachlässigung der Druckbewehrung sind große Abweichungen festzustellen(1.307-0.171-0.131).

Fig. 6 Momenten-Krümmungs-Beziehungen von Stahlprofilblech Verbunddecken

3.3 Momentenumlagerung

Für die Bestimmung der Schnittgrößenverteilung von Stahlprofilblech-Verbunddecken an statisch unbestimmten Systemen wurde ein Rechenprogramm geschrieben, das auf folgenden Voraussetzungen beruht:
- Die Querschnitte bleiben eben.
- Die Schubverformungen sind klein gegenüber den Biegeverformungen und werden deshalb vernachlässigt.

Es wurden verschiedene Parametereinflüsse untersucht. Besonderes Augenmerk wurde dem Einfluß unterschiedlicher Bewehrungsgrade

über der Innenstütze auf die Gesamttragfähigkeit des Konstruktionssystems und auf den Umlagerungsgrad des Stützenmomentes zugewandt (Figur 7).

Für extreme Bewehrungsverhältnisse wurden Umlagerungsgrade α_u bis zu 80 % nachgewiesen.
Der Vergleich der analytisch gefundenen Versagenslasten mit den Versuchsergebnissen, die an 4 Zweifeldecken gewonnen wurden, ergab für das Last-Verformungs-Verhalten gute Übereinstimmung.

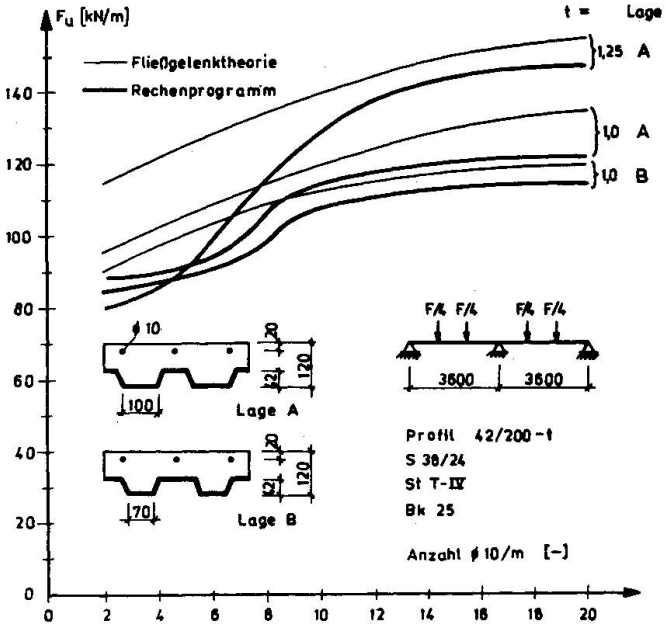

Fig. 7 Versagenslasten unterschiedlich bewehrter Zweifelddecken

LITERATURVERZEICHNIS

1. KIND S., Experimentelle und analytische Untersuchungen zum Tragverhalten von Stahlprofilblech-Verbunddecken. TH Leipzig, Dissertation, September 1984.

2. Berechnung, bauliche Durchbildung und Ausführung von stahlblechbewehrten Decken (Stahlblech-Verbunddecken). Vorschrift der Staatlichen Bauaufsicht, 7. Entwurf 09/84, VEB Metallleichtbaukombinat- Forschungsinstitut.

3. GOEBEN H.-E., KIND S., Weltstandsanalyse über Stahlprofilblech-Verbunddecken und Ausblick auf Anwendungsmöglichkeiten in der DDR. Wissenschaftliche Berichte der TH Leipzig, 1980, Heft 1.

4. MARX S., KIND S., GOEBEN H.-E., Verbundkonstruktionen im Stahlbau - Ein Beitrag zur Walzstahleinsparung. Wissenschaftliche Berichte der TH Leipzig, 1984, Heft 1.

5. REHM G., Über die Grundlagen des Verbundes zwischen Stahl und Beton. Deutscher Ausschuß für Stahlbeton, 1961, Heft 138.

6. FRANKE L., Einfluß der Belastungsdauer auf das Verbundverhalten von Stahl in Beton (Verbundkriechen). Deutscher Ausschuß für Stahlbeton, 1976, Heft 268.

7. DILGER W., Veränderlichkeit der Biege- und Schubsteifigkeit bei Stahlbetontragwerken und ihr Einfluß auf Schnittkraftverteilung und Traglast bei statisch unbestimmter Lagerung. Deutscher Ausschuß für Stahlbeton, 1966, Heft 179.

8. RÜSCH S., STÖCKL S., Versuche zur Festigkeit der Biegedruckzone und Einflüsse der Querschnittsform (Dreieck, Rechteck, Plattenbalken). Deutscher Ausschuß für Stahlbeton, 1969, Heft 207.

Composite Beams Using Newly Developed H-Shaped Steel with Protrusions

Poutres composites employant des profilés nouveaux en H avec saillies

Verbundträger aus neuentwickelten H-Stahlprofilen mit Oberflächenerhebungen

Ben KATO
Professor
Tokyo University
Tokyo, Japan

Suguru SAKAMOTO
Dr. Eng.
Sumitomo Metal Industries Ltd.
Hasaki-machi, Japan

Fumio OHTAKE
Dr. Eng.
Sumitomo Metal Industries Ltd.
Hasaki-machi, Japan

Keiichi TAKADA
Research engineer
Sumitomo Metal Industries Ltd.
Hasaki-machi, Japan

Koichiro OKUTO
Staff Manager
Sumitomo Metal Industries Ltd.
Osaka, Japan

Hiroshi NOSE
Staff Manager
Sumitomo Metal Industries Ltd.
Tokyo, Japan

SUMMARY

For steel-concrete composite structures an H-shaped steel with high shear bond performance to concrete by forming protrusions on its outer flange surface has been developed. The configuration of protrusions was determined as a result of many push-out tests, to find out the most effective configuration. The applicability of this H-shape steel to composite beam construction has been confirmed by full-scale model tests and field tests.

RÉSUMÉ

Pour les structures composites en acier-béton, on a mis au point les profilés en H avec une bonne adhésion transversale au béton en formant des saillies sur ses larges rebords extérieurs. Dans cette mise au point on a effectué un grande nombre d'essais d'extrusions afin de déterminer la meilleure configuration des saillies. De plus, la possibilité d'application de ce profilé en H aux poutres composites de bâtiments a été également confirmée au cours d'essais de modèle en vraie grandeur ainsi que d'essais sur le terrain.

ZUSAMMENFASSUNG

Für Stahl-Betonverbundkonstruktionen sind H-Stahlprofile entwickelt worden, welche auf der Flanschaussenseite Oberflächenerhebungen zur Steigerung der Schubverbundwirkung aufweisen. Die Anordnung der Oberflächenerhebungen wurde durch viele «Anstossversuche» bestimmt, um zur leistungsfähigsten Lösung zu gelangen. Die Eignung dieser H-Stahlprofile für Verbundträger in Hochbauten wurde durch Versuche im Massstab 1:1 und Feldmessungen bestätigt.

1. INTRODUCTION

Steel and concrete composite beams are widely used in bridge and building structures throughout the world. From the structural point of view, the mechanism of transfering shear stress at the interface of steel and concrete is the most important aspect. The flat surface of structural steel shapes, for example,does not exhibit any significant bond performance at all. A substantial number of shear connectors are required to be studded when beams are designed as steel and concrete composite beams. An extensive research and development work has been carried out by authors to introduce new concept of composite beams using new structural H-shapes, "Embossed H-Shapes". They have series of protrusions on their flange surfaces.

This paper reports the results of experimental research works carried out to fully investigate the hehavior of these composite beams formed by "Embossed H-Shapes". The bond characteristics of protrusions was investigated firstly by performing a number of push-out tests. The concept of shape factor for optimum configuration of protrusions has been introduced. The successful method to produce "Embossed H-Shapes" has been developed in the mean time as the result of several trial productions. Eleven full scale model specimens of different length were constructed and subjected to structural testings. The concept was then applied to several building steelworks as their sub-beams, and field tests were conducted there.

2. BOND CHARACTERISTICS

2.1 Test procedures

Twenty specimens for push-out tests were prepared. The protrusions were formed by machining flange surfaces this time. Line-type and dot-type protrusions as shown in Fig.1 were studied. The effect of parameters such as height (h), width (w_1,w_2), interval (i_1,i_2), rising angle (θ) of protrusions and concrete strength (Fc) was investigated. Details of these parameters and some of corresponding results of push-out tests are summarized in Table 1. Figure 2 illustrates the test specimens and procedures. The vertical load is applied statically and the slip between steel and concrete slab is detected by dial gauges. During the vertical loading, the pressure of 0.3 N/mm^2 was constantly applied to the interface between the steel and the concrete by the horizontal clamping apparatus.

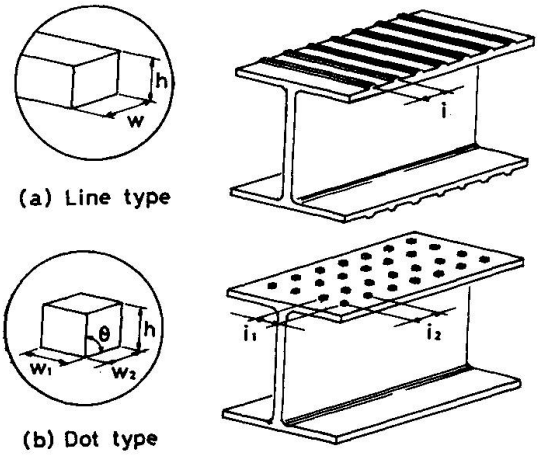

Fig.1 Type of protrusions of push-out test

2.2. Test results

Typical load-slip curves observed are compared in Fig.3. Maximum shear bond strength (τ_{max}) tabulated in Table 1 is in the form of the uniform stress acting over the whole matting area of steel to concrete. The deformation capacity(δ_{90}) is defined as the slip observed at the load of 90% of Pmax after the experiencing ultimate load Pmax.

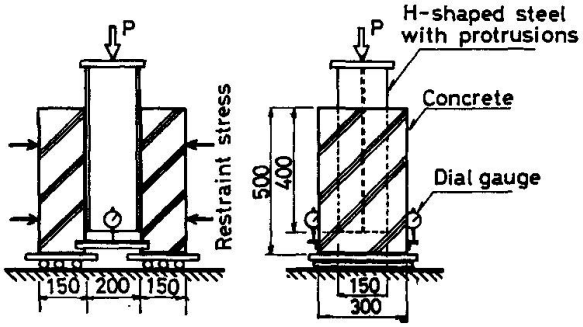

Fig.2 Test procedure of push-out test

The failure occurred in the concrete surface in all specimens. Two types of failure mode were observed. They are illustrated in Fig.4. One is the shearing failure and another is bearing failure [1]. Failure mode of each specimen is also listed in Table 1.

2.3. Discussion

The failure modes and the bond characteristics can be expected to be explained by introducing the concept of shape factor (As/Ab) of protrusions, where Ab is bearing area of the protrusions and As is their shearing area as illustrated in Fig.5 [2].

Fig. 6 shows the relationship between the bond strength in terms of concrete strength(τ_{max}/Fc) and the shape factor (As/Ab). It is seen in this figure that the bond strength increases as the shape factor decreases. The failure mode changes at the shape factor of about 9. The shearing failure occurs when (As/Ab) is less than 9 and the bearing failure does otherwise.

Fig. 7 shows the deformation capacity δ_{90} in relation to the shape factor. It is seen there that the shearing failure is associated with very little deformation capacity. This phenomenon is also illustrated in Fig. 3 by curves L-2 and D-8, which indicate that the load decreases abruptly right after reaching the Pmax. The successful bond characteristics with stable bond strength cannot be expected in the range where shape factor (As/Ab) is less than 9 when shearing failure always occures in brittle nature.

The rising angle (θ) showed little influence on the shear bond strength if the rising angle is greater than 60° (D-10 in Table 1). It could also be said that all the other parameters than As/Ab, such as the type of protrusions, do not exhibit significant influences on the bond strength. It has been concluded therefore that the optimum configuration of protrusions can be expected when their shape factor lies in the range of 10 to 20.

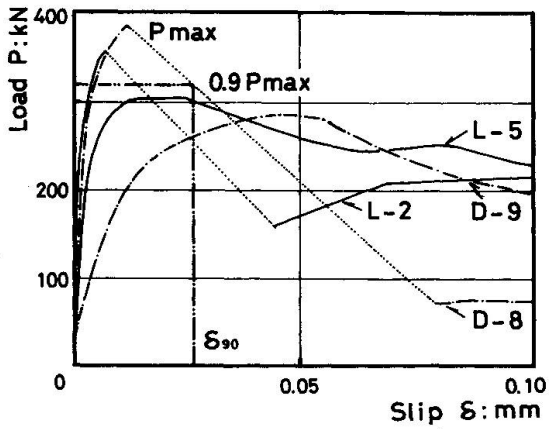

Fig.3 Typical load-slip curves

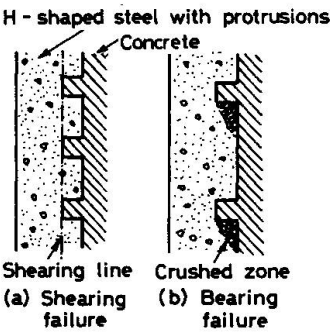

Fig.4 Failure modes

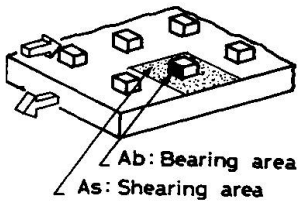

Fig.5 Shape factor As/Ab

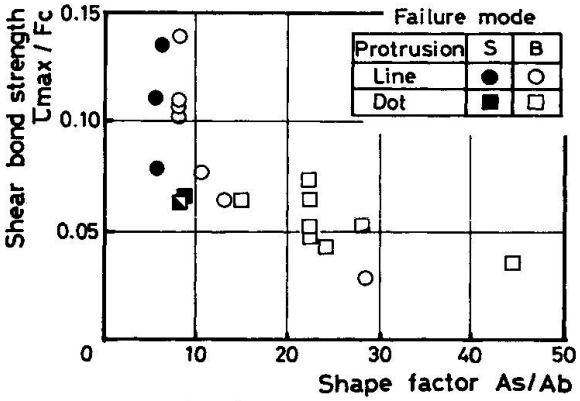

Fig.6 Bond strength

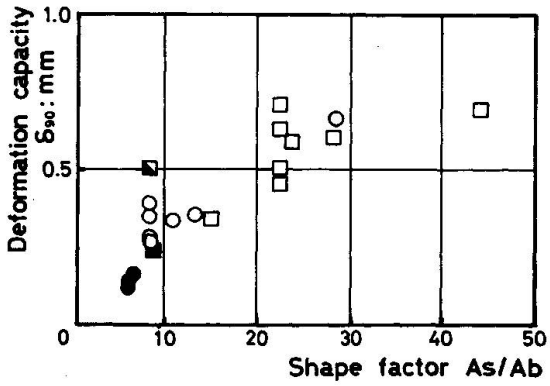

Fig.7 Deformation capacity

Specimen	Protrusions			Shape factor	Concrete strength	Bond strength	Deformation cap.	Failure mode*1
	Height h (mm)	Interval $i(i_1 \times i_2)$ (mm)	Width $w(w_1 \times w_2)$ (mm)	As/Ab	F_c (N/mm^2)	τ_{max} (N/mm^2)	δ_{90} (mm)	
L-1	2	15	3	6.0	31.8	2.48	0.12	S
L-2	2	15	3	6.0	25.6	2.88	0.14	S
L-3	2	20	3	8.5	25.6	2.62	0.27	B
L-4	2	20	3	8.5	25.6	3.57	0.35	B
L-5	2	20	3	8.5	25.6	2.73	0.39	B
L-6	2	25	3	11	25.6	1.99	0.34	B
L-7	2	30	3	13.5	25.6	1.64	0.42	B
L-8	2	60	3	28.5	31.8	0.98	0.66	B
L-9	3	30	4.5	8.5	25.6	2.81	0.29	B
L-10	6	50	1.0	6.7	36.3	4.90	0.17	S
D-1	3	15x15	4.5x4.5	15.2	31.8	2.04	0.34	B
D-2	3	18x18	4.5x4.5	22.5	36.9	1.88	0.51	B
D-3*2	3	18x18	4.5x4.5	22.5	20.2	0.94	0.46	B
D-4	3	18x18	4.5x4.5	22.5	20.2	1.30	0.71	B
D-5*2	3	15x30	15x4.5	8.5	20.2	1.23	0.50	B+S
D-6	3	20x20	4.5x4.5	28.1	31.8	1.67	0.60	B
D-7	3	25x25	4.5x4.5	44.8	31.8	1.13	0.69	B
D-8	5	20x20	7.5x7.5	9.2	31.8	2.13	0.27	S
D-9	5	30x30	7.5x7.5	22.5	31.8	2.32	0.64	B
D-10*3	3	18x18	6.2x6.2	23.7	36.9	1.52	0.63	B

Note : *1, In failure mode, S is shearing failure and B is bearing failure
*2, D-3 and D-5 have staggered protrusions
*3, D-10 has protrusions with the rising angle θ=60°

Table 1 Specimens and test results of push-out test

3. CONFIGURATION OF PROTRUSIONS OF EMBOSSED H-SHAPES

Interpreting the test results explained so far, the final configuration of protrusions to be roll-formed on the Embossed H-Shapes has been determined as shown in Fig. 8. The shape factor, As/Ab, of the protrusions is about 16. Embossed H-Shapes available at present from Sumitomo are in the form of universal beams whose flange width is 200mm and their height range from 300mm to 600mm, being commonly applied to the sub-beams of the structural steelworks in various buildings. Portions of flange surfaces about 50 mm from their edges are prepared flat without protrusions, so that they can easily support the ends of steel decks of cold formed light gauge sheets which in turn act as the concrete forms.

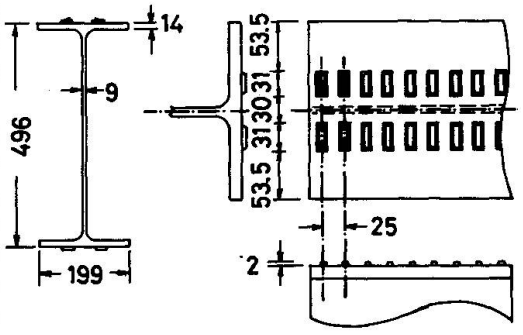

Fig.8 Embossed H-shape

4. APPLICABILITY OF EMBOSSED H-SHAPE TO COMPOSITE BEAMS

4.1 Bond strength of Embossed H-Shapes in composite beams

4.1.1 Specimen and test procedure

The higher bond stress is expected in composite beams than in push-out tests, because greater restraint force exists by pressing concrete slab vertically to the flange surface. Therefore, the shear bond strength of Embossed H-Shapes was investigated in the form of composite beams with short bending span, which are illustrated in Fig. 9. The specimens were designed to have failed in bond

failure before the yield of concrete or steel occurred. The upper half of Table 2 tabulates the parameters of six test specimens prepared. The methods of concrete placement and concrete characteristics are the main parameters. The sixth specimen, NA-1, was included for the purpose of comparison. This was a composite beam with a usual plain universal shape and shear connectors studded onto it, and with the same section as DA-2. Both NA-1 and DA-2 were formed with light gauge steel decks (JIS-ALM12). The deflection of beams, the slip between steel shapes and concrete slab and the strain distribution over several cross sections were the items measured during these short span tests.

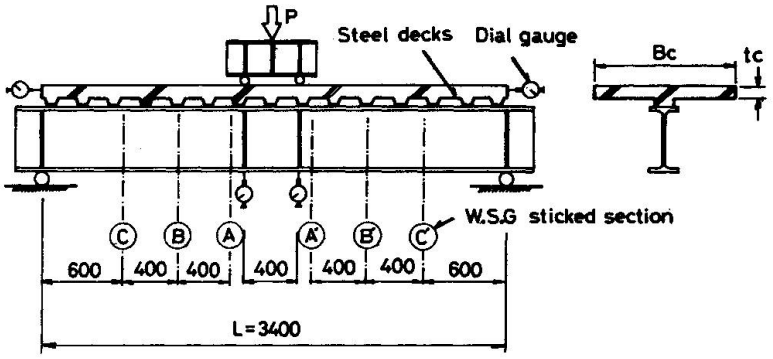

Fig.9 Short span test

Specimen		RC-slab: Width Bc (mm)	RC-slab: Thickness tc (mm)	RC-slab: Steel deck*1	Concrete: Sort*2	Concrete: F_c (N/mm²)	Test results: Maximum load P_{max} (KN)	Test results: Slip load P_s (KN)	Test results: Shear bond Strength τ_{max} (N/mm²)	$\frac{\tau_{max}}{F_c}$
Short span test	DA-1	1500	90	non	N	28.9	967	431	4.08	0.142
	DA-2	"	85	ALM-12	N	27.5	984	470	4.19	0.152
	DA-3	"	90	non	N	19.9	843	372	2.74	0.138
	DA-4	"	90	non	L1	23.7	872	402	3.19	0.135
	DA-5	"	90	non	L2	29.8	804	392	3.53	0.118
	NA-1	"	85	ALM-12	N	27.3	1101	-	-	-
Ordinary span test	DB-1	2800	85	ALM-12	N	23.3	607	607	4.56	0.196
	DB-2	"	90	non	N	18.2	568	372	3.21	0.176
	DB-3	"	50	ALM-12	N	17.5	631	441	2.63	0.150
	NB-1	"	85	ALM-12	N	29.8	768	-	-	-
	DC-1	"	90	non	N	22.8	735	395	3.70	0.162

Note : *1, ALM-12 deck is a JIS-Standard deck with 1.2mm in thickness and 75mm in web height.
*2, N is normal concrete. L_1 and L_2 are light weight aggregate concrete with the specific gravity of 1.8 and 1.6, respectively.

Table 2 Specimens and test results of composite beam test

4.1.2 Test results and discussions

The load slip curves are shown in Fig. 10. The conventional beam, NA-1, shows a ductile behavior, but the slip occurs in the early stage of loading, see Fig.10, so that it's initial rigidity is lower than DA-2 with Embossed H-Shape. Although the behavior of Embossed-H composite beams is less ductile after the initial slip of concrete occurred on the flange surface of steel shapes, the complete composite action with no slip movement can be expected before then.

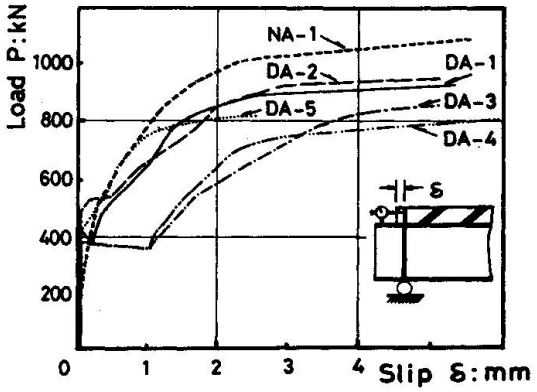

Fig.10 Load-slip curves in short span test

The maximum shear bond stress (τ_{max}) of Embossed H-Shapes is calculated by dividing the increments of axial force of the steel cross-section by the resisting area which, in turn, is the multiple of the incremental beam length times protruded width of 100mm, see Fig. 8, indifferent of the method of concrete placement with or without cold formed steel forms. The results are also tabulated in Table 2. The maximum shear bond strength (τ_{max}) of Embossed H-Shapes is plotted against concrete strength (Fc) as shown in Fig.11. A linear relationship ($\tau_{max} = 2 \times Fc/15$) can be observed, and by utilizing this and certain value of factor of safety,a design method can be formulated. For Japanese domestic application, the factor of safety of two (2) was adopted.

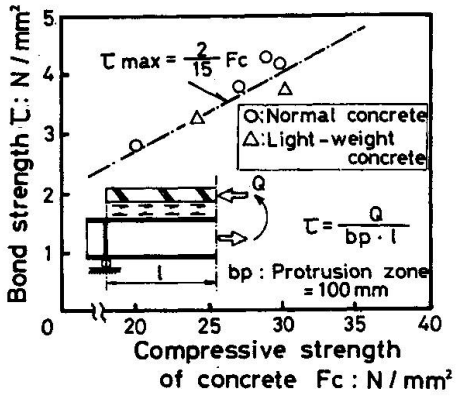

Fig.11 Relation between concrete strength and bond strength

4.2. Full-scale model tests

4.2.1 Specimen and test procedure

Five full scale composite beam with ordinary length of sub-beams were prepared. Specimen configurations are illustrated in Figs. 12 and 13. The lower half of Table 2 tabulated the details of these specimens.

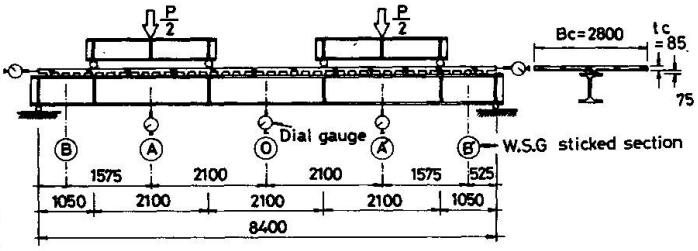

Fig.12 Ordinary span test in simple beam

Dimensions and cross-sectional properties of the specimen DB-1 are the exact duplication of composite sub-beams recently constructed in Japan, utilizing Embossed H-Shapes of mild steel. The concrete slab was placed on the light gauge steel deck, JIS-ALM12. The concrete of the specimen DB-2 was placed over the usual and supported concrete form,without using steel deck. The specimen DB-3 is with steel deck but its slab is thinner than DB-1. NB-1 is the specimen of conventional composits beam by a plain universal beam, the size of which is the same as that of DB-1, with shear connectors studded on its flange surface. The cross-section of DC-1 is the same as that of DB-2, but this was tested under the condition of seemingly continuous beam. The same sections are connected at both ends of the DB-2 specimen, as shown in Fig. 13. This is the configuration of usual sub-beams, connected to main girders with high-strength bolts. Nearly central span of sub-beams at both ends of the specimen DC-1 was restricted from any upward deflection, so that some negative bending moment occurred at the location of connections to girders. Load were applied as illustrated in these figures and measurements obtained were the deflection of beams, the slip between the steel shape and concrete slab and strains at various cross-sections.

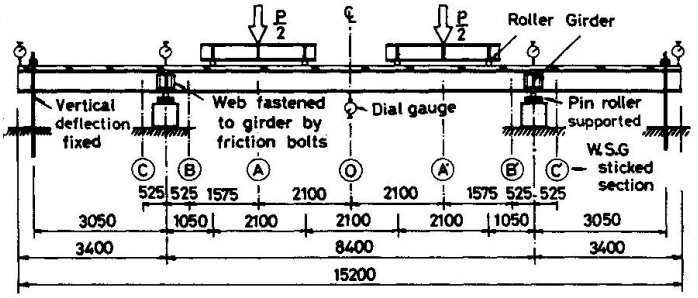

Fig.13 Ordinary span test in continuous beam

4.2.2. Test results and interpretations

Figure 14 illustrates the load-deflection relationships of two specimens, DB-1, a composite beam with an Embossed H-Shape and NB-1,a composite beam with an ordinary universal beam with shear connectors. Pys there is the calculated load at which the steel shapes in the composite cross section yield. Pub is the shear strength calculated for Embossed H-beam,DB-1, using the results of short span tests (τ max = 2x Fc/15). Both specimens were subjected to repeated loading up to Pys for six cycles. The same characteristics as observed in short span tests can be confirmed also in this figure. Studded beam,NB-1, starts to loose its rigidity at the load much less than Pys, and residual deflection is accumulated during six repetitions of cycle loading. Embossed H-beam DB-1, on the other hand, maintains its initial rigidity even when Pys is reached. It can be concluded that, at least in the elastic range, composite beams with Embossed H-Shapes behave in the same manner as, or rather more rigidly than those with ordinary beams and shear connectors.

Specimens DB-2 and DC-1 are compared in Fig. 15. Some cracks appeared in the concrete slab at the location over the steel connections to girders at fairly early stage thus loosing the rigidity of the continuous slab specimen, DC-1. The behavior of this beam then becomes similar to that of DB-2,a simply supported beam,and nearly at Pys the slip between steel and concrete was observed both in DB-2 and DC-1, as was seen in above mentioned test of DB-1. Many slip-like saw shapes seen in the curve of DC-1 are attributed to the frictional slips occurred at high-strength bolts connecting a sub-beam to main girders. Throughout the whole test period,the curve of DC-1 stayed higher than DB-2.

The behavior of DB-3, the specimen with thinner concrete slab, is illustrated in Fig.16. The shear bond strength of this specimen was designed much less than Pys, the yield of steel, and this was confirmed in the behavior of the test beam. No other significant failures anticipated due to thinner concrete slabs were observed during the test.

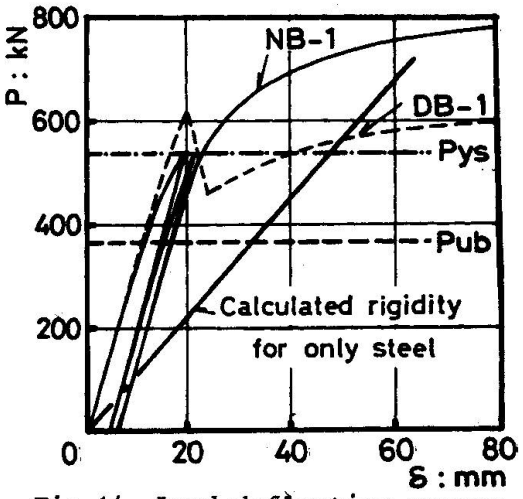

Fig.14 Load-deflection curves of DB-1 and NB-1

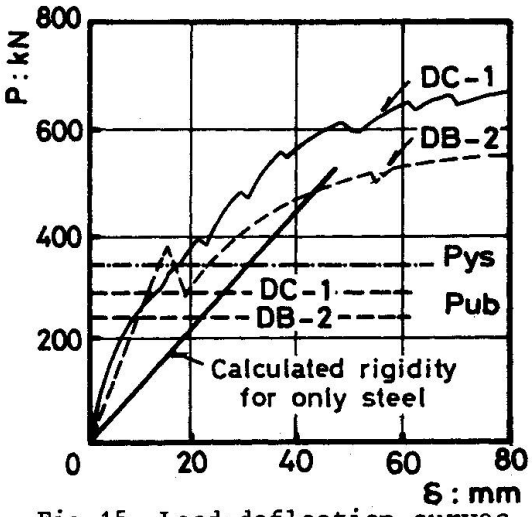

Fig.15 Load-deflection curves of DB-2 and DC-1

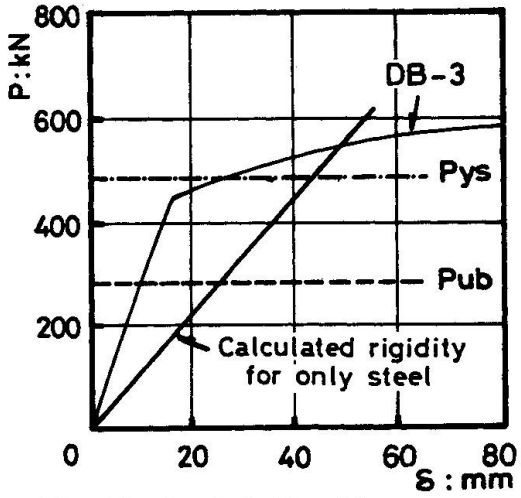

Fig.16 Load-deflection curves of DB-3

The shear bond strength of these composite beams is also tabulated in Table 2. These figures are somewhat higher than those obtained by short span tests. Slip loads at which the initial slips occur in these beams are also higher than those in short span tests. It is seen that in short span tests the load applied is rather concentrated,while it is more uniform in these full scale model tests. Therefore,the shear bond strength is considered to be greater when the concrete slab is pressed down onto the flange surface more effectively. From this point of view, the optimum condition exists in the beams loaded by uniformly distributed loads. The shear bond strength obtained by short span tests is, therefore, considered to stay in safety side, when this is used in the design formula for the conditions of uniformly distributed load.

Higher rigidity of floor beams offers less vibration. Vibration problems of floor beams are getting more strict nowadays. Steel and concrete composite construction increases the rigidity of frame members and thus decreases the vibration troubles. Factor of increase in its rigidity over the simple steel construction is said to be 2 to 3 [3]. About ten buildings have been constructed so far using Embossed H-Shapes as sub-beams. Number of field tests up to their design load were performed in some of these buildings. The results were compared with those of laboratory tests described in this report, and the applicability of Embossed H-Shapes was further confirmed successfully. The use of the Embossed H-shaped for composite construction exhibits large economic advantages in addition to the simplification of field works.

5. CONCLUSIONS

(1) Universal beams (Embossed H-Shape) which exhibit substantial shear bond performance with concrete have been developed by roll-forming protrusions on their flange surfaces in univesal mills.

(2) Extensive Push-out tests have revealed that the most dominant factor to affect the shear bond characteristics is the shape factor (As/Ab) It has been found out that, as the shape factor decreases, the shear bond strength increases but that there exists the lower bound of the shape factor below which no ductility of bond characteristics can be expected.

(3) The configuration of protrusions to be roll-formed on the flange surface of the Embossed H-Shapes has been determined by the results obtained by these extensive push-out tests.

(4) The shear bond strength has been investigated by full scale composite beams with Embossed H-Shapes and the results have been formulated as $\tau_{max}=2\times Fc/15$.

(5) It has been confirmed further, for example by several field tests, that the composite beams with Embossed H-Shapes exhibit the complete composite behavior at least in the elastic range untill the bond stress reaches its ultimate strength.

REFERENCES

[1] TSUBOI Y. and YASHIRO H., Experimental Study by Deformed Bar. Journal of Institution of Industrial science, Univ. of Tokyo, vol.15,No.1,1953

[2] CLARK A.P., Comparative Bond Efficiency of Deformed Concrete Reinforcing Bars. Journal of A.C.I.,Dec.1946

[3] HIRANO M.,Present Status of Progress of Composite Structures in Buildings in Japan. Society of Steel Construction of Japan,vol.13,No.143,1977

[4] KATO B.,NISHIDA A.,MURAKAMI N.,SAKAMOTO S.,OHTAKE F. and TAKADA K.,Bond Characteristics of H-Shaped Steel with Protrusions on Its Surfaces.Annual Meeting of Architectural Institude of Japan (A.I.J.),Oct.1977

[5] KATO B.,SAKAMOTO S.,OHTAKE F. and TAKADA K.,Mechanical Properties of Composite Beam by Embossed H-Shape(Part I,II),Annual Meeting of A.I.J.,1981,1982

Behaviour of Concrete In-Filled Tubular Columns

Comportement des colonnes mixtes formées de tubes remplis de béton

Verhalten von betongefüllten Stahlhohlprofilstützen

C.N. SRINIVASAN
Partner
M/s C.R. Narayana Rao
Madras, India

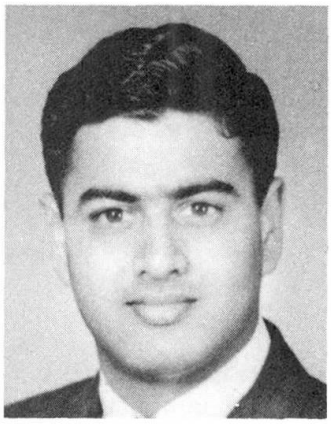

Completed his Under-Graduate Degree in Indian Institute of Technology, Kharagpur. Got his Post-Graduate Degree and Training in United States. He is involved in Design of Structures, both Concrete and Steel for Industrial Buildings and High rise buildings.

SUMMARY

Concrete in-filled tubular columns represent a class of structure where the best properties of steel and concrete are used to their maximum advantage. Aspects governing strength and behaviour over the entire range of loading have been studied and capacity interaction diagrams proposed based on the stress strain relationship for the constituent material properties.

RÉSUMÉ

Les colonnes mixtes formées de tubes remplis de béton représentent le type d'élément structurel utilisant au mieux les caractéristiques de l'acier et du béton. Les phénomènes gouvernant leur comportement et leur résistance face aux différentes sollicitations possibles sont étudiés et des diagrammes d'interactions basés sur les relations contrainte-dilatation des matériaux constitutifs sont donnés.

ZUSAMMENFASSUNG

Betongefüllte Stahlhohlprofilstützen stellen ein Bauelement dar, bei dem die besten Eigenschaften von Stahl und Beton am vorteilhaftesten kombiniert werden. Aspekte, welche die Festigkeit und das Verhalten über den ganzen Belastungsbereich beeinflussen, wurden studiert, und ein Tragfähigkeitsinteraktionsdiagramm wird aufgrund des Spannung-Dehnungs-Verhältnisses der beteiligten Materialien vorgeschlagen.

Concrete in-filled tubular columns represent a class of structure where the best properties of steel and concrete are used to their maximum advantage. The following aspects governing the strength and behaviour have been studied. (1)

1. Confining action in circular and square CITC.
2. Triaxial effects on the core and biaxial effects on the shell.
3. Presence of lateral strain compatibility and complete interaction of core and the shell, over entire range of loading.
4. Effect of method of loading and a study of connections.
5. Factors governing the service and the ultimate load behaviour.

The test programme included -

In the first phase, 150 mm dia circular and square tubes of 300 mm to 1200 mm lengths were tested to develop a stress strain relationship for core and shell and to study items 1 to 3 above. 6 Nos. circular short specimens of CITC have been tested to verify the validity of the proposed lead-strain relationship.

In the second phase, CITC, of lengths 1200 mm, 1840 mm and 2500 mm have been tested for both axial and eccentric loaded conditions and to study the connection details and transfer of load from horizontal (beams and slabs) to vertical member (CITC).

A total of 12 specimens were tested for axially loaded condition, out of which 8 were for the study of connections. 13 specimens were tested for eccentrically loaded condition. In addition, 8 specimens were tested to study the presence of bond at the concrete steel interface. 6 specimens were tested to study the effect of k, the lateral load enhancement factor with slenderness ratio.

Table I and II summarises the results of eccentrically and axially loaded sections. Fig. 1 shows a specimen under test.

Stress strain relationship of the constituent materials of the CITC was studied to prepare an equivalent stress strain relationship for the laterally confined core of concrete and biaxially stressed steel shell (overcoming the difficulty of defining the areas of cross section and ratios of module of the constituent materials) that would be applicable for the entire range of loading, taking into account progressively increasing degree of confinement applied continuously over the length of the specimen.

The following additional factors affecting stress strain relationship have been studied.

1. Effect of lateral load enhancement factor with reference to slenderness.
2. Effect of variation of Poisson's ratio of concrete with stress level and its effect on bond between core and shell.
3. Percentage load carried by shell and core over the entire range of loading, which reverses from service load to ultimate load requiring different load factors are to be applied to service load and ultimate load stages. (Fig. 2)

As opposed to reinforced concrete columns and concrete encased steel columns, in the CITC, lateral strain compatibility and composite action is absent upto a load level, $\frac{P}{P_Y} = 0.50$. Consequently, the core of CITC is laterally

confined at advanced stages of loading only and at the earlier stages of loading it is under a uniaxial stage of stress. Thus for a realistic representation of actual behaviour under progressively increasing loads, different stress-strain relationship are to be employed to represent service stage and ultimate stage behaviour. Based on all the foregoing, a stress strain relationship is proposed. (1) (2)

Based on the study of connections (beam to column and flat slab to column) on the strength and behaviour, it is concluded that methods of transferring load from horizontal members (beam or slabs) to vertical members (CITC) affect the strength and behaviour of CITC as also the load-strain behaviour of constituent material. Flat slab to column type of connection , particularly when the connection is such, where the shell and core are loaded together or where the core alone is loaded (Fig. 3) is an effective connection detail, where the enhanced strength of the concrete core, is best exploited. Beam to column type of connection where shell alone is loaded first, does not lend itself for a proper exploitation of CITC. In fact this type of connection is unsafe andnot reliable.

Capacity interaction formulae for square and circular CITC, for service and ultimate load stages, based on the true stress strain curves for CITC, and taking into account percentage of load shared by the core and the shell of different stages of loading, have been developed. A typical interaction diagram for circular and square CITC is shown in Fig. 4 and 5. Effect of wall thickness, diameter and strength of concrete mix have also been studied in this investigation.

On the study of the square and circular CITC, the strength and behaviour of square and circular CITC are governed by different parameters. The confinement effect of a circular shell is far higher than the square one, all the more so, if beam to column type of bracketted connections are employed, i.e., when the connection transfers the force to the shell of the column. CITC shows large enhancement of load carrying capacity and can sustain large strains and deformations. This reserve of strength and deformation makes CITC, asideal structural element in certain special conditions, as in a seismic design. This study has indicated that for effective exploitation of CITC, high strength tubes are to be employed. In the ranges tested, i.e., relatively short specimen of $\frac{L}{d} < 12$ and small eccentricity $\frac{e}{d} < 0{\cdot}2$, the failure load is even more than one and a half times the failure load calculated employing uniaxial stress strain relationship for steel and concrete.

A design method to take into account the enhanced strength is proposed in this study. A design method has also been developed as a part of this study.

REFERENCES

1. SRINIVASAN C.N. Behaviour of Concrete In-filled Tubular Columns. Thesis submitted for the award of Doctor of Philosophy - Indian Institute of Technology, Madras 1981.

2. SEN H.K. Triaxial effects in concrete filled Tubular Steel Columns. Thesis submitted to University of London 1969.

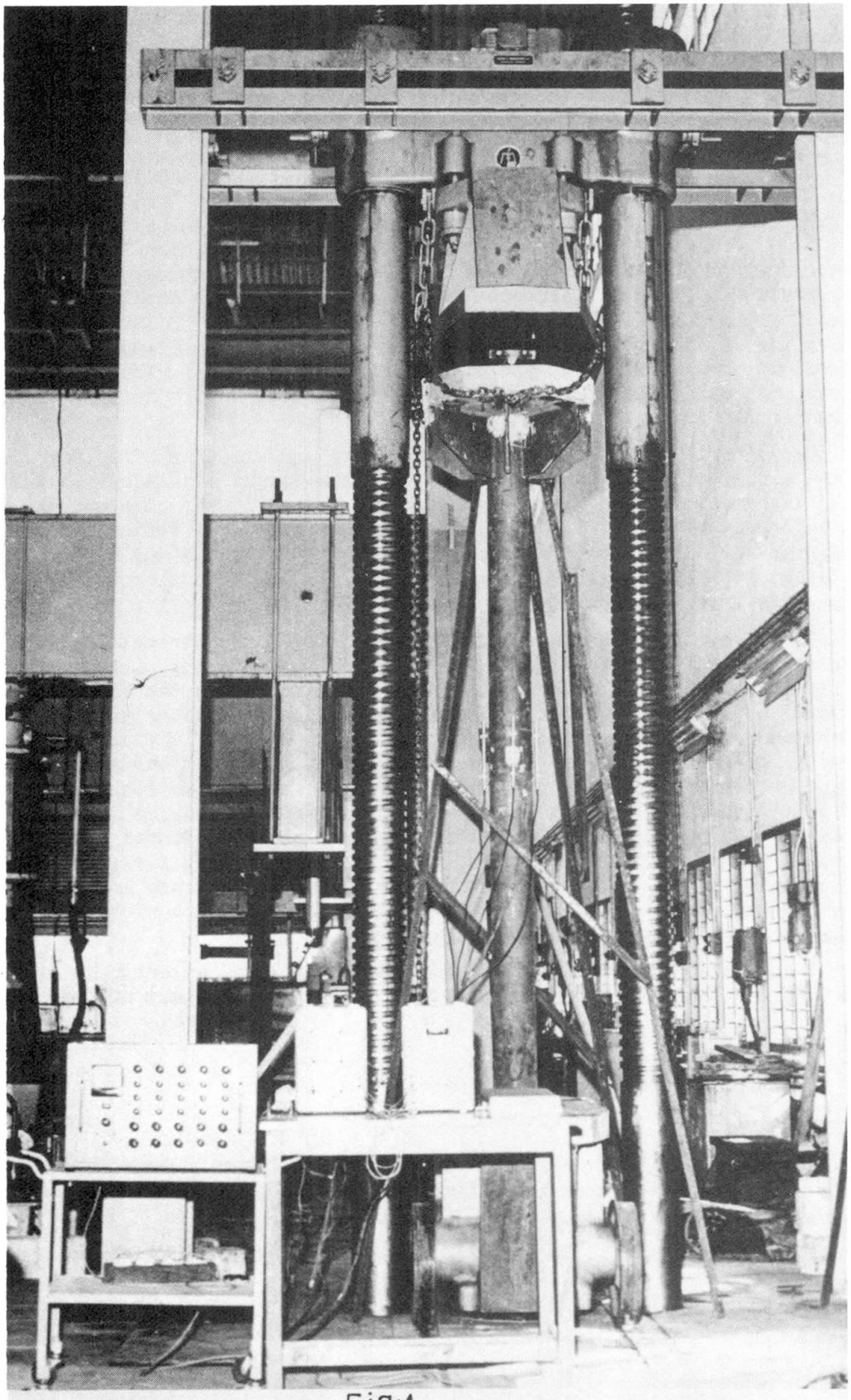

Fig:1

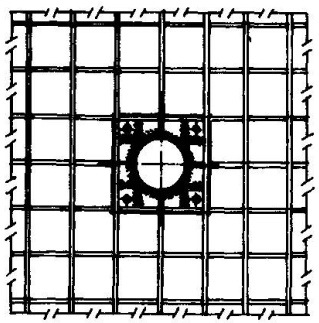

PLAN OF JOINT

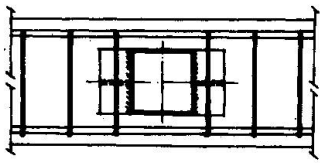

PLAN OF SEATING BRACKET.

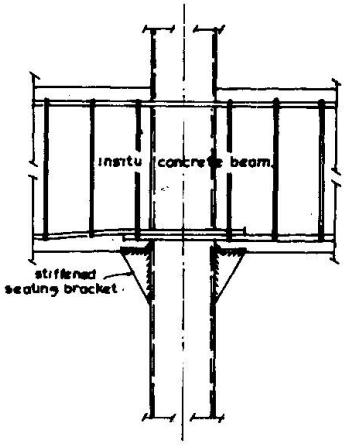

b. CONTINUOUS COLUMN TO FLOOR BEAM.

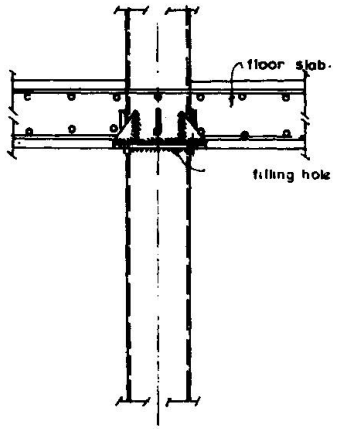

a FLUSH FLOOR JOINTING.

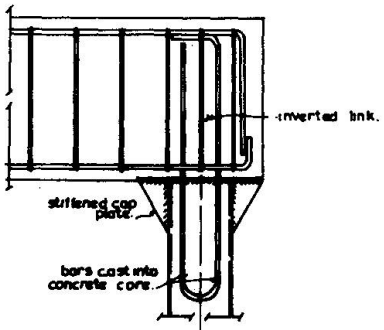

c PERIMETER COLUMN TO FLOOR BEAM.

FIG: 3 TYPICAL CONNECTIONS. COLUMNS TO CONCRETE FLOOR CONSTRUCTION

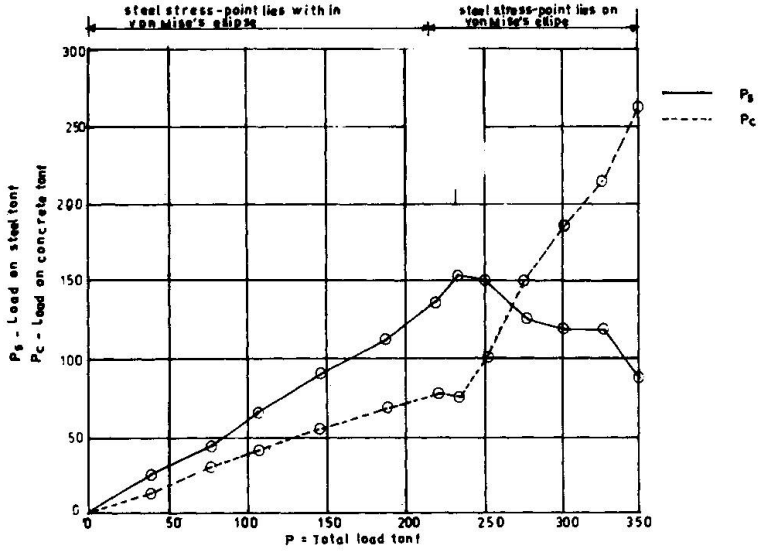

Fig: 2(a) TYPICAL DIAGRAM SHOWING LOAD SHARED BY STEEL AND CONCRETE OVER ENTIRE RANGE OF LOADING (BASED ON SEN. 22)

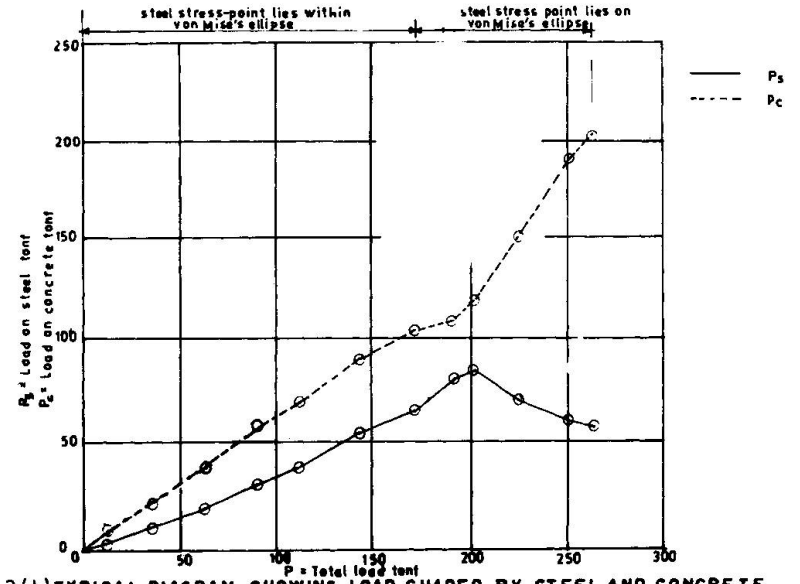

Fig: 2(b) TYPICAL DIAGRAM SHOWING LOAD SHARED BY STEEL AND CONCRETE OVER ENTIRE RANGE OF LOADING (BASED ON SEN. 22)

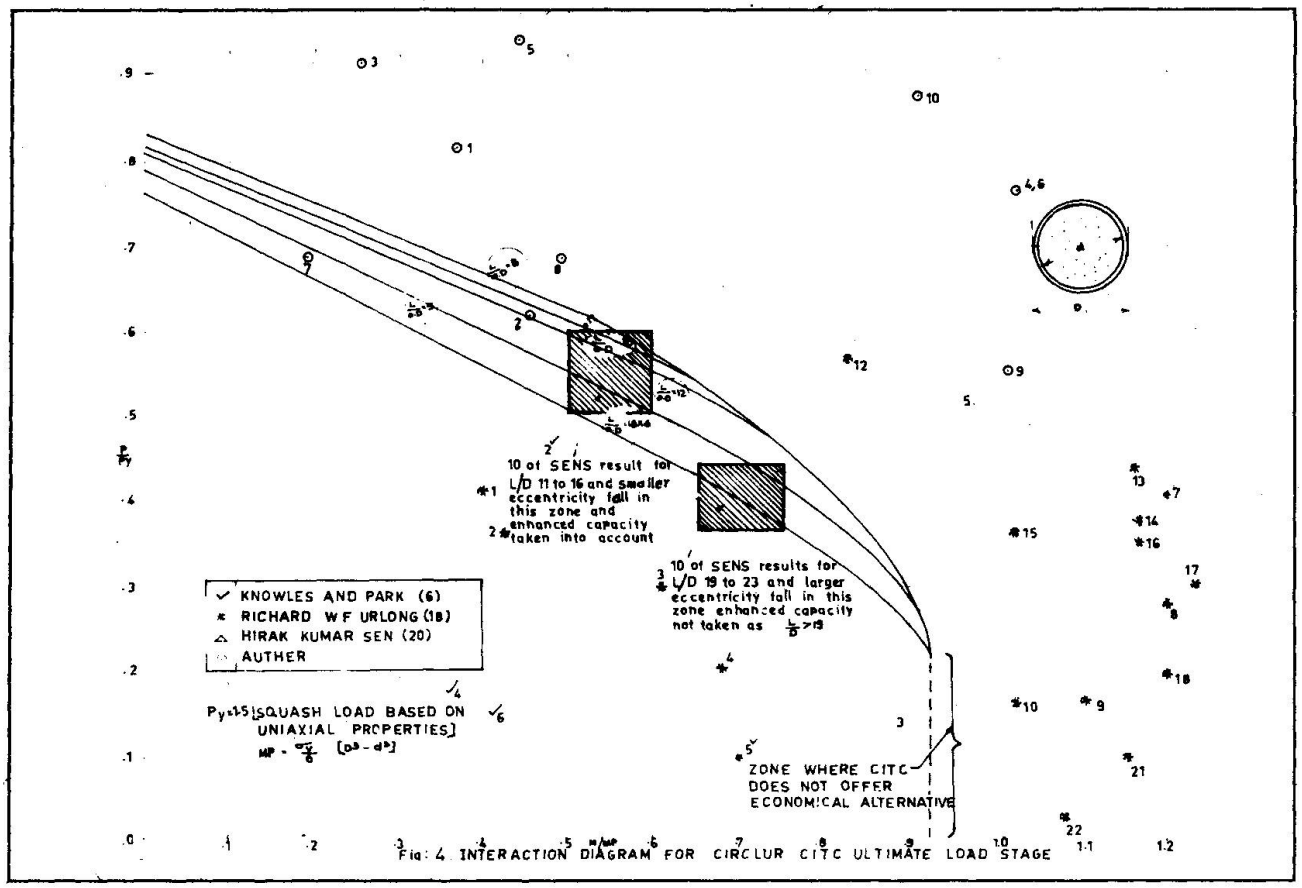

Fig: 4 INTERACTION DIAGRAM FOR CIRCLUR CITC ULTIMATE LOAD STAGE

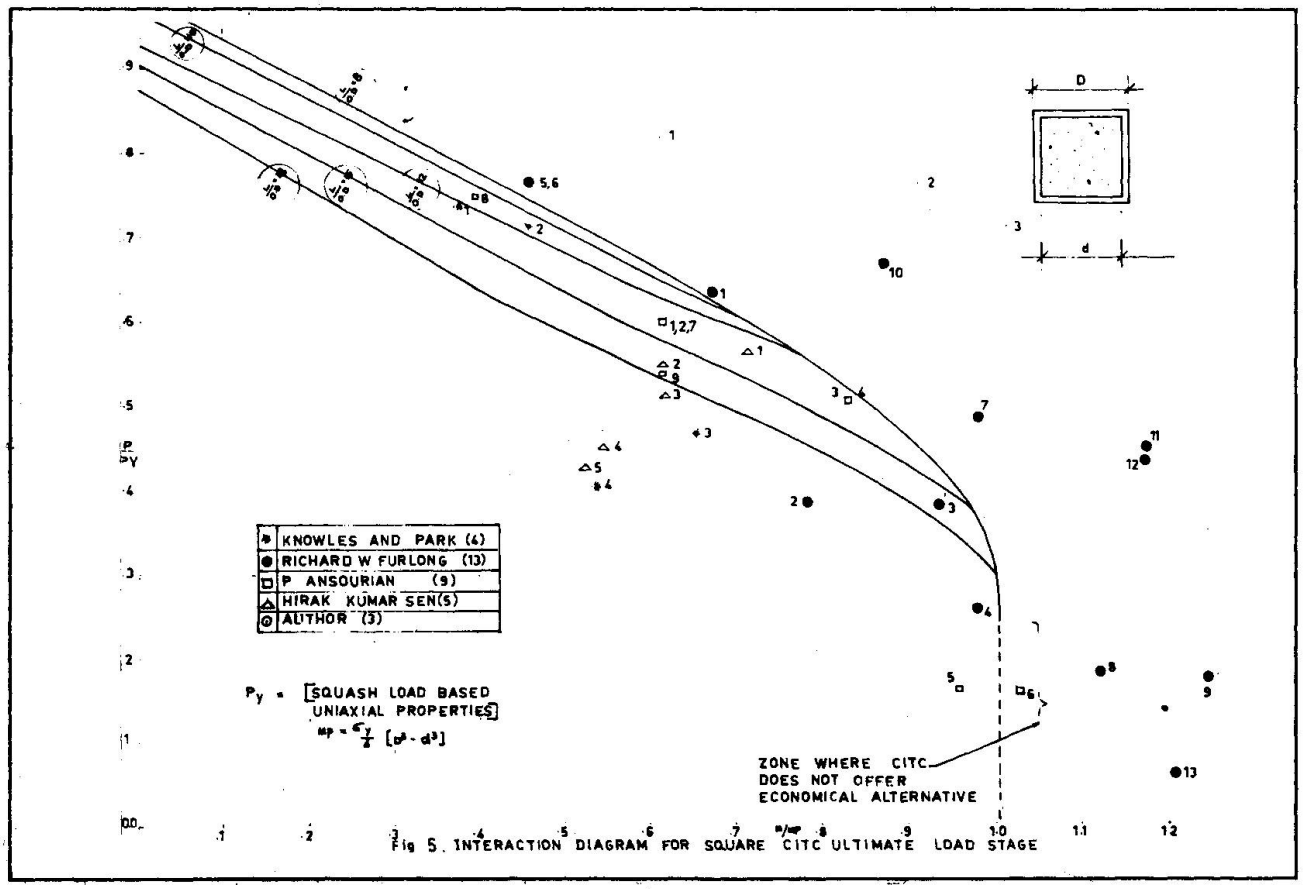

Fig 5. INTERACTION DIAGRAM FOR SQUARE CITC ULTIMATE LOAD STAGE

TABLE I

TEST RESULTS OF AXIALLY LOADED SPECIMEN TO STUDY THE INFLUENCE OF METHOD OF LOADING.

DESCRIPTION : 15 cm. nominal dia. or 15 cm. square x 6 mm wall thickness x 122 cm long tube infilled concrete corresponding to a 15 cm cylinder strength of 300 kg/cm^2

Brief Description of Loading.	Failure load (Tonne)	Observations at Failure.
Infilled circular tube core only loaded.	185	Formation of Luder Lines and spalling of mill scales and kind at mid-height.
Infilled circular tubes both shell and core loaded.	200	Luder lines with spalling of mill scales and kink at mid-height.
Infilled circular tube, bracketed arrangement beam to column type connection-shell loaded.	110	Bulges at top and local buckling.
Hollow circular tube.	90	Bulges at top and local buckling.
Infilled circular tube, shell only loaded.	85	Bulges at top and local buckling.
Infilled circular tube flat slab to column connection core and shell loaded.	205	Formation of Luder lines, bending with kink at mid-height.
Square tubes - core only loaded.	200	Cracks formation at the welds
Square tubes - both core and shell loaded.	240	Cracks at the welds.
Infilled square tube-bracketed arrangement, 'Beam to Column' type connection - shell loaded.	120	Bulges at top and local buckling.
Hollow square tube.	75	Bulges at top and local buckling.
Infilled square tube, shell only loaded.	88	Bulges at top and local buckling.
Infilled square tube - flat slab to column type connection - core and shell loaded.	250	Formation of Luder lines and bending with kink at mid-height.

TABLE II

TEST RESULTS OF ECCENTRICALLY LOADED CIRCULAR AND SQUARE CITC.

DESCRIPTION :

(1) 15 cm. nominal dia. x 6 mm wall thickness Circular CITC. 122 cm. long.
(2) Do Do 184 cm. long.
(3) Do Do 250 cm. long.
(4) 15 cm. x 15 cm. x 6 mm square CITC. 122 cm. long.

Concrete mix of the infill corresponds to 15 cm. cylinder strength of 200 kg/cm.^{2}

S.No.	Brief Description.	Length in cm.	Eccentrically applied in load in cm.	Observed failure load in tonnes.	
1.	Circular CITC Core only loaded.	184	1.0	118.0	Core only loaded with loading head-bearing through 5 cm. thick close fitting loading head.
	Do	184	1.6	98.0	
	Do	122	0.6	133.0	
2.	Circular CITC Core and shell loaded.	122	1.0	140.0	Concrete face finished smooth.
	Do	122	3.0	120.0	
	Do	250	0.6	100.0	
3.	Circular CITC beam to column type bracketed connection shell only loaded.	122	1.5	100.0	Shell only loaded through stiffened bracket.
	Do	250	4.0	80.0	
4.	Circular CITC- Flat slab to column type connection Core and shell loaded together.	122	2.0	127.0	
5.	Square CITC- Core and shell loaded.	122	2.5	112.0	Concrete face finished smooth.
6.	Square CITC beam to column type bracketed connection shell only loaded.	122	4.0	105.0	
	Do	122	5.0	95.0	
	Enhanced Failure load of Circular CITC (under axial load).			145.35	tonnes.
	Failure load of Square CITC (under axial load).			134.00	"
	Moment capacity of circular CITC.			306.78	" cm.
	Moment capacity of square CITC.			459.00	" cm.

Battened Composite Columns

Colonnes diaphragmées mixtes

Verschalte Verbundstützen

Hassan SHAKIR-KHALIL
Lecturer
University of Manchester
Manchester, Great Britain

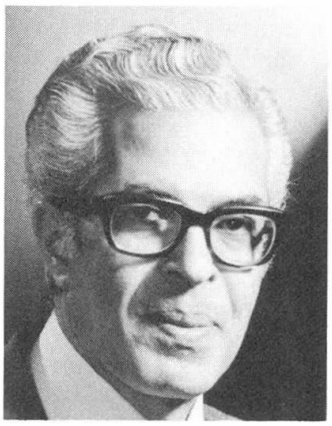

Hassan Shakir-Khalil graduated in Civil Engineering from Cairo University, Egypt, where he also obtained his Masters degree. He obtained his PhD degree from Cambridge University. During 1958–60 he worked in the Bridge Department with Krupp, Rheinhausen. He spent most of his working life in the academic field.

Yasser M. HUNAITI
On study leave
University of Jordan
Amman, Jordan

Yasser M. Hunaiti, born in Jordan in 1956, obtained his BSc (Eng.) in 1978 from Garyounis University, Libya. He was awarded a scholarship from University of Jordan, and obtained his MEng from McGill University, Canada, and has been reading for his PhD degree in Engineering at Manchester University, England since January 1983.

SUMMARY

The paper deals with a new type of composite column which consists of two steel channels facing each other and connected together with end and intermediate batten plates. The rectangular shaped core so formed is then filled with insitu plain concrete. Full scale tests have been carried out on this new type of column with a view to establishing that this form of composite column can be safely designed in accordance with both the new British Bridge Code and the European recommendations of the ECCS for Composite Structures.

RÉSUMÉ

Cet article décrit un nouveau type de colonnes mixtes composées de deux profilés en C réunis par des diaphragmes; l'espace intérieur ainsi créé est ensuite bétonné au chantier. Des essais ont été conduits pour montrer que ce type de colonnes peut être dimensionné en toute sécurité avec les Normes Britanniques et les Recommendations Européennes.

ZUSAMMENFASSUNG

Der Vortrag behandelt einen neuen Typ von Verbundstützen, welcher aus zwei sich gegenüberliegenden U-Stahlprofilen besteht, die an den Enden wie auch an Zwischenstellen mit Schalplatten verbunden sind. Der rechteckig geformte Kern wird mit Ortsbeton gefüllt. An diesem neuen Stützentyp wurden im Massstab 1:1 Versuche durchgeführt, mit dem Ziel zu beweisen, dass diese Art von Verbundstützen sowohl nach den Britischen Brückenbaunormen, wie nach den Europäischen Empfehlungen der EKS für Verbundkonstruktionen, sicher bemessen werden können.

1. INTRODUCTION

Composite columns of steel and concrete have been in use for several decades. Until recently, the methods of design for such columns have been of the empirical type, and were based on the experimental results of few full-scale tests and on very little research [1]. Two methods of design have now become available for the design of composite columns, namely the British Bridge Code [2] and the European recommendations for composite structures by the ECCS [3], referred to hereafter as the Bridge Code and the ECCS method. Both these methods of design are applicable to concrete-encased steel sections as well as to concrete-filled tubes. In the case of concrete-encased steel sections, sufficient longitudinal and transverse reinforcements are required to ensure full composite action up to failure between the structural steels and concrete elements, including the reinforcement. In the case of concrete-filled hollow steel sections, although no reinforcement is needed to ensure the composite action between the structural steel and concrete elements, reinforcement can be used for fire protection requirements.

2. WHY BATTENED COMPOSITE COLUMNS?

The concrete-encased type of composite column was a natural development of the traditional use of light concrete encasement as a means of fire protection for the structural steel section. This type of composite column suffers from the present situation in the construction industry in which the cost of the labour element has been rising steeply in the last few decades. The column requires a complete shuttering as well as a reinforcement cage which is further complicated by the presence of the steel core within. The concrete-filled hollow section requires neither shuttering nor real reinforcement since the tube is filled with plain in-situ concrete. However, the structural steel element of this type of composite column is exposed, being on the outside, and hence requires some form of fire protection. Furthermore, when using this type of column with standard flooring, it can be seen that the beam-column connections are neither of the simple type nor are they easily accessible as when the structural steel element of the column is of the rolled steel type.

The proposed battened composite column consists of two steel channel sections, battened together by means of end and intermediate batten plates, and the inside is then filled with plain in-situ concrete. This type of column compares favourably with the traditionally used composite columns given above. However, similar to the concrete-filled steel tubes, it has no concrete encasement, and therefore requires some form of fire protection. Compared to the traditional composite column sections, the battened composite column offers the following advantages:

- it requires shuttering of a simple and cheap form
- requires no reinforcement cage
- is more versatile since its load-carrying capacity can be altered simply by changing the depth of the column.
- makes very efficient use of the structural steel element since the steel is placed on the outside where it is most needed.
- provides easy access to the inside core, and hence, unlike concrete-filled tubes, makes for easy beam-column connections.

Tests have been carried out on full-scale battened composite columns and the results published elsewhere [4]. Further tests have been performed on another series of columns in which extensive strain measurements were taken, and which established the full composite action between the structural steel and concrete core up to failure [5]. Simple expressions have also been developed for the

design of this type of column [6] and were based on an approach proposed by Johnson and Smith [7].

3. DESIGN OF COMPOSITE COLUMNS

The load carrying capacity of a short composite column is a function of its squash load N_u, the design ultimate moment of resistance M_u, and also the concrete contribution parameter α [8]. The squash load N_u is defined as the ultimate axial load for a short column, and for short-term loading is given by:

$$N_u = A_s f_{sd} + A_c f_{cd} \quad (1)\ a$$

$$= A_s f_{sk} + 0.83 A_c f_{cu} \quad (1)\ b$$

where the symbols are as given in the list of notation, and the material partial factors of safety are taken equal to unity. The design ultimate moment of resistance M_u of the section of a composite column can be calculated from the conditions of equilibrium across the section. The solution is based on the standard rectangular stress blocks used when analysing a composite steel - concrete section, and in which the concrete in tension is ignored. The concrete contribution parameter α , is given by the ratio of the portion of the squash load which is carried by the concrete core to the total value of the squash load of the composite section.

Under the combined effect of an axial load N and a bending moment M on a composite section, dimensionless interaction graphs of the type shown in Figure 1 could be developed by consideration of equilibrium conditions across the section. It can be seen that under a small axial load, the design ultimate moment of resistance of the section could be exceeded as a result of the stabilising effect the compressive force has on the equilibrium of the composite section.

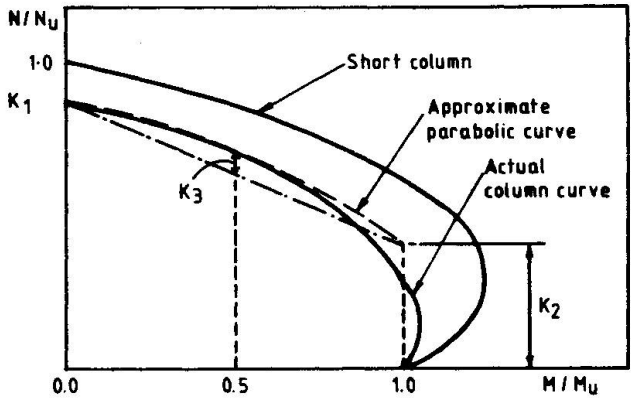

FIG. 1. TYPICAL INTRACTION GRAPHS FOR COMPOSITE COLUMNS.

The ultimate load-carrying capacity of an axially loaded composite column is given by:

$$N_k = K_1 N_u \quad (2)$$

where K_1 is a reduction factor which depends on the slenderness of the column. Both the Bridge Code [2] and the ECCS method [3] take K_1 as a function of $\bar{\lambda}$, where $\bar{\lambda}$ is the equivalent slenderness ratio of the column, and which is given by:

$$\bar{\lambda} = (N_u/N_{cr})^{\frac{1}{2}} = L_e/L_c \quad (3)$$

The ultimate load-carrying capacity of a composite column under axial compression and bending is given by:

$$N_k = K N_u \quad (4)$$

where K is a reduction factor which depends on the reduction factor K_1 for axially loaded columns, the material and cross-section properties of the column section, and also on the shape and ratios of the bending moment distributions in the column. In this respect the design is simplified by the introduction of new factors K_2 and K_3 which are used to modify the actual interaction graphs as shown in Figure [1].

The Bridge Code as well as the ECCS for Composite Structures are only applicable to concrete-encased steel sections and concrete-filled steel tubes. Neither method is applicable to the proposed battened composite column since the structural steel part of the column is not included in either table C16.1, Figure 16.1 or Figure C16.1 of the European recommendations [3]. It was therefore necessary to provide experimental evidence that both the Bridge Code and the ECCS could be safely applied in the design of the proposed column.

4. TESTS ON BATTENED COMPOSITE COLUMNS

4.1 Test rig

Full scale tests on battened composite columns were carried out in a 10 000 kN capacity test rig which has been described elsewhere [10]. The load was applied to the columns by way of a pair of crossed knife-edges acting through a pair of 75mm thick plates at each end. The loading system consisted of 38mm round bars positioned in either 15mm deep V-shaped notches or in 5mm deep, 40mm diameter circular grooves in the loading plates. A system of holes in the set of loading plates nearer the column ends, and to which the column end plates were bolted, enabled the columns to be accurately fixed to the thick loading plates giving a high degree of accuracy in applying the load at the required eccentricities.

4.2 Test specimens

Figure 2 and Table 1 give details of the tested columns. End plates 15mm thick were welded to the column ends using 6mm fillet welds. The cross-sectional areas of the channels given in Table 1 were estimated by their weight; this was in preference to the use of the tables which gave only the nominal dimensions. The sizes of the batten plates used are given in Table 1, and are seen to be substantially smaller than required in accordance with the design specifications of bare structural steel battened columns [1]. The maximum size of aggregate used for the concrete was 10mm, and the properties of the concrete mix were 1: 1.9 : 2.4 /0.55. All columns were cast and tested horizontally, which of course would not be the case in practice.

Figure 3 shows the details of the column ends when tested with end eccentricities larger than half the column depth or breadth measured along the minor and major axes respectively. In such cases, the end plates were taken large enough to accomodate the applied compressive force within their dimensions. Triangular stiffening plates were welded to both the end plates and column ends to ensure that premature failure of the columns would not occur as a result of local failure at the column ends.

4.3 Instrumentation

The columns were instrumented to measure the longitudinal strains in the steel channels using electrical strain gauges, and in the concrete using a Demec strain gauge. The Demec gauge was also used to detect and measure the transverse separation between the flanges of the steel channels and the concrete at positions midway between the battens. Only one half of each column

length was instrumented for strain measurements, and typical positions of the various gauges are shown in Figure 4. The electrical strain gauges on the batten plates, which were only used in a few of the tested columns, showed that the batten plates acted only as ties between the steel channel flanges, and that the battens were not subjected to bending moments as in the case of battened bare steel columns. Dial gauges were used to measure the column defflections at mid-span both in the minor and major axes directions. Resin was also applied to parts of the columns which were not instrumented in order to observe the progress and extent of the yielding of the structural steel elements.

TABLE 1 : DETAILS AND PROPERTIES OF COLUMNS

Column No.	Size of channel	Depth of column	Batten plates			Steel channels				Concrete core				Effective length	
			Thickness	Length of end battens	Length of intermediate battens	Area $A_{s/2}$	Characteristic strength f_{sk}	Yield strain ϵ_y	Elastic modulus E_s	Area A_c	Cube strength f_{cu}	Elastic modulus		L_{ex}	L_{ey}
												Bridge Code	ECCS		
	mm x mm	mm	mm	mm	mm	mm^2	N/mm^2	%	kN/mm^2	mm^2	N/mm^2	kN/mm^2	kN/mm^2	mm	mm
1	152x76	352	10	150	100	2242	267	NR*	205.0#	48860	45.0	32.0	22.4	3174	2904
2	152x76	352	8	180	120	2273	270	"	"	48790	37.0	29.7	18.4	3180	2910
3	152x76	352	8	180	120	2274	268	"	"	48790	35.0	29.2	17.4	3180	2910
4	203x89	428	10	200	140	3579	274	"	"	80220	41.0	30.8	20.4	3180	2910
5	203x89	428	10	200	140	3579	279	"	"	80220	38.0	29.9	18.9	3180	2910
6	254x76	402	10	220	150	3621	337	"	"	94360	41.0	30.8	20.4	3180	2910
7	254x76	402	10	220	150	3621	333	"	"	94360	47.0	32.5	23.4	3180	2910
8	152x76	352	8	150	120	2342	330	"	"	48860	39.0	30.3	19.4	3180	2910
9	152x76	352	8	150	120	2342	330	"	"	48860	46.0	32.2	22.9	3180	2910
10	152x76	350	6	120	90	2269	312	"	207.0#	48800	38.3	30.0	19.1	3180	2910
11	152x76	350	6	120	90	2268	314	"	"	48800	40.6	30.7	20.3	3180	2910
12	152x76	350	6	120	90	2386	298	0.24	203.4	48570	38.9	30.3	19.3	3180	2910
13	152x76	350	6	120	90	2388	295	0.22	203.4	48560	36.6	29.5	18.3	3180	2910
14	152x76	350	6	120	90	2335	267	0.25	211.7	48670	42.4	31.3	21.1	3180	2910
15	152x76	350	6	120	90	2277	274	0.30	221.3	48790	41.6	31.0	20.8	3180	2910
16	152x76	350	6	120	90	2292	278	0.30	221.6	48760	38.8	30.3	19.3	3180	2910
17	152x76	350	6	120	90	2272	277	0.30	225.5	48800	34.3	29.0	17.1	3180	2910
18	152x76	350	6	120	90	2285	323	NR*	207.0#	48770	42.0	31.0	20.9	2910	3180
19	152x76	350	6	120	90	2268	310	"	"	48800	48.2	33.0	24.0	2910	3180
20	152x76	350	6	120	90	2365	296	0.22	233.7	48610	36.6	29.5	18.3	2910	3180
21	152x76	350	6	120	90	2380	272	0.21	230.0	48580	39.5	30.5	19.7	2910	3180
22	152x76	350	6	120	90	2300	278	0.29	205.4	48740	35.2	29.3	17.5	2910	3180
23	152x76	350	6	120	90	2300	288	0.28	204.1	48740	33.7	28.9	16.8	2910	3180
24	152x76	350	6	120	90	2300	272	0.29	207.4	48740	33.4	28.8	16.6	2910	3180
25	152x76	350	6	120	90	2300	291	0.30	204.8	48740	42.6	31.3	21.2	2910	3180
26	152x76	350	6	120	90	2300	273	0.30	208.3	48740	38.6	30.2	19.3	2910	3180

* Values were not recorded # Average values Material partial safety factors are ignored.

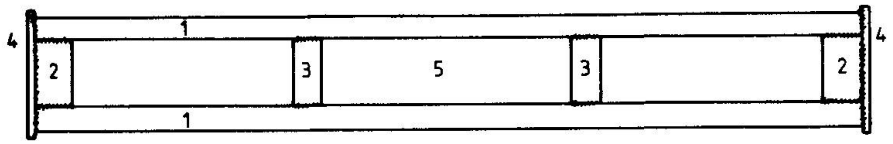

1. Steel channels (2·7m long) 2. End batten plates
3. Intermediate batten plates 4. End plates 5. Plain concrete core.

FIG. 2. DETAILS OF COLUMN SPECIMENS.

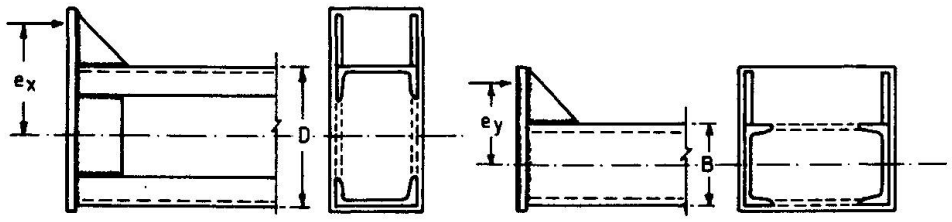

a) Bending about major axis b) Bending about minor axis

FIG : 3. DETAILS OF COLUMN ENDS SUBJECTED TO LARGE ECCENTRICITIES

4.4 Test results

Some of the test results of columns 1-9 have been published elsewhere [4]. Moreover, the results of the extensive strain measurements on columns 10-26 have also been published, and showed clearly the presence of full composite action between the structural steel and concrete elements of the battened composite column up to failure [5].

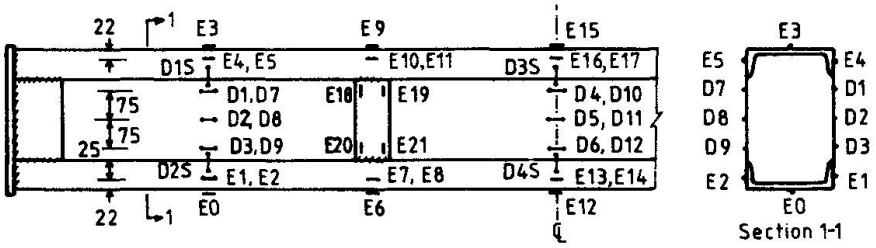

E : Electrical resistance strain gauges D: Demec gauges (S for separation)

FIG : 4. TYPICAL POSITION OF STRAIN GAUGES
(Distances given in mm for channel size 152 x 76)

Figure 5 shows some typical load-deflection curves of the tested columns. Columns subjected to minor axis bending showed negligible deformations in the minor axis direction, and such deflections were therefore omitted from the figure. On the other hand, columns subjected to major axis bending suffered a small minor axis bending due to their self weight. The minor axis moments were further magnified by the effect of the compression force, and consequently the columns deflected in both the major and minor axis direction. The last two columns in the series were subjected to biaxial bending and therefore exhibited deformations in both directions as seen in Figure 5. The deflections measured in the major axis direction were always measured using dial gauges resting against the flanges of both steel channels, and hence the angle of twist of the mid-span section could also be evaluated. Under large eccentricities, columns tested under major axis bending showed very little twist. The largest recorded angle of twist at failure was 2×10^{-2} radian for column 12 (e_x = 120mm). The other major axis columns suffered angles of twist of less than 3.5×10^{-3} radian at failure.

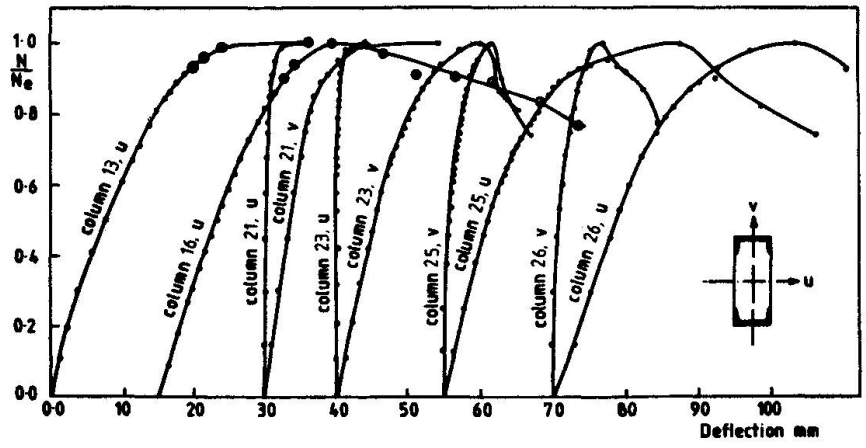

FIG 5. LOAD-DEFLECTION CURVES

Tables 1 and 2 show the details and results of all tests carried out on full scale battened composite columns. With the exception of column 9, which was tested in double curvature, all columns were tested in single curvature. Each column was made by using a 6.0m long steel channel section, from which a 5.4m length was used for the column, and the remaining 0.6m was used to determine

the material properties of the steel channel. The characteristic strength of steel was determined from tests on tension specimens machined from the 0.6m long channel section, usually one or two specimens from the web and one from each flange. The characteristic strength of concrete was determined for each column from an average value of tests on at least four 100mm cubes.

TABLE 2 : TEST RESULTS OF COLUMNS

Column No.	Eccentricity		Eccentricity ratio		Squash load	Conc. contribution factor	Ult. moment of resistance		Exp. Failure load	Mid-span deflection at failure		Mid-span moment at failure		Bridge Code			ECCS		
	About major axis e_x	About minor axis e_y	About major axis e_x/D	About minor axis e_y/B	N_u	α	M_{ux}	M_{uy}	N_e	v	u	M_{ex}(*)	M_{ey}(#)	Reduction factor K_B	Ult. load N_{kB}	$\frac{N_e}{N_{kB}}$	Reduction factor KE	Ult. load N_{kE}	$\frac{N_e}{N_{kE}}$
	mm	mm			kN		kNm	kNm	kN	mm	mm	kNm	kNm		kN			kN	
1	0	0	0	0	3022	0.604	-	80.4	2610	-	4.5	-	11.8	0.755	2283	1.14	0.851	2571	1.01
2	0	8	0	0.05	2726	0.550	-	81.4	2290	-	11.2	-	44.0	0.657	1790	1.28	0.701	1911	1.20
3	0	40	0	0.26	2636	0.538	-	80.6	1338	-	18.8	-	78.7	0.406	1070	1.25	0.411	1082	1.24
4	0	10	0	0.05	4691	0.582	-	174.0	4250	-	7.2	-	73.1	0.747	3502	1.21	0.776	3639	1.17
5	0	30	0	0.15	4527	0.559	-	176.3	3093	-	14.8	-	138.6	0.589	2665	1.16	0.594	2687	1.15
6	0	12	0	0.05	5652	0.568	-	261.3	5063	-	4.0	-	81.0	0.792	4479	1.13	0.803	4538	1.12
7	0	25	0	0.10	6092	0.604	-	261.3	4432	-	9.6	-	153.4	0.673	4097	1.08	0.675	4110	1.08
8	0	0	0	0	3121	0.505	-	101.5	2539	-	4.5	-	11.4	0.761	2375	1.07	0.838	2615	0.97
9	0	50	0	0.33	3403	0.546	-	102.4	1776	-	N.R.	-	-	0.554	1884	0.94	0.547	1861	0.95
10	0	40	0	0.26	2967	0.523	-	93.4	1357	-	N.R.	-	68.0*	0.402	1192	1.14	0.407	1208	1.12
11	0	40	0	0.26	3069	0.536	-	94.2	1494	-	10.1	-	74.9	0.394	1209	1.24	0.400	1228	1.22
12	0	60	0	0.39	2990	0.524	-	93.8	1185	-	31.5	-	108.4	0.319	955	1.24	0.321	961	1.23
13	0	80	0	0.52	2884	0.512	-	92.6	986	-	35.1	-	113.5	0.272	784	1.26	0.272	784	1.26
14	0	100	0	0.66	2960	0.579	-	83.2	777	-	28.8	-	100.1	0.211	626	1.24	0.213	630	1.23
15	0	120	0	0.79	2932	0.574	-	83.2	643	-	29.0	-	95.8	0.186	546	1.18	0.187	549	1.17
16	0	140	0	0.92	2844	0.552	-	84.6	553	-	24.8	-	91.1	0.172	488	1.13	0.172	489	1.13
17	0	160	0	1.05	2648	0.525	-	83.0	491	-	26.4	-	91.5	0.162	429	1.14	0.162	429	1.14
18	40	0	0.11	0	3176	0.535	225.7	-	2252	14.7	4.3	123.2	-	0.566	1797	1.25	0.615	1952	1.15
19	80	0	0.23	0	3359	0.581	215.0	-	1825	18.4	3.5	179.6	-	0.455	1528	1.19	0.487	1635	1.12
20	120	0	0.34	0	2877	0.513	214.1	-	1521	21.0	9.1	214.5	-	0.408	1175	1.29	0.432	1244	1.22
21	160	0	0.46	0	2887	0.552	198.0	-	1346	24.5	5.4	248.3	-	0.350	1011	1.33	0.368	1061	1.27
22	200	0	0.57	0	2703	0.527	195.5	-	1212	17.4	4.0	263.4	-	0.313	845	1.43	0.322	870	1.39
23	280	0	0.80	0	2688	0.507	202.6	-	950	20.3	4.4	285.2	-	0.247	665	1.43	0.257	690	1.38
24	360	0	1.03	0	2602	0.519	191.3	-	728	19.6	7.4	276.4	-	0.191	498	1.46	0.198	513	1.42
25	80	40	0.23	0.26	3062	0.563	204.7	89.1	1205	6.8	32.5	104.5	87.4	0.281	861	1.40	0.285	873	1.38
26	160	80	0.46	0.52	2817	0.554	192.0	83.4	664	7.0	33.8	110.9	75.6	0.180	508	1.31	0.180	506	1.31

(*) $M_{ex} = N_e (e_x + v)$ (#) $M_{ey} = N_e (e_y + u)$ *Deflection assumed to be the same as column 11

The elastic modulus of steel was either determined for each column from the test results on the tension specimens, or was taken 205 kN/mm^2 or 207 kN/mm^2; these being very close to the average experimental values obtained for a group of columns. The elastic modulus of concrete given in Table 1 was obtained in accordance with the Bridge Code and the ECCS recommendations. As seen from Table 2, the actual failure loads of the columns are all in excess of the predicted values as obtained by the Bridge Code and the ECCS recommendations. It should be noted that in using these methods of design, it was decided to use curve "a" of the European buckling curves for bare steel columns. It was originally thought that curve "c" was more appropriate for use for the bare steel section of the battened composite column, but further considerations indicated that curve "a" should be used. The choice of curve "a" for the design of battened composite columns was supported by the test results which showed that the use of curve "c" gave predicted failure loads which were very conservative.

The ratios of the failure loads to the predicted values are shown graphically in Figure 6 both for minor and major axis bending. The two recommended methods of design seem to be in fairly good agreement, with the Bridge Code giving ultimate loads which are marginally lower than those predicted by the ECCS method. As seen from Figure 6, the failure to predicted load ratio reaches a peak at eccentricity ratios of 0.5 and 0.6, after which it levels off at values of 1.15 and 1.45 for minor and major axis bending respectively. The closest agreement between the experimental and predicted values is for the case of axial compression where the eccentricity is equal to zero.

Figure 7 shows the failure loads of the columns in which steel channels of size 152 x 76 were used. The failure loads are shown against the interaction graph of a short column of the same dimensions and for which a concrete contribution parameter of α = 0.55 was taken; this being an average value for the tested

columns as seen from Table 2. The interaction curves obtained on the basis of the Bridge Code and the ECCS recommendations are shown also in Figure 7, and are plotted using the factors K_1 K_2 and K_3 as obtained by the design recommendations. It can be seen from the figure that all the experimental failure loads are higher than predicted by both methods of design.

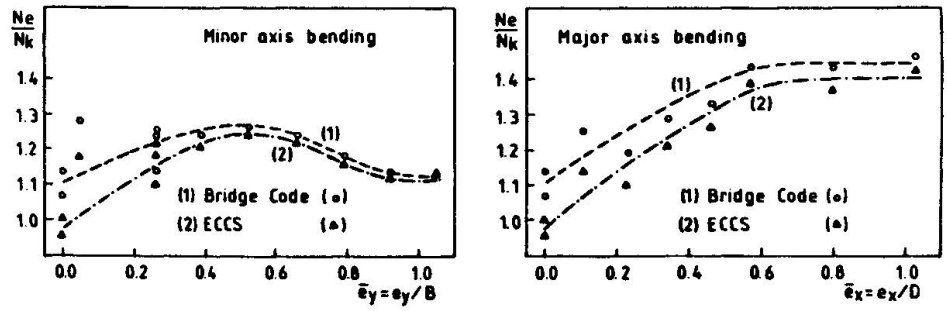

FIG. 6 FAILURE LOAD V. ECCENTRICITY FOR COLUMNS

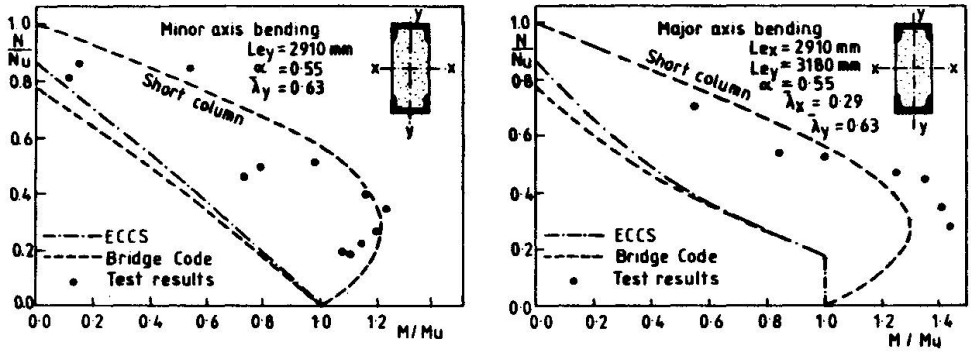

FIG. 7 INTRACTION CURVES UNDER UNIAXIAL BENDING FOR COLUMNS USING 152 x 76 STEEL CHANNELS

5. CONCLUSIONS

Results of tests on battened composite columns reported both here and elsewhere, confirm that full composite action up to failure is present between the structural elements of the column, namely the concrete core and the structural steel channels. The results also show that both the Bridge Code and the ECCS recommendations could be safely used for the design of the column since the experimental failure loads were always in excess of the predicted values. The experimental investigation thus confirms that the battened composite column is a practical way of combining concrete and structural steel in such a way that the best use is made of their material properties.

6. NOTATION

A_c, A_s	:	Area of concrete core and structural steel section respectively.
B, D	:	Breadth and depth of section respectively.
E_c, E_s	:	Elastic modulus of concrete and structural steel respectively.
e_x, e_y	:	Eccentricity about the major and minor axes respectively.
$\bar{e}_x$, $\bar{e}_y$	:	Eccentricity ratios e_x/D and e_y/B respectively.
f_{cu}	:	Cube strength of concrete
f_{cd}, f_{sd}	:	Design strength of concrete and steel respectively
f_{ck}, f_{sk}	:	Characteristic strength of concrete and steel respectively.
K_1	:	Reduction factor for an axially loaded composite column.
K_{1B}, K_{1E}	:	K_1 as obtained from Bridge Code and ECCS respectively.

K	:	Reduction factor for a composite column subjected to compression and bending.
K_B, K_E	:	Reduction factor K as obtained from Bridge Code and ECCS respectively.
L_e	:	Effective column length about appropriate axis
L_c	:	Critical length of column for which its squash load equals its Euler critical load.
M	:	Factored moment on composite column
M_u	:	Design ultimate moment of resistance of composite section.
M_{ux}, M_{uy}	:	M_u value about major and minor axis of section respectively.
N_e, M_e	:	Experimental failure load and moment respectively.
N	:	Factored normal force on composite column
N_{cr}	:	Euler critical load of composite column
N_u	:	Squash load of composite column
N_k	:	Ultimate load-carrying capacity of composite column
N_{kB}, N_{kE}	:	N_k value as obtained from the Bridge Code and ECCS recommendations respectively.
u, v	:	Deflections at column mid-span in the direction of the X and Y axes respectively.
α	:	Concrete contribution parameter
λ	:	Slenderness ratio of column.
$\bar{\lambda}$	:	Equivalent slenderness ratio of column.

7. REFERENCES

1. BS 449: Part 2, "The use of structural steel in buildings", British Standard Institution, 1969.
2. BS 5400: "Steel, concrete and composite bridges, Part 5: Code of Practice for design of composite bridges", British Standard Institution, 1979.
3. European Convention of Constructional Steelwork (ECCS): "Composite Structures",1981.
4. TAYLOR, T., SHAKIR-KHALIL, H., YEE, Y.M., "Some Tests on a new type of composite column", Proc. Instn. Civ.Engnrs, Part 2, vol. 75, June 1983.
5. SHAKIR-KHALIL, H. and HUNAITI, Y.M., "Behaviour of battened composite columns", Conference, Applied solid mechanics, University of Strathclyde, Glasgow, U.K., March 1985.
6. YEE, Y. M., SHAKIR-KHALIL, H., TAYLOR R., "Design expressions for a new type of composite column", Journal of Constructional steel research, vol.2, No.2, June 1982.
7. JOHNSON, R.P. and SMITH, D.G.E., "A simple design method for composite columns", The Structural Engineer, vol. 58A, No. 3, March 1980.
8. BASU, A.K. and SUMMERVILLE, W., "Derivation of formulae for the design of rectangular composite columns", Proc. Instn. Civ.Engnrs, Supp. vol., 1969.
9. VIRDI, K.S. and DOWLING, P.J., "A unified design method for composite columns", Publications, IABSE, vol. 36 II, 1976.
10. HORNE, M.R., and NARAYANAN, R., "Ultimate capacity of longitudinally stiffened plates used in box girders", Proc. Instn. Civ.Engnrs, Part 2, vol. 61, June 1976.

Leere Seite
Blank page
Page vide

Confinement of Steel Buckling by Concrete in Composite Members

Effet stabilisant du béton dans les éléments mixtes

Begrenzung des Beulens von Stahl durch den Beton im Verbundbau

Masami SAKAI
Dr. Eng.
Nippon Kokan K.K.
Kawasaki, Japan

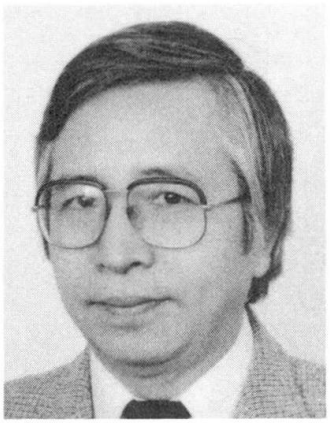

Masami Sakai, born 1938, did research on steel structures for a Master's degree of Yokohama National Univ. 1967, awarded Dr. of. Eng. by Tokyo Univ. 1985 and is now working on composite materials and structures.

Nobuhiko CHIDA
Structural Eng.
Nippon Kokan K.K.
Kawasaki, Japan

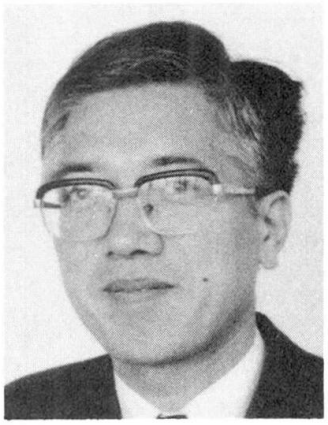

Nobuhiko Chida, born 1939, did research on differential settlement of foundations at Tohoku Univ. He designed steel structures for 19 years at N.K.K. and is now working on new materials for buildings.

Toshio NASU
Structural Eng.
Nippon Kokan, K.K.
Kawasaki, Japan

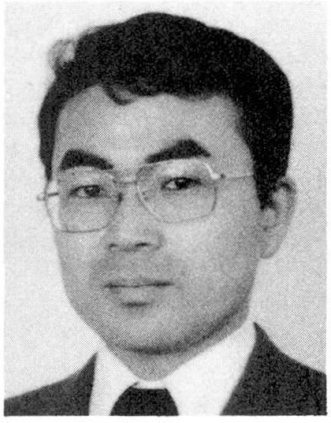

Toshio Nasu, born 1950, did research on cracking of concrete for a Master's degree of Osaka Univ. 1977, worked on the aseismic design of steel structures for 4 years at N.K.K., and is now working on steel and concrete composite structures.

SUMMARY

A steel plate element in a composite member of steel and concrete may be confined by concrete, hence it is possible to prevent the occurrence of local buckling even if the plate element has a large width-thickness ratio. In this study, experiments were first conducted on 76 specimens. Then, theoretical investigation was made by use of the Energy Method on the ductility of H steel flange. As a result, the effect of concrete on the ultimate strength, ductility and stiffness of composite members could be quantitatively determined.

RÉSUMÉ

Les éléments plans des profilés en H sont stabilisés au voilement par le béton, dans le cas de colonnes ou de poutres composites; il est possible de prévenir ce phénomène même pour des élancements (rapport largeur/épaisseur) élevés. On a tout d'abord expérimenté 76 éprouvettes pour étudier le voilement, la ductilité et la rigidité. Ensuite, sur ces critères, une étude théorique a été conduite, utilisant la méthode énergétique. Ainsi, les auteurs ont pu montrer l'effet stabilisant du béton.

ZUSAMMENFASSUNG

Ein Stahlplattenelement in einem Verbundbauteil aus Stahl und Beton kann durch den Beton gehalten werden, weshalb es möglich ist, dass das lokale Beulen des Plattenelementes verhindert wird, auch wenn das Breite- zu Dicke-Verhältnis gross ist. Im Rahmen dieser Studie wurden 76 Versuchskörper getestet. Anschliessend wurden theoretische Untersuchungen des Verformungsverhaltens von Flanschen bei H-Profilen mittels der Energie-Methode durchgeführt. Als Ergebnis konnte die Wirkung des Betons auf die Tragfähigkeit, Verformbarkeit und Steifigkeit von Verbundelementen quantitativ bestimmt werden.

1. OUTLINE OF EXPERIMENT

The experimental parameters are given in Table 1, the section types of specimen are shown in Fig.1 and the loading types in Fig.2.

2. RESULTS OF EXPERIMENT

2.1 Buckling mode of steel

The steel buckling mode of section type H-1 is shown in Fig.3(a). On the contrary, in the case of the section type H-3, the effect of inside concrete is shown in Fig.3(b). In the case of section type H-4, it is as shown in Fig.3(c). Accordingly, the stronger the confinement by concrete is, the smaller the buckling wave length is (Fig.4). Fig.5 shows the relation between the position of hoop reinforcement and the curvature

Table .1 Experimental parameters

Parameter	Level
B/t_f	9.5,10,15,20,23,30,33,48,62.5
Pw(%)	0, 0.1,0.2,0.4
tc(mm)	0, 20, 40, 64
N/No	0, 0.15, 0.3, 0.6, 1.0

B/t_f: Width-thickness ratio
Pw: Hoop reinforcement ratio
tc: Thickness of concrete cover
N/N_o: Compression ratio
No: Yield compression load of steel

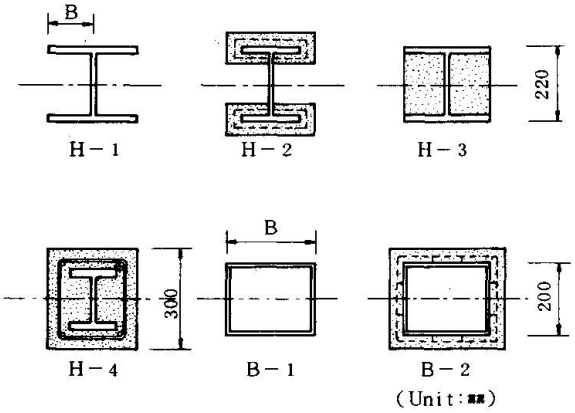

Fig.1 Section types of specimen

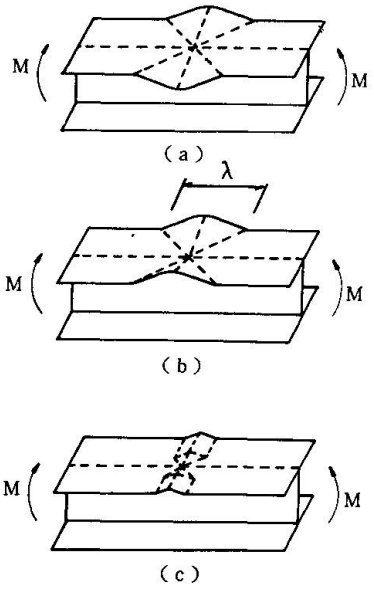

Fig.3 Buckling mode of steel

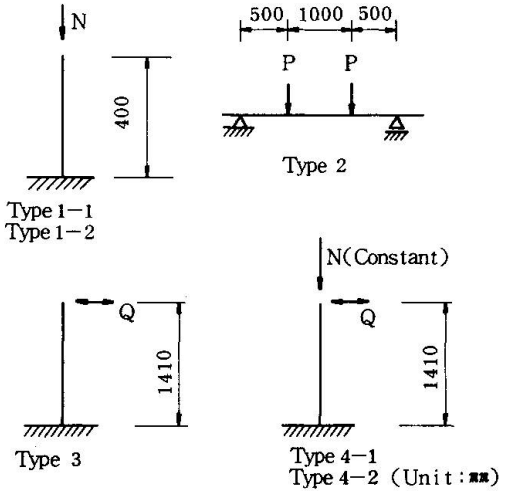

1-1, 4-1 Steel is only compressed
1-2, 4-2 Steel and concrete are compressed

Fig.2 Loading types

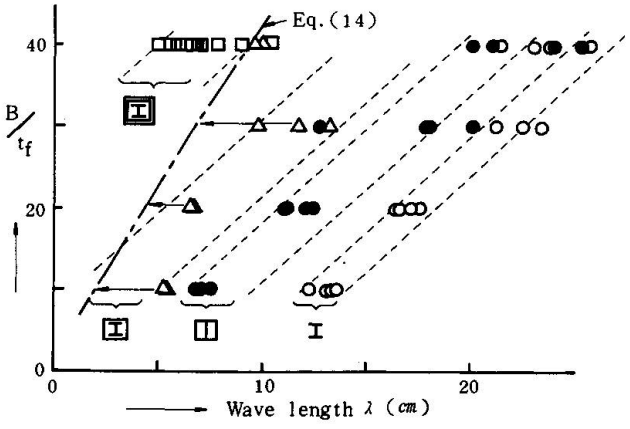

Fig.4 Variation of λ (Loading type 1-1)

distribution of steel flange obtained from test. As is clear from this figure, buckling of flange is under the influence of hoop reinforcement pitch. In this experiment, the buckling wave length was 1.5p on the average for the H-type.

2.2 Failure mode of concrete cover

In the case of loading type 1-1 and section type H-4 bending crack(1) are observed in the center of concrete (Photo.1-(a)). This fact indicates that the steel flange will first push the central area of concrete cover. In the case of section type B-1, the wave corresponding to the flange and that corresponding to the web shift by half wave-length to each other. In the presence of confinement by concrete, however, both the shifting of wave-length and wave length itself become smaller.
In terms of loading type 1-2, the concrete cover is pushed-out due to local buckling of steel either prior to the collapse of concrete (Photo. 1-(b)) or after the collapse of concrete. The former was observed in case of no hoop reinforcement and the latter was observed in the case when the concrete was firmly confined by hoop reinforcement.

2.3 Failure of hoop reinforcement

Fig.6 shows the strain of hoop reinforcement of loading type 1-1. Step 1 is the value just after cracking, and Step 2 is the value just before collapse. The strain of point (4) is distinguished at the initial stage, but at the final stage, the strain

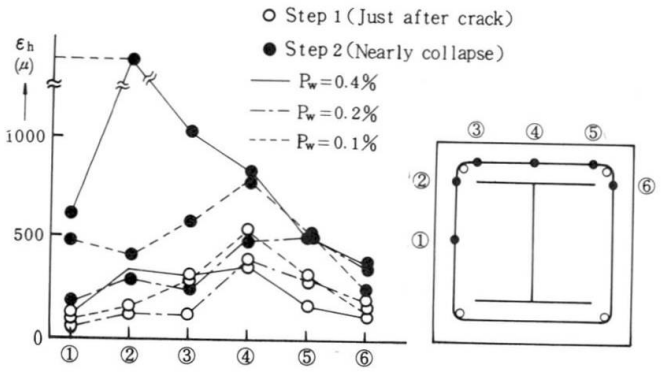

Fig.6 Strain of hoop reinforcement

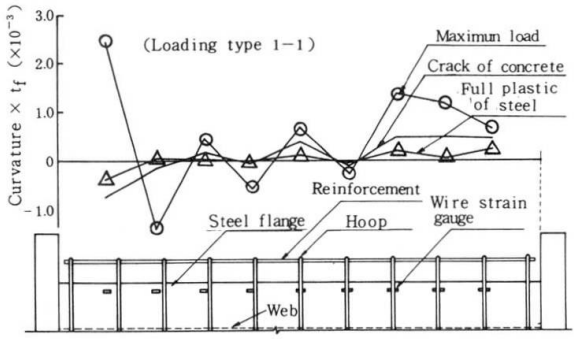

Fig.5 Deformation of steel flange (Pw=0.2%)

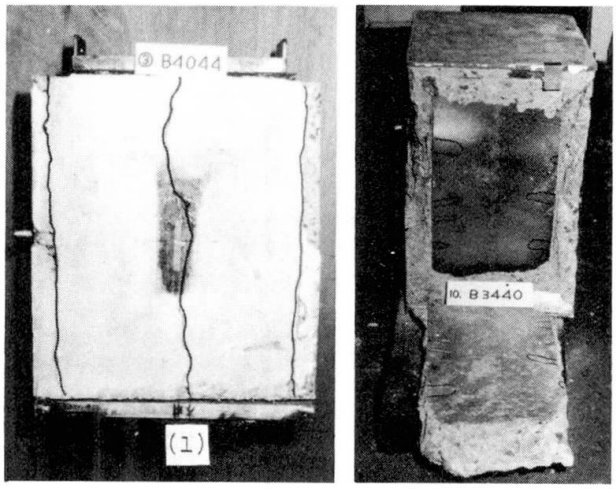

(a) Loading type 1 - 1 (b) Loading type 1 - 2

Photo.1 Failure mode of concrete cover

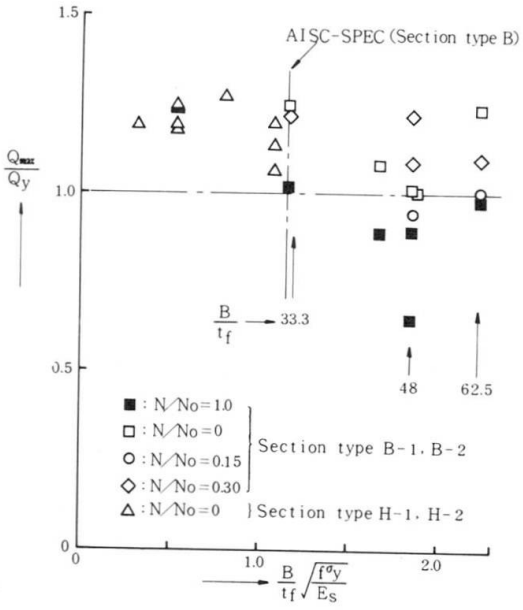

Fig.7 Maximum load and B/t_f (Loading type 3, 4-1)

on or around the flange end is sharply increasing toward the failure.

2.4 Ultimate strength of member

Fig.7 shows the ultimate strength of composite members obtained from the experiments of section type H-1,H-2,B-1,B-2 loading type 3,4-1. Even if the width-thickness has a ratio of B/tf = 62.5, it is possible to secure the full plastic strength of steel with the aid of the effect of confinement by concrete. However, the larger the compression ratio N/No is, the lower the ultimate strength is. Fig.8 shows the ultimate strength of section type H-1,H-3,H-4 loading type 1-1 paying close attention to the degree of confinement by concrete. By coating grease on the steel surface its bond with the concrete was broken. This figure indicates that as the degree of confinement by concrete increases, it approaches full plastic strength.

Fig.9 shows the data of loading type 4-2. Likewise in a situation when only the steel was compressed, the larger the width-thickness ratio B/tf and compression ratio are, the lower the ultimate strength is. With the aid of confinement by concrete, however, it is possible to secure the full plastic strength. Judging from these results, it has been proven that the confinement by concrete can improve the ultimate strength of steel. The Eq.(1) is the regression formula for determination of the ultimate strength of section type B-2 induced from the experiment.

$$\frac{Mmax}{Mthe} = (2.36-2.09\frac{N}{No})\frac{tc}{100t_f} + 9.04\times10^{-4}(\frac{B}{t_f})^2 - 0.1\frac{B}{t_f} + 3.5 \quad ---(1)$$

where, Mmax: Maximun resisting moment of section
Mthe: Theoretical full plastic moment of steel

The Eq.(1), the full plastic moment (Theoretical 1) and the maximum moment on the assumption that all the section has been subjected to strain hardening (Theoretical 2) are compared in Fig.10.

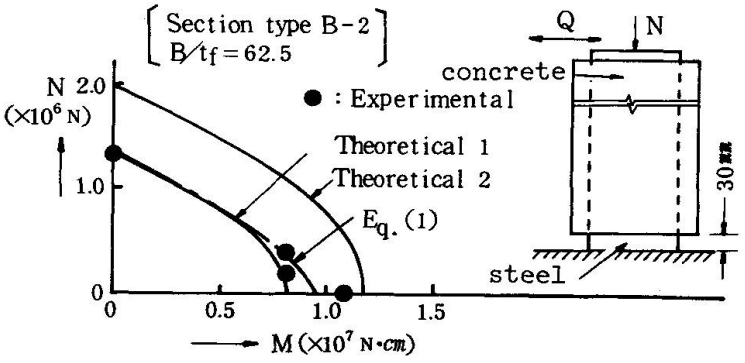

Fig.10 Maximum load (Loading type 4-1)

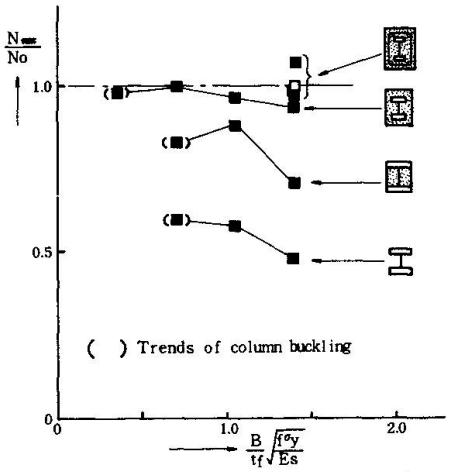

Fig.8 Maximum load and B/tf (Loading type 1-1)

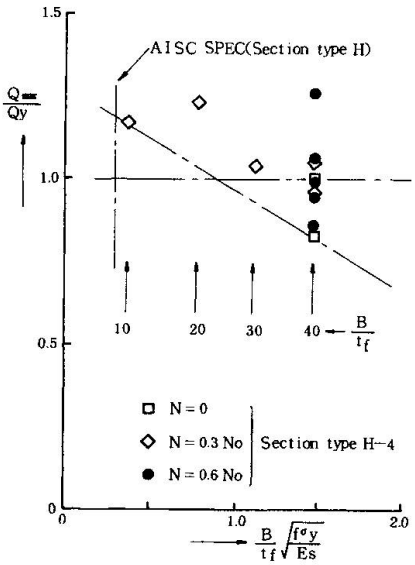

Fig.9 Maximum load and B/tf (Loading type 4-2)

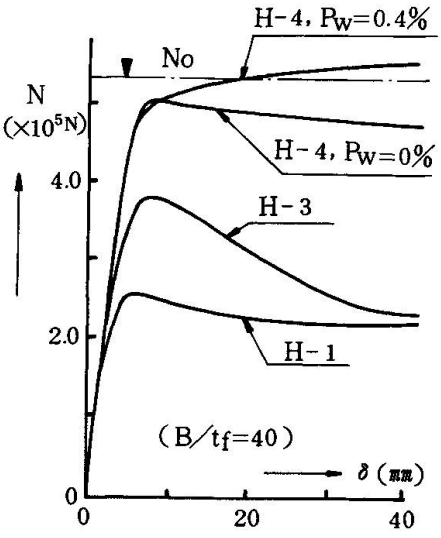

Fig.11 N-δ (Loading type 1-1)

2.5 Ductility of member

Fig.11 is the load-deformation curve of loading type 1-1. The steel surface have been greased. With the increase of flange confinement, ductility is improved. For the deformation at the ultimate strength, the effect of hoop reinforcement is particularly significant. Fig.12 shows the influence of flange width-thickness ratio in case of loading type 3. This figure indicates that, with the increase of width-thickness ratio, the ductility is lowered. However, if the hoop reinforcement is increased in volume, the ductility will be improved as is shown in Fig.13. It should be noted that, in the case when the similar experiment is conducted in loading type 4-2, the ductility may not be much improved. In this case the concrete cover is liable to separate from the inside concrete because of the small pitch of hoop reinforcement.

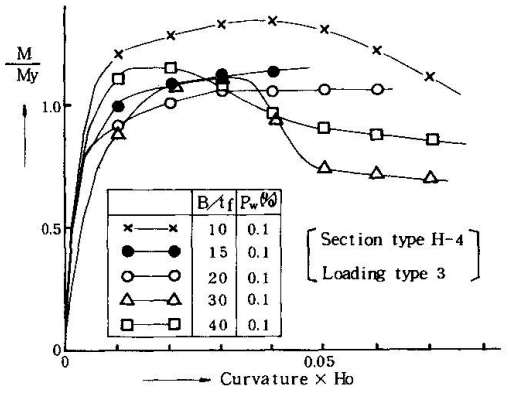

Fig.12 Moment-Curvature

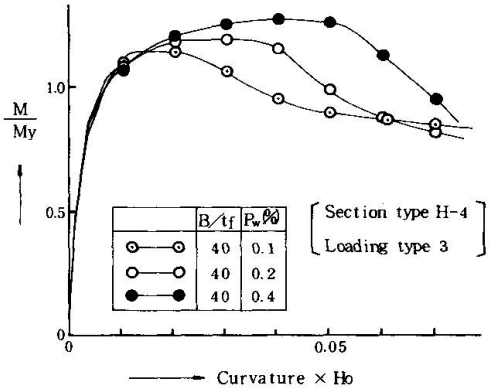

Fig.13 Moment-Curvature

2.6 Stiffness of member

Fig.14 shows the specimen's stiffness EI made dimensionless form by the theoretical stiffness of steel EsIs. It is clear from this figure that, with an increase in the compression ratio, the stiffness is higher. Then contribution rate of concrete for stiffness @ will be determined from the experimental values. For the section type B-2 and loading type 4-1, Eq.(2) is established.

$$\alpha = -0.0564 + (0.00462 + 0.0687 \frac{N}{N_o}) \frac{tc}{t_f} \quad ---(2)$$

provided that, when $\alpha < 0$, $\longrightarrow$ $\alpha = 0$

3. DUCTILITY OF STEEL FLANGE PLATE

For the study of ductility in plastic region of steel plate, there is one method in which the stabilizing conditions for the plate are deduced using the plastic flow theory (Haaijer[3],etc.) and another one where they are deduced by the Energy Method based on the assumed buckling mode of the plate (Kato & Hukuchi[1]). In this study, theoretical investigation are made on the ductility of steel plate by the latter method which permits comparatively easy determination of the influence by each confining factors.

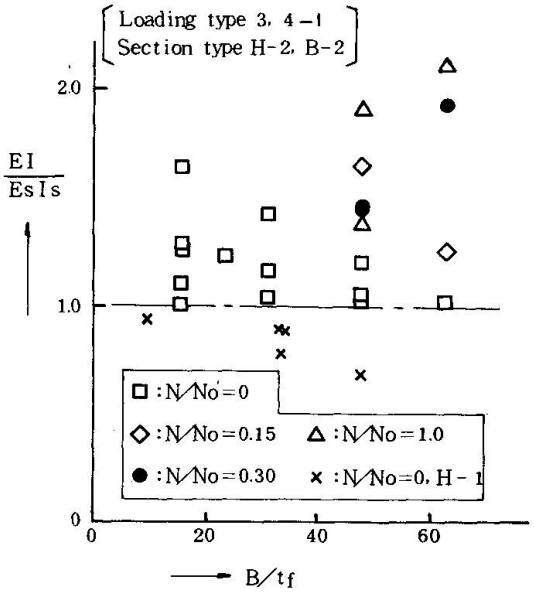

Fig.14 Stiffness of composite member

3.1 Assumptions for analysis

(1) The section type H-4 is to be investigated.

(2) Assuming that the bond between the steel and concrete is zero, the steel is only compressed.

(3) In the axial direction of each member, the web does not confine the flange deformation, but deforms together with the flange.

Based on these assumptions, the buckling and the failure modes of flange plate and concrete cover are defined and the volume of internal work nessesary for such deformation is expressed as a numerical formula. Then, from the experimental work equilibrium, the resisting moment per unit length in the hinge line of flange plate is determined. On the other hand the maximum possible moment per unit length in the hinge line is also deduced by using expanded Von Mises's yielding condition up to the strain hardening range. From these formulae the limit strain sEmax of flange plate at the ultimate strength is deduced.

3.2 Defining of buckling mode

For steel flange plate it is assumed that plastic rotation takes place around the yield hinge line indicated in Fig.15, up to the ultimate strength of member. The pentagon $A_1A_2CA_4A_3$ is assumed to be contracted by δ from both sides into the pentagon $A_1'A_2'CA_4'A_3'$. At this time the triangles $A_2'CB_2'$, $A_4'CB_4'$, A_2A_4C and B_2B_4C are subject to shearing strain. The collapse mechanism of cover concrete is shown in Fig.16. As is also clear from Photo.1, the steel flange cannot be released from the confinement except for making cracks on the concrete cover along the line of flange end. Even in the case when there is no hoop reinforcement, it is considered that the comfinement of flange plate is effective if the concrete on both ends of flange is sound.

3.3 External work

The external work at the time when the flange plate deforms by 2δ under the yield compression load $2B \cdot t_f \cdot f\sigma_y$ is

$$ {}^{o}W = 4B \cdot t_f \cdot f\sigma_y \cdot \delta \quad ---(3) $$

3.4 Internal work

(1) The shearing strain work iWs1 of flange plates $A_2'CB_2'$ and $A_4'CB_4'$ is

$$ {}^{i}W_{s1} = 2\lambda \cdot t_f \cdot \delta \cdot \tau = 2\lambda \cdot t_f \cdot \delta \cdot {}_f\sigma_y \cdot \sin\phi \cos\phi \quad ---(4) $$

(2) The shearing strain work iWs2 of flange plates A_2CA_4 and B_2CB_4 is

$$ {}^{i}W_{s2} = \lambda^2 \cdot t_f \left(\frac{1}{\cos\theta} - 1\right) {}_f\sigma_y \cdot \sin\phi \cos\phi \quad ---(5) $$

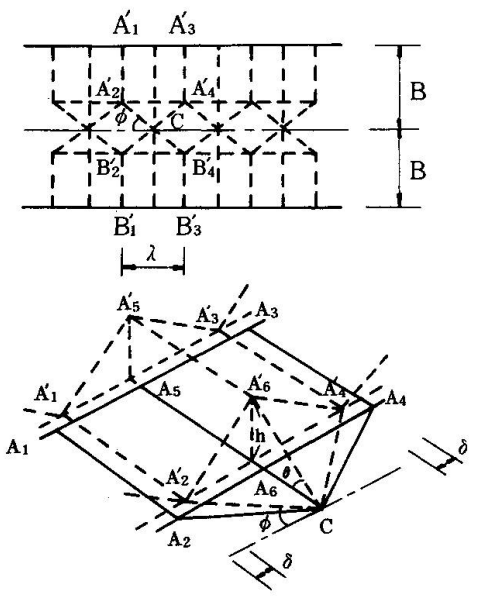

Fig.15 Buckling model of flange

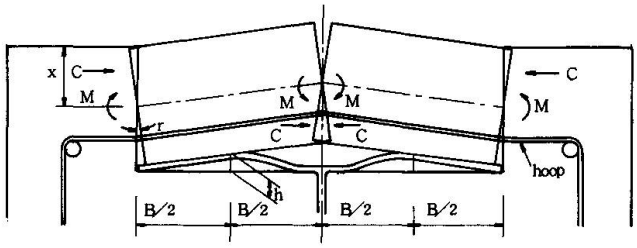

Fig.16 Collapse mechanism of concrete cover

(3) The work iWbs by rotation of flange plate hinge is

$$i^{W}_{bs} = \int_o^{\theta} (\Sigma M)\, d\theta \quad \text{----------(6)}$$

(4) The work iWbc by rotation of concrete cover's hinge is

$$i^{W}_{bc} = 4M\theta = k_1 k_3 (1-k_2) \cdot Fc \cdot l_o \cdot \frac{\lambda}{B} \cdot tc^2 \cdot \tan\theta \quad \text{---(7)}$$

(5) The work of hoop reinforcement iWbh, using the elongation rate, is

$$i^{W}_{bh} = {}_h\sigma_y \cdot P_w \cdot (B+d) \cdot l_o \cdot 2\{\sqrt{(2h)^2+B^2} - B\} \quad \text{----(8)}$$

3.5 Equilibrium of work and limit strain

From the equilibrium of work, oW = iW, iWbs is determined as follows:

$$i^{W}_{bs} = K_1(1-\sqrt{1-\tan\theta}) - K_2(\frac{1}{\cos\theta}-1) - K_3\tan\theta - K_4(\sqrt{\tan^2\theta+(\frac{B}{\lambda})^2} - \frac{B}{\lambda}) \quad \text{---------(9)}$$

$$K_1 = (4Bt_f \cdot {}_f\sigma_y - 2\lambda t_f \tau)\frac{\lambda}{2} \qquad K_2 = \lambda^2 t_f \cdot \tau$$

$$K_3 = k_1 k_3 (1-k_2) tc^2 \cdot \lambda \cdot l_o Fc/B \qquad K_4 = 2 \cdot {}_h\sigma_y \cdot Pw(B+d) \cdot \lambda \cdot l_o \quad \text{-------(10)}$$

Therefore, the resisting moment M per unit length of hinge line determined from Eq.(6) with the total length of hinge line expressed as L is :

$$M = \frac{\Sigma M}{L} = \frac{1}{L} \cdot \frac{d(i^{W}_{bs})}{d\theta} \fallingdotseq \frac{1}{L}(\sqrt{2\varepsilon} \cdot K_1 - \sqrt{2\varepsilon} \cdot K_2 - K_3 - \frac{\lambda}{B}\sqrt{2\varepsilon} \cdot K_4) \quad \text{-------------(11)}$$

On the other hand, the maximum possible value of M is determined by expanding Von Mise's formula for strain hardening range in the same manner of Ref.[1] :

$$M = \frac{1}{4} {}_f\sigma_y t_f^2 m, \quad m = \frac{\beta^2 - (2\sin^2\phi - \cos^2\phi)^2}{2\beta}, \quad \beta = \sqrt{\cos^4\phi + 4\{(\frac{f\sigma_u}{f\sigma_y})^2 - \cos^2\phi\,(1+2\sin^2\phi)\}} \quad \text{--(12)}$$

The limit strain of flange is derived from the Eq.(11) and Eq.(12). and expressed as Eq.(13) :

$$s\varepsilon_{max} = \frac{(\frac{1}{4} \cdot f\sigma_y \cdot m \cdot \bar{L} + \bar{K}_3)^2}{2(\bar{K}_1 - \bar{K}_2 - k \cdot \bar{K}_4)^2} \cdot (\frac{t_f}{B})^2$$

$$= K(\frac{t_f}{B})^2 \quad \text{----------(13)}$$

$$\bar{K}_1 = 2k \cdot {}_f\sigma_y - k^2 \cdot \tau \qquad \bar{K}_2 = 2k^2 \cdot \tau$$

$$\bar{K}_3 = k_1 k_3 (1-k_2)\frac{l_o}{B}(\frac{tc}{t_f})^2 Fc \cdot k$$

$$\bar{K}_4 = 2 \cdot {}_h\sigma_y \cdot l_o Pw(B+d)k/(B \cdot t_f)$$

$$\bar{L} = \sqrt{2k} + 3, \quad k = \lambda/B$$

Moreover, the buckling length of flange is expressed by Eq.(14) by partially differentiating the value of K in Eq.(13) by λ

$$\lambda = F(\frac{f\sigma_u}{f\sigma_y}, \frac{tc}{t_f}, Pw, d) \quad \text{---(14)}$$

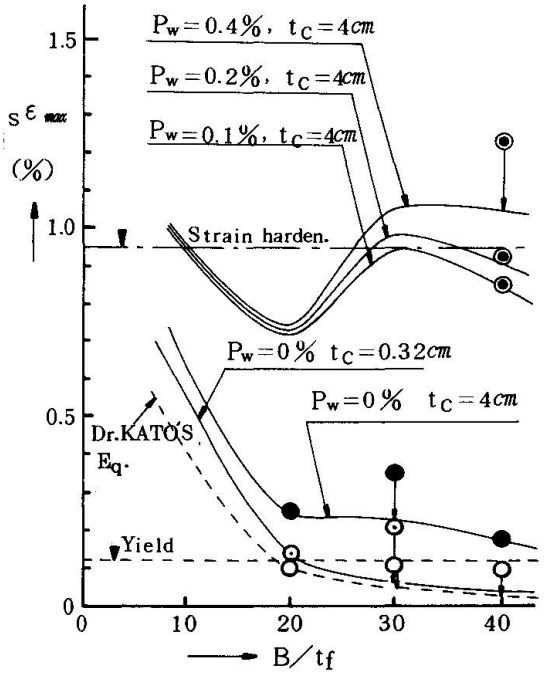

Fig.17 Limit strain of steel flange (Loading type 1-1, section type H-1, H-3, H-4)

The theoretical value of λ determined for the section type H-4 from Eq.(14) is shown in Fig.4. The value of $_s\varepsilon_{max}$ determined by substituting Eq.(14) in Eq.(13) using the width-thickness ratio B/tf as a parameter is shown in Fig.17. Judging from Fig.17, it seems that the larger the width-thickness ratio B/tf is the greater effect the concrete cover and hoop reinforcement have.

4. CONCLUSION

The findings of this study are as follows:

1) The buckling mode of steel flange varies greatly with the presence of concrete. In particular the buckling wave length of flange was significantly smaller due to the effect of confinement of concrete.

2)To secure the theoretical yield strength of composite members, the width-thickness ratio of steel flanges could be increased up to 40(H type) and 62.5(B type) through proper choice of concrete cover.

3) The ductility of composite members was significantly improved by the concrete cover. Especially the use of sufficient volume of hoop reinforcement is very effective to the ductility properties.

4) The limit strain of steel flange under the confinement of concrete was evaluated with various parameters using the Energy Method. And simulation of experimental values could be attained to a certain degree.

Notation

B: Half width of flange
t_f: Flange thickness
tw: Web thickness
tc: Concrete cover thickness
H: Height of steel section
Ho: Height of specimen's section
λ: Buckling wave length
p: Pitch of hoop reinforcement
Pw: Hoop reinforcement ratio
N/N_o: Compression ratio
C: Compressive force of concrete
k_1, k_2, k_3: $k_1 \cdot k_3 = 0.83, k_2 = 0.42$
θ : Angle of flange plate rotation
γ: Angle of concrete cover rotation
ϕ : Angle of external force with flange hinge line
Mmax: Maximum resisting moment of section
lo: Effective length of concrete cover contributing to the confinement
d: (Beam width-2B)/2
δ: Deformation of flange
τ: Shearing Stress $(={}_f\sigma_y \cdot \sin\phi \cos\phi)$
Fc: Compressive strength of concrete
Es: Elastic modulous of flange
ε: Strain of flange
$_h\sigma_y$: Yield stress of hoop
$_f\sigma_y$: Yield stress of flange
$_f\sigma_u$: Ultimate stress of flange
$_oW$: External work
$_iW$: Internal work
α: Contribution rate of stiffness (El/Esls-1)

References:

[1] B.Kato & Y.Hukuchi "Flange local buckling in plastic range"(in Japanese), TRANSACTIONS of AIJ May,1968
[2] M.G.Lay "Flange Local Buckling in Wide Flange Shapes",ASCE,December,1965
[3] G.Haaijer "Plate Buckling in the Strain Hardening Range",ASCE,TRANSACTIONS paper,No.2968,1958
[4] M.Kimura "The Stiffening Effect for Local Buckling of High Strength Steel by Mortar"(in Japanese),Research Reports of AIJ Kanto Branch,1976